ALL-CELLULOSE COMPOSITE LAMINATES: THE PROCESSING-STRUCTURE-PROPERTY RELATIONSHIPS FROM THE MACRO- TO THE NANOSCALE

Jan Wolfgang Dormanns

A thesis submitted in partial fulfilment of the requirements for the Degree of Doctor of Philosophy in Mechanical Engineering in the University of Canterbury.

October 2015

Jan Wolfgang Dormanns: *All-cellulose composite laminates: The processing-structure-property relationships from the macro- to the nanoscale,* Department of Mechanical Engineering, University of Canterbury, Christchurch, New Zealand

"For all knowledge and wonder (which is the seed of knowledge)
is an impression of pleasure in itself."

— Sir Francis Bacon (The Advancement of Learning, 1605)

Dedicated to my son Samuel with your endless curiosity and happiness.
Never stop exploring my little adventurer!
* 26.01.2014

CONTENTS

Of the gladest moments in human life, methinks is
the departure upon a distant journey to unknown lands.
— Sir Richard Francis Burton (1856)

ACKNOWLEDGEMENTS

Even though the world was quite different and far more unexplored in Burton's days, it was with slightly nervous joy that Katharina and I headed off to Christchurch in 2012 and it is with a laughing and a crying eye that I see this thesis being submitted. New Zealand has been a fantastic home in the past three years and I want to thank all those who helped me during this time.

I wish to express my most sincere gratitude to Dr. Mark Staiger, Prof. Dr. Jörg Müssig and Dr. Benoît Duchemin for their valuable supervision. Thank you for all the advice and help over the past years, it was a great experience.

I want to thank all the technicians at UC for their great assistance, especially Kevin Stobbs, Mike Flaws, Helen Devereux, Gary Turner, Manfred Ingerfeld and Jan McKenzie.

A big thanks to the MacDiarmid Institute for funding my research trips, the MacDiarmid Emerging Scientist Association for great workshops and connecting students all over New Zealand, and Dr. Michelle Dickinson at the University of Auckland for granting access to the nanoindenter.

My thanks also go to Dr. Céline Picard and Vincent Loisel for their assistance during my stay in Le Havre; and Dr. Mark Tobin and the IR-team at the Australian Synchrotron, and the Royal Society of New Zealand for funding the synchrotron experiments and travel assistance to Melbourne (AS151/IRM/ Proposal 9060).

I want to thank the University of Canterbury for granting a UC Doctoral Scholarship, which made my studies possible in the first place.

A special thanks to Dr. Tim Huber and Dr. Jeremias Schuermann for their help and advice, as well as countless discussions on ACCs; and to all the other students I had the honour to share an office with for the great atmosphere. I also want to thank Felix Weiler, Tom Pawley and Christian Hannes for their contributions during their internships in our research group.

Thanks to André Miede for providing the classic thesis style and the LaTeX-community for discussing every single typesetting problem and all the energy that goes into web fora. Also a big thanks to all open source developers for making great software available.

Finally, I want to thank all my friends here in New Zealand, back home in Germany and all over the world, thanks for being the wonderful people you are. I want to show my deepest gratitude to my parents and my family, thanks for all your trust and confidence, supporting me wherever I go, whatever I do and always being there for me when I need you the most.

My biggest and loudest "Thank you!" goes to my beloved wife Katharina and our son Samuel, the two of you are the wonderful core of my life.

ABSTRACT

Cellulose is an excellent resource for the manufacture of sustainable materials, due to its availability and biodegradability. All-cellulose composites (ACCs) are an emerging class of bio-based composites in which both the fibre and matrix phase consist of cellulose. Thereby, ACCs overcome the chemical incompatibility often encountered when hydrophilic cellulose is used as reinforcement of hydrophobic polymer matrices in bio-based composites.

The mechanical properties of ACCs are reported to exceed those of traditional bio-based composites, which makes ACCs a promising material in the search for an alternative to petrochemical-derived thermoplastics. However, the manufacture and characterisation of ACCs has been limited to thin films (< 1 mm). Recently, solvent infusion processing (SIP) based on partial dissolution of cellulose fibres in an ionic liquid (IL) has been developed. SIP presents a pathway that allows the manufacture of thick ACC laminates (> 4 mm), which widens the range of potential applications. The aim of this work was the characterisation of the structure and properties of ACC laminates from the macroscopic laminate scale down to the individual fibre and matrix phases on the microscopic scale.

The occurrence of size effects in composites reported in the literature poses the question whether increasing the dimensions of ACC laminates impairs the mechanical properties. In this work the effect of increasing thickness on the structure and mechanical properties of ACC laminates based on a woven rayon textile and manufactured by SIP was investigated. A positive size effect of increasing strength with increasing thickness was found. Ultimate tensile strength increased from 80 MPa in a single lamina of 0.42 mm thickness to 106 MPa in an ACC laminate of 8 laminae with a thickness of 3.36 mm. A strengthening mechanism for ACC laminates based on a woven rayon textile is proposed. Furthermore, a transition from low-strain fail-

ure to tough and high-strain failure with increasing thickness and a scale effect of increasing crystallinity towards the core of thick ACC laminates was observed.

SIP has been developed using imidazolium-based ILs, which offer a high cellulose solubility and facilitate controlled dissolution by adjusting the processing temperature. However, ILs are also known to be toxic and non-biodegradable, making them non-ideal solvents for manufacturing a green material. In this work the use of an aqueous 7 wt. % NaOH/12 wt. % urea solution (NaOH/urea) as cellulose solvent for SIP has been explored as an environmentally friendly and cost-effective alternative to ILs. The effect of infusion temperature, dissolution time and cooling during processing were investigated. NaOH/urea facilitated rapid processing of ACC laminates with partial dissolution achieved in 5 min and when compared to IL-processed laminates a similar Young's modulus in the range of 7 to 8 GPa and a 28 % increase in ultimate tensile strength to 123 MPa was found. Cooling the SIP setup and the solvent to -12 °C prior to infusion and continuous cooling during infusion were required to achieve homogeneous and optimum mechanical properties.

Fourier-transformed infrared spectroscopy (FTIR) and elemental analysis were utilised to confirm the complete removal of IL and NaOH/urea from thick ACC laminates by washing in distilled water. Measuring the conductivity of the washing bath was established as a measure of the solvent content and to determine completion of solvent removal from ACCs.

Micromechanical characterisation of the individual fibre and matrix phases by nanoindentation revealed a lower modulus of the matrix in comparison to the fibres, indicative of structural changes with ACC processing. FTIR-microspectroscopy and transmission electron microscopy suggest a more amorphous matrix in comparison to the fibres in ACC laminates. A significant decrease in modulus from 9.5 GPa of as-received fibres to values in the range of 7.9 to 8.9 GPa of fibres in ACC laminates measured by nanoindentation leads to the conclusion that not only the surface but also the core of the cellulose reinforcement is affected by processing.

DECLARATION

I declare that this dissertation is my own unaided work. It is being submitted for the degree of Doctor of Philosophy at the University of Canterbury. It has not been submitted for any other degree or examination in any other University.

Jan Wolfgang Dormanns
Christchurch, 30.10.2015

PUBLICATIONS

The work presented in this thesis includes the following publications:

Chapters 1 – Introduction – and 2 – Literature Review – include passages of the following book chapter:
Title: "From Cellulose Dissolution and Regeneration to Added Value Applications – Synergism Between Molecular Understanding and Material Development"
Authors: Poonam Singh, Hugo Duarte, Luís Alves, Filipe Antunes, Nicolas Le Moigne, **Jan Dormanns**, Benoît Duchemin, Mark Peter Staiger and Bruno Medronho
Book: "Cellulose", ISBN 978-953-51-4411-3
Publisher: IntechOpen, Rijeka, Croatia

Material covered in Chapter 4 – Size and scale effects in all-cellulose composite laminates – has been accepted for publication subject to amendments, revision under review as of 24.02.2016:
Title: "Positive size and scale effects in all-cellulose composite laminates"
Authors: **Jan Dormanns**, Felix Weiler, Jeremias Schuermann, Jörg Müssig, Benoît Duchemin, Mark Peter Staiger
Journal: Composites Part A: Applied Science and Manufacturing, Elsevier, Amsterdam, Netherlands

Material covered in Chapter 5 – Solvent Infusion Processing Using Aqueous Sodium Hydroxide/Urea Solution – has been peer-reviewed and published:

Title: "Solvent Infusion Processing of All-Cellulose Composite Laminates Using Aqueous Sodium Hydroxide/Urea Solution"

Authors: **Jan Dormanns**, Jeremias Schuermann, Jörg Müssig, Benoît Duchemin, Mark Peter Staiger

Journal: Composites Part A: Applied Science and Manufacturing, Elsevier, Amsterdam, Netherlands (Vol. 82, pp. 130-140)

LIST OF FIGURES

LIST OF TABLES

1

INTRODUCTION

1.1 BACKGROUND

1.1.1 *Composites, bio-based composites and green composites*

Composites represent an important class of engineering materials and are generally made up of two or more distinct phases. A strong and stiff component, often in fibrous form, is used as the reinforcement by embedding it in a more compliant phase, that is referred to as the matrix. A synergistic effect is achieved by the combination of matrix and reinforcement, such that the mechanical properties of the composite exceed those of either phase alone. A central point in composites is the concept of load transfer. An externally applied load is transferred from the compliant matrix to the reinforcement, such that the bulk of the load is carried by the stronger and stiffer fibres. One of the main advantages of composites is that high strength and stiffness can be achieved in materials of relatively low density. Advanced composites are nowadays used in a wide range of lightweight, structural applications in the aerospace, automotive and sports industries [Hull and Clyne, 1996].

The 21st century is marked by an increase in public awareness of environmental concerns. The drawbacks of relying on depleting fossil resources has led to changes in the development of materials and materials selection. There has been much effort in the development of sustainable and

environmentally-friendly alternatives to petrochemical-derived plastics, such as bio-based polymers and composites. Cellulose has gained interest in this context due to its high strength and stiffness, availability and biodegradability [Wertz et al., 2010]. A large body of research has focused on replacing the traditional reinforcement of composites, such as glass fibres, with natural, lignocellulosic fibres [Mohanty et al., 2002; John and Thomas, 2008; Faruk et al., 2012]. The most commonly used natural fibres are flax, hemp, sisal, jute and wood [Bledzki and Gassan, 1999; Müssig, 2010] and it has been shown that their high strength and stiffness give bio-based composites mechanical properties that can compete with glass fibre-reinforced composites, especially when density is accounted for [Wambua et al., 2003].

Comparative life cycle assessment of natural fibre-reinforced composites and traditional glass fibre-reinforced composites conducted by Joshi et al. [2004] shows that the use of natural fibres as reinforcement is environmentally favourable due to (i) the lower environmental impact of natural fibres during production, (ii) the higher fibre fraction of bio-based composites required to achieve equivalent mechanical performance, which reduces the environmentally concerning matrix phase, (iii) the lower density and accordingly high specific modulus and strength of bio-based composites, that improves fuel efficiency and reduces emissions in transport applications and (iv) the recovered energy and carbon credits from incineration of natural fibres at the end-of-life disposal [Joshi et al., 2004].

A prime example of the application of bio-based composites is the automotive industry, which is aware of the necessity to reduce its carbon footprint, a development that is driven by the demand of consumers and government regulations. The carbon footprint is reduced by (i) designing more fuel efficient engines or alternative electric drives and (ii) designing lighter components made from sustainable materials. Henry Ford used hemp fibre-

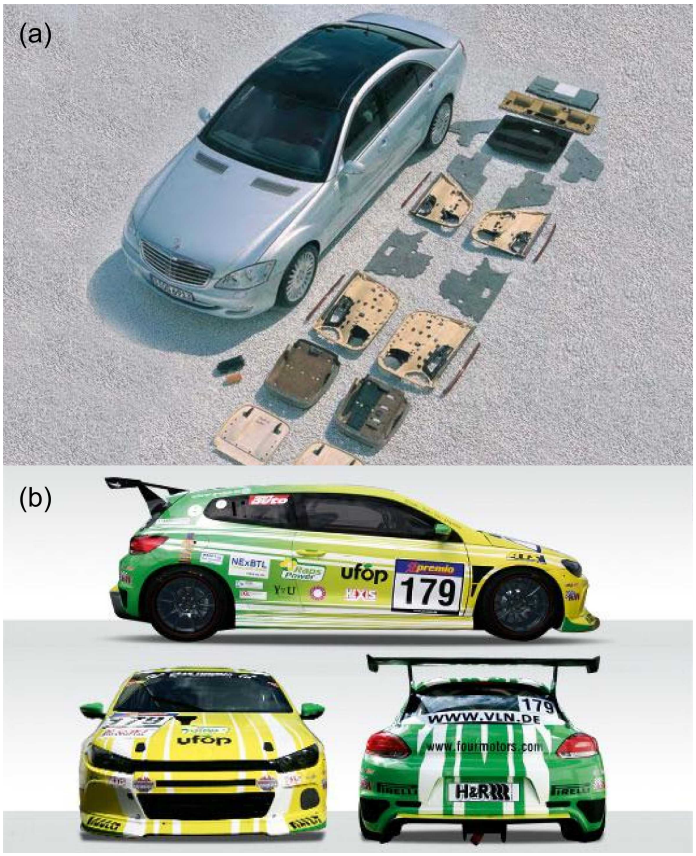

Figure 1: (a) Natural fibre-reinforced components in Mercedes S class (Bledzki et al., 2006, reproduced with kind permission of John Wiley and Sons). (b) Bioconcept car based on a Volkswagen Scirocco with natural fibre-reinforced chassis (www.fourmotors.com, 21.05.2015).

reinforced components in his cars already in 1941 and the Trabant, introduced in 1957 and the most common vehicle in former East Germany, was equipped with a natural fibre-reinforced chassis [Karus et al., 2005]. Since then research and development on bio-based composites has progressed continuously and natural fibre-reinforced components are nowadays used in many interior, e.g. door panels and seat backs (Figure 1a), and some exterior applications, e.g. an Abaca fibre-reinforced under floor protector in the Mercedes A class [Bledzki et al., 2006].

Glass and carbon fibre-reinforced components have dominated high-performance applications, due to specifications of high strength and stiffness.

However, other factors, such as cost, weight and sustainability, have gained in importance and led to a shift towards greater use of bio-based composites. The "Bioconcept Car" (Figure 1b), based on a Volkswagen Scirocco, is the result of a sustainable racing project. It runs on biofuel and is one of the world's first racing cars with a chassis made entirely from natural fibre-reinforced composites [Endres and Habermann, 2013; Fan et al., 2011]. The car was honoured with the "Composite Pioneer Award" in 2009 (www.fourmotors.com) and is an inspiring example in the development of bio-based composites.

However, the use of bio-based reinforcements is only the first step towards the final goal of completely bio-based, biodegradable and CO_2-neutral materials. In parallel, there has been intensive research on the development of bio-based polymers as matrix systems [Faruk et al., 2012; Reddy et al., 2013]. Composites that are a mix of bio-based and synthetic materials are known as *bio-* or *ecocomposites*, while those completely composed of bio-based materials are referred to as *green composites*.

The replacement of synthetic fibre by natural fibre is a promising advancement. However, chemical incompatibility may exist between a hydrophilic fibre reinforcement and hydrophobic polymer matrix that leads to weak interfacial fibre-matrix bonding. Poor fibre-matrix bonding leads to inefficient load transfer between the two phases such that the high mechanical properties of natural fibres are not reflected in the performance of bio-based composites [Bledzki and Gassan, 1999; Faruk et al., 2012]. The relatively poor mechanical properties of bio-based composites are significantly improved by chemically treating the fibre and/or matrix using chemical grafting, corona discharge and silane or alkaline treatments; although, such treatments add processing complexity and cost [Mohanty et al., 2001; George et al., 2001; Kalia et al., 2013].

1.1.2 *Single polymer composites*

Single polymer composites (SPCs), also referred to as one-polymer composites, self-reinforced composites, all-polymer composites or homocomposites, are an emerging class of materials and have received attention in several recent review articles [Matabola et al., 2009; Kmetty et al., 2010; Fakirov, 2013; Karger-Kocsis and Bárány, 2014]. The concept of SPCs is to use two varieties of the same polymer as matrix and reinforcement in a composite and it was first presented by Capiati and Porter [1975] using high-density polyethylene (HDPE). HDPE fibres with highly aligned and extended polymer chains, having an increased melting temperature of 140.1 °C and strength comparable to that of glass fibre, were used as reinforcement. A second variety of HDPE with low degree of polymerisation (DP) and therefore comparably low melting temperature of 131.1 °C was used as matrix. The difference in melting temperature of 9 °C was utilised to embed the fibres in the molten matrix [Capiati and Porter, 1975].

Based on this principle of variations in the melting temperature of a given polymer depending on e.g. DP, orientation, branching or co-polymerisation, several processing pathways for thermoplastic SPCs, such as film stacking, co-extrusion and hot compaction, have been developed and are summarised in the reviews by Kmetty et al. [2010] and Fakirov [2013].

SPCs offer two specific advantages: (i) SPCs overcome the issue of chemical incompatibility seen in natural fibre-reinforced composites. By using the same polymer for fibre and matrix a high level of chemical bonding can be achieved, resulting in high interfacial strength and efficient load transfer. (ii) SPCs possess "ultimate recyclability" *via* reprocessing (remelting), as there is no need for separation of fibre and matrix phase, which poses a difficulty for

traditional composites and bio-based composites [Capiati and Porter, 1975; Matabola et al., 2009; Kmetty et al., 2010; Karger-Kocsis and Bárány, 2014].

The recent increase in environmental awareness also led to growing interest in green SPCs. A high performing class of green SPCs are all-cellulose composites, in which both phases consist of cellulose.

1.1.3 *All-cellulose composites*

All-cellulose composites (ACCs) are green composites that have been developed using the SPC concept. In ACCs, both the reinforcing and matrix phases are based on cellulose, leading to high chemical compatibility at the fibre-matrix interface. Although high performance ACCs have recently appeared in the literature [Nishino et al., 2004; Qin et al., 2008; Soykeabkaew et al., 2009a], there are historically a number of materials that could be categorized as ACCs. For example, currently used materials such as vulcanized fibre and paper were patented in 1859 [Brown, 1999], cellophane was patented in 1918 [Brandenberger, 1918] and the processing of vegetable parchment is a technology dating back to the 19th century, as well [Cartier et al., 1994].

1.1.3.1 *Processing pathways of all-cellulose composites*

Generally, non-derivatised ACCs are processed *via* one of two different pathways (Figure 2). The first pathway involves two distinct processing steps in which (i) cellulose is first fully dissolved in a solvent and then (ii) regenerated in the presence of an undissolved cellulose reinforcement. The first example of the 2-step method was reported by Nishino et al. [2004] who combined unidirectional ramie fibre with fully dissolved wood pulp. The regeneration of the wood pulp created a matrix phase that provided adhesion between the undissolved ramie fibres. The second pathway is essentially a

single processing step that involves wetting a cellulose reinforcement with a solvent and partially dissolving the cellulose. Regeneration of the dissolved portion of cellulose leads to the *in situ* formation of a matrix phase that binds together the undissolved portion of cellulose. Gindl and Keckes [2005] were the first to report the use of the 1-step method for creating an ACC, and it has been variously referred to as partial dissolution [Huber et al., 2012a], surface-selective dissolution [Soykeabkaew et al., 2008] and natural fibre welding [Haverhals et al., 2010]. It is important to note that the processing of ACCs *via* the 1-step method follows a transforming instead of an adding concept. Partial dissolution transforms the outermost part of cellulose fibre into the matrix, instead of adding a separate matrix.

An advantage of the 1-step method is the relatively high volume fraction of fibres that can be achieved, e.g. $\leqslant 88$ vol.% are reported by Soykeabkaew et al. [2009a]. Thus, the volume fraction of fibres in an ACC approaches the theoretical maximum of 90.7 % that exists for a hexagonal packing arrangement. Maximising the volume fraction of fibres and minimising that of the matrix is desirable as it leads to improved mechanical properties [Hull and Clyne, 1996].

1.1.3.2 *Derivatised all-cellulose composites*

Processes such as esterification [Matsumura et al., 2000], benzylation [Lu et al., 2002, 2003] and oxypropylation [de Menezes et al., 2009a,b] have been used to derivatise cellulose and subsequently produce all-plant or all-wood fibre composites. Derivatisation turns cellulose into a thermoplastic polymer and ACCs can subsequently be produced by methods like hot compaction or compression moulding. Introducing thermal processability to cellulosic materials is a remarkable feature of derivatised ACCs, however, the intensive chemical modification with long processing times and associated

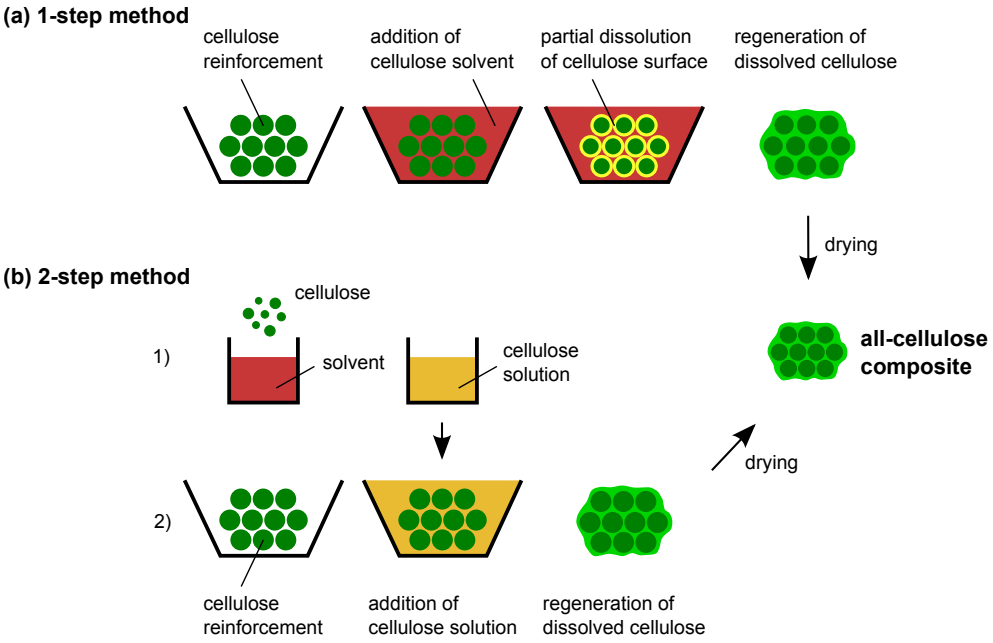

Figure 2: Processing of ACCs *via* (a) the 1-step method and (b) the 2-step method (Adapted from Huber et al., 2012c).

costs cannot be justified by their mechanical properties, as tensile strength and Young's modulus are inferior when compared to non-derivatised ACCs [Huber et al., 2012b]. The relatively low mechanical properties are probably due to a comparably low volume fraction of fibres (30 to 40 %) and incomplete impregnation of the fibres due to the high viscosity of the benzylated cellulose matrix [Lu et al., 2002].

1.1.3.3 *Cellulose reinforcements in all-cellulose composites*

The choice of cellulose source determines the type of composite that will be obtained. Isotropic ACCs have been created from micro- or nanofibrillated cellulose [Gindl and Keckes, 2005; Duchemin et al., 2009a; Abbott and Bismarck, 2010; Pullawan et al., 2013], wood pulp [Gindl et al., 2006c], bacterial cellulose [Soykeabkaew et al., 2009b; Zhou et al., 2009] and filter paper [Duchemin et al., 2009a]. Uni- or multidirectional ACCs have been prepared from natural fibre including ramie [Nishino et al., 2004; Qin et al.,

2008; Soykeabkaew et al., 2008] and flax [Gindl-Altmutter et al., 2012], and regenerated cellulose fibre including Lyocell [Gindl-Altmutter et al., 2012], Cordenka [Huber et al., 2012d,a] and Bocell [Soykeabkaew et al., 2009a].

1.1.3.4 *Solvents used for processing all-cellulose composites*

A solvent for industrial scale manufacture of ACCs ideally facilitates cellulose dissolution without pretreatment in a short time, while having a low environmental impact and being cost efficient. In the majority of studies, ACCs were processed using the lithium chloride/dimethyl acetamide (LiCl/DMAc) solvent system [Nishino et al., 2004; Gindl and Keckes, 2005; Duchemin et al., 2007, 2009b; Qin et al., 2008; Soykeabkaew et al., 2008; Pullawan et al., 2013; Yousefi et al., 2013]. LiCl/DMAc is a direct solvent of cellulose with very low chain degradation during dissolution and solubility of 15 wt.% [Liebert, 2009; Olsson and Wesman, 2013]. However, cellulose needs to be activated in a polar medium for 6 to 24 h and dissolution times of 2 to 6 h are necessary for processing fibres to ACCs by partial dissolution [Qin et al., 2008; Soykeabkaew et al., 2008]. These long processing times make LiCl/DMAc less attractive.

N-methyl-morpholine-N-oxide (NMMO) is known as a relatively environmentally friendly solvent used on industrial scale for regenerated cellulose fibre production (Lyocell process) [Loubinoux and Chaunis, 1987; Fink et al., 2001]. However, NMMO is thermally unstable and additives are necessary to prevent dangerous exothermic side reactions during cellulose dissolution [Navard et al., 2012; Rosenau et al., 2002], and it has been hardly used for manufacturing ACCs [Ouajai and Shanks, 2009].

A class of solvent that has recently received a lot of attention after Swatloski et al. [2002] highlighted their ability to dissolve cellulose are room temperature ionic liquids (ILs). The high cellulose solubility (> 20 wt.%) and direct

dissolution capability of ILs have since led to their use for ACC processing in many studies. ACCs have been prepared using ILs *via* the 2-step method by Zhao et al. [2009], who used rice husks as reinforcement and dissolved filter paper as cellulose matrix. Several groups have also performed 1-step processing of ACCs using ILs. Duchemin et al. [2009a] used the IL 1-butyl-3-methylimidazolium chloride (BmimCl) to prepare ACCs by partial dissolution of microcrystalline cellulose and filter paper. Huber et al. used the IL 1-butyl-3-methylimidazolium acetate (BmimAc) in partial dissolution approaches to produce ACC laminates by compression moulding [Huber et al., 2012d] and the solvent infusion process [Huber et al., 2012a]. Haverhals et al. used the IL 1-ethyl-3-methylimidazolium acetate (EmimAc) to transform loose natural fibres (hemp and cotton) into a composite structure by partial dissolution and termed the process "natural fibre welding" [Haverhals et al., 2010, 2012]. Similar approaches using IL for ACC processing have also been reported in other studies [Yousefi et al., 2011; Ma et al., 2011; Shibata et al., 2013a,b].

An alternative class of cellulose solvents that meets the criteria of direct and rapid dissolution and a low environmental impact are NaOH-based aqueous solutions. The discovery of aqueous NaOH as cellulose solvent dates back to the 1930's [Davidson, 1934] and Sobue et al. established that direct dissolution is possible in a narrow window of NaOH concentration (7 to 10 wt. %) and temperature (-10 to +4 °C) [Sobue et al., 1939]. Both cellulose solubility and stability of the solution can be enhanced by additives such as urea and thiourea [Zhou and Zhang, 2000; Cai and Zhang, 2005; Zhang et al., 2002]. Aqueous NaOH-based solvents appear promising for the processing of ACCs due to their low environmental impact, low cost, no necessary pretreatment of the cellulose and short dissolution times of 2 to 5 min [Cai and Zhang, 2005; Qi et al., 2008a]. However, NaOH/urea solvents

have only been used in few ACC studies and processing has been limited to the 2-step method. Cellulose solutions in NaOH/urea were mixed with cellulose nanocrystals [Qi et al., 2009; Wang and Chen, 2011; Pullawan et al., 2014] or short ramie fibres [Yang et al., 2010] to obtain isotropic ACCs and nano-ACCs with tensile strength and Young's modulus in the range of 120 to 140 MPa and 3 to 12 GPa, respectively, depending on the mass fraction of the reinforcement. 1-step processing of an ACC based on filter paper was performed by Han and Yan [2010] using the additive polyethylene glycol (PEG) in an aqueous 10 wt. % NaOH/ 1 wt. % PEG solution. However, an extensive dissolution time of 12 h was required to achieve the highest Young's modulus and ultimate tensile strength of 0.8 GPa and 75 MPa, respectively [Han and Yan, 2010].

1.1.3.5 *Mechanical properties of all-cellulose composites and comparison to bio-based composites*

The mechanical properties of ACCs strongly depend on the type of reinforcement and processing conditions. One of the main factors is the dissolution time and its effect is best explained with the example of a unidirectional ACC. With increasing dissolution time a larger portion of the fibres is transformed into the matrix, which decreases the longitudinal tensile strength due to the reduction of the fibre-volume fraction. Simultaneously transverse strength increases due to the higher matrix-volume fraction and better interfacial adhesion [Nishino et al., 2004; Soykeabkaew et al., 2008]. The dissolution time has an effect on the microstructure and crystallinity of ACCs, as well as the DP of the processed cellulose [Soykeabkaew et al., 2008; Duchemin et al., 2009b]. A similarly important parameter is the regeneration rate, with ACCs formed by slow precipitation displaying higher crystallinity, Young's modulus and tensile strength [Duchemin et al., 2009b].

The mechanical properties of ACCs can also be influenced by wet drawing. Stretching a regenerated, but still wet ACC leads to a preferred orientation of cellulose crystallites in the stretching direction [Gindl et al., 2006b; Pullawan et al., 2013]. The crystalline orientation is maintained after drying and a linearly increasing relationship of tensile strength and Young's modulus with the applied draw ratio was found. Applying a draw ratio of 1.5 leads to an increase in tensile strength from 202 to 428 MPa and Young's modulus from 9.9 to 33.5 MPa [Gindl et al., 2006b]. Similarly, the orientation of nanowhiskers within an ACC can be influenced by a magnetic field to achieve an increase in mechanical properties in a preferred direction [Li et al., 2010; Pullawan et al., 2012].

The comparison of mechanical properties of ACCs in the literature is problematic due to variations in cellulose type and processing parameters. A broad overview of the mechanical properties of ACCs was presented by Huber et al. [2012b]. A comparison of ACCs with other bio-based composites shows that ACCs are highly competitive in terms of their properties (Figure 3a). The Young's modulus of isotropic ACCs is relatively high when compared to conventional bio-based composites, which is attributed to the high properties of the regenerated cellulose matrix [Huber et al., 2012b]. The situation is different for unidirectional composites, where the Young's modulus of ACCs falls in the same range as that of bio-based composites (Figure 3b). This may be due to either a decrease in the fibre modulus caused by solvent interaction in the processing of ACCs or the modulus of bio-based composites is mainly determined by the fibre modulus and the interfacial strength is of little influence [Huber et al., 2012b]. Regarding ultimate tensile strength, ACCs perform significantly better than isotropic and unidirectional bio-based composites.

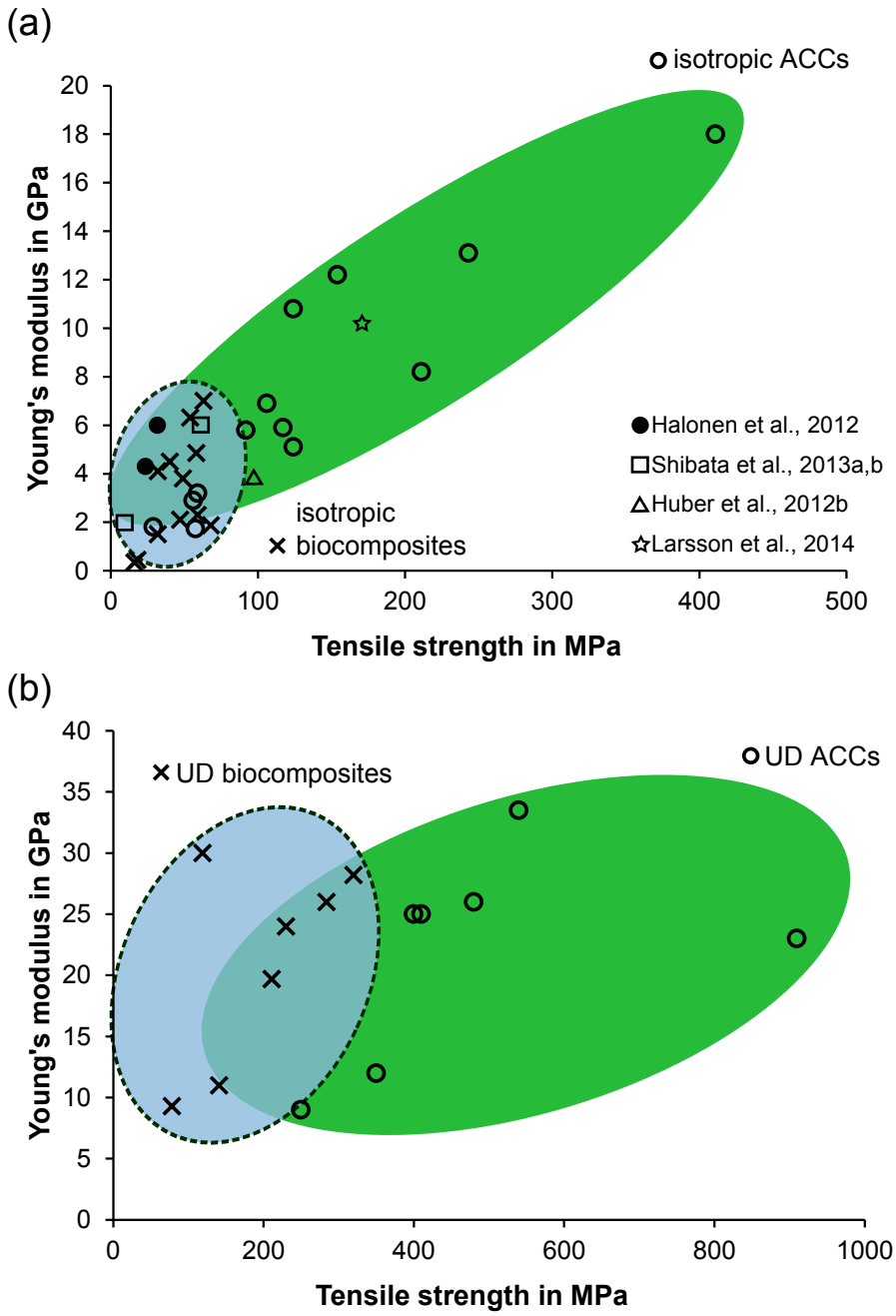

Figure 3: Comparison of mechanical properties of (a) isotropic and (b) unidirectional bio-based composites and ACCs. Underlying data was presented in the review of Huber et al. [2012b], updated with more recently published studies on isotropic ACCs [Halonen et al., 2012; Huber et al., 2012a; Shibata et al., 2013a,b; Larsson et al., 2014].

1.1.3.6 *Developing industrial scale manufacturing pathways for all-cellulose composites*

The majority of literature studies of ACCs have produced and characterised films of ACCs with thicknesses in the range of 0.3 to 1 mm. However, the expansion of ACCs into different applications will likely require greater thicknesses of material. The manufacture of ACCs relies on wet processing and necessitates a washing and drying step. The removal of solvent and subsequent drying result in a volumetric shrinkage approximately equal to the ratio of solvent to cellulose. ACC films are typically cast from 5 to 25 vol. % cellulose and hence a shrinkage of >75 % is to be expected, that is significantly higher than the shrinkage of 1 to 3 % observed during injection moulding of thermoplastics [Rosato and Rosato, 1995]. Furthermore, the removal of solvent from the dissolved portion of cellulose also results in *differential* shrinkage due to the stronger shrinkage of the regenerated matrix phase in comparison to the undissolved reinforcement [Duchemin et al., 2009b]. Differential shrinkage is problematic for two reasons: (i) internal residual stresses are generated that compromise the mechanical performance of the composite; and (ii) dimensional stability of the material is decreased following the final drying step (i.e. warpage occurs). Hence, it is clear that extensive experimental studies and development of predictive models of shrinkage in ACCs are still required in order to meet the requirements of the composite industry. Finally, the disposal and/or recycling of the solvent and identification of cost-effective sources of cellulose are important aspects in the context of industrial manufacturing that require further research and development.

Processes based on the 1-step method seem more promising for larger scale manufacture of ACCs, due to the higher cellulose/solvent ratio and minimal transformation of cellulose precursor to matrix, which limits the overall and differential shrinkage. Industrial-scale composite manufacturing

techniques (e.g. compression moulding, resin infusion) have been explored and adapted for larger scale 1-step manufacturing of ACCs [Huber et al., 2012d,a]. A common characteristic of these processing routes is the application of pressure to consolidate the material during all stages of processing so as to manage the shrinkage and ensure dimensional stability. Conventional compression moulding of composites involves the use of a rigid double-sided mould through which pressure and heat are applied to consolidate the reinforcement and matrix materials [Mazumdar, 2001]. Compression moulding of ACC laminates was carried out by Huber et al. [2012d]. Initially, several layers of a woven regenerated cellulose fibre textile were impregnated with an IL as the solvent, followed by stacking and compression of the layers. The application of heat and pressure (110 °C, < 2.5 MPa, 80 min) leads to partial dissolution of the fibres within the textile layers, resulting in the *in situ* formation of the matrix phase. The compression moulded ACC laminates were formed into dimensionally-stable, flat sheets with a final thickness of 2 mm, tensile strength of 70 MPa, and Young's modulus of 2.5 GPa.

Vacuum-assisted resin transfer moulding (VARTM) is a liquid moulding process that is used to fabricate complex-shaped, high quality composite laminate parts. Typically, a woven textile preform is placed on a one-sided rigid mould that is then covered with a vacuum bag. The application of a vacuum forces resin to flow through the textile preform, while also acting to remove voids and compact the laminate stack [Mazumdar, 2001; Glancey, 2010].

As an adaptation of the VARTM process, a method called solvent infusion processing (SIP) was developed by Huber et al. [2012a] for the fabrication of larger scale ACC laminates. During SIP, a cellulosic textile is placed on a one-sided rigid mould, sealed with a vacuum bag and then homogeneously wetted by infusing it with a cellulose solvent, rather than a resin as in regular

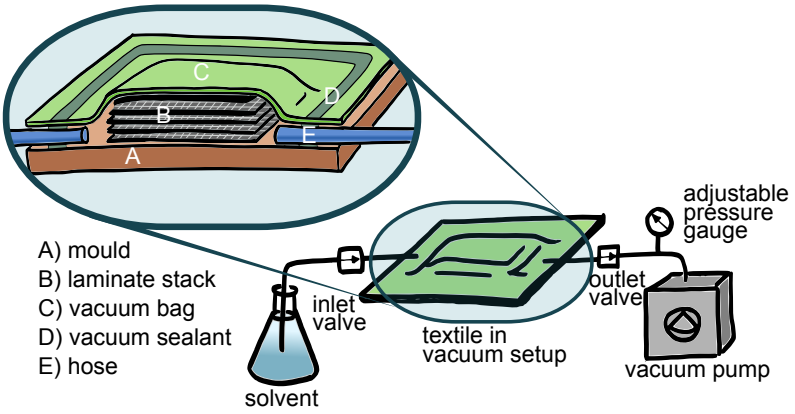

Figure 4: Setup of the solvent infusion process (SIP) as developed by Huber et al. [2012a].

VARTM (Figure 4). Huber et al. used the IL BmimAc for the development of SIP, where further compaction and partial dissolution of the cellulose reinforcement after infusion are then achieved using external pressure and heat. Regenerating the dissolved fibre portion leads to the formation of the matrix phase and the final ACC laminate is obtained by drying [Huber et al., 2012a].

SIP results in ACC laminates with a high fibre volume fraction (70 to 90 vol. %) with minimal void content. The thickness of the ACC laminates is easily adjusted by varying the number of textile layers. The mechanical properties of the final laminate can be tailored through the choice of precursor (i.e. fibre preform). ACCs based on rayon fibre processed *via* SIP have been shown to exhibit high tensile and flexural strength of 95 MPa and 135 MPa, respectively, and outstanding impact resistance with a puncture impact strength of 2 kN mm^{-2} and an unnotched Charpy impact strength of 42 kJ m^{-2} [Huber et al., 2012a, 2013].

1.2 RESEARCH MOTIVATION AND OBJECTIVES

1.2.1 *Motivation*

Cellulose represents an ideal choice as raw material for sustainable materials, due to the combination of availability, biodegradability and high mechanical properties [Wertz et al., 2010]. The use of cellulose in bio-based composites has advanced in recent years, however, chemical incompatibility between hydrophobic polymer matrices and hydrophilic natural fibres can limit the strengthening effect of the reinforcement [Bledzki and Gassan, 1999; Faruk et al., 2012]. ACCs as single-polymer composites overcome this problem and offer a promising new approach to utilise cellulose as raw material for green composites [Nishino et al., 2004; Huber et al., 2012b].

The research conducted in the field of ACCs has concentrated on thin films, however, composites of greater thickness will be necessary to transfer ACCs from research on a laboratory scale to replacing petrochemical polymers in actual applications. Partial dissolution has been identified as a promising processing pathway and SIP has been introduced as an upscalable method with high potential [Huber et al., 2012a], providing the starting point for this work.

This thesis sets out to investigate open questions in upscalable processing of ACCs *via* SIP, deepen the understanding of structural reorganisation of cellulose by partial dissolution and its effect on the mechanical properties of the individual fibre and matrix phases and the overall composite material.

In all experiments a regenerated cellulose fibre is used as starting material. The structural and chemical homogeneity of regenerated fibres is advantage-

ous for analysing the effects of processing on the structure and properties of ACC laminates, as discussed in Section 2.3.2.1.

1.2.2 *Objective 1: Upscaled manufacturing and size effect in all-cellulose composite laminates*

SIP has been shown to be a viable processing pathway for the fabrication of thick ACC laminates [Huber et al., 2012a]. The ability of processing ACCs with increased dimensions widens the range of potential applications. However, composites are known to exhibit a size effect of decreasing strength with increasing dimension [Zweben, 1994; Bažant et al., 1996; Wisnom, 1999; Sutherland et al., 1999a]. Therefore, the question is raised whether the mechanical performance of ACCs is impaired by the process of upscaling the dimension of laminates.

The first objective of this thesis is to determine whether an increase in ACC laminate thickness has an influence on their mechanical properties and investigate the underlying mechanisms of a potential size effect.

1.2.3 *Objective 2: Aqueous sodium hydroxide/urea solution as alternative solvent for solvent infusion processing*

SIP is the most promising manufacturing route for ACCs published thus far that can be potentially extended to an industrial scale. SIP was initially explored using 1-butyl-3-methylimidazolium acetate (BmimAc), an ionic liquid (IL), as cellulose solvent [Huber et al., 2012a]. Various ILs are direct solvents for cellulose offering cellulose solubility of up to 25 wt.% [Swatloski et al., 2002]. However, ILs are associated with several drawbacks: The production

of ILs on a relatively small scale makes them expensive solvents [Pinkert et al., 2009; Zhu et al., 2006]. In contrast to their image as green solvents due to their low volatility, the toxicity of imidazolium-based ILs has been documented [Ranke et al., 2004; Bernot et al., 2005; Zhao et al., 2007; Jastorff et al., 2005; Matzke et al., 2007], and is a potential environmental issue when processing ACCs on a larger scale and suggests the use of alternative solvents.

An aqueous solution of 7 wt.% NaOH/12 wt.% urea (NaOH/urea) appears promising for industrial scale manufacture of ACCs due to its low environmental impact, low cost, no necessary pretreatment of the cellulose and short dissolution times of 2 to 5 min [Cai and Zhang, 2005; Qi et al., 2008a]. In the field of ACCs, NaOH/urea solvents have been limited to composite processing *via* the 2-step method by preparing a fully dissolved cellulose solution that is combined with cellulose nanocrystals [Qi et al., 2009; Wang and Chen, 2011; Pullawan et al., 2014] or short ramie fibres [Yang et al., 2010].

Using NaOH/urea for upscaled manufacturing presents challenges due to the limited cellulose solubility of 5 to 7 wt. % and subambient temperatures (-12.5 °C) required for dissolution [Cai and Zhang, 2005; Jin et al., 2007; Egal et al., 2008]. Consequently, the second objective of this thesis is to determine whether an aqueous NaOH/urea solution can be used as cellulose solvent for processing ACC laminates *via* SIP.

1.2.4 *Objective 3: Removal of solvent from all-cellulose composite laminates*

Processing of ACCs requires the use of solvents, due to the non-thermoplastic nature of cellulose in its non-derivatised form. In the processing steps following (partial) dissolution, the cellulose solvent diffuses from the ACC into the regeneration and washing medium. The removal of solvent from ACCs is

important for economical, environmental, health and safety, and engineering reasons. However, regenerated cellulose films and fibres are reported to contain solvent residues after washing [Mahadeva and Kim, 2012; De Silva et al., 2015].

Hence, the third objective of this thesis is to investigate whether the solvents used for partial dissolution in this work, ILs and aqueous NaOH/urea solution, are completely removed by washing or remain trapped, particularly in the core of thick ACC laminates.

1.2.5 *Objective 4: Individual structural and mechanical characterisation of fibre and matrix phases in all-cellulose composite laminates*

When processing ACCs by partial dissolution, a portion of the cellulose reinforcement is reshaped into the matrix phase. Changes in cellulose structure in the process of dissolution and regeneration of the matrix phase have been reported. Generally, a decrease in crystallinity was found with processing, indicating that the relatively high crystallinity of the reinforcement is decreased and an amorphous or paracrystalline matrix is formed [Nishino et al., 2004; Duchemin et al., 2007, 2009b]. Furthermore, the structure and mechanical properties of ACCs depend on the dissolution and regeneration conditions, as e.g. the regeneration rate and the regeneration medium are known to affect the formation of cellulose during coagulation [Duchemin et al., 2009b; Mao et al., 2006; Zhang et al., 2005b]. Additionally, not only the surface of the reinforcement, but also the core may be affected by solvent interaction. However, thus far a combined analysis of the changes in the fine structure of cellulose and the mechanical properties of the individual phases is missing in the literature.

Accordingly, the fourth objective of this thesis is to characterise the individual fibre and matrix phases in ACC laminates structurally and mechanically, and investigate the influence of the dissolution time and regeneration medium.

2

LITERATURE REVIEW

2.1 CELLULOSE

Cellulose is the structural element of plants and its molecular structure with the formula $(C_6H_{10}O_5)_n$ was first described by Anselme Payen in 1838. It is the main molecule in the cell wall of higher plants and is also produced by algae, certain bacteria, protozoans and animal tunicates [Wertz et al., 2010]. With an estimated annual biomass production of approximately 1.5×10^{12} tons [Klemm et al., 2005] cellulose is the most common organic polymer on earth and can be considered an almost inexhaustible raw material for environmentally friendly products. Today cellulose is mainly used in the construction, paper and textile industry, but also in pharmaceuticals, foodstuffs and cosmetics [Klemm et al., 2005].

2.1.1 *Molecular structure*

Cellulose is a carbohydrate polymer formed by a linear chain of glucose molecules. A covalently bonded C-O-C group between the C1 and C4 carbon atoms of two adjacent anhydroglucopyranose units (AGU) is formed by a condensation reaction, resulting in a cellobiose unit (Figure 5). The cellulose chain has a twofold helical conformation with every second AGU rotated

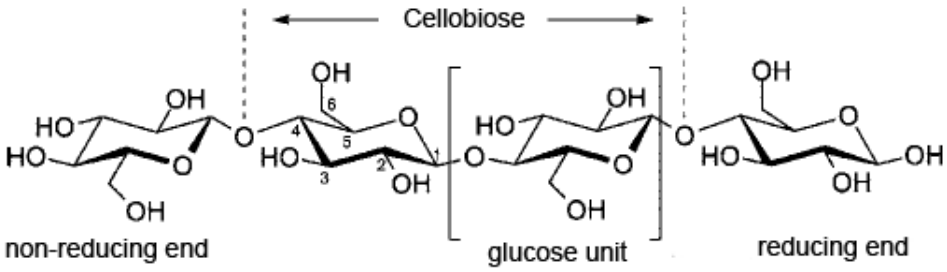

Figure 5: Molecular structure of cellulose (adapted from Pinkert et al., 2010).

by 180 °. This results in a flat ribbonlike structure that is stabilised by intramolecular hydrogen bonds [Klemm et al., 2005; Wertz et al., 2010].

The degree of polymerisation (DP) of cellulose is a measure of the chain length, i.e. the number of linked AGUs. The DP varies with cellulose source and typical values are in the range of 10000 in wood; 3000 to 15000 in cotton; 6500 to 8000 in bast fibres, such as flax and ramie; up ot 10000 in bacterial cellulose; 300 to 700 in wood pulp; and 150 to 300 in powdery microcrystalline cellulose [Klemm et al., 2005; Keijsers et al., 2013].

Typical properties of cellulose, such as hydrophilicity, biodegradability, chirality and broad chemical reactivity due to the manifold hydroxyl groups (3 per AGU), are based on the molecular structure. The hydroxyl groups are also the basis for an extensive hydrogen bond network, leading to several crystalline arrangements and semicrystalline structures [Klemm et al., 2005].

Cellulose organises in a highly hierarchical fashion to form the cell wall of plants (Figure 6), consisting of the primary wall (P) and several secondary walls (S1 and S2, substructured into lamellae), of which the S2 wall is the thickest with the highest cellulose content (1 to 10 µm compared to 0.1 to 0.5 µm for P and 0.1 to 0.3 µm for S1). Within the cell walls cellulose microfibrils are held together by hemicelluloses, lignins and pectins. These components act as matrix and make wood and other lignocellulosics a com-

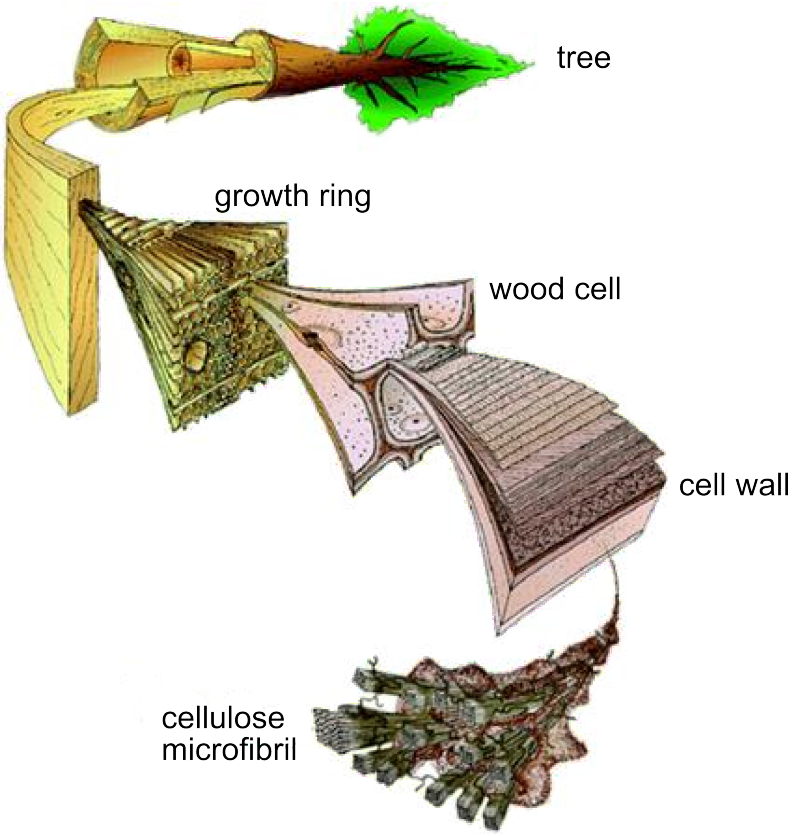

Figure 6: Hierarchical structure of cellulose from microfibril to tree (Image credit: Mark Harrington, University of Canterbury).

plex natural composite. The orientation of the cellulose fibrils, referred to as the microfibril angle, varies greatly in the different cell wall layers, e.g. from 2 to 20 ° and 85 to 90 ° in alternating lamellae of bamboo cell wall [Parameswaran and Liese, 1976]. The microfibrils can be found in bundles, e.g. in wood and bast fibres such as hemp and flax, or as individual fibres, e.g. in cotton [Klemm et al., 2005; Wertz et al., 2010].

2.1.2 *Secondary structure*

Cellulose chains assemble to complex structures *via* intermolecular hydrogen bonds. These cellulose aggregates show different degrees of order, which

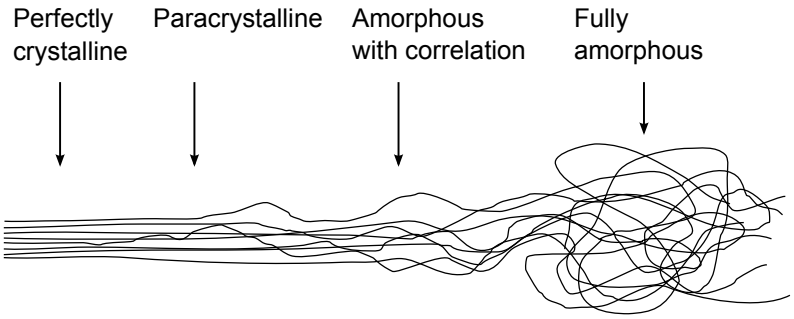

Figure 7: Schematic of cellulose chains (hypothetically) arranged in different degrees of order, from perfectly crystalline to fully amorphous (adapted from Howsmon and Sisson, 1954).

can range from low, referred to as amorphous, to dense and regular, referred to as crystalline (Figure 7). Due to the mixture of low and highly ordered domains, cellulose is regarded as a semicrystalline polymer and its fine structure has been investigated for almost a century [Herzog et al., 1923; Staudinger, 1930; Ingersoll, 1946].

Models of the fine structure of cellulose were developed early on and a fringed-fibril structure first proposed by Hearle and Peters [1963] describes continuous crystalline regions, from which fibrils branch off at different lengths (Figure 8). Crystalline domains, also referred to as crystallites, consequently alternate with amorphous domains [Fink et al., 1995]. The dimension of the crystallites varies with origin. Typical values for width range from 3 to 5 nm in wood pulp, 7 nm in cotton to 20 nm in the alga *Valonia* and crystallite length ranges from 100 to 300 nm in Cotton to up to 2000 nm in *Valonia* [Imai et al., 1998; Araki et al., 1998; Dong et al., 1998; Fleming et al., 2001].

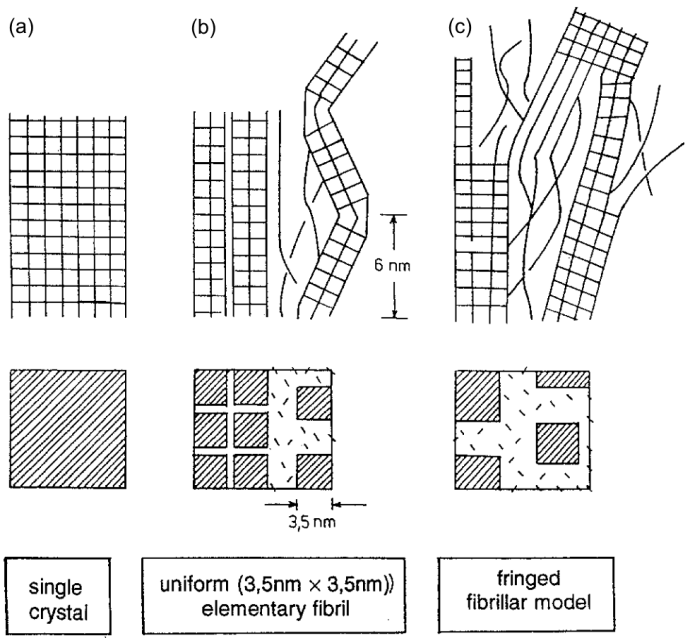

Figure 8: Models for the supermolecular structure of (a) crystalline and (b & c) semicrystalline cellulose (Fink et al., 1995; reproduced with kind permission of Springer Science and Business Media).

2.1.3 *Crystal structure and polymorphy*

The crystal structure of cellulose has been extensively studied by nuclear magnetic resonance, infrared and diffraction methods and seven polymorphs of cellulose are known (I_α, I_β, II, III_I, III_{II}, IV_I and IV_{II},), which can be interconverted (Figure 9, O'Sullivan, 1997). Cellulose I is the native and most studied form and it was found that it presents a mixture of two polymorphs, I_α and I_β, of which I_α is triclinic and metastable and can be converted to the monoclinic I_β by annealing at 260 ° in dilute alkali solution [VanderHart and Atalla, 1984; Sugiyama et al., 1991]. Cellulose I is irreversibly converted to cellulose II by (i) dissolution and regeneration or (ii) mercerisation (swelling in concentrated NaOH solution). Cellulose III_I and III_{II} are obtained by a treatment with liquid ammonia or amines of cellulose I or II, respectively.

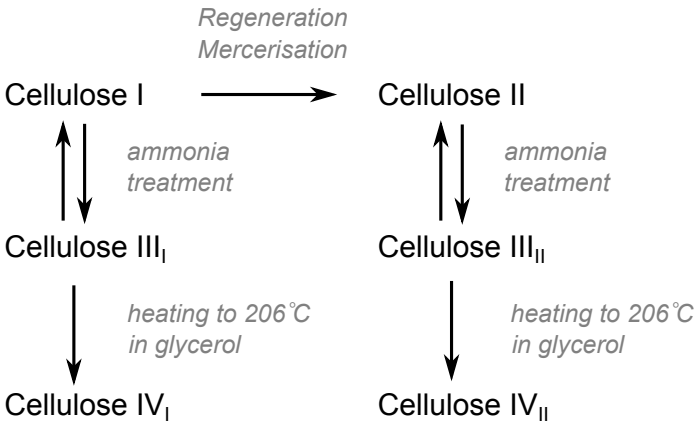

Figure 9: Interconversion of cellulose polymorphs (adapted from O'Sullivan, 1997).

Heating cellulose III_I or III_{II} in glycerol to 206 °C results in the conversion to cellulose IV_I and IV_{II}, respectively [O'Sullivan, 1997].

The conversion of cellulose I to cellulose II changes the chain packing arrangement and hydrogen bonding pattern. During mercerisation or dissolution and regeneration the parallel chains of cellulose I rearrange to the more stable antiparallel packing of cellulose II [Kolpak and Blackwell, 1976]. An interdiffusion model for this change was proposed by Okano and Sarko [1985], where neighbouring mirofibrils (each of parallel packed cellulose I) of opposite orientation take up NaOH solution and are turned into intermediate Na-cellulose. Mobilisation of chains allows their interdiffusion, such that upon washing and drying microfibrils of antiparallel packing are present [Zugenmaier, 2008].

Furthermore, the intra- and intermolecular hydrogen bond patterns change. Cellulose I has two intramolecular hydrogen bonds at O(5)-OH(3) and OH(2)-O(6) and an intermolecular O(6)-O(3), while cellulose II has an intramolecular hydrogen bond at OH(3)-O(5) and intermolecular hydrogen bonds at OH(6)-O(2) for corner chains and at OH(6)-O(3) centre chains (Figure 10, O'Sullivan, 1997). Cellulose II also has an inter-sheet interaction at OH(2)-

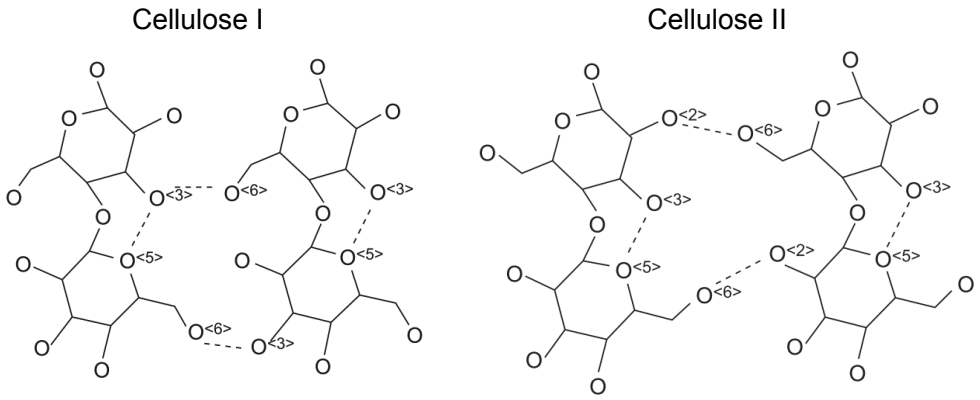

Figure 10: Hydrogen bonding pattern of cellulose I and cellulose II (adapted from O'Sullivan, 1997).

O(2) between corner and centre chains, which is not present in cellulose I [O'Sullivan, 1997].

2.1.4 *Amorphous cellulose*

The amorphous domains between crystallites are characterised by a relatively low order in their arrangement, however, the wide variability of order between fully amorphous and perfectly crystalline (Figure 7) impedes a clear definition of amorphous cellulose, as even the non-crystalline parts exhibit a certain degree of order. Relatively crystalline cellulose can be turned into true amorphous cellulose by ball-milling, grinding, saponification or regeneration with ethanol from solution in SO_2-diethylamine-dimethylsulfoxide [Nelson and O'Connor, 1964; Fink et al., 1987; Ciolacu et al., 2011]. Fink et al. [1987] characterised the structure of amorphous cellulose by X-ray diffraction (XRD) and concluded that cellulose chains have a bent and twisted backbone and an increased intermolecular distance compared to the crystalline state. The hydrogen bonding pattern of amorphous cellulose was analysed by Fourier-transformed infrared spectroscopy (FTIR), indicating that

the OH(2) and OH(3) hydroxyl groups are involved in intermolecular hydrogen bonding, while OH(6) forms an intrachain hydrogen bond. It is concluded that amorphous cellulose consists of randomly coiled chains with local domains of higher order held together by intermolecular hydrogen bonding [Kondo and Sawatari, 1996].

Interestingly, amorphous cellulose can recrystallise. Moisture induces plasticisation and allows recrystallisation of fully amorphous cellulose into a cellulose II lattice, while the presence of nuclei in partially crystalline cellulose is necessary to restructure into a cellulose I lattice [Bhama Iyer et al., 1984].

2.1.5 *Crystallinity*

The ratio of crystalline to amorphous cellulose fractions is expressed as crystallinity and can be assessed by several techniques, such as XRD, FTIR, Raman spectroscopy, solid state nuclear magnetic resonance (NMR) and moisture absorption [Wakelin et al., 1959; Segal et al., 1959; O'Connor et al., 1958; Agarwal et al., 2009]. Crystallinity indices have been defined for the different techniques, of which XRD can be considered the standard method. In a comparative assay Röder et al. [2006] show the correlation of crystallinity obtained by FTIR, Raman and NMR with XRD, highlighting that care needs to be taken when directly comparing crystallinity values obtained by different methods, as e.g. XRD returns higher values than NMR and FTIR higher values than XRD. Typical crystallinity values for cellulose of different origin ordered from high to low are $>80\,\%$ in algae, 65 to 79 % in bacterial cellulose, 56 to 65 % in cotton, approximately 45 % in ramie, flax and hemp [Klemm et al., 2005] and 25 to 40 % in regenerated cellulose fibres [Röder et al., 2006].

2.2 CELLULOSE DISSOLUTION

Many cellulose applications necessitate reshaping of cellulose to e.g. fibres, films or membranes, however, in contrast to thermoplastics cellulose decomposes at elevated temperatures. Therefore, dissolution is the main processing route of cellulose. Dissolution of cellulose is challenging, it is insoluble in water and common organic solvents and can only be dissolved by a selection of solvents [Navard et al., 2012; Olsson and Wesman, 2013]. The general train of thought is that breaking the inter- and intramolecular hydrogen bonding network is the key for dissolving cellulose [Zhang et al., 2002; Chen et al., 2007; Jin et al., 2007; Qi et al., 2011; Navard et al., 2012].

Lindman et al. [2010] have critically questioned the importance of hydrogen bonding and suggest that van der Waals forces and hydrophobic interactions are elementary to cellulose solubility, as well. The importance of the amphiphilic character of cellulose and hydrophobic interactions between cellulose sheets has been highlighted and discussed in several recent articles [Medronho et al., 2012; Medronho and Lindman, 2014b,a; Alves et al., 2015].

The specific mechanisms for dissolution of cellulose in the solvents used in this study, aqueous NaOH/urea solution and ionic liquids, are given in detail in Sections 2.2.3 and 2.2.4, respectively.

2.2.1 *Derivatising cellulose solvents*

Cellulose solvents are generally divided into two categories, derivatising and non-derivatising solvents. Derivatising solvents were historically developed first and involve a conversion step in which a soluble intermediate is formed that will be reverted to pure cellulose after processing, meaning that the dis-

solved polymer is actually not cellulose [Olsson and Wesman, 2013]. The most common example of derivatising dissolution is the viscose process initially developed by Cross et al. [1893]. In the viscose process, cellulose xanthogenate is formed by a reaction with carbon disulfide in sodium hydroxide. The metastable cellulose xanthogenate can be dissolved in aqueous sodium hydroxide, resulting in a viscous solution suitable for fibre extrusion. Precipitation in an acid bath follows, leading to simultaneous neutralisation and regeneration. The end product is consequently pure cellulose. The viscose process is widely used for the production of viscose fibres, textiles and cellophane, although alternatives have been developed to overcome the environmental concerns associated with the sulfuric reagents and heavy metals used in the viscose process [Olsson and Wesman, 2013].

One of the alternatives to the viscose process uses cellulose carbamate, produced in a reaction with urea. Cellulose carbamate can subsequently be dissolved in aqueous NaOH solution and is recovered by an acidic treatment. This procedure builds up on the viscose process and resolves the environmental concerns, but is not in industrial use at present [Navard et al., 2012]. Other derivatising pathways use nitrocellulose or cellulose acetate (Fortisan process) as intermediates to achieve dissolution. However, derivatising solvents play a minor role in the context of ACCs [Huber et al., 2012b] and the review will concentrate on the relevant direct solvents of cellulose.

2.2.2 *Non-derivatising cellulose solvents*

Direct dissolution without a derivative intermediate is advantageous for general processing and may even be necessary for analytical purposes. The dissolution procedure is simplified, as processing steps can be omitted and recycling of solvents is more straightforward, as no by-products are generated

[Olsson and Wesman, 2013]. According to Navard et al. [2012] and Olsson and Wesman [2013] the group of the most widely used non-derivatising cellulose solvents includes:

- aqueous alkali solution (LiOH, NaOH; enhanced by additives, such as urea, thiourea or poly-ethylene glycol)
- inorganic metal complexes
- acidic solutions (e.g. phosphoric acid)
- dimethyl acetamide/lithium chloride (DMAc/LiCl)
- dimethylsulfoxide/tetrabutylammonium (DMSO/TBAF)
- N-methyl-morpholine-N-oxide (NMMO)/water
- ionic liquids (IL),

of which NMMO, DMAc/LiCl, aqueus NaOH/urea and ILs are the most commonly used for processing cellulose to ACCs [Huber et al., 2012b].

The NMMO/water solvent system

Aliphatic and cyclo-aliphatic amine oxides were first described as cellulose solvents by Graenacher and Sallmann [1939] and a series of patents using NMMO/water mixtures for cellulose dissolution were issued in the 1960s [Navard et al., 2012]. Up to date NMMO (Figure 11a) is the most industrially used direct solvent, due to the fact that no pretreatment or activation of the cellulose is necessary and the high concentration of cellulose (ca. 17 wt. %) achievable. Furthermore, NMMO has a recycling potential of 99 % after processing [Olsson and Wesman, 2013].

The NMMO/water solvent system is both temperature and composition dependent, as evident from the phase diagram developed by Biganska and

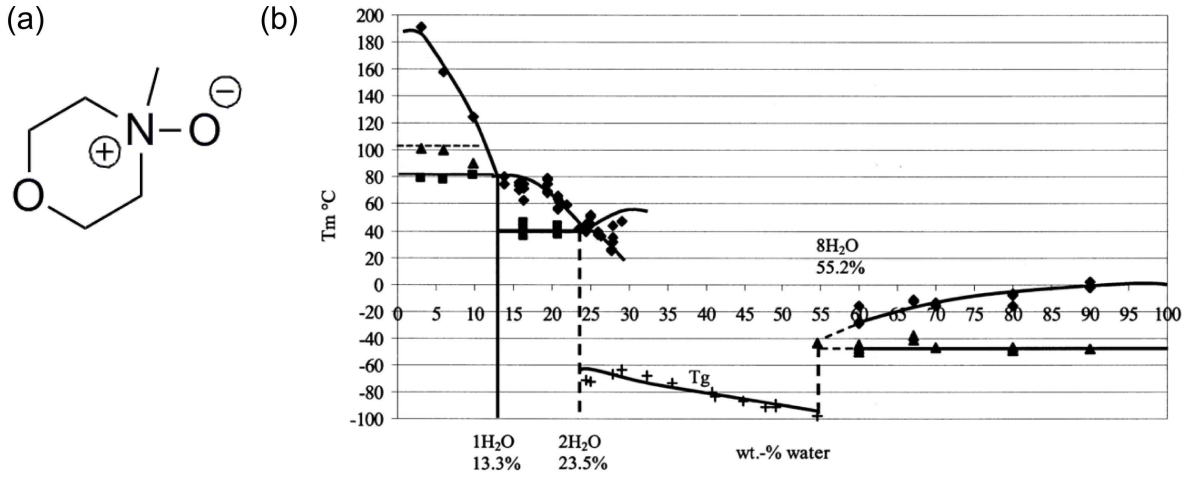

Figure 11: (a) Chemical structure of NMMO [Olsson and Wesman, 2013]. (b) Phase diagram of the NMMO/water solvent system [Biganska and Navard, 2003].

Navard [2003] (Figure 11b). At low water concentrations (< 10 %) temperatures in excess of 100 °C are necessary to keep the solvent liquid, which leads to cellulose and solvent degradation. Furthermore, NMMO is thermally unstable and stabilisers are added to avoid dangerous exothermic side reactions [Navard et al., 2012; Rosenau et al., 2002].

Consequently, cellulose dissolution in NMMO usually starts at high water concentrations with the further advantage of low viscosity, which eases mixing. Water content is subsequently removed at temperatures in the range of 100 to 120 °C under reduced pressure. A solution of 14 % cellulose, 10 % water and 76 % NMMO is then used for producing regenerated cellulose fibres known as Lyocell [Olsson and Wesman, 2013].

NMMO has rarely been used for processing ACCs [Huber et al., 2012b]. Ouajai and Shanks [2009] used NMMO to prepare hemp-based ACCs *via* the 2-step method. The isotropic ACCs exhibited relatively low tensile strength and Young's modulus of 28.9 MPa and 1.82 GPa, respectively.

The DMAc/LiCl solvent system

DMAc/LiCl is a relatively inert and thermally stable solvent system and was patented by Charles McCormick in 1979. It can dissolve up to 15 % of relatively high molecular weight cellulose with negligible chain degradation. Furthermore, the solvent does not form chemical bonds with cellulose, making it the preferred choice for analytical work, such as molecular weight determination *via* size exclusion chromatography [Liebert, 2009; Olsson and Wesman, 2013]. However, the incomplete recycling of this relatively expensive solvent system still prevents its use in large scale industrial application [Liebert, 2009].

Cellulose has to be activated in a polar medium before it can be effectively dissolved in DMAc/LiCl. The polar medium is necessary to open the pores of cellulose to allow the penetration and dissolution by LiCl. However, any medium other than DMAc used for swelling, such as acetone, methanol or isopropanol, needs to be completely removed in order to not hinder dissolution [Turbak et al., 1981]. Dissolution can then follow either of two procedures: (i) the DMAc/LiCl solvent mixture is prepared first and cellulose directly added, or (ii) cellulose is dispersed in DMAc followed by addition of LiCl [Seurin and Sixou, 1987]. The presence of moisture causes a significant decrease in cellulose solubility in DMAc/LiCl. Contamination has to be minimised during preparation of solution, however, this is challenging as both components are hygroscopic [Olsson and Wesman, 2013]. Care has to be taken to maintain the solution at a temperature below 150 °C, to prevent chain degradation during dissolution [Turbak et al., 1981].

DMAc/LiCl has been used extensively for processing ACCs *via* both the 1- and 2-step method Huber et al. [2012b]. Isotropic and unidirectional ACCs with high and exceptionally high mechanical properties have been reported. In the initial publication of Nishino et al. [2004] that introduced the concept

of ACCs, ramie fibres were impregnated by a solution of kraft pulp dissolved in DMAc/LiCl to obtain unidirectional ACCs with a tensile strength of 480 MPa. Also the strongest ACCs reported thus far with a tensile strength of 910 MPa were prepared by partial dissolution of Bocell fibres in DMAc/LiCl solution [Soykeabkaew et al., 2009a].

2.2.3 *Cellulose dissolution in aqueous sodium hydroxide solution*

The discovery of cellulose solubility in mixtures of NaOH and water dates back to the 1930s, when Davidson reported the dissolution of modified cotton in an aqueous solution of 10 wt.% NaOH in a series of articles [Davidson, 1934, 1936, 1937]. It was shown that a higher solubility is achieved when the temperature is decreased from +15 °C to -5 °C (Figure 12). Furthermore, molecular weight was identified as an important property in cellulose dissolution and a high solubility of 80 % was reported for hydrocellulose [Davidson, 1934, 1936, 1937].

The complex relationship of cellulose and aqueous NaOH was explored by Sobue et al. [1939], who developed a ternary phase diagram (Figure 13, although a recent study by Duchemin [2015] suggests that the ice region at temperatures < 0 °C and NaOH concentrations < 10 wt. % needs to be revisited). At relatively high concentrations of NaOH (>i̇0 wt. %) and temperatures (10 to 100 °C) cellulose is not dissolved, but swells and changes morphology and crystal structure to a variety of Na-celluloses and cellulose II. This process is referred to as mercerisation and is used in the textile industry, e.g. to improve lustre, smoothness, dye-ability and mechanical properties of cotton fabrics. Cellulose dissolution only occurs in the "Q-region", a narrow window of concentration and temperature, 7 to 10 wt.% NaOH and +2 to -10 °C, respectively [Navard et al., 2012].

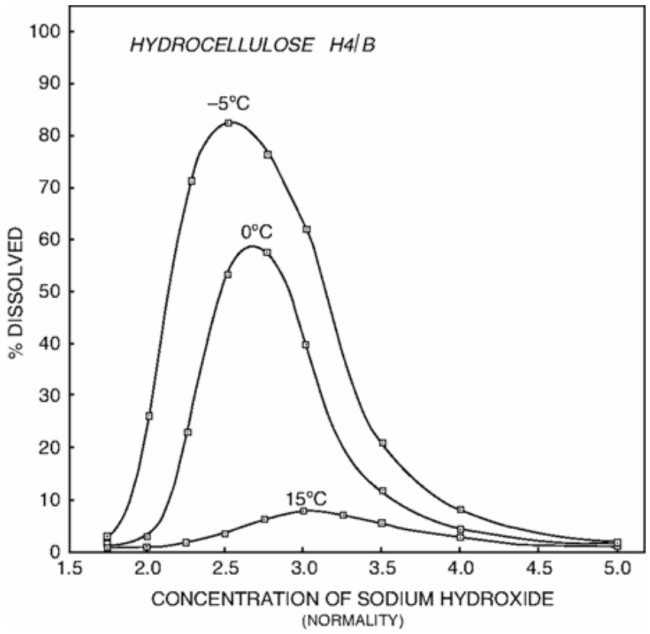

Figure 12: Solubility of modified cotton in aqueous NaOH solution as a function of NaOH content and temperature (Davidson, 1934, in Navard et al., 2012).

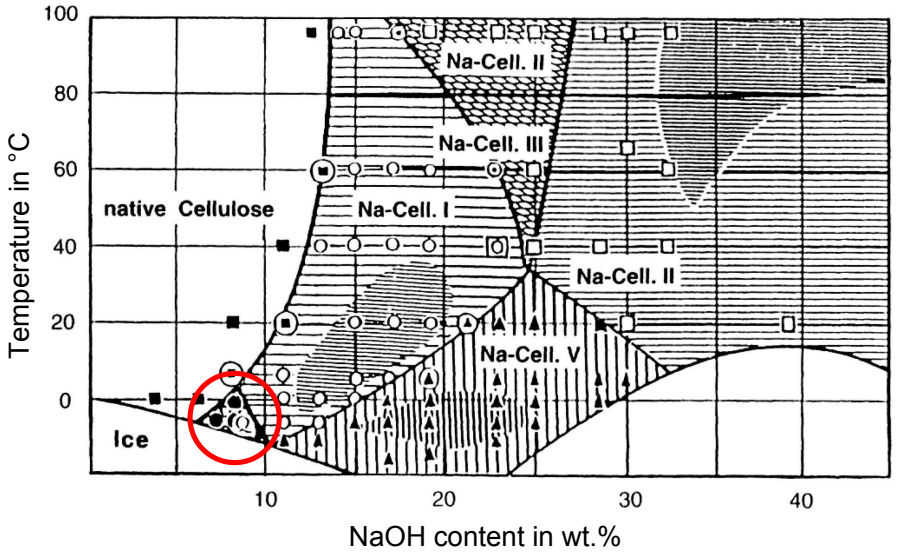

Figure 13: Ternary phase diagram of cellulose-NaOH-water mixtures developed by Sobue et al. [1939]. Red circle marks the "Q-region" of cellulose solubility (adapted from Navard et al., 2012).

Egal et al. [2007] showed that the number of NaOH molecules linked to one AGU of cellulose varies with the mass ratio of cellulose to NaOH (M_{cell}/M_{NaOH}). At low cellulose concentrations, $M_{cell}/M_{NaOH} < 0.25$, 20 or more NaOH molecules are bound to one AGU. The number of NaOH molecules per AGU decreases with increasing M_{cell}/M_{NaOH} and reaches a lower limit of 4 NaOH molecules per AGU. As the molar mass of an AGU is $m_{AGU} = 162\,g\,mol^{-1}$ and that of NaOH is $m_{NaOH} = 40\,g\,mol^{-1}$, it follows that the limit of cellulose dissolution is reached at equal masses of cellulose and NaOH in a given solution. The highest concentration of NaOH that allows direct dissolution is 10 wt.%, consequently the theoretical maximum of cellulose dissolution is 10 wt.% [Egal et al., 2007].

In practice, lower values in the range of 4 to 6 wt.% cellulose in solution have been found experimentally and undissolved residues remain of samples with a relatively high DP of 750 and more [Isogai and Atalla, 1998; Cai and Zhang, 2005; Jin et al., 2007]. The addition of compounds such as urea, thiourea or PEG enhance solubility of cellulose in aqueous NaOH solution and their stability, although the underlying mechanisms are still a matter of debate [Olsson and Wesman, 2013]. Solvent mixtures of 7 wt.% NaOH/12 wt.% urea and 8 wt.% NaOH/ 6.5 wt.% thiourea/ 8 wt.% urea were found to have the highest dissolution yields (Table 1) and allow preparation of a stable extrusion dope for the production of regenerated fibres [Qin et al., 2012; Qi et al., 2008a; Jin et al., 2007].

Cai and Zhang [2005] proposed the following dissolution mechanism of cellulose in precooled aqueous NaOH/urea. When cellulose is added to the solvent, hydrolised Na^+ and OH^- ions and urea hydrates, as well as free water surround the cellulose molecules (Figure 14a). Na^+ and OH^- ions and urea hydrates start to penetrate the cellulose and destroy inter- and intramolecular hydrogen bonds, leading to swelling and solvation of cellulose

Table 1: Solubility of cellulose in NaOH-based aqueous solutions of different composition (References [1] Isogai and Atalla, 1998; [2] Qin et al., 2012; and [3] Jin et al., 2007).

Cellulose type	DP	solvent composition (wt.%) NaOH / urea / thiourea	absolute (and relative) cellulose solubility	Reference
MCC (Avicell)	190	5 / 0 / 0	2 wt.% (100 %)	[1]
Cotton linter	850	5 / 0 / 0	0.64 wt.% (32 %)	[1]
Regenerated cotton linter	750	5 / 0 / 0	1.8 wt.% (94 %)	[1]
Cotton linter pulp	580	7 / 12 / 0	6.5 wt.% (-)	[2]
Cotton linter pulp	520	8 / 8 / 6.5	7.6 wt.% (100 %)	[3]
Cotton linter pulp	620	8 / 8 / 6.5	6.5 wt.% (100 %)	[3]
Cotton linter pulp	1400	8 / 8 / 6.5	2.1 wt.% (83 %)	[3]

chains (Figure 14b). The ions and hydrates continue to penetrate the cellulose and ultimately a coat of hydrates and free water forms around dissolved cellulose chains in a transparent solution (Figure 14c, Cai and Zhang 2005). Xiong et al. [2013] showed that the OH^- anions are responsible for breaking the hydrogen bonding network of cellulose, while the cations form a complex with cellulose molecules that stabilise the solution.

In recent studies the importance of the amphiphilic character of cellulose for its dissolution was emphasised [Medronho et al., 2012; Medronho and Lindman, 2014b,a; Alves et al., 2015]. In the glucopyranose ring of cellulose all hydroxyl groups are located on equatorial positions, giving the molecule a hydrophilic character in equatorial direction. In contrast to this the axial direction of the ring is hydrophobic, due to the hydrogen atoms of the axial C-H bonds. A hydrophobic pairing energy then favours the stacking of the hydrophobic, flat sides of the cellulose ribbons in crystalline structures [Bergenstrahle et al., 2010; Medronho and Lindman, 2014b]. These hydrophobic interactions need to be overcome during dissolution and it has been shown that additives, such as urea, contribute to cellulose dissolution *via* such hydrophobic interactions. Additionally, urea hydrates serve as hydrogen bond-

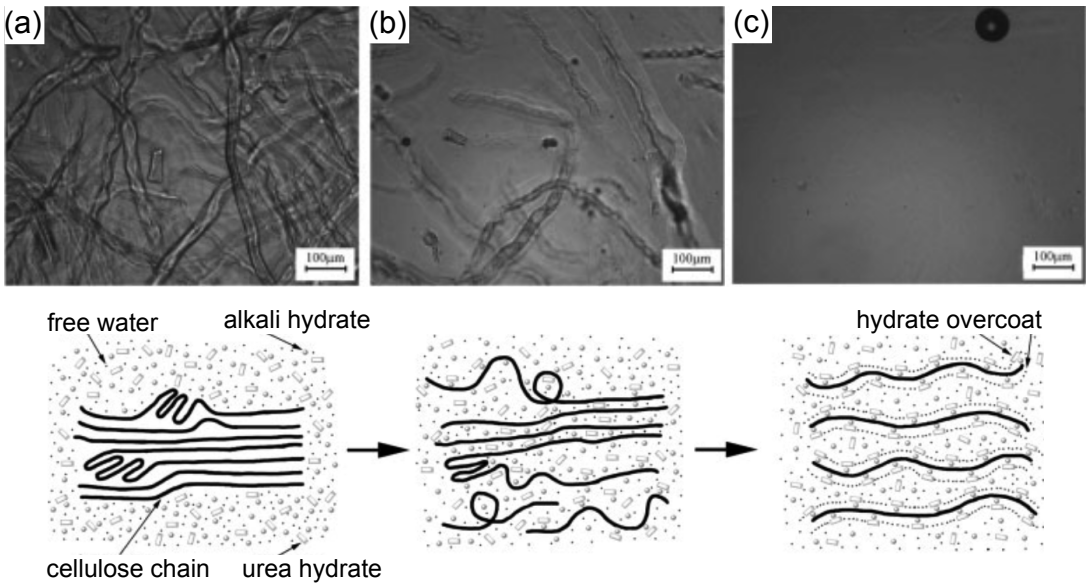

Figure 14: Optical microscopy and schematic of the dissolution process of cellulose in aqueous NaOH/urea solution precooled to -10 °C from (a) the initial undissolved to (b) the swollen and (c) fully dissolved state (Cai and Zhang, 2005; with kind permission of John Wiley and Sons).

ing donor and receptor between solvent molecules, hence enhancing dispersion and preventing re-association of cellulose chains [Cai and Zhang, 2005].

The recycling of NaOH-based solvents may be facilitated by evaporation and hyperfiltration. The review of Ren [2000] reveals that NaOH in waste water streams from textile production can be recovered economically at concentrations greater than 2 %. Furthermore, strategies such as counter-current washing can enhance washing efficiency and allow the recovery of NaOH from waste water for direct reuse.

In the context of ACCs, NaOH/urea solvents have been limited to processing *via* the two-step method to create isotropic ACCs by adding cellulose nanocrystals or short ramie fibres to a predissolved cellulose solution [Qi et al., 2009; Wang and Chen, 2011; Pullawan et al., 2014; Yang et al., 2010].

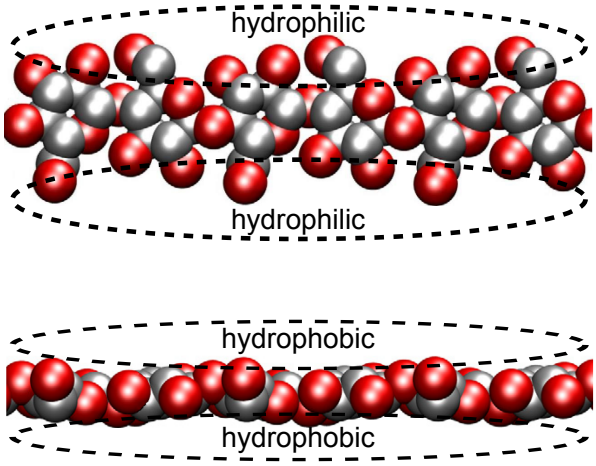

Figure 15: Van der Waals force representation of the cellulose chain shown perpendicular (top) and parallel (bottom) to the equatorial direction of the glucopyranose rings with hydrophobic and hydrophilic parts indicated by ellipses. Oxygen atoms are shown in red, non-polar carbon atoms in black, hydrogen atoms have been omitted for clarity (adapted from Bergenstrahle et al., 2010, and Medronho and Lindman, 2014b; with kind permission of Elsevier).

2.2.4 *Cellulose dissolution in ionic liquids*

Ionic liquids are salts with a low melting point composed of an organic cation and an organic or inorganic anion. Graenacher [1934] already found and patented the use of liquefied quarternary ammonium salts for preparing cellulose solutions, however, this received little attention at its time. It was the publication of Swatloski et al. [2002], who reported the dissolution of up to 25 wt.% cellulose in ILs with 1-butyl-methylimidazolium (Bmim) cations and several different anions, that triggered renewed interest in this class of solvent. Since then the use of room temperature ILs for processing cellulose has resulted in diverse research outputs, as evident from manifold reviews [Zhu et al., 2006; Seoud et al., 2007; Feng and Chen, 2008; Pinkert et al., 2009; Gibril et al., 2012b].

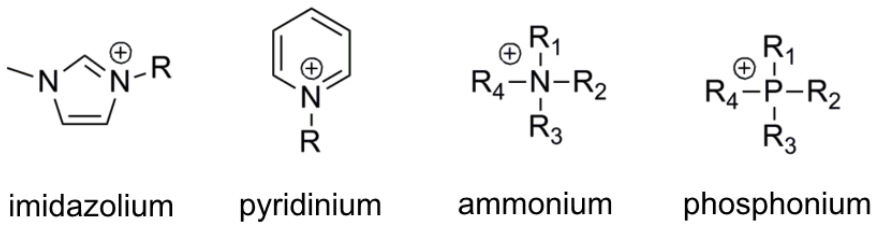

Figure 16: Commonly used cations of ILs used for cellulose dissolution (Olsson and Wesman, 2013).

There are thousands of possible combinations for pairing cations and anions, allowing the adjustment of chemical and physical properties of ILs in many ways. Several classes of cations combined with a multitude of anions have proved to facilitate the dissolution of cellulose, of which the most commonly used cations include imidazolium, pyridinium, ammonium and phosphonium (Figure 16). The imidazolium cation in combination with different alkyl substituents has developed into the most popular choice for cellulose dissolution [Olsson and Wesman, 2013].

The capability of ILs to dissolve cellulose is attributed to their ionic character, high polarity and the ability to form hydrogen bonds [Feng and Chen, 2008; Pinkert et al., 2009; Olsson and Wesman, 2013]. It is suggested that both anion and cation contribute to the dissolution process. Electron donor-acceptor (EDA) complexes are formed by the oxygen and hydrogen atoms of cellulose. The cation of an IL acts as the electron acceptor centre and the anion as electron donor centre. If the two centres of the IL are close enough to the EDA complexes of cellulose, the IL will interact with the cellulose and open the hydrogen bonded structure of cellulose chains, resulting in dissolution (Figure 17; Feng and Chen, 2008; Pinkert et al., 2009; Olsson and Wesman, 2013).

The solubility of cellulose in IL increases with (i) decreasing DP of the cellulose, (ii) decreasing side chain length of the IL and (iii) increasing dissolu-

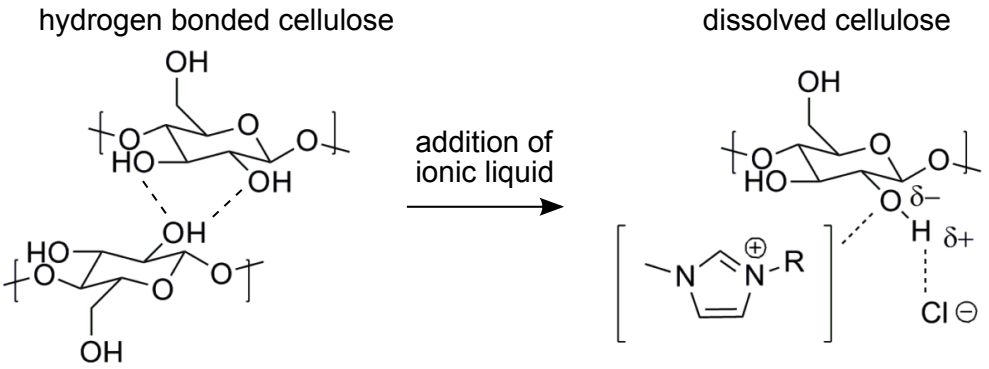

Figure 17: Interaction of an imidazolium-chloride ionic liquid with cellulose (based on Feng and Chen, 2008, and Olsson and Wesman, 2013).

tion temperature [Swatloski et al., 2002; Feng and Chen, 2008]. Dissolution is generally performed in the temperature range of 80 to 130 °C and extended dissolution times also lead to an increase in solubility, although this may be accompanied by cellulose chain degradation [Pinkert et al., 2009; Kosan et al., 2007; Seoud et al., 2007]. Heinze et al. [2005] found that a pyridium-based IL exhibits a higher cellulose solubility of 39 wt. % when compared to an imidazolium-based IL, which showed a solubility of only 18 wt. % under the same dissolution conditions. However, the pyridium-based IL also lead to a stronger decrease in DP. The temperature during dissolution needs to be controlled accurately, as some ILs, such as ethyl-methylimidazolium-chloride (EmimCl) and BmimCl, start degrading at ca. 120 °C [Olsson and Wesman, 2013].

ILs are generally hygroscopic and hence absorb water from the ambient atmosphere [Pinkert et al., 2009]. Moisture absorption is relevant to cellulose processing in ILs, as the experiments of Swatloski et al. [2002] have shown that cellulose solubility is impaired at water contents > 1 wt. %. It is therefore necessary to dry both the IL and the cellulose prior to dissolution.

The use of ILs as cellulose solvent in ACC processing has been a comparatively popular choice. ILs are attractive due to the direct dissolution, high

cellulose solubility and relative ease of controlling dissolution by changes in temperature. Many studies report on isotropic and unidirectional ACCs, prepared *via* both the 1- and 2-step process [Zhao et al., 2009; Duchemin et al., 2009a; Haverhals et al., 2010, 2012; Yousefi et al., 2011; Ma et al., 2011; Shibata et al., 2013a,b]. ILs have also been the solvent of choice for upscaled manufacturing of ACCs, thus far [Huber et al., 2012d,a].

2.2.5 *Regeneration of dissolved cellulose*

The regeneration of a cellulose solution occurs upon its contact with a coagulant. The process of regeneration relies on the counter-diffusion between the solvent in the solution and the non-solvent in the coagulant. When the solvent leaves the solution and the non-solvent penetrates into the cellulose solution, the cellulose starts to lose its solubility. This diffusion process results in the formation of a semi-solid cellulose precipitate, by re-establishing the intra- and intermolecular hydrogen bonds [Zhang et al., 2005b].

Miyamoto et al. [2009] have resolved the structural reformation of cellulose in detail by molecular dynamics simulations. The regeneration in water is described as a three-staged process (Figure 19): Firstly, cellulose molecules start aggregating in a sheet like structure due to hydrophobic stacking of the glucopyranose rings. Secondly, these hydrophobically stacked sheets associate *via* intermolecular hydrogen bonding, as precipitation proceeds. Some regions pack tightly, leading to the formation of thin crystals. Upon the incorporation of defects more amorphous regions are formed. Thirdly, the randomly dispersed structural units come in contact and adhere together by a diffusion-limited cluster-cluster aggregation mechanism. Regenerated cellulose with a mixture of crystalline and amorphous regions is formed. Simultaneously, the solvent is squeezed out from the precipitating cellulose gel,

which results in shrinkage and the uniplanar orientation of the $(1\bar{1}0)$ crystal plane. Following this process, the regeneration of cellulose in an aqueous coagulant results in the formation of a relatively crystalline arrangement [Miyamoto et al., 2009]. Isobe et al. [2012] have also shown the initiation of cellulose regeneration by hydrophobic stacking and subsequent formation of intermolecular hydrogen bonding in synchrotron experiments.

The regeneration mechanism depends on the coagulation medium and cellulose structure formation changes when liquids other than water are used. Miyamoto et al. [2009] simulated the regeneration of cellulose in benzene, where wavy cellulose sheets are formed by hydrogen bonding, followed by hydrophobic stacking of the wavy sheets, leading to the formation of predominantly amorphous cellulose domains. Upon contact of these domains, large clusters of amorphous cellulose are formed.

The molecular dynamics simulations of Miyamoto et al. [2009] predict a lower crystallinity for coagulation media with low dielectric constants (DC), such as benzene and toluene (DC 2.27 and 2.38, respectively), and acetone and ethanol (DC 21 and 25, respectively), when compared with water and a high DC of 80. This trend has been confirmed by regeneration experiments, where a crystallinity of only 6 % was found in cellulose films regenerated by immersion in toluene [Yamane et al., 2006].

Not only crystallinity, but also porosity, density and mechanical properties of the regenerated material depend on the regeneration conditions. Bang et al. [1999] show that a reduced solvent diffusion of NMMO, i.e. a slower regeneration rate, results in a reduced pore size and higher density of regenerated cellulose films, as well as a higher crystallinity. The diffusion rate of solvents is known to decrease with decreasing temperature and with increasing solvent content in the washing bath, i.e. a lower concentration gradient [Bang et al., 1999; Jiang et al., 2011].

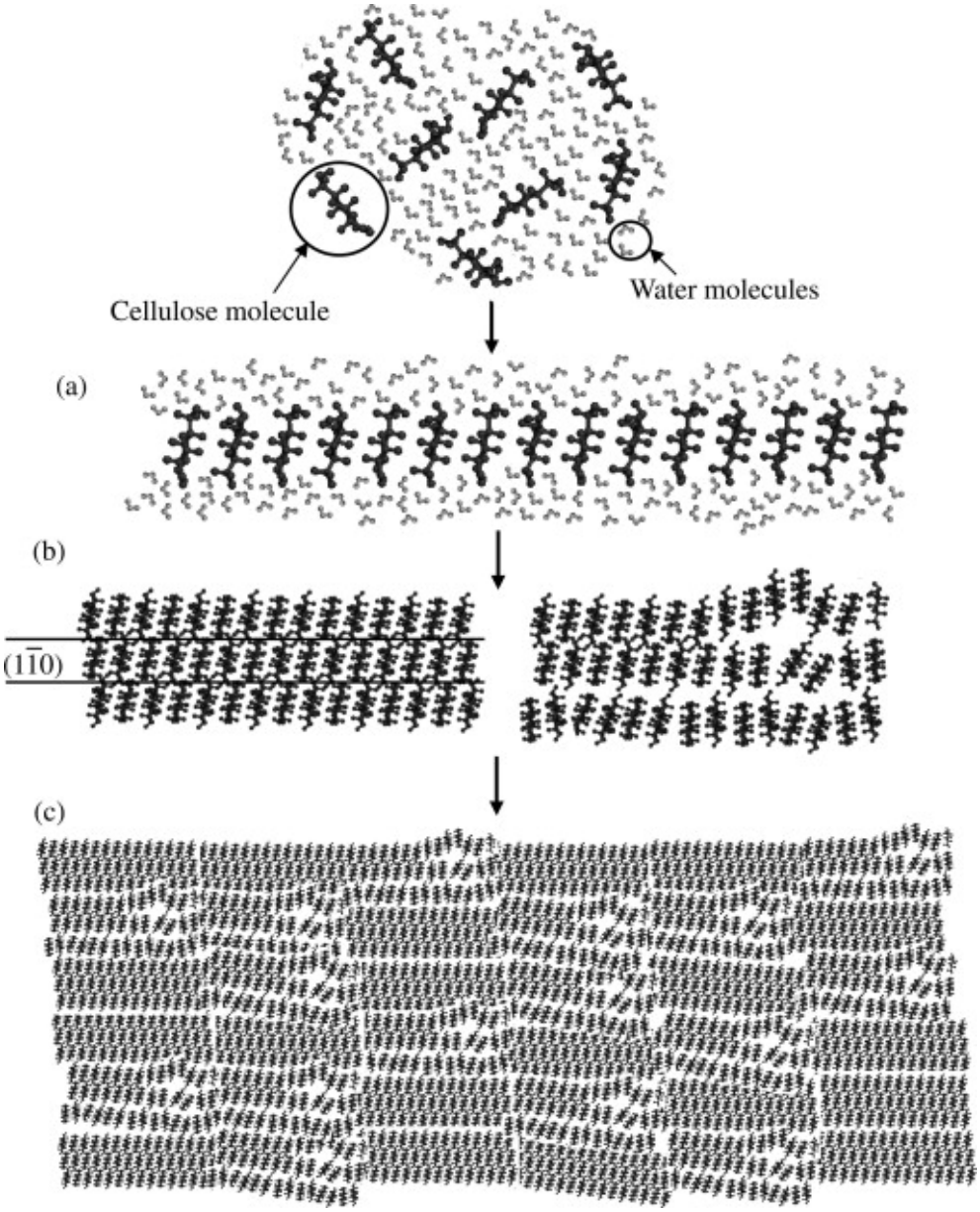

Figure 18: Schematic model for the structural formation of cellulose by regeneration in water: (a) formation of molecular sheets by hydrophobic stacking and van der Waals forces; (b) piling up of the molecular sheets by hydrogen bonds to form seeds of crystalline (left, (1$\bar{1}$0) crystal lattice plane indicated) and amorphous domains (right); (c) contact and sticking together of the structural units to form regenerated cellulose (reproduced from Miyamoto et al., 2009, with kind permission of Elsevier).

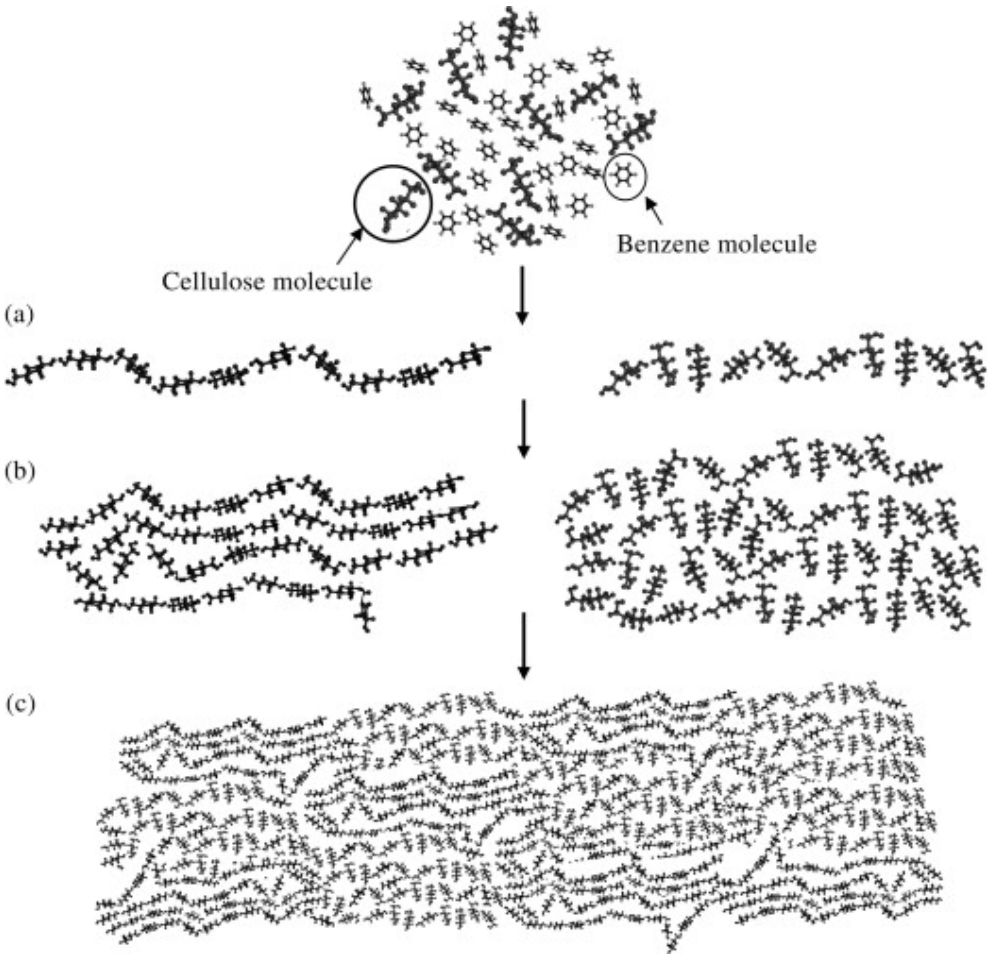

Figure 19: Schematic model for the structural formation of cellulose by regeneration in benzene: (a) formation of a wavy cellulose sheet with hinge-like joints by hydrogen bonding; (b) formation of predominantly amorphous regions by hydrophobic interactions; (c) contact and sticking together of the structural units to form mostly amorphous regenerated cellulose (reproduced from Miyamoto et al., 2009, with kind permission of Elsevier).

A comparison of cellulose films regenerated from cotton linter pulp dissolved in 7.5 wt. % NaOH/ 11 wt. % urea is presented by Mao et al. [2006]. Thin films were regenerated by immersion in a coagulant for 5 min followed by washing under running water and then distilled water, before air-drying at ambient temperature. The results indicate that regeneration in 5 wt. % sulfuric acid results in formation of films with a smaller pore size of 30.6 nm when compared to 34.4 nm in distilled water. Interestingly, regeneration in acetone led to the films with the smallest pores of 25.7 nm, whereas regeneration in ethanol produced the largest pores of 56.8 nm. The overall porosity was not affected significantly by coagulation in acid, water or ethanol (85 to 87 %), only regeneration in acetone led to a drop in porosity to 81 %. The strongest films were prepared in a 5 wt. % sulfuric acid/ 5 wt. % sodium sulfate bath and exhibited 98.1 MPa tensile strength at an elongation at break of 10.8 %. Regeneration in water, ethanol and acetone resulted in weaker films with a strength of 70.6 MPa, 56.9 MPa and 79.2 MPa, respectively. Lower elongations at break of 4.0 %, 3.6 % and 5.1 % were observed [Mao et al., 2006].

In addition to the finding of Mao et al. [2006] that coagulation in acid results in stronger films in comparison to water, the strength of the acid is of importance, too. Zhang et al. [2001] found that films prepared from cotton linter dissolved in 6 wt. % NaOH/ 4 wt. % urea exhibit a 10 to 20 MPa higher tensile strength for regeneration in sulfuric acid compared to regeneration in acetic acid.

Furthermore, not only the coagulation medium, but also the coagulation method affects cellulose formation. Remarkable differences between immersion and vapour precipitation have been reported. While immersion results in semicrystalline films, Song et al. [2013] have shown that crystalline cellulose spherulites can grow from concentrated cellulose solution in IL by very

slow vapour precipitation. Spherulite growth occurred in thin films of cellulose solution precipitated at RH levels < 30 % at cellulose concentrations > 12 wt. %. An increase in spherulite size from 10 to 70 µm was observed for increasing crystallisation temperatures from 20 to 60 °C and increasing cellulose concentrations from 12 to 19 wt. % [Song et al., 2013].

Similar crystallisation effects have been observed for ACCs. Duchemin et al. [2009b] have found that ACCs prepared from partially dissolved MCC exhibit a higher crystallinity of 48 % for slow regeneration by vapour precipitation compared to 36 % for fast regeneration by immersion in water. Slow regeneration also resulted in significantly improved tensile properties with a strength and Young's modulus of 102 MPa and 7.6 GPa, respectively, compared to 29 MPa and 1.8 GPa for fast regeneration [Duchemin et al., 2009b].

2.3 CELLULOSE FIBRES

2.3.1 *Natural fibres*

On a first level, natural fibres are categorised in two main groups, organic and inorganic fibres (Figure 20). Inorganic fibres are of mineral origin and include e.g. asbestos. Organic fibres are further categorised into plant- and animal-based fibres. Animal fibres are made of proteins and include hair, wool and silk [Müssig, 2010]. While inorganic and animal fibres are of technical relevance as well, this review will concentrate on plant-based fibres and their use as reinforcement in composites.

Plant-based fibres are further subdivided into six categories depending on their origin within the plant. These six categories and common examples are bast fibres (flax, hemp, ramie), leaf fibres (sisal, abaca), seed fibres (cotton,

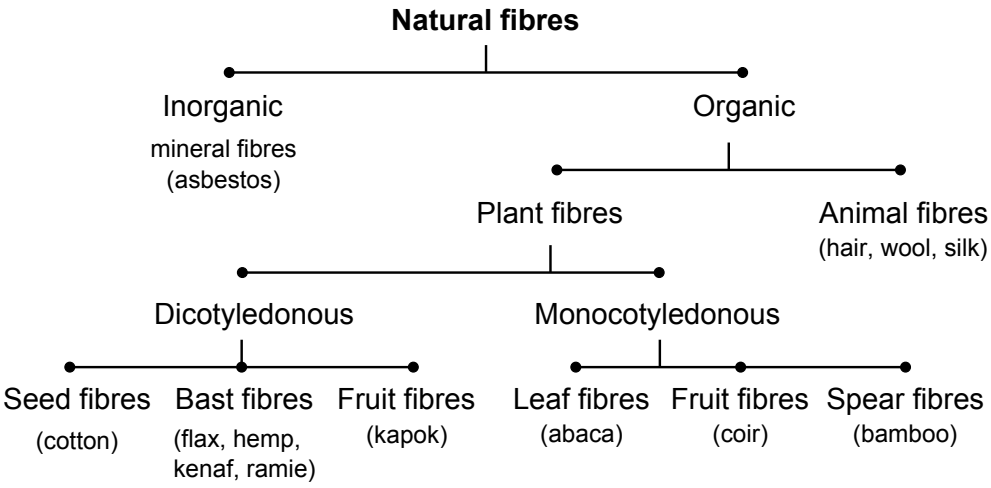

Figure 20: Overview of natural fibres (adapted from Müssig, 2010).

coir), core fibres (kenaf), grass and reed fibres (wheat, corn) and all other types (wood, roots) [Bledzki and Gassan, 1999]. The use of bast and leaf fibres dominates in long fibre-reinforced bio-based composites, wood fibres are extensively used in wood-plastic composites (WPC), and other cellulosic fibres are suitable as reinforcement in bio-based composites, as well [Mohanty et al., 2002; John and Thomas, 2008; Faruk et al., 2012].

Before bast fibres can be extracted from the plants, the stems need to undergo a process named retting. During retting the stems are degummed, i.e. the gummy substance that connects fibres and other parts of the stem are removed by enzymatic and bacterial activity. This degumming process commonly takes 10 to 20 days, depending on water conditions, such as temperature, pH and macro-nutrients, although it should be noted that water retting is nowadays considered a polluting technique and is not applied in Europe any more. Retting is then followed by decortication to yield the fibres. Manual decortication using knives still prevails, although mechanical decorticators are becoming more common. The quality of the final fibres can differ widely in properties such as colour, fineness, strength, density, root proportion and tenderness [Franck, 2005].

The use of natural fibres for replacing glass fibres as reinforcement in composites offers several advantages: lower density, biodegradability, low cost, lower energy consumption during production, carbon storage during use, as well as less abrasion to machinery during production [Wambua et al., 2003; Joshi et al., 2004]. However, a drawback of natural fibre is the large inherent scatter in properties due to differences in growing and harvesting conditions, necessitating rigorous quality management to ensure consistent composite properties [Müssig, 2010; Keller et al., 2001].

Fibre structure and properties

The main component of plant fibres is cellulose, usually present in the native cellulose I polymorph. Furthermore, the fibres contain varying amounts of hemicelluloses, lignins, pectins and waxes. The chemical composition may vary with species and within different parts of the same plant. The chemical components are distributed over the cell wall, which consists of several layers, of which the secondary cell wall layer is the thickest and structurally most important (Figure 21). Each cell wall layer is composed of many laminae. Within each lamina the cellulose fibrils are parallel, but the orientation of the laminae varies within the cell wall layers. The orientation of the microfibrils in regard to the fibre axis is known as the microfibrillar angle [Klemm et al., 2005; Bledzki and Gassan, 1999].

The mechanical properties of plant fibres depend on the cellulose content, cellulose crystallinity and on the average microfibrillar angle. For example, the lower orientation of microfibrils in cotton at an angle of $\sim 18\,^{\circ}$ leads to a relatively low Young's modulus and higher elongation at break when compared to bast fibres like hemp and flax with a typical microfibrillar angle of $\sim 4\,^{\circ}$, resulting in stiff and strong fibres [Klemm et al., 2005; Bledzki and Gassan, 1999].

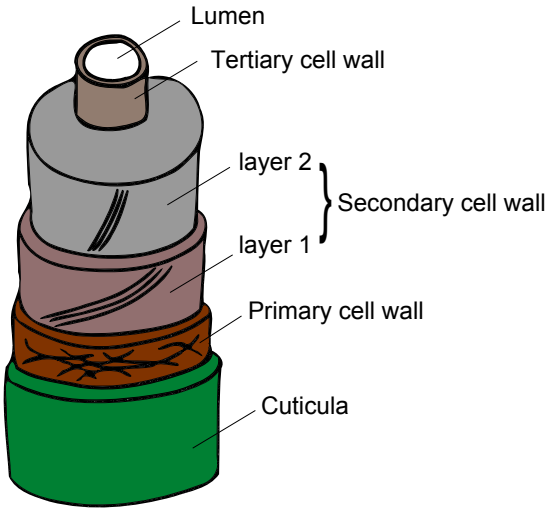

Figure 21: Schematic of the cell wall structure of plant fibres, different microfibrillar angles are outlined in the secondary cell wall layers (Adapted from Klemm et al. 2005 and Bledzki and Gassan 1999).

It should be noted that the term "fibre" needs to be used and interpreted with care in the case of natural fibres. The fibre length of plant fibres corresponds to the length of individual cells. Fibres on the individual cellular level are referred to as single fibres, while often the general term fibre is used to refer to fibre bundles. In most cases, these fibre bundles are the textile fibres that are used as reinforcement in bio-based composites. The length of single fibres varies significantly with plant species. The shortest single fibres are found in sisal and jute (1 to 8 mm) and the longest in ramie (40 to 250 mm). Fibre bundles are typically in the range of 300 to 900 mm in flax and 1000 to 3000 mm in hemp [Franck, 2005].

2.3.2 *Man-made cellulose fibres*

In contrast to natural fibres, man-made cellulose fibres are produced as continuous, endless fibres and consist only of cellulose. Several manufacturing processes *via* both derivatising and non-derivatising pathways have been

Table 2: Overview of properties of selected natural fibres compared to E-glass fibres [Franck, 2005]. Crystallinity values taken from [a] Klemm et al., 2005; [b] Mwaikambo and Ansell, 1999; [c] Arévalo et al., 2010; [d] Gindl-Altmutter et al., 2012.

Fibre	Tensile strength in MPa	Young's modulus in GPa	Density in g cm^{-3}	Cellulose content in %	Hemicellulose content in %	Lignin content in %	Pectin content in %	Cellulose crystallinity in %
Flax	800-1500	60-80	1.40	68-85	10-17	3-5	5-10	44[a]-78[d]
Hemp	550-900	70	1.48	68-85	10-17	3-5	5-10	44[a]-88[b]
Jute	400-800	10-30	1.46	70-75	12-15	10-15	1	78[b]
Cotton	280-840	12	1.51	92-95	5.8	0	1.2	56[a]-80.6[c]
E-glass	2400	73	2.55	-	-	-	-	-

developed and reached industrial maturity. Generally speaking, cellulose is dissolved and the solution extruded into fibres, which are subsequently re-generated and dried to obtain man-made cellulose fibre (Figure 22).

The annual global fibre production accounts to approximately 90 million tons, of which the largest share are petrochemical-derived synthetic fibres with 63 %, followed by cotton with 30 %. Man-made cellulose fibres have a market share of 6.7 %, followed by wool with 1.3 %. The production of man-made fibres showed higher growth rates than natural fibres over the last years and manufacturers expect their growth to continue, due to the so called "cellulose-gap". A demand overhang of cellulose fibres is expected due to global population and prosperity growth and a limited cotton supply caused by competition over land and water resources [Hämmerle, 2011]. However, world fibre production exceeded global demand in 2014 with cotton production being 2 million tons higher than use [www.lenzing.com, www.thefiberyear.com, 4.8.2015].

At first, man-made cellulose fibres were referred to as "artificial silk". At present the term "viscose rayon" is commonly used, of which viscose is derived from the *viscous* cellulose solution the fibres are created from and

Figure 22: Processing steps in the production of regenerated cellulose fibres (www.lenzing.com, 19.02.2015)

rayon was introduced by a committee formed by the U.S. Department of Commerce and several commercial associations as a compound word for sun*ray*, due to the brightness and cott*on* due to the similar appearance and comfort of the fibres [Shaikh et al., 2012]. The fact that man-made cellulose fibres are produced by dissolving the natural polymer or one of its derivatives which is then regenerated after extrusion, leads to them also being called regenerated cellulose fibres [Woodings, 2001]. Viscose rayon offers similarly high comfort when wearing on skin as cotton, high moisture absorbance, and good dye- and drapability, which has led to its widespread use as an apparel fabric. It is also used as a technical fibre. High-tenacity rayon is used as reinforcement of mechanical rubber goods, such as tyres, conveyor belts and hoses [Shaikh et al., 2012]. The rayon fibre used throughout this work (Cordenka) is extensively used in the carcass of car tyres. The carcass determines the load bearing capacity of a tyre and due to its well-balanced proportion of strength and elasticity Cordenka rayon results in a comfortable ride, and is hence also referred to as tyre-cord [Wunderlich and Zimmerer, 2011; Adusumali et al., 2006].

Fibre processing

A short history of the development of regenerated fibres is given by Woodings [2001], who names George Audemars as the first person to produce a man-made cellulose fibre. In 1855, Audemars dissolved nitrated cellulose in ether and alcohol and discovered that fibres could be formed by drawing the solution in the air. Although the fibres could be woven into a textile, they had the serious drawback of being explosive. In 1889, Count Hilaire de Chardonnet presented a new variety of nitrocellulose fibres. His process was used commercially until 1949 and earned him a reputation as "Father of Rayon", although the denitration step that made the fibres safe led to a deterioration of their strength and appearance [Woodings, 2001].

The discovery of Cross et al. [1893] that cellulose could be dissolved after derivatisation to cellulose xanthate triggered a new development and led to the success of the viscose process. Woodings [2001] presents a detailed description of the viscose process, which is summarised as follows: In the derivatisation step, cellulose xanthate is obtained by a NaOH and carbon disulfide treatment of cotton or wood cellulose. Dissolution is subsequently achieved by mixing the xanthate in an aqueous NaOH solution, where the ratio of xanthate to NaOH determines the fibre quality. For example, textile yarns are obtained from a 7.5:6.5 ratio, while strong and high wet modulus rayon requires a 6.0:6.0 ratio. A lower xanthate content allows the use of higher DP cellulose to be dissolved, which is beneficial for the strength of regenerated fibres. After dissolution the viscose dope still contains too many air bubbles and particles, and has a too high degree of xanthation for fibre formation. Dexanthation, filtration and degassing occur during ageing of the dope prior to the fibre formation process. The viscose dope is then pumped through a spinneret to form fibres, which are pulled through a coagulation bath. The coagulation bath contains 5 to 15 % sulfuric acid, 0.05 to 7 % zinc

sulfate and 10 to 28 % sodium sulfate. The fibre of viscose dope coagulates at the interface with the acid bath, first forming a cuticle that develops into a skin, through which the rest of the regeneration is controlled. The fibre consequently has a skin-core non-uniformity, a characteristic of rayon. The regeneration rate can be controlled by temperature and coagulation bath composition. E.g. the addition of zinc sulfate slows down the regeneration by forming a cellulose xanthate intermediate and allows higher draw ratios of the fibres. The sulfuric acid in the coagulation bath converts the regenerated fibres back to pure white cellulose. Fibre formation and regeneration are followed by washing and drying steps to finalise fibre processing [Woodings, 2001].

Modifications to the viscose process have been developed in order to (i) improve fibre properties and (ii) reduce environmental impact caused by the release of CS_2 and heavy metal compounds. The technical use of rayon as reinforcement of e.g. car tyres necessitates stronger fibres. Tyre cord with an increased strength (+50 to 100 %) are obtained by increasing the zinc content in the regeneration bath, which allows higher draw ratios and leads to a thicker skin than in regular viscose. Furthermore, modifiers such as monoamine and quarternary ammonium lead to a prolonged life of the zinc cellulose xanthate gel that again allows higher draw ratios. A mix of modifications to tyre cord lead to the development of Modal fibres, exhibiting a high wet modulus [Woodings, 2001]. Several approaches have led to a reduction of hazardous by-products of regenerated fibre production. The CarbaCell process is based on the viscose route, however, CS_2 is substituted by urea to obtain the cellulose derivative carbamate, which can be dissolved and extruded on existing viscose fibre production systems [Klemm et al., 2005].

An alternative to the derivatising cellulose dissolution in the viscose process is the direct dissolution of cellulose. The earliest fibres produced by dir-

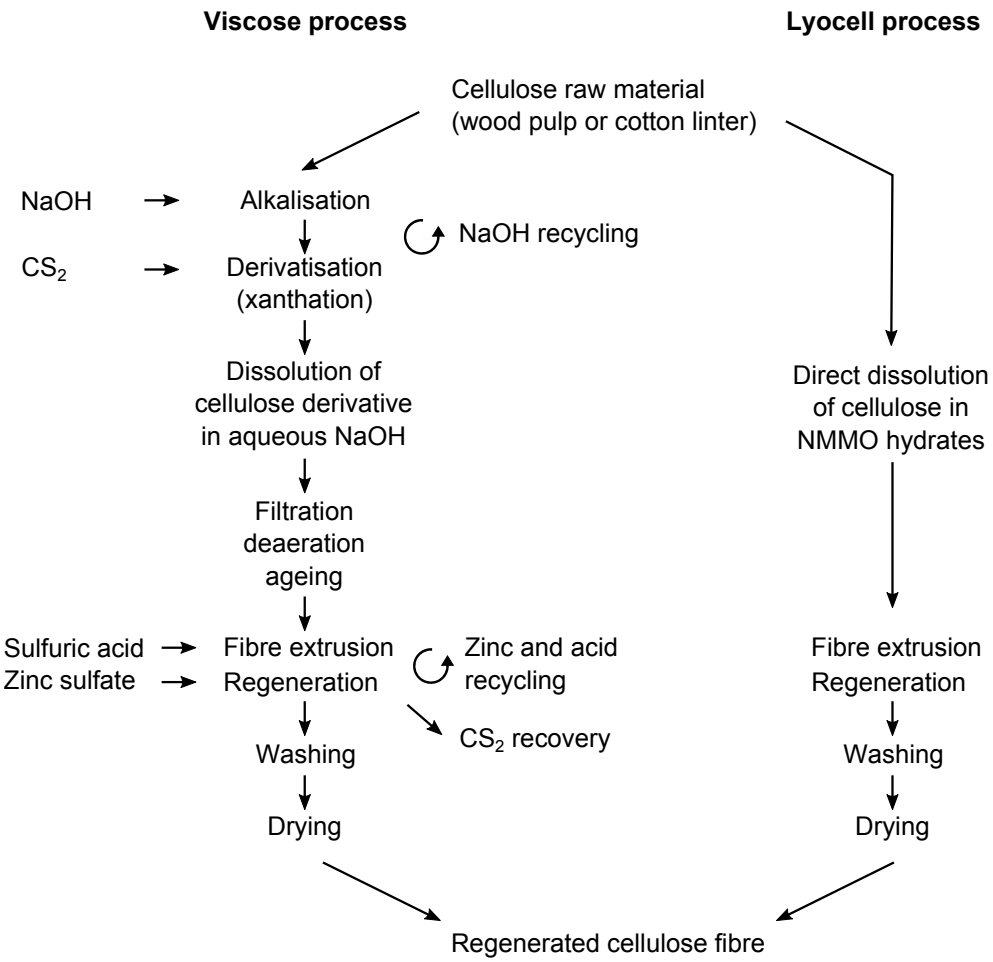

Figure 23: Processing steps of regenerated cellulose fibres *via* the viscose and Lyocell process (adapted from Woodings, 2001, and Klemm et al., 2005).

ect dissolution were obtained from cuprammonium solutions (Cupro silk), however, the copper ammonia technology also poses environmental hazards [Klemm et al., 2005].

Boerstoel et al. [2001] found that anhydrous phosphoric acid is a powerful direct solvent of cellulose (solutions of up to 38 wt.% cellulose) and fibres can be produced from liquid crystalline solutions. The so called "Fibre B", or Bocell, exhibits an extraordinarily high tensile strength of 1700 MPa and a Young's modulus of 44 GPa [Northolt et al., 2001]. However, the only direct dissolution process that developed to commercial maturity is the Lyocell

process [Klemm et al., 2005]. The NMMO solvent system is used to prepare fibres by extruding a highly viscous solution through an air gap, and high draw ratios result in a highly oriented fibre with mechanical properties comparable to tyre yarns. Due to their high orientation Lyocell fibres have the tendency to fibrillate, necessitating surface treatments for textile applications [Perepelkin, 2007].

Fibre structure and properties

The quality of regenerated cellulose fibres depends directly on the purity of the raw material. Strong fibres require the use of high purity pulps with an alpha cellulose content of > 96 %. All other substances, such as hemicellulose and lignin, have to be removed. Additionally, the DP has to be within a suitable range [Woodings, 2001].

Furthermore, the structure of regenerated cellulose fibres depends on the processing conditions, which in turn determines the mechanical properties. Overall, the mechanical properties of regenerated fibres depend upon (i) DP and distribution of chain length, (ii) preferred orientation of crystallites and molecules and the distribution of this orientation, (iii) the degree of crystallinity, and (iv) the average distribution of the above over the cross-section of the fibre [Hermans, 1941; Ingersoll, 1946; Ward, 1950].

As expected, regenerated cellulose fibres with a higher DP exhibit higher tensile strength [Kreze and Malej, 2003]. The draw ratio during fibre processing determines the fineness and degree of orientation of crystallites in yarns. Increasing the draw ratio leads to an increasing orientation of crystalline domains, which is correlated to an increase in Young's modulus and tensile strength and a decrease in elongation at break [Perepelkin, 2007; Loubinoux and Chaunis, 1987; Soykeabkaew et al., 2009a; Sun et al., 2015]. Similarly, a higher degree of crystallinity also correlates to a higher strength

and Young's modulus of the fibres [Ward, 1950; Hindeleh, 1980; Kreze and Malej, 2003].

Due to the fibre formation and regeneration process viscose rayon exhibits a skin-core structure. The formation of a skin originates from a friction induced orientation of cellulose chains at the outside of the extrusion jet. The orientated micelles at the skin are then precipitated first when the yarn comes in contact with the regeneration bath, while the coagulation medium diffuses more slowly into the core which then regenerates in a state of less preferred orientation. The thickness of the skin can be varied by controlling the composition of the viscose dope and the coagulation bath [Morehead and Sisson, 1945].

Müller et al. [2000] have shown by X-ray microbeam and electron diffraction that the skin exhibits a higher degree of crystallite orientation, although no significant difference in crystallinity and mean crystallite size is found when comparing the skin to the core. Interestingly, Gindl et al. [2006a] have shown by nanoindentation that the difference in crystalline orientation does not result in a variation of mechanical properties. No significant variation of the indentation modulus and hardness over the diameter of Lyocell and viscose rayon fibres was found.

In man-made fibres cellulose is present in the cellulose II polymorph, due to the dissolution and regeneration during processing. However, depending on the processing conditions a mixture of cellulose II and cellulose IV may exist [Hindeleh, 1980]. It may be of interest to note, that according to Chaudhuri et al. [1983] the typical cellulose II structure is obtained by X-ray diffraction, but electron diffraction reveals residues of cellulose I crystals. It is possible for cellulose I nuclei to resist the conversion to cellulose II during alkali treatment and Chaudhuri et al. argue that these nuclei are too small to satisfy the diffraction requirement of X-rays, but are detectable by elec-

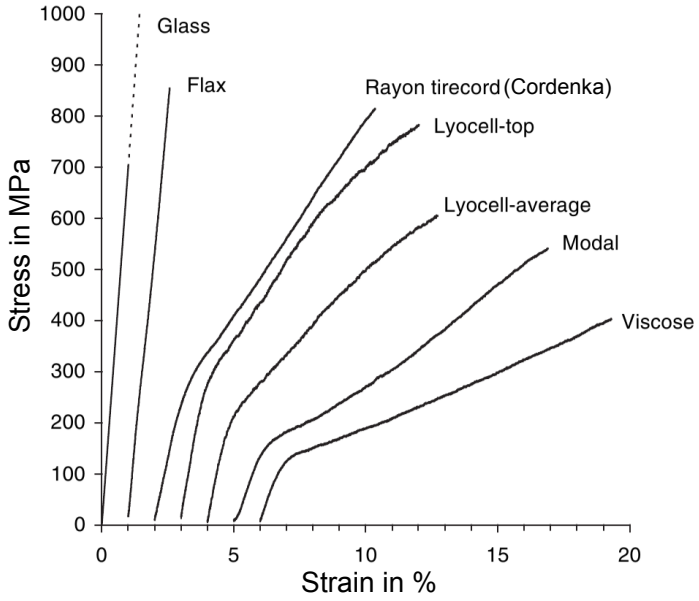

Figure 24: Representative stress-strain curves of glass, flax and various regenerated cellulose fibres. The stress-strain curve of glass fibre extends to 3000 MPa and is not fully shown. Curves are horizontally shifted by 1 % [Adusumali et al., 2006].

tron diffraction. The crystallinity of regenerated cellulose fibres is generally found to be lower (30 to 40 %) when compared to natural fibres (70 to 90 %) [Ward, 1950].

2.3.2.1 *Differences between natural and man-made cellulose fibres and the preferred choice as cellulose precursor for ACCs*

An important aspect to consider when working with natural fibres is the inherent variability of properties originating from natural variation and differences in growing and harvesting conditions [Müssig, 2010; Franck, 2005]. In comparison, the structural and mechanical properties of man-made fibres can be controlled by processing parameters and tailored to specific needs within a narrow distribution (Figures 24 and 25). Such reliable properties are desirable from a composite engineering perspective as composite properties are easier to predict and control [Adusumali et al., 2006].

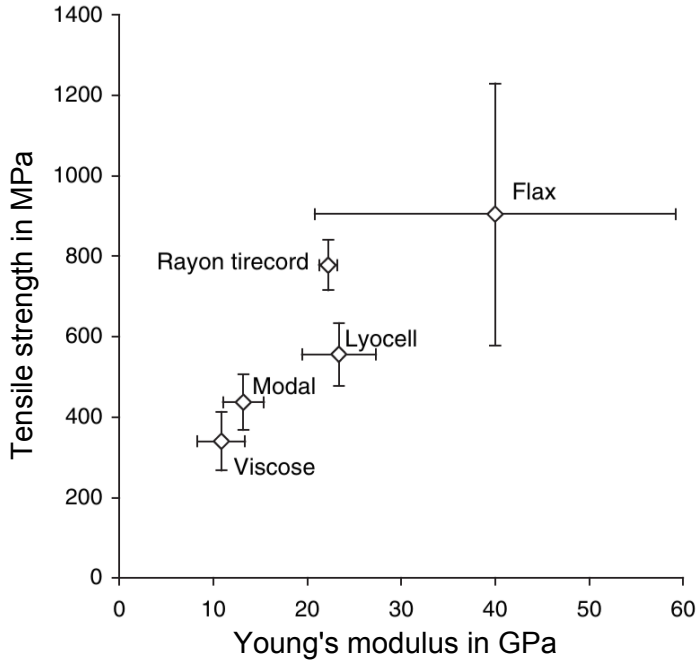

Figure 25: Comparison of average tensile strength and Young's modulus of natural and man-made cellulose fibres [Adusumali et al., 2006].

In the context of ACCs a further difference is of critical relevance. The complex structure of the multi-layered cell wall of natural fibres leads to special phenomena when interacting with cellulose solvents. In good solvents, such as NMMO with a low water content (< 16 wt.%), natural fibres break into fragments and dissolve. In bad solvents, such as NMMO with higher water content (> 20 wt.%), and in aqueous NaOH-based solvents, a ballooning phenomenon is observed, as described for cotton and wood fibres Cuissinat and Navard [2006]; Le Moigne et al. [2008, 2010]. Some parts of the fibres swell into balloons and the inner secondary S2 layer of the cell wall is dissolved first. Only then the secondary S1 layer, which forms the membrane of the balloons, slowly dissolves. Helices and collars around the balloons formed by the primary cell wall are not dissolved easily and break under the expansion of the secondary wall during swelling of the balloons. It is hence revealed that the dissolution of natural fibres occurs inhomogeneously over

the length of the fibre and exhibit a radial gradient of dissolution that proceeds from the inside to the outside [Cuissinat and Navard, 2006; Le Moigne et al., 2008, 2010].

On the contrary, the dissolution of man-made fibres proceeds radially from the skin to the core, as shown by Chaudemanche and Navard [2011] for Lyocell fibres dissolved in NMMO. A homogeneous radial dissolution was found independent of the quality of the solvent (high and low water content in NMMO). In addition, regenerated fibres do not show the rotation observed in cotton and wood fibres during dissolution [Le Moigne et al., 2010]. Furthermore, cellulose II dissolves more readily than native cellulose I [Isogai and Atalla, 1998].

As a consequence of the complex dissolution pattern of natural fibres, complications may arise when applying the partial dissolution approach of 1-step ACC processing. A thin matrix layer on the surface of the reinforcement is desired to achieve bonding between fibres. However, the inner S2 layer dissolves first and partial dissolution of natural fibres may therefore result in the transformation of the fibre core to matrix, instead of the surface. In addition, the S2 layer represents the major portion of the plant cell wall and commonly exhibits the lowest microfibrillar angle, which makes it the most important portion regarding mechanical reinforcement [Klemm et al., 2005]. Partial dissolution may therefore break down the strong core of a natural fibre and result in incomplete wetting of the fibre surface, leading to relatively poor mechanical performance of an ACC based on natural fibres.

The relatively poor performance of flax-based ACCs when compared with Lyocell-based ACCs prepared by partial dissolution in an IL, with tensile strengths of 34 and 78 MPa, respectively, may be explained by the mechanism outlined above, as Gindl-Altmutter et al. [2012] attribute the low mechanical properties of their flax-based ACC to the structural deterioration of

the flax fibres. Huber et al. [2012d] also observed a lower tensile strength and Young's modulus of 46 MPa and 0.86 GPa, respectively, for ACC laminates based on a flax textile, when compared to ACC laminates based on a rayon textile with tensile strength and Young's modulus of 70 MPa and 2.5 GPa, respectively. The lower mechanical properties of flax-based ACCs were attributed to a lower solubility of the more crystalline cellulose in flax fibres and non-cellulosic constituents that may interfere with dissolution [Huber et al., 2012d].

The successful creation of unidirectional ACCs by partial dissolution of ramie fibres in LiCl/DMAc by Soykeabkaew et al. [2008] indicates that the mechanical performance of ACCs may depend on the species of natural fibre and type of solvent system. Ramie based ACCs with a high tensile strength of 460 MPa were prepared. However, the strength of the individual ramie fibre used was 768 MPa and the high fibre fraction of more than 80 % and low void content of less than 1 vol.% suggests that the fibres have been weakened by partial dissolution [Soykeabkaew et al., 2008].

Regenerated cellulose fibres can also be favourable in terms of environmental impact. Life cycle assessment conducted by Shen et al. [2010] shows that regenerated cellulose fibres have a lower overall impact than cotton and synthetic fibres made from polyethylene terephthalate (PET) and polypropylene (PP). Cotton has the least favourable score because of its high land and water use, the eutrophication associated with fertilisers, as well as comparably high human- and eco-toxicity. Viscose, and other regenerated cellulose fibres, are the environmentally preferred choice, because of their low toxicity, as well as low fossil energy requirements during production and a lower global warming potential [Shen et al., 2010]. Environmental impact will however depend on the type of natural fibre and the production facility of the regenerated cellulose fibre, as e.g. viscose produced in Asia has

a global warming potential of ca. 6000 kg CO_2 eqivalent per tonne of fibre compared to < 2000 kg CO_2 equivalent for the same fibre produced in Austria [Shen et al., 2010].

In summary, the purity, low variation in mechanical properties, homogeneous radial dissolution, and cellulose II polymorph make regenerated fibres the preferable starting material for ACCs over natural fibres and are used as precursor in all experiments of this thesis.

3

EXPERIMENTAL PROCEDURES

3.1 MATERIALS

3.1.1 *Cellulose precursor*

An unsized batch of regenerated cellulose fibre (rayon, Cordenka® 700, Cordenka GmbH, Obernburg, Germany, Table 3) in the form of a 2D textile (2/2 twill weave) was used as precursor for fabricating single- and multi-layered ACC laminates. The areal mass of the textile was 450 g mm^{-2}, while the yarn density was 13 yarns cm^{-1} in warp and 10 yarns cm^{-1} in weft direction. The continuous fibres had an average diameter of 12 µm and a DP of 440, as measured by viscometry [Schuermann, 2014]. The crystallinity of rayon is generally reported in the range of 18 to 45 % [a.M. Hindeleh and Johnson, 1974; Hindeleh, 1980] with recent comparative measurements being in a narrower range of 26 to 30 % as measured by XRD and 32 to 46 % by FTIR [Röder et al., 2006]. As no amorphous cellulose material was available for this study, the crystallinity of as-received rayon was standardised to an average value of 32 % presented in the literature. The information on the precursor material used throughout this work is summarised in Table 3.

Table 3: Summary of information about the cellulose precursor according to the manufacturer [Cordenka, 2009; Wunderlich and Zimmerer, 2011] and single fibre testing reported in the literature [Volkmann et al., 2012; Ganster and Fink, 2006].

fibre	
type	Cordenka 700
diameter	ca. 12 µm
single fibre modulus	15.4 ± 3.4 to 20.6 ± 3.4 GPa
single fibre strength	762 ± 87 to 899 ± 64 MPa
elongation at break	12.0 ± 1.0 to 19.4 ± 2.7 %
yarn	
linear density	1840 dtex
number of filaments	1000
twist	Z 100 t m^{-1}
textile	
weave	2/2 twill
yarn density warp	13 cm^{-1}
yarn density weft	10 cm^{-1}
areal mass	450 g mm^{-2}

3.1.2 *Solvents*

The ILs 1-butyl-3-methylimidazolium acetate (BmimAc) and 1-ethyl-3-methylimidazolium acetate (EmimAc) with a purity of $\geqslant 95$ %, (BASF, Ludwigshafen, Germany) and aqueous NaOH/urea solution were used as cellulose solvents. The ILs were dried under vacuum at 95 °C for at least 5 days before use. The aqueous NaOH/urea solution was prepared by mixing 7 wt.% NaOH, 12 wt.% urea (chemicals of analytical grade, purchased from Sigma Aldrich) and 81 wt.% distilled water in a glass beaker and stirring with a magnetic stirrer at room temperature until clear and is referred to as NaOH/urea.

3.2 PREPARATION OF ALL-CELLULOSE COMPOSITE LAMINATES

ACC laminates were prepared using SIP as described by Huber et al. [2012a] and summarised schematically in Figure 26. Rectangular strips of the rayon textile were cut and dried at 95 °C and vacuum for 24 h before processing (The equilibrium moisture content of the rayon is 10.3 ± 0.4 wt.% and maximum mass loss of the textile under the drying conditions given above was reached within 18 h.). The dry textile strips were stacked to form a laminate stack with symmetric layup, where the laminae were aligned such that the weft direction was parallel to the infusion direction. A flat steel plate was used as mould onto which the laminate stack was placed and sealed with a vacuum bag. The sealed laminate stack was then connected to a vacuum infusion setup with an inlet for the solvent and an outlet in line with a pressure gauge and vacuum pump (Laboport N 820.3, KNF Neuberger GmbH, Freiburg, Germany). An absolute pressure of 200 mbar was applied for infusion, unless otherwise specified. The connecting hoses were fitted with a valve at inlet and outlet to control the flow of solvent.

When using IL as solvent, the infusion was performed with cellulose and solvent at room temperature (20 ± 2 °C). Partial dissolution was achieved by placing the setup in a laboratory hot press (Gibitre Instruments, Bergamo, Italy) at 95 °C under an applied pressure of 1 MPa for a dissolution time of 60 min, unless specified otherwise. The procedure for using NaOH/urea as solvent is described in the corresponding chapter (Section 5.2).

Following the dissolution step, the laminate stack was carefully removed from the vacuum setup and its mass measured with a laboratory balance

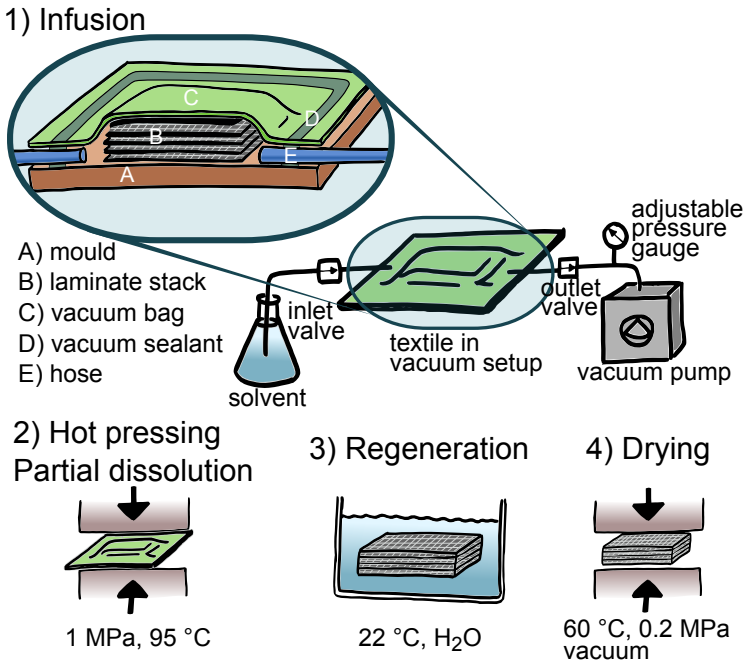

Figure 26: Setup and processing steps of the solvent infusion process (SIP) as developed by Huber et al. [2012a].

(ED2249, accuracy 0.1 mg, Sartorius AG, Göttingen, Germany). The solvent uptake U in mass % of the conditioned textile was calculated as

$$U = \frac{m_i - m_c}{m_c} \times 100 \tag{1}$$

where m_i and m_c are the masses after infusion and conditioning, respectively.

Subsequently the laminate was regenerated and washed in distilled water at room temperature (20 ± 2 °C). The water was exchanged at least two times within 24 h until no further increase in conductivity of the water bath was measured using a portable multiparameter meter (HQ40d, HACH LANGE GmbH, Düsseldorf, Germany). In addition, removal of solvent was confirmed by Fourier-transformed infrared spectroscopy. Spectra of ACC laminates showed no traces of typical solvent peaks.

The regenerated material was cut for scanning electron microscopy (SEM) and tensile testing using a sharp blade, while still wet. The specimens were then dried between porous polytetrafluoroethylene (PTFE) sheets (2 mm thick, pore size 20 µm, DIA-Nielsen GmbH & Co. KG, Düren, Germany) at 60 °C under vacuum and an external pressure of 0.2 MPa until their mass was constant.

3.3 PREPARATION OF CELLULOSE FILMS

As a comparison to the cellulose matrix created in the ACC laminates by partial dissolution, unreinforced cellulose films were cast from cellulose solutions. Rayon fibres were cut into short fragments of ~2 mm length and dried at 95 °C in a vacuum oven for 24 h. Solutions containing 5 wt. % rayon were obtained by dissolution in IL and NaOH/urea at 95 °C and -12 °C, respectively. The solutions where stirred using an overhead stirrer (Eurostar power-b, IKA-Werke, Staufen, Germany) for dissolution times of 60 min and 5 min for IL and NaOH/urea, respectively, unless specified otherwise. Subsequently the solutions were subjected to centrifugation at 3000 rpm for 10 min for degassing and to separate dissolved from undissolved cellulose portions.

The clear, dissolved portion was cast into a rectangular mould consisting of a 3 mm thick polypropylene plate with a rectangular opening of 55 mm length and 35 mm width sandwiched between two sheets of porous PTFE. The mould was submerged in distilled water (or other regeneration medium, as indicated) so as to infiltrate the porous PTFE. The film was left to regenerate over night, carefully removed from the mould and subsequently washed in distilled water until no further increase in conductivity indicated complete

solvent removal. The cellulose films were then dried in the same conditions as the ACC laminates, between porous PTFE sheats at 60 °C under vacuum and an external pressure of 0.2 MPa.

3.4 MATERIALS CHARACTERISATION

3.4.1 *Mechanical testing*

The tensile properties of ACCs and unreinforced cellulose films were determined by tensile testing according to ASTM D 3039 using a universal testing machine (Criterion 43, MTS Systems Corporation, Eden Prairie, USA) equipped with a 10 kN, 2.5 kN or 500 N loadcell, as appropriate, and a constant crosshead speed of 2 mm min^{-1} was applied. Specimen dimensions are given in the respective experimental sections of each results chapter. Strain was measured using a videoextensometer (Genie 1400, Teledyne DALSA, Waterloo, Canada). Specimens were conditioned at 23 °C and 50 % RH for a minimum of 24 h prior to testing. The Young's modulus was measured as tangent modulus between strains of 0.1 and 0.3 %. Yield strength was determined at an offset of 0.2 % strain. The work to fracture was determined by numerically integrating the stress-strain curve. A minimum of 5 replicates were tested.

3.4.2 *Microscopy*

Cross sections and fracture surfaces of ACCs and cellulose films were examined by scanning electron microscopy (SEM). A thin slice was cut off the wet ACC cross section with a virgin razorblade to create a smooth surface for

microscopy, followed by drying under the same conditions as the laminates. All samples were sputter coated with gold for 180 s at 25 mA. Images were obtained with a 7000F FE-SEM (JEOL, Peabody, USA) at 5 kV accelerating voltage.

3.4.3 *Density*

The density of ACC laminates was determined according to ASTM-D792 using an analytical balance equipped with the corresponding density determination kit (XP 105, accuracy $d = 0.01$ mg, Mettler Toledo, Greifensee, Switzerland). Specimens were oven-dried to a constant mass at 95 °C in a vacuum oven. Their dry mass was measured in air (m_{air}) and in immersed in distilled water (m_{water}), while making sure that no air bubbles adhered to the specimen. The influence of water uptake by the immersed samples was kept to a minimum by relying on the first stable measurement after approximately three seconds of immersion. The density ρ was subsequently calculated as

$$\rho = \frac{m_{air}}{m_{air} - m_{water}}(\rho_{water} - \rho_{air}) + \rho_{water} \tag{2}$$

where ρ_{water} is the density of distilled water at the temperature measured during the experiment (0.99875 kg m^{-3} at 17.3 °C) and ρ_{air} is the density of air (0.0012 kg m^{-3}).

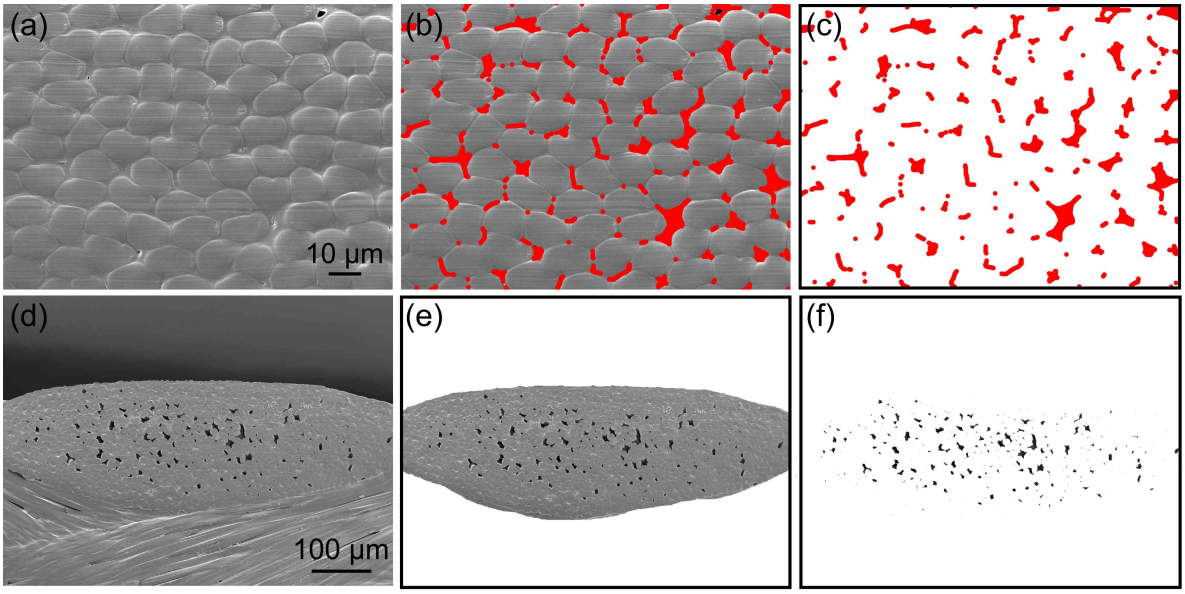

Figure 27: Procedure for determination of matrix (a-c) and void fraction (d-f) in ACC laminates by image analysis.

3.4.4 *Determination of matrix and void fraction*

The volume fraction of matrix (V_m) and voids (V_v) of the ACCs was determined by image analysis. The low contrast between fibre and matrix in the micrographs obtained by SEM required manually delineating the matrix phase by image manipulation (GIMP 2.8.2, www.gimp.org). The resulting high contrast images were analysed using the threshold tool in ImageJ 1.49g (Wayne Rasband, National Institute of Health, USA). V_m was calculated by dividing the number of matrix pixels by the number of pixels of the full image, V_v by dividing the void pixels by the yarn pixels (Figure 27). In order to account for variations in the volume fractions within a given composite, two images at 1000 × magnification from three separate yarns were analysed.

Additionally, V_v was calculated from the density of ACC laminates (ρ_{ACC}) according to ASTM-D2734, based on the assumption that a theoretical void

free ACC exhibits a density equal to that of rayon fibres (ρ_{rayon} = 1.52 g cm^{-3}; Woodings, 2001). Hence, V_v was calculated as

$$V_v = (\rho_{rayon} - \rho_{ACC})/\rho_{rayon} \times 100 \quad (3)$$

3.4.5 *Wide angle X-ray diffraction*

Equipment and measurements

A X'Pert diffractometer (PANalytical, Almelo, Netherlands) equipped with a sample spinner was used for wide angle X-ray diffraction (WAXD) analysis of ACC samples in transmission and powder mode. In transmission, the samples were clamped in between two polyimide foils that are transparent to X-radiation. A cobalt anode (λ = 1.79031 Å) was excited at a 40 kV voltage and a 40 A current. Data acquisition was performed in steps of 0.1 ° over an angular range of 10 to 45 ° 2θ. Each step was 300 s long. The incident beam was collimated by 0.04 rad Soller slits, a fixed anti-diffusion slit at 1/4 °, an anti-scatter slit at 1/2 ° and a 10 mm mask. The diffracted radiation was collimated with large 0.04 rad Soller slits. The Kβ radiation was filtered with an iron plate. The signal was received by a Pixcel 1D detector before being recorded with the PANalytical data collector software.

In the literature the use of a copper anode to generate X-rays prevails over the cobalt anode used in this work. In order to make results directly comparable, the diffraction angle θ was converted from the wavelength of cobalt λ_{Co} = 1.79031 Å to the wavelength of copper λ_{Cu} = 1.54184 Å by the following equation:

$$\frac{\lambda_{Cu}}{\sin\theta_{Cu}} = \frac{\lambda_{Co}}{\sin\theta_{Co}} \quad (4)$$

Determination of cellulose crystallinity and crystallite size

Cellulose crystallinity was determined as the indices CrI_{Segal} based on the ratio of maximum and minimum intensities according to Segal et al. [1959], CrI_{area} based on the integral method described by Wakelin et al. [1959].

CrI_{Segal} is calculated by

$$CrI_{Segal} = \frac{I_c - I_a}{I_c} \times 100, \tag{5}$$

where I_c is the maximum intensity at the principal crystalline diffraction peak and I_a is the minimum intensity between peaks attributed to scattering by amorphous cellulose. For analysing cellulose I samples as initially defined by Segal et al. [1959], the peak for I_c is found at 22.7 ° and I_a is found at 18 °. The conversion of cellulose I to cellulose II results in a shift of the peaks in diffractograms and I_c is found at 20 ° and I_a at 16 ° [Nelson and O'Connor, 1964; Revol et al., 1987; Azubuike et al., 2012; French and Cintrón, 2012; Nam et al., 2016].

To determine CrI_{area} the peaks of a diffractogram were fitted using Pearson VII profiles in Fityk (Version 0.9.8; Wojdyr, 2010). A curve of the amorphous background scattering was computed from data presented by Duchemin et al. [2012] and Ciolacu et al. [2011]. The fitted curves were integrated in Matlab (R2014a, MathWorks, Natick, MA, USA) from 10 to 40 °2θ to receive the corresponding areas. The area attributed to crystalline diffraction ($A_{crystalline}$) is calculated by subtracting the area of the amorphous scattering (A_{amorph}) from the total area under the diffractogram (A_{total}) and crystallinity is subsequently calculated as

$$CrI_{area} = \frac{A_{crystalline}}{A_{total}} \times 100 \tag{6}$$

The crystallite size (τ) perpendicular to the lattice plane of the corresponding peak was determined by the Scherrer equation

$$\tau = \frac{K\lambda}{\beta cos\theta} \tag{7}$$

where K is the crystal shape factor, typically 0.89 for cellulose [Reddy and Yang, 2005], λ the wavelength of the X-ray beam and β the full width at half height of the diffraction peak at the angle θ [Scherrer, 1918; Langford, 1978]. Crystallite sizes of cellulose determined by the Scherrer equation typically deviate by less than 10 % from the real values, hence no correction is necessary [Fink et al., 1995].

3.4.6 *Fourier transformed infrared spectroscopy*

The ACCs and solvents were characterised by Fourier transformed infrared spectroscopy (FTIR) with an attenuated total reflection (ATR) equipped spectrometer (Frontier, Perkin Elmer, Waltham, MA, USA). Three specimens of each sample were analysed by averaging 64 scans in the wavenumber range 4000 to 650 cm^{-1}. The three spectra acquired for each sample were averaged in Spekwin32 (F. Menges, Version 1.71.6.1, www.effemm2.de). The total crystallinity index (TCI) was calculated as the ratio of the intensity measured at 1372 cm^{-1} and 2900 cm^{-1} according to Nelson and O'Connor [1964]. Area normalisation was performed in Fityk (Version 0.9.8; Wojdyr, Wojdyr [2010]) to visualise changes in the spectra with varying processing conditions.

In this context it is important to note that partial dissolution and regeneration of native cellulose may result in the transformation of highly crystalline cellulose I to (i) amorphous cellulose and (ii) semicrystalline cellulose II. The characterisation methods WAXD and FTIR are sensitive to a transformation

of cellulose polymorph [French, 2014; Nelson and O'Connor, 1964]. Throughout this work, rayon fibres consisting of cellulose II are used as cellulose precursor. Therefore, no changes in polymorph are expected with dissolution and regeneration. All changes in WAXD and FTIR results are consequently attributed to changes in the ratio of crystalline to amorphous domains.

3.5 STATISTICS

The experimental data were tested for normal distribution (Shapiro-Wilk test) and homogeneity of variances (Bartlett's test, Fligner-Killeen test) and differences were tested for statistical significance at a probability level of $\alpha = 5\,\%$ by analysis of variances followed by post-hoc testing (Tukey's procedure, Wilcoxon rank sum test) using the programming language R [R Core Team, 2013]. Results are given as arithmetic mean $\pm$ standard deviation.

4

SIZE AND SCALE EFFECTS IN ALL-CELLULOSE COMPOSITE LAMINATES

4.1 INTRODUCTION

Size effects refer to changes in the mechanical properties of a material specimen caused by changes in the physical volume of the specimen. In general, size effects are attributed to the presence of flaws and the higher probability of a large volume in comparison to a small volume to contain a critical flaw that causes premature failure [Wisnom, 1999; Sutherland et al., 1999a]. In ductile materials, the stress concentration arising from a flaw of critical size is diminished by local plastic deformation. However, in a brittle material, the stress concentration around a flaw initiates local failure that propagates and results in global failure [Odom and Adams, 1992]. Most composites, such as glass and carbon fibre-reinforced polymers, are quasi-brittle materials that exhibit a negative size effect in which the strength decreases with increasing specimen dimensions [Zweben, 1994; Bažant et al., 1996; Wisnom, 1999; Sutherland et al., 1999a].

The size effect in composites can be described by the modified weakest link model, where Weibull theory is applied to anisotropic materials [Wisnom, 1999; Tabiei and Sun, 2000]. The modified weakest link model predicts a straight line of slope -1/m, where m is the Weibull modulus that quantifies

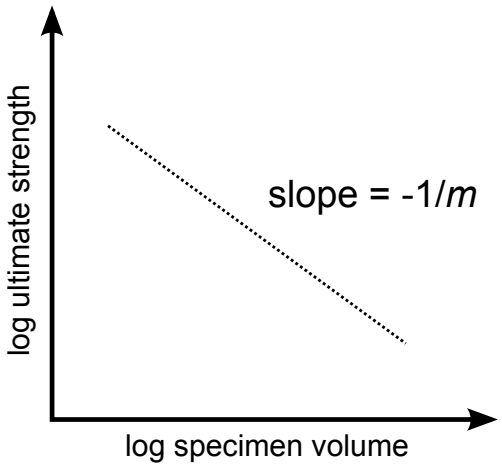

Figure 28: Logarithmic plot of a strength size effect as predicted by the modified weakest link model with Weibull modulus m [Sutherland et al., 1999a].

the size effect of a given material, for a logarithmic plot of strength as a function of specimen volume (Figure 28, Sutherland et al., 1999a). The modified weakest link model was found to match experimental data of glass and carbon fibre-reinforced composites [O'Brien and Salpekar, 1993; Wisnom and Atkinson, 1997; Wisnom, 1999].

The existence of size effects has been reported in a wide range of materials, reviewed by Bažant and Chen [1997] and Bažant [1999], and size effects in composites have been summarised in several reviews [Zweben, 1994; Bažant et al., 1996; Wisnom, 1999; Sutherland et al., 1999a].

In addition to size effects, an increase in dimensions can give rise to scale effects [Sutherland et al., 1999a]. The quality of composites may differ between small laboratory scale samples for testing and full-scale manufacturing, e.g. due to variations between nominally identical batches of resin or reinforcement, warp-weft distortions in large areas of textile, and differences in the cure of small and large volumes of epoxy resin. Sutherland et al. [1999b] found that the scale effect arising from upscaled production of com-

posites is more influential than a strength size effect in ship-building grade glass fibre-reinforced composite laminates.

SIP is the first upscalable manufacturing pathway of ACC laminates and facilitates processing of ACCs with increased dimensions [Huber et al., 2012a]. However, it is yet unknown whether size and scale effects occur in ACCs when the dimensions of the laminates are increased. In this chapter the manifestation of size and scale effects in ACC laminates is investigated by characterising ACCs of increasing laminate thickness by tensile testing, WAXD, and SEM. Furthermore, the evolution of damage with increasing strain is examined in a series of interrupted tensile tests followed by microstructural characterisation using SEM.

4.2 EXPERIMENTAL PROCEDURES

4.2.1 *Preparation of all-cellulose composite laminates*

ACCs were manufactured *via* SIP as described in Section 3.2. A laminate stack of 180 mm width and 350 mm length with 1, 2, 4 or 8 laminae was infused with the IL BmimAc, partially dissolved at 95 °C under an applied pressure of 1 MPa for 60 min and regenerated in water (Figure 29a). The regenerated material was cut to SEM and tensile testing specimens using a sharp blade prior to drying. Tensile tests were performed on rectangular coupons with a length and width of 140 and 14 mm, respectively, at a gauge length of 60 mm.

Unreinforced cellulose films were prepared as a representation of the matrix phase as described in Section 3.3 by dissolving rayon fibres of ~2 mm length in BmimAc at a temperature of 95 °C for 60 min. Tensile tests were

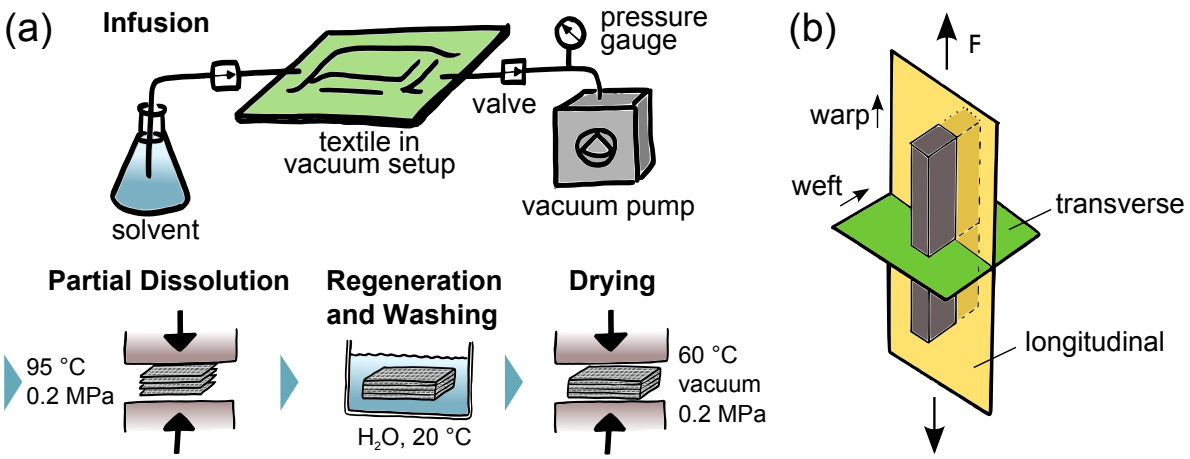

Figure 29: (a) Schematic of solvent infusion processing of ACC laminates. (b) Schematic of the warp and weft directions in the laminates. The longitudinal and transverse planes describe the cross-sectional cuts for the microstructural analysis. Arrows indicate the direction of the applied load F during tensile testing.

performed on rectangular strips with a length and width of 30 and 4 mm, respectively, at a gauge length of 16 mm.

4.2.2 *Materials characterisation*

Cellulose crystallinity determination with increasing thickness

Sections of 60 µm in thickness were microtomed from an ACC with 8 laminae from the surface (skin) through to the core. A selection of five sections representing the skin, intermediate and core volume of the ACC laminate, was analysed by WAXD performed in powder mode in steps of 0.1° over a 2θ range of 10° to 40° using a X'Pert powder diffractometer (PANalytical, Almelo, Netherlands) equipped with a sample spinner. The procedures for cellulose crystallinity determination are given in Section 3.4.5.

Damage evolution

The damage evolution in ACC laminates under tensile load was investigated following the approach proposed by Lomov et al. [2008]. Damage analysis started with tensile testing specimens to failure. Characteristic strain levels for a *post-mortem* investigation were then determined from the stress-strain curves. Specimens were loaded to strains of 0.5 % (ε_1), 1.5 % (ε_2) and 4.5 % (ε_3) after which the specimens were immediately unloaded. The specimens were then analysed by SEM to observe the accumulated damage.

Longitudinal and transverse cross sections of the tensile specimens (Figure 29b) were obtained by cutting 10 mm long blocks from within the gauge volume. The blocks were then immersed in distilled water to soften so that a smooth surface for SEM analysis could be prepared by cutting with a razor blade. The prepared blocks were dried under the same conditions as the laminate and gold coated for 180 s at 25 mA (Emitech K975X, Quorum Technologies Ltd, East Grinstead, UK). Three replicates per strain level were examined with a scanning electron microscope (7000F FE-SEM, JEOL, Tokyo, Japan) using an accelerating voltage of 5 kV. Sample preparation did not introduce artefacts or alter damage present in specimens. No differences in microstructure were found when comparing as-fabricated ACC specimens which were directly cut before drying with samples that were dried, re-wetted, cut and re-dried. Furthermore, no damage was found in the transverse sections, when cracks were already present in the longitudinal sections, indicating that softening, cutting and re-drying do not influence the presented results.

4.3 RESULTS AND DISCUSSION

4.3.1 *Microstructure*

Processing of ACCs by SIP resulted in dimensionally stable laminates with well consolidated laminae and fibres. The fibres were surrounded by a 1 to 5 µm thin layer of matrix, indicating successful partial dissolution. Longitudinal and transverse cross sections revealed identical microstructures with alternating warp and weft yarns according to the weave pattern of the textile used as precursor (Figure 30). Low numbers of voids (~10 µm diameter) were observed between the laminae and in between fibres.

4.3.2 *Tensile behaviour*

The stress-strain curve of ACC laminates with 4 laminae exhibited linear elastic behaviour up to a yield point at 62 to 67 MPa and ca. 1.5 % strain (Figure 31). A stress plateau was observed to follow yielding, continuing until a failure strain of 4.8 ± 2.1 %. The stress-strain curve could be divided into four distinct stages: (I) linear-elastic, (II) yielding, (III) stress plateau after yielding and (IV) final failure (Figure 31). A detailed microstructural characterisation of the accumulated damage in Stages I to IV was carried out at nominal strains of 0.5 % (ε_1), 1.5 % (ε_2), 4.5 % (ε_3) and strain to failure (ε_f).

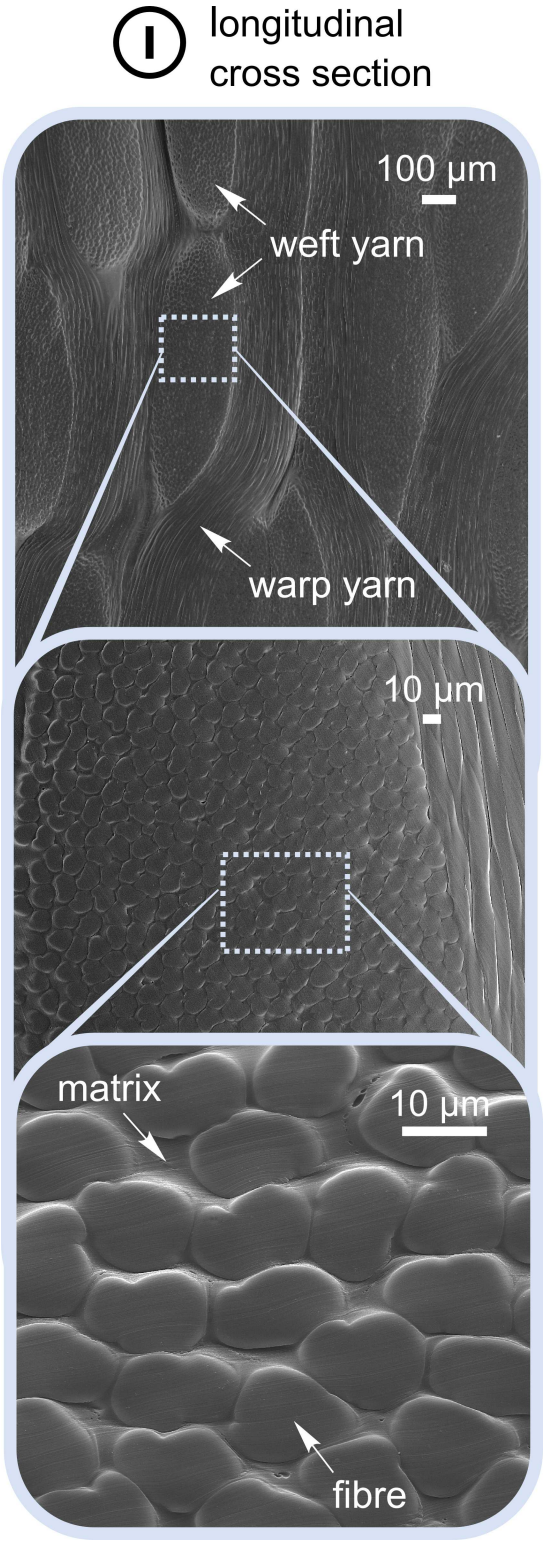

Figure 30: Scanning electron micrographs of the longitudinal cross section of an as-fabricated ACC laminate with 4 laminae at varying magnifications.

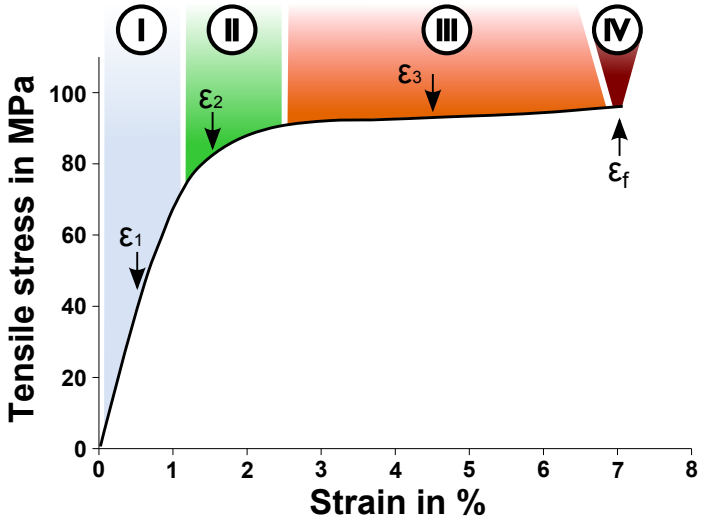

Figure 31: Representative stress-strain curve of an ACC laminate with 4 laminae characterised by four stages: linear-elastic (I), yield (II), stress plateau (III) and final failure (IV). The accumulated damage was examined at ε_1, ε_2, ε_3 and ε_f.

4.3.3 *Damage evolution in all-cellulose composite laminates*

The as-processed ACC laminates were translucent, indicating a low void content and high interfacial adhesion between the fibre and matrix [Soykeabkaew et al., 2008]. A similar level of translucency was retained in specimens strained to 0.5 % and 1.5 % (Figure 32). Microscopic observations revealed no difference in microstructure between as-processed and 0.5 % strained specimens. No cracks or debonding of fibre and matrix were observed in longitudinal and transverse cross sections in Stage I.

The initiation of failure occurred in Stage II upon yielding, resulting in the appearance of microcracks observed in specimens strained to 1.5 % (Figure 33). Microcracks of 2 to 10 µm length were orientated perpendicular to the applied tensile load, and appeared to mainly originate from microvoids (Figure 33). No damage was evident in the transverse cross section.

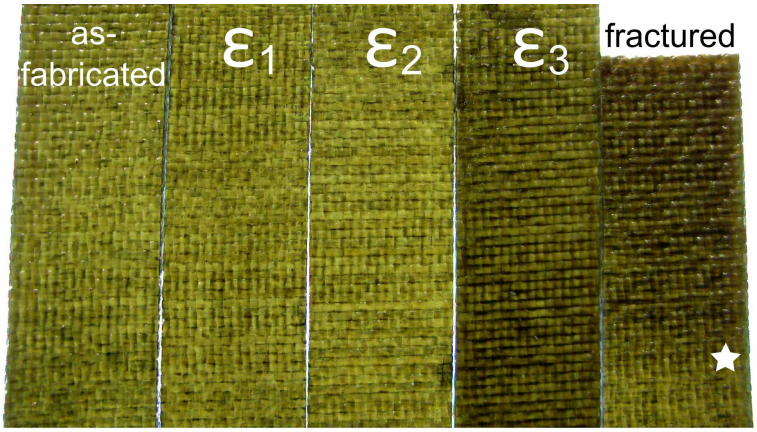

Figure 32: Photograph of specimens with 4 laminae showing increasing opacity with increasing strain. The white star indicates the transition from gauge length (opaque) to gripped section (lighter, at bottom) of the fractured sample. The width of each specimen is 14 mm.

Larger cracks of 10 to 30 µm width and 100 to 300 µm length were observed running through the transverse weft yarns after applying a strain of 4.5 % (Stage III, Figure 34). The opacity of specimens increased due to the presence of cracks, along with the appearance of dark lines at a strain of 4.5 % (ε_3, Figure 32). While the transverse yarns were split by cracks, the longitudinal warp yarns remained intact, effectively acting as crack arresters. There were pockets of matrix phase between weft yarns that exhibited cracking. The separation of yarns from each other was also observed, resulting in local delamination of adjacent layers (Figure 34).

Longitudinal cross sections of fractured specimens (Stage IV) exhibited extensive accumulation of cracks and delamination (Figure 35), accompanied by a further increase in opacity in the gauge section up to the strain of failure (Figure 32). Approximately half of the transverse yarns were split completely, some by two or more cracks (Figure 35). The cracks in transverse yarns propagated in between fibres with some fibres separated from the edge of cracks (Figure 36a,b). Fibre splitting rarely occurred (Figure 36c).

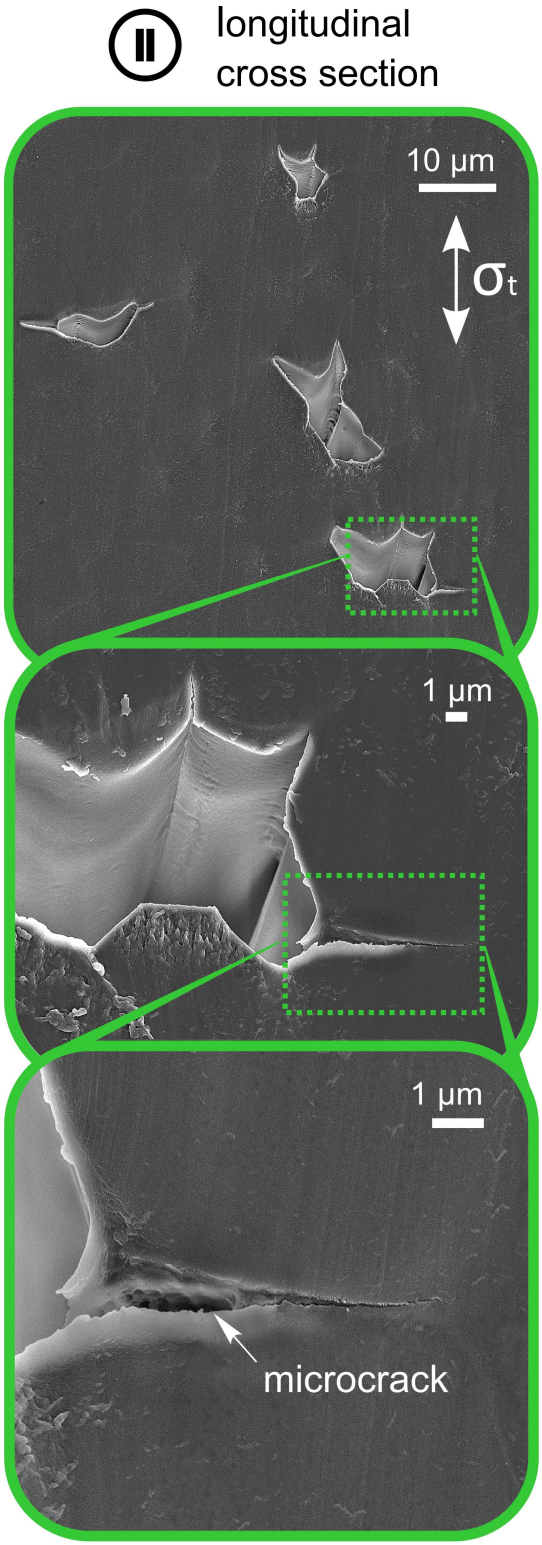

Figure 33: Scanning electron micrographs of the longitudinal cross section of an ACC laminate with 4 laminae strained to 1.5 % elongation (Stage II). Direction of the applied tensile stress σ_t is indicated by arrows (↕).

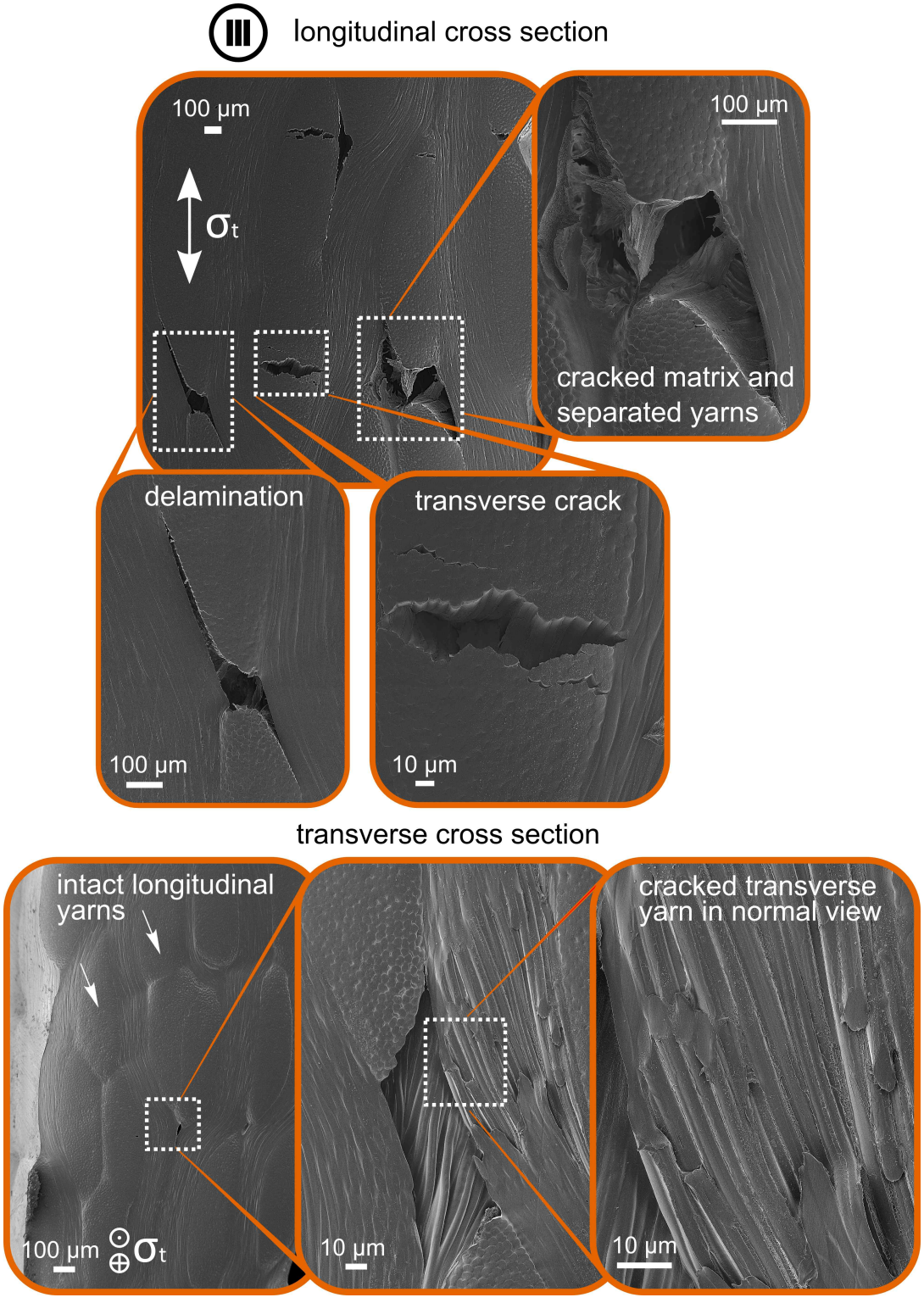

Figure 34: Scanning electron micrograph of the longitudinal and transverse cross section of a 4-layered ACC laminate strained to 4.5 % elongation (Stage III). Direction of the applied tensile stress σ_t is indicated by arrows (↕) for in plane and signs (⊙ & ⊕) for out of plane stress.

Local delamination was caused by long cracks originating from the fracture surface and propagating longitudinally in between laminae (Figure 35). Pull-out of complete yarns could be observed at the fracture surface (Figure 37a). However, there was little evidence of individual fibre pull-out (Figure 37b,c).

The increase in opacity was only observed in thick laminates with 4 and 8 laminae. 1 and 2 laminae specimens strained to failure still exhibited the translucent appearance of as-fabricated specimens. However, visual observation revealed individual transverse cracks close to the site of fracture (Figure 38).

4.3.4 *Properties of all-cellulose composite laminates as a function of laminate thickness*

4.3.4.1 *Thickness and density*

The thickness of the ACC laminates increased from 0.42 ± 0.04 mm for 1 lamina to 3.36 ± 0.04 mm for 8 laminae (Table 4). Laminate thickness increased by 703.6 %, which was slightly higher than the theoretically expected value of 700 %. Simultaneously, the density of the ACC laminates decreased by 1.3 % from 1.501 ± 0.002 g cm^{-3} for 1 lamina to 1.481 ± 0.005 g cm^{-3} for 8 laminae (Table 1). The final density of the ACC (ρ_{ACC}) should be equal to that of the dry rayon fibres (ρ_{rayon} = 1.52 g cm^{-3}; Woodings, 2001) if the ACC is void-free and exhibits a constant overall crystallinity. Hence, the void content ($(\rho_{rayon} - \rho_{ACC})/\rho_{rayon} \times 100$) of a single lamina is 1.3 %, which increases to 2.6 % for an 8 laminae ACC (Table 4), if potential crystallinity changes are ignored.

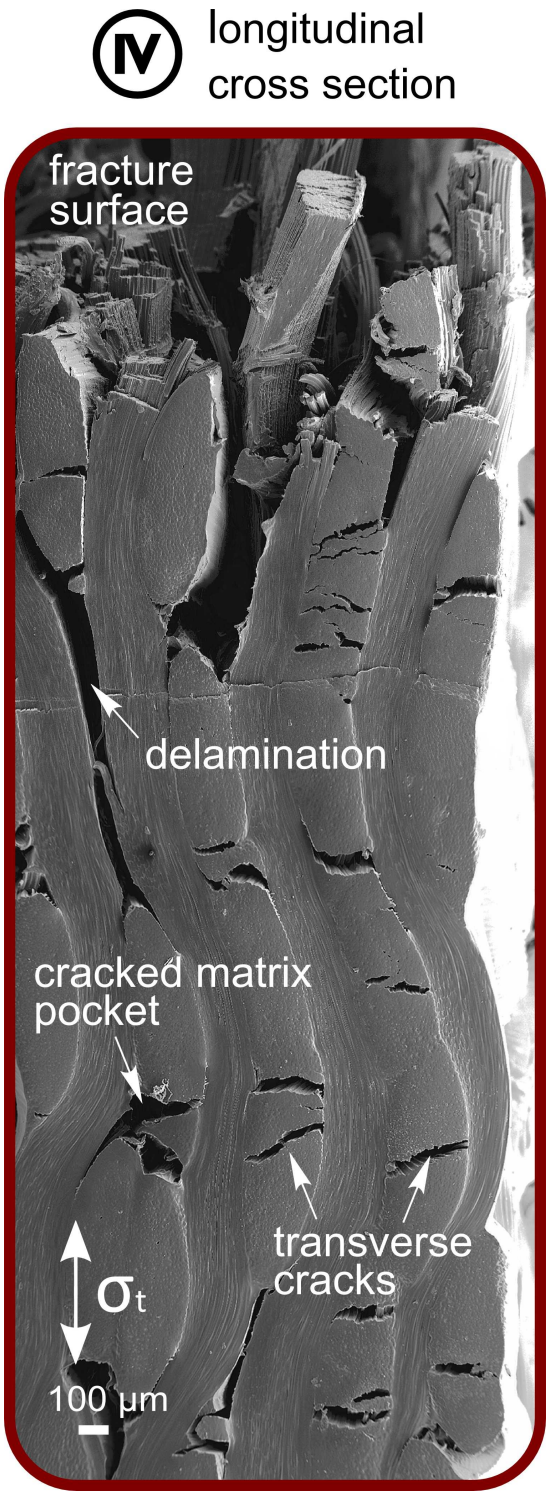

Figure 35: Scanning electron micrograph of a fractured 4 layer ACC laminate (Stage IV). Direction of the applied tensile stress σ_t is indicated by arrows (↕).

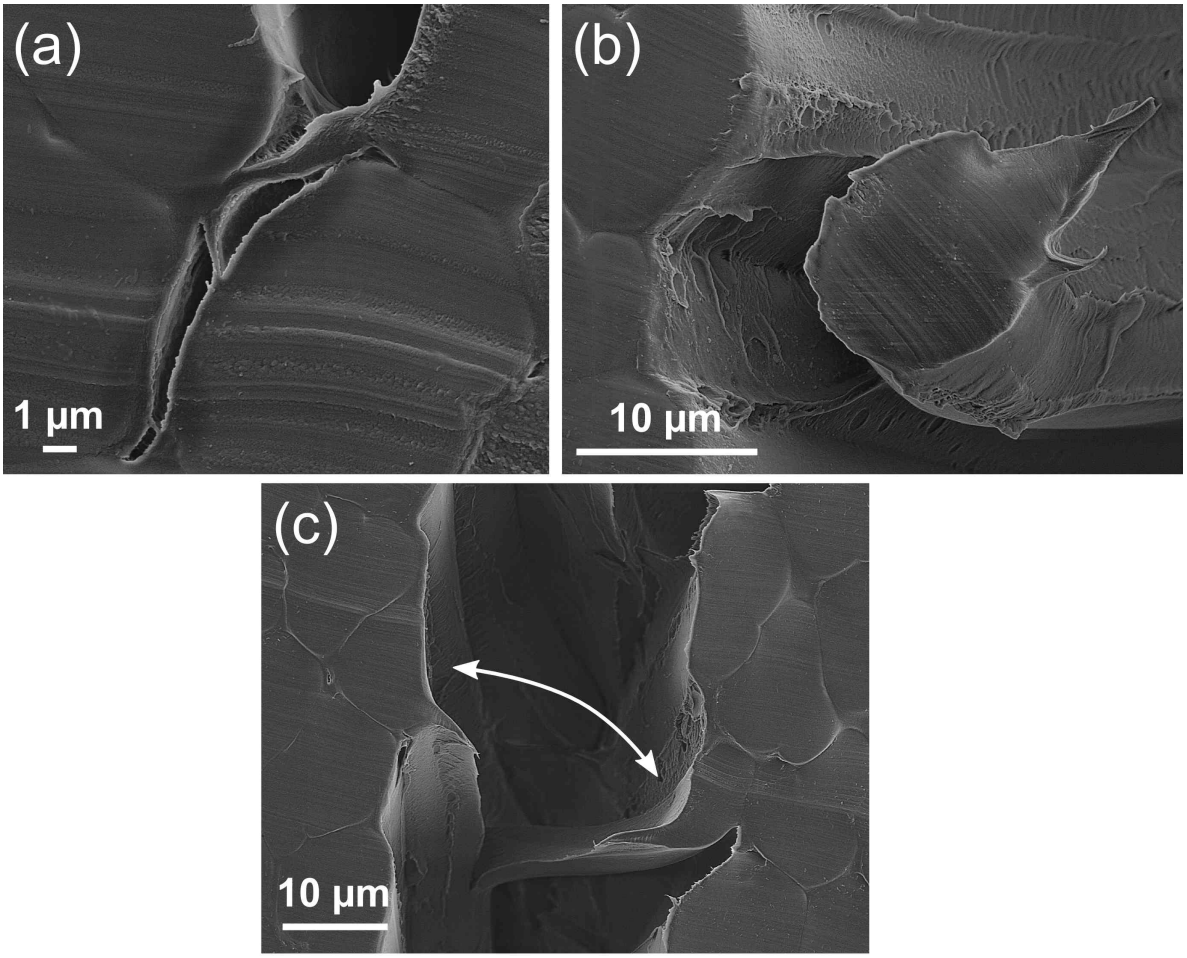

Figure 36: Scanning electron micrographs of details in longitudinal cross sections of ACC laminates in Stages III and IV. (a) Transverse crack running in between fibres. (b) Single fibre separated from other fibres in a yarn and protruding into a transverse crack. (c) Micrograph of the only observed instance of a fibre split by a transverse cracks. The arrow indicates the separated halves of the split fibre.

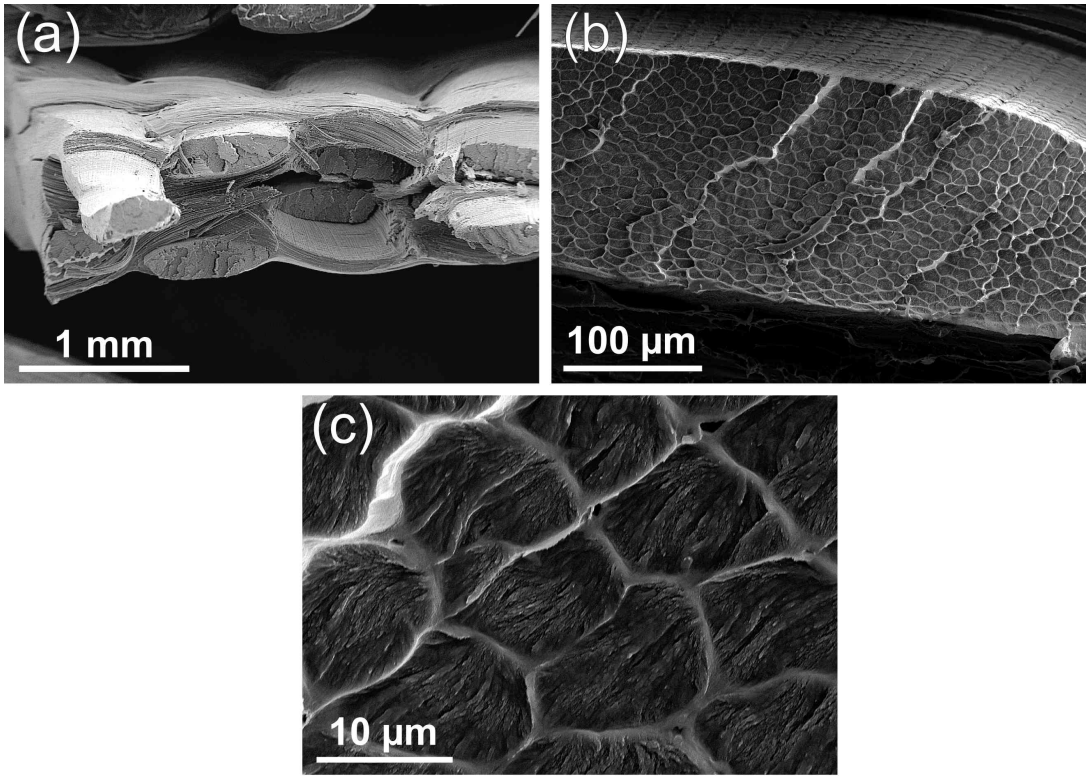

Figure 37: Scanning electron micrographs of the tensile fracture surface of an ACC laminate with 4 laminae, on laminate (a), yarn (b) and fibre level (c).

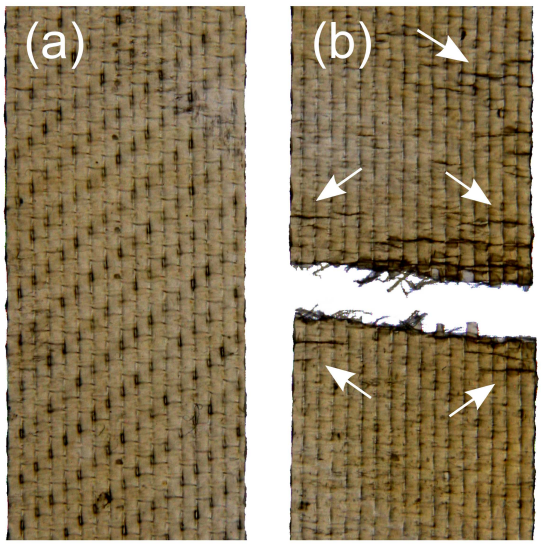

Figure 38: Photographs of (a) an as-fabricated (b) and fractured 1 lamina specimen. Arrows indicate the location of individual transverse cracks. The width of each specimen is 14 mm.

Table 4: Mechanical and physical properties of ACC laminates and unreinforced cellulose film (Unr. cell. film). (* significant differences in ultimate tensile and yield strength are indicated by different superscript letters, no significant difference in Young's modulus was found, $\alpha = 0.05$).

	Tensile* strength in MPa	Yield* strength in MPa	Young's* modulus in GPa	Elongation at break in %	Thickness in mm	Density in g cm^{-3}	V_v (density) in %
Unr. cell. film	66.9 ± 5.3^{a}	56.5 ± 6.4^{a}	7.1 ± 0.6	2.0 ± 0.9	0.26 ± 0.10		
1 lamina	79.7 ± 2.4^{b}	60.9 ± 0.3	7.3 ± 0.4	3.1 ± 1.2	0.42 ± 0.04	1.501 ± 0.002	1.3
2 laminae	86.0 ± 6.5^{c}	62.4 ± 3.7	7.6 ± 0.3	1.9 ± 0.2	0.88 ± 0.04	1.463 ± 0.019	3.7
4 laminae	96.3 ± 3.3^{d}	64.9 ± 2.6^{b}	7.8 ± 0.9	4.8 ± 2.1	1.55 ± 0.05	1.477 ± 0.007	2.8
8 laminae	105.8 ± 4.2^{e}	66.5 ± 3.3^{b}	7.5 ± 0.5	8.9 ± 1.0	3.36 ± 0.04	1.481 ± 0.005	2.6
change from 1 to 8 laminae	+32.8 %	9.2 %	+2.7 %	+187.1 %	+703.6 %	-1.3 %	+1.3 %

4.3.4.2 *Variation of cellulose crystallinity with all-cellulose composite laminate thickness*

As expected, the WAXD diffractograms of all samples produced diffraction peaks at 2θ of 12.3 °, 20 ° and 22 ° (Figure 39a) that are assigned to the diffracting planes $(1\bar{1}0)$, (110) and (020) of cellulose II [French, 2014]. It is concluded, that the cellulose II polymorph known for rayon fibres [Röder et al., 2009] remains unchanged with processing into ACC laminates.

CrI_{area} of an 8 laminae ACC was determined as a function of thickness. It increased from 64 % at the skin to 79 % at the core of the laminate (Figure 39b)[1]. Cellulose is a semicrystalline polymer and its crystallinity is known to change with dissolution and subsequent regeneration [Bang et al., 1999; Zhang et al., 2005b; Duchemin et al., 2009b]. The regeneration of cellulose from a solution relies on the counter-diffusion between the non-solvent in

1 The low WAXD signal intensity obtained from the thin slices did not allow for standardisation of the amorphous background with literature values. Hence, the thickness dependent crystallinity should be interpreted as relative differences within this sample only and the absolute values should not be compared to other samples.

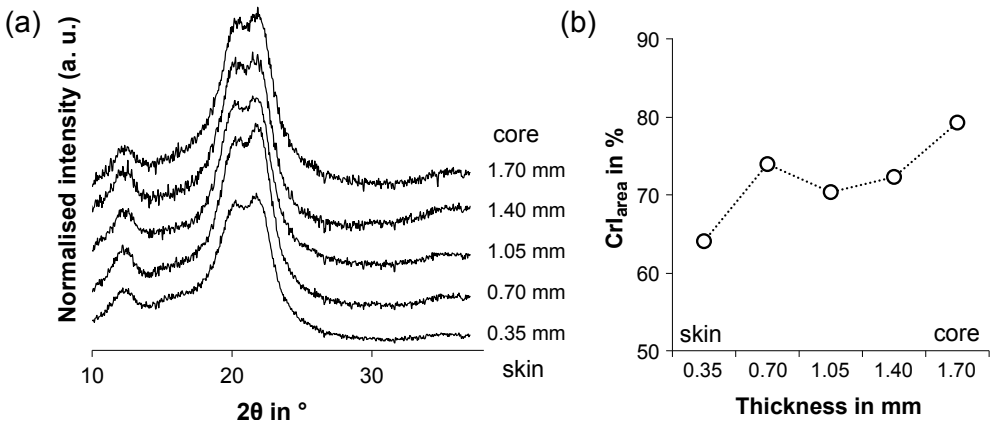

Figure 39: (a) Area-normalised WAXD diffractograms (shifted vertically for clarity) and (b) cellulose crystallinity as function of thickness of an 8 laminae ACC from skin to core.

the coagulant, in this case water, and the solvent in the cellulose solution [Zhang et al., 2005b]. As the water penetrates into the cellulose solution and the IL diffuses into the water bath, the intra- and intermolecular hydrogen bonds are reformed and the cellulose precipitates. Jiang et al. [2011] have shown that the diffusion of IL from a cellulose solution in water follows Fick's Law. The IL diffuses from regions of high concentration to regions of low concentration along a concentration gradient, and the diffusion coefficient depends on temperature, cellulose content in the solution and IL concentration in the regeneration bath [Bang et al., 1999; Jiang et al., 2011]. Thin ACC laminates have a high surface to volume ratio such that the IL and water need only diffuse short distances to allow rapid regeneration of the partially dissolved rayon. Thick laminates have a lower surface to volume ratio and an increased length over which IL and water must diffuse, resulting in longer regeneration times. Furthermore, only the skin is directly exposed to the water bath. In accordance with Fick's law, at any given time following regeneration, the relative IL concentrations are higher in thicker laminates. The slower regeneration results in a more crystalline arrangement of cellu-

lose chains [Bang et al., 1999; Zhang et al., 2005b; Duchemin et al., 2009b; Song et al., 2013] and hence the crystallinity increases towards the core of thick laminates (Figure 39).

The increase in crystallinity has an impact on the density of ACC laminates, as amorphous cellulose is 5 to 6 % less dense than crystalline cellulose [Hermans et al., 1946]. Crystallinity is generally speaking the ratio of amorphous to crystalline domains ($R_{a/c}$), and thus a change in density caused by a variation in crystallinity can be estimated by applying the rule of mixtures. Given the density of crystalline and amorphous cellulose II is 1.58 g cm^{-3} [Woodings, 2001] and 1.47 g cm^{-3} [Ishikawa et al., 1997], respectively, a change in $R_{a/c}$ from 0.36/0.64 at the skin to 0.21/0.79 at the core of 8 layer laminates results in a 1.1 % higher density at the core. Averaged over the full thickness of an ACC laminate, this equates to an increase in density of 0.55 % for a laminate with 8 laminae when compared to 1 lamina.

However, the overall change in density of ACC laminates by increasing the number of laminae is negative. The increase in density by approximately 0.5 % due to the higher crystallinity at the core of 8 laminae (Figure 39) is counteracted by the laminate thickness increasing by 3.6 % more than the expected 700 % (Table 4). This leads to the observed increase in void content by 1.3 % when comparing laminates with 1 and 8 laminae.

4.3.4.3 *Variation of mechanical properties with increasing all-cellulose composite laminate thickness*

The ACC laminates were found to exhibit a positive size effect of increasing ultimate tensile strength, yield strength and elongation at break with increasing thickness. The ultimate tensile strength increased from 79.7 ± 1.4 MPa in a single lamina to 105.8 ± 4.2 MPa (+32.8 %) in the 8 laminae ACC (Table 4). The Young's modulus of all laminates was in the range of 7.3 ± 0.4 GPa to

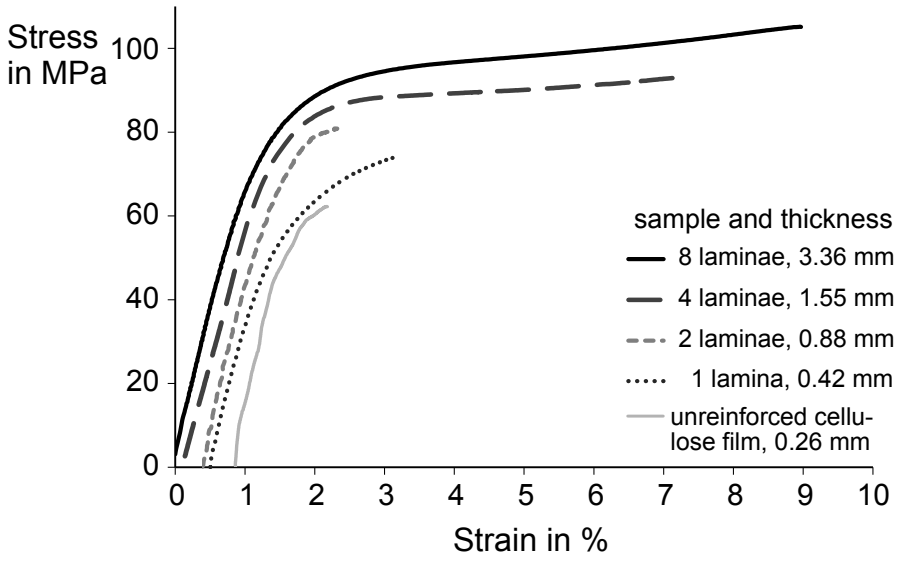

Figure 40: Representative stress-strain curves of ACC laminates with increasing number of laminae and unreinforced cellulose film. Graphs have been shifted horizontally for clarity.

7.8 ± 0.9 GPa and no significant differences were found. The yield strength increased from 60.9 ± 0.3 MPa to 66.5 ± 3.3 MPa by increasing the number of laminae from 1 to 8 (Table 4).

The shape of the stress-strain curves of ACC laminates changed with increasing the number of laminae (Figure 40). Initially, all of the laminates exhibited linear elastic behaviour prior to yielding between 1 and 2 % strain. A more pronounced plateau in stress was observed following yielding of laminates with 4 and 8 laminae. The stress plateau extended from approximately 3 to 9 % strain with 8 laminae. This led to an increase in strain to failure by 187 % from 3.1 ± 1.2 % to 8.9 ± 1.0 % when the number of laminae was increased from 1 to 8.

The unreinforced film of fully dissolved rayon exhibited a tensile strength of 66.9 ± 5.3 MPa and Young's modulus of 7.1 ± 0.6 MPa. The film fractured at a comparably low strain of 2.0 ± 0.9 % without the stress plateau after yield seen in ACC laminates (Figures 40 and 41).

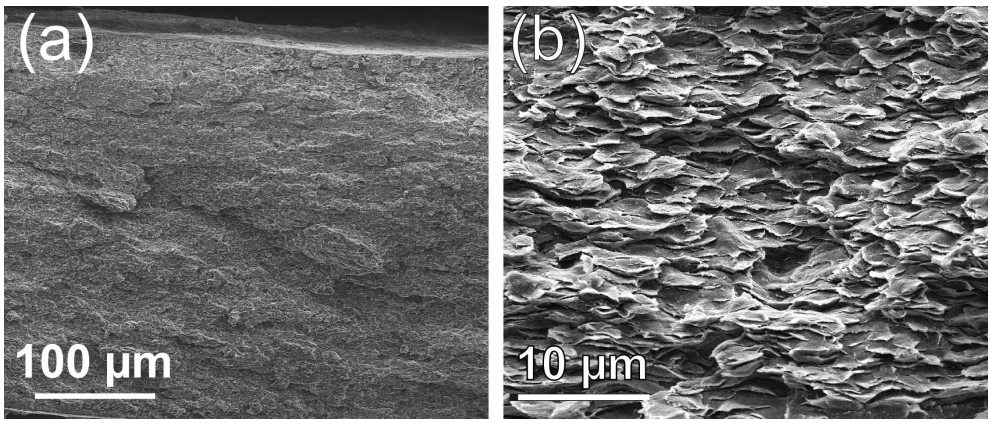

Figure 41: Scanning electron micrographs of the fracture surface of the unreinforced cellulose film at low (a) and high (b) magnification.

4.3.5 *Positive size effect on the tensile strength of all-cellulose composite laminates*

The increase in mechanical properties with increasing thickness of ACC laminates is surprising, as a size effect of decreasing strength with increasing volume is generally known for composites [Wisnom, 1999; Bažant et al., 1996]. The reasons for the increased mechanical properties were found to lie within the structure and damage evolution of ACC laminates, as discussed in the following sections.

4.3.5.1 *Strengthening mechanism in thick all-cellulose composite laminates*

The most prominent difference in the tensile characteristics of thin (1 and 2 laminae) and thick ACC laminates (4 and 8 laminae) is the stress plateau of Stage III following yield (Figure 40). This plateau coincides with an increase in opacity of the thicker laminates during tensile testing (Figure 32). The opacity of the specimens can be correlated with damage that accumulates during Stage III. Cracking of transverse yarns and local delamination are observed, that lead to scattering of light and hence an increase in opacity (Fig-

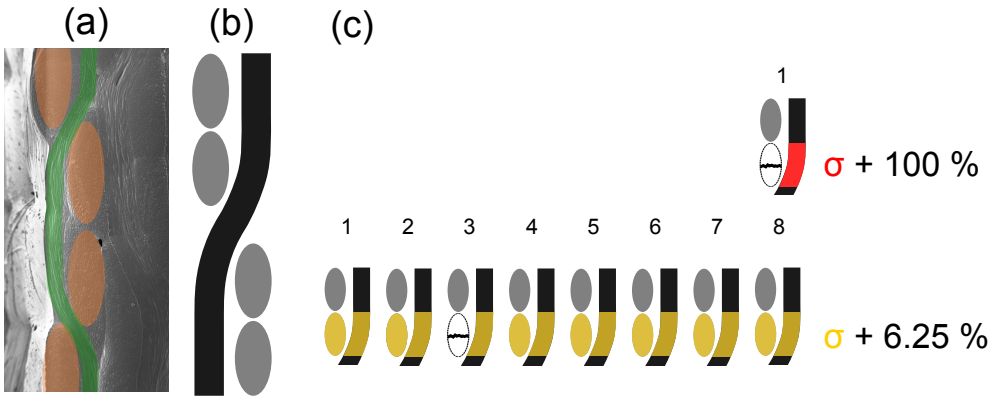

Figure 42: (a) SEM micrograph with false-coloured inlay showing longitudinal warp (green) and transverse weft yarns (orange). (b) Schematic of the warp and weft yarns of the twill weave textile within the ACC laminates. (c) Schematic of ACCs with 1 lamina and 8 laminae with one fractured transverse yarn and the corresponding increase in stress in the remaining cross-sectional area.

ure 34). The opacity of thick laminates increased during deformation, while the single lamina ACC remained translucent during deformation, indicating a distinct difference in damage accumulation. Furthermore, the longitudinal cross section of fractured thick laminates shows accumulated cracks and local delamination across the entire gauge length. This leads to the conclusion that thick laminates are more damage tolerant and the following strengthening mechanism is proposed.

Transverse cracking and delamination lead to the separation of longitudinal yarns from transverse yarns, such that the longitudinal yarns can straighten in the direction of the applied load. The straightening allows the yarns to relax from their crimped shape imposed by the weave, thereby reducing tensile stress at a given strain, allowing individual yarns to remain intact up to higher loads. Furthermore, load is transferred to the remaining cross sectional area when a transverse yarn cracks, leading to a local stress concentration. In a single lamina such a crack running through a transverse yarn corresponds to a loss of 50 % of the cross-sectional area that carries load,

which equals a stress increase of 100 % (Figure 42). This local jump in stress by 100 % exceeds the strength of the remaining cross section and causes failure of the laminate. Consequently, the first transverse crack that spreads over the full width of a specimen causes a single lamina to fail. In an 8 layer laminate the cracking of a transverse yarn translates to a stress increase of only 6.25 %, the adjacent longitudinal yarns act as crack arresters and the load is transferred to the remaining 7.5 layers (Figure 42). A local increase in stress of 6.25 % does not cause failure and as transverse cracks originate from randomly distributed defects, they occur in the entire gauge volume and the stress redistribution allows the accumulation of many transverse cracks in thick laminates.

In summary, thick laminates have a higher damage tolerance due to crack arresting and stress redistribution. The accumulation of damage within the gauge volume results in the delocalisation of strain, due to the straightening of detached longitudinal yarns. This leads to a transition from early fracture of thin laminates with 1 and 2 laminae at low strains to failure, to failure at higher strains and stresses with an increased toughness of thick laminates with 4 and 8 laminae.

4.3.6 *Size effects in composites and polymers*

In the field of composites, the vast majority of studies cover *negative* size effects of decreasing strength with increasing volume [Wisnom, 1999; Bažant et al., 1996, 1999]. Sutherland et al. [1999a] mention the existence of a *positive* or reverse size effect of increasing strength with increasing dimensions in composites in their review, although no citations to respective studies are provided. Evidence for the existence of a negative size effect in composites is summarised by Zweben [1994] and there are many studies that present

experimental evidence [Gurvich and Pipes, 1995; Bažant et al., 1996; Wisnom and Atkinson, 1997].

Bažant et al. [1996] have shown that Bazant's size effect law applies to composites, according to which the logarithm of strength over the logarithm of specimen size transitions smoothly from a horizontal asymptote predicted by the strength criterion of plastic limit analysis to an inclined asymptote with a slope of -0.5 predicted by linear elastic fracture mechanics. However, their study investigated two-dimensional scaling (primarily width) at constant thickness, which is not adequate for comparison to the thickness dependent size effect presented in this work.

In general, the negative size effect in composites is attributed to the higher probability of a larger volume to contain a critical defect and it can be modelled by applying Weibull theory to anisotropic materials (modified weakest link model) [Wisnom, 1999; Tabiei and Sun, 2000]. The size effect of quasi-brittle composites following the modified weakest link model is characterised by a negative slope in a log-log plot of strength as a function of specimen dimension (Figure 43), which fits experimental data for carbon and glass fibre-reinforced composites [Wisnom, 1999]. On the contrary, ACC laminates of increasing thickness show a positive slope (Figure 43). It needs to be noted, that the application of Weibull theory to size effects in composites must be treated with care. As Wisnom [1999] and Sutherland et al. [1999a] point out in their reviews, Weibull theory assumes that failure occurs catastrophically from a critical defect. Carbon and glass fibre-reinforced composites often fail suddenly, with failure initiating from a defect and resulting in brittle fracture [Sutherland et al., 1999a; Wisnom, 1999]. In contrast, the failure of ACC laminates is characterised by extensive damage accumulation, which distinguishes ACCs from composites that are characterised by a Weibull-type size effect.

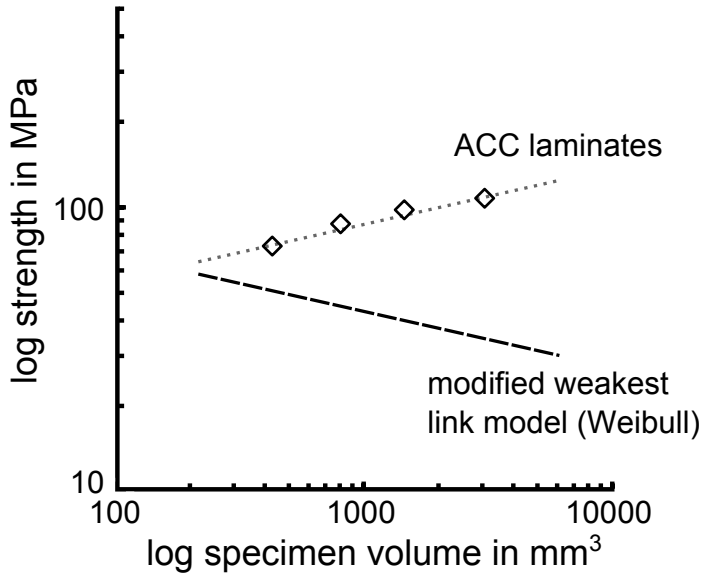

Figure 43: Log-log plot of tensile strength over specimen volume with a positive slope seen for ACC laminates and a typical negative slope for other composites following Weibull theory [Wisnom, 1999; Sutherland et al., 1999a]

A fundamental difference between conventional composites and ACCs is that in carbon and glass fibre composites brittle fibres are embedded in a more ductile matrix and the overall properties resemble a quasi-brittle material. However, in the ACC laminates presented here, ductile rayon fibres are embedded in a matrix of dissolved and regenerated rayon that fractures at a comparably low strain of 2.0 ± 0.9 % (Table 4, Figures 40 & 41) without the stress plateau after yield observed in laminates, and overall the laminates exhibit a ductile tensile behaviour.

It needs, however, to be mentioned that the matrix may exhibit a different behaviour than the unreinforced film, as the matrix created by partial dissolution is confined in between fibres that may act as nucleation sites during regeneration. Furthermore, the matrix layer in ACCs is only 1 to 5 µm thick, hence a size effect may be present in the much larger volume of regenerated cellulose tested in the unreinforced film with a thickness of 0.26 mm.

Size effects are generally attributed to the presence of defects in the material. The potential of thick ACC laminates to accumulate damage shows that the existence of defects is not detrimental to their ultimate tensile strength, but is instead part of the strengthening mechanism described above. A higher void content has been shown to lead to a decrease in strength of carbon-epoxy [Almeida and Neto, 1994] and flax-epoxy composites [Li et al., 2015]. In ACC laminates, on the contrary, the increase in void content with increasing laminate thickness (Table 4) could be beneficial to the strengthening mechanism by initiating transverse cracks (Figure 33). However, an increase in void content also leads to a decrease in interfacial shear strength of 7 % per 1 % voids [Judd and Wright, 1978]. The relative contribution of increased void content and reduced interfacial shear strength to initiation and accumulation of damage is not evident from the present work and should be addressed in the future.

While a negative size effect is known for a variety of materials, e.g. concrete, rock, ceramics and wood [Bažant and Chen, 1997] as well as metals such as aluminium [Bažant et al., 1987], a positive size effect as seen in ACC laminates is rare. Exceptions to the negative size effect have been reported for concrete in splitting tensile tests, depending on the loading configuration [Zhou et al., 1998; Tang et al., 1992], for sea ice under certain conditions [Bažant and Guo, 2002], and in hot extruded magnesium alloy depending on thickness and orientation [Zhang et al., 2013].

Polymers and polymer fibres are also subject to a negative size effect caused by the higher number of flaws and their increasing size with increasing specimen volume [Wagner, 1989; Odom and Adams, 1992]. The toughness of brittle polymers can be increased by several mechanisms as outlined by Argon and Cohen [2003]. While an increase in microstructural perfection to avoid critical flaws by optimising polymer processing is either fundament-

ally not possible or costly, a transition to ductile failure in semi-crystalline polymers can be achieved by lowering the plastic resistance. An effective way of enhancing plasticity is the quasi-uniform cavitation of a polymer by the introduction of particles. Upon the application of stress, the particles cause cavitation or debond and the polymer undergoes large scale strain in the interparticle ligaments, leading to global delocalisation of strain and a transition to ductile behaviour [Argon and Cohen, 2003].

The same toughening concept applies to ACC laminates. The transverse cracking of weft yarns leads to their local debonding from the longitudinal yarns. The straightening of longitudinal yarns from their crimped weave pattern in turn results in an increase in strain. As transverse cracking is a global phenomenon occurring in the entire gauge volume of thick laminates, it results in global strain delocalisation and an overall transition to ductile failure of thick ACC laminates. In addition to strain delocalisation, crack deflection and interlaminar debonding observed in ACC laminates strained to 4.5 % (Figure 34) are known as efficient energy absorbers in composites [Hull and Clyne, 1996] that contribute to the increase in toughness with increasing ACC laminate thickness, with the work to fracture of $1.3 \pm 0.4\,\mathrm{MJ\,m^{-3}}$ in 1 lamina increasing to $8.2 \pm 1.1\,\mathrm{MJ\,m^{-3}}$ in 8 laminae ACCs (Figure 40).

It is important to note that the biaxial weave of the cellulose precursor is a prerequisite for the observed positive size effect. The cracking of transverse yarns and crack arresting by longitudinal yarns is a vital part of the proposed strengthening mechanism with increasing number of laminae. It is likely that the positive size effect is limited to ACCs based on woven precursors and the influence of increasing dimensions on unidirectional ACCs has to be investigated independently.

4.3.7 *Initiation of failure in all-cellulose composite laminates*

The yielding of ACC laminates occurs at 1 to 2 % strain, which is similar to rayon fibres [Eichhorn et al., 2001; Adusumali et al., 2006]. The typical double-linear increase in stress with strain of regenerated cellulose fibres is due to a linear change in orientation of crystalline and amorphous domains. The disruption of interfibrillar hydrogen bonds at yield leads to a decrease in slope at higher strains [Gindl et al., 2008; Northolt and Vries, 1985]. However, the change in slope after yield is less pronounced in rayon fibres than in ACC laminates. The stress-strain curve of rayon fibres increases from ca. 300 MPa to ca. 800 MPa after yield [Adusumali et al., 2006], whereas the increase in stress plateaus after yield in ACC laminates (Figure 40). It is therefore concluded that the onset of microstructural damage in ACC laminates coincides with the yield point, confirmed by the first occurrence of microcracks in transverse yarns in Stage II (Figure 33).

Damage is expected to initiate in either the fibres, the matrix or at the interface. Splitting of fibres was only observed once and therefore transverse failure of fibres is ruled out as the dominating initiator of damage (Figure 36c). The matrix is observed to separate from fibres by microcracking (Figure 36a) and comparably brittle fracture of the unreinforced cellulose film was observed at stress and strain levels similar to the yield strength of laminates (Figures 40 and 41), suggesting that the matrix strength is reached with yield. The interfacial strength of a cellulose fibre bonded to a matrix of regenerated cellulose is not known. However, the fracture surface of ACC laminates showed no fibre pull-out (Figure 37), which indicates strong interfacial bonding [Hull and Clyne, 1996]. Unfortunately, the low contrast between fibre and matrix in SEM micrographs impedes a clear distinction between interfacial and matrix failure.

4.3.8 *Scale effects in all-cellulose composite laminates*

Sutherland et al. [1999b] point out that a scale effect, i.e. a difference in manufacturing quality between small samples and large structures, can dominate over a size effect, as shown for glass fibre-reinforced composites. All samples in this study were processed using the same equipment and great care was taken to prevent a scale effect. However, the void content and crystallinity of ACC laminates are affected by scaling. An increase of laminate thickness by increasing the number of laminae increases the likelihood of air inclusions during SIP. Hence, the higher void content of thicker laminates is considered a scale effect. The regeneration of dissolved cellulose is affected by scale, due to the reduction of diffusion rates with increased thickness, as discussed in Section 4.3.4.2. Therefore, the higher crystallinity at the core of thick laminates is also considered a scale effect.

4.4 SUMMARY

It has been demonstrated that the solvent infusion process allows the upscaled manufacture of ACC laminates without compromising their mechanical properties. Increasing the thickness of solvent infusion processed ACC laminates based on a woven textile precursor leads to a transition from failure of thin laminates (1 and 2 laminae) at comparatively low strains and stresses to a macroscopically ductile behaviour of thick laminates (4 and 8 laminae) with failure at higher stress and strain levels and a six-fold increase in work to fracture.

The increase of ultimate tensile strength with increasing laminate thickness is due to a combination of scale and size effects. The positive size effect

of increasing ultimate tensile strength is attributed to a higher damage tolerance of thick laminates. Stress redistribution upon cracking of transverse yarns and crack arresting by longitudinal yarns allow damage accumulation in thick laminates, which results in global strain delocalisation, increased ductility and higher ultimate tensile strength.

Increasing the thickness of ACCs by the addition of laminae leads to a higher void content in thick laminates. This increase in void content is a scale effect that contributes to the strengthening mechanism, as transverse cracking initiates from voids. A further scale effect is the increase in cellulose crystallinity at the core of thick laminates due to a decreased rate of regeneration with increased laminate thickness.

5

SOLVENT INFUSION PROCESSING USING AQUEOUS SODIUM HYDROXIDE/UREA SOLUTION

5.1 INTRODUCTION

SIP facilitates the production of thick laminates, as demonstrated in Chapter 4, and is a promising candidate for upscaled manufacturing of ACCs. SIP was initially explored using the IL BmimAc as cellulose solvent [Huber et al., 2012a]. However, there is substantial evidence of the toxicity of imidazolium based ILs for unicellular organisms [Ranke et al., 2004], aquatic life [Bernot et al., 2005; Zhao et al., 2007] and terrestrial plants and invertebrates [Jastorff et al., 2005; Matzke et al., 2007]. In combination with the non-biodegradable character of ILs [Romero et al., 2008], potential environmental concerns arise if ILs were to be used for processing ACCs on an industrial scale. It is therefore desirable to use alternative solvents for the manufacture of ACCs.

A solvent for industrial scale manufacture of ACCs ideally facilitates cellulose dissolution without pretreatment in a short time, while having a low environmental impact and being cost efficient. A class of cellulose solvents that meets these criteria are NaOH-based aqueous solutions with additives such as urea to enhance cellulose solubility. In contrast to synthesised ILs, both NaOH and urea occur naturally. Urea is a product of the liver when metabolising protein, it is excreted through urine and has a very low toxicity [Reece

et al., 2013]. NaOH occurs e.g. in limestone and does not produce systemic toxicity [ATSDR, 2014]. For instance, NaOH is part of the action potential in neuronal activity in the human body and only dangerous due to its tissue corrosiveness at high concentrations. Hence, NaOH does not impose health risks at low concentrations in aqueous solution and is used for preparing alkaline drinking water [Whang, 1994].

Various methods of dissolving cellulose in NaOH-based solvents have been described. Firstly, Isogai and Atalla [1998] dispersed cellulose in an aqueous 9 wt.% NaOH solution at room temperature to first swell the cellulose. Subsequently, dissolution was achieved by freezing the solution at -20 °C and then diluting the thawed solution with water to attain a concentration of 5 wt.% NaOH. Secondly, Qi et al. [2011] describe a two-step procedure consisting of dispersing cellulose in a 14 wt.% NaOH solution precooled to 0 °C followed by adding a 24 wt.% urea solution, resulting in an aqueous 7 wt.% NaOH/ 12 wt.% urea solution, while stirring vigorously. Thirdly, several studies report direct dissolution in a single step by adding cellulose to aqueous 7 wt.% NaOH/12 wt.% urea or 8 wt.% NaOH/ 8 wt.% urea/ 6.5 wt.% thiourea solution precooled to -12 °C and stirring the mixture [Jin et al., 2007; Qi et al., 2008a; Qin et al., 2012].

The highest solubility of cellulose in NaOH-based solvents (7.6 wt.%, cotton linter pulp, DP520) is achieved with an aqueous 8 wt. % NaOH/ 6.5 wt. % thiourea/ 8 wt. % urea solution [Jin et al., 2007]. However, the solubility-enhancing compound thiourea is carcinogenic and toxic [McCann et al., 1975; Dieke et al., 1947], which is the reason for the choice of solvent used in this study being 7 wt.% NaOH/12 wt.% urea aqueous solution, which can dissolve cellulose concentrations of up to 6.5 wt.% (cotton linter pulp, DP 580) in times as short as 2 min [Qi et al., 2008a; Qin et al., 2012].

An aqueous solution of 7 wt.% NaOH/12 wt.% urea appears promising for industrial scale manufacture of ACCs due to its low environmental impact, low cost, no necessary pretreatment of the cellulose precursor and short dissolution times of 2 to 5 min [Cai and Zhang, 2005; Qi et al., 2008a]. Processing of ACCs using NaOH/urea solvents has thus far been limited to the 2-step method [Qi et al., 2009; Wang and Chen, 2011; Pullawan et al., 2014; Yang et al., 2010].

In this chapter, the use of an aqueous solution of 7 wt.% NaOH/12 wt.% urea (NaOH/urea) for 1-step processing of ACC laminates *via* SIP is explored. The influence of the infusion temperature, cooling conditions during infusion and dissolution time on the structure and mechanical properties of ACC laminates were investigated, in order to find the optimum processing conditions for 1-step processing of regenerated cellulose fibres to ACCs. The microstructure, mechanical properties and fine structure of ACC laminates were characterised by tensile testing, SEM, WAXD and FTIR. ACC laminate preparation by SIP was also compared to a simple immersion technique in NaOH/urea.

5.2 EXPERIMENTAL PROCEDURES

5.2.1 *Preparation of all-cellulose composite laminates by solvent infusion*

Solvent infusion processing was performed as described by Huber et al. [Huber et al., 2012a] and in Section 3.2, with modifications to accommodate the requirements of aqueous NaOH/urea solution. The rayon textile was cut in strips of 120 mm width and 100 mm length (the infusion direction was parallel to the shorter length, along the weft direction of the textile) and two

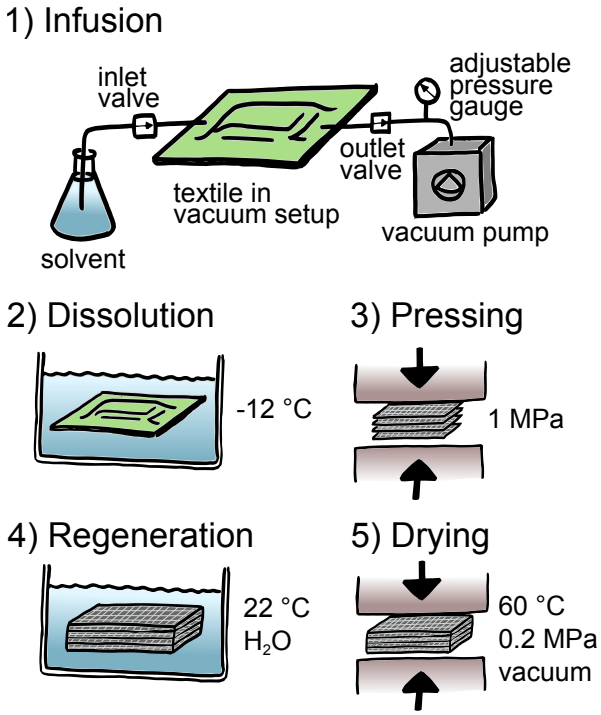

Figure 44: Processing steps of solvent infusion processing (SIP) using aqueous NaOH/urea solution as solvent.

layers stacked symmetrically to form a laminate stack which was then sealed with a vacuum bag. The same infusion setup as described for IL was used (Figure 44) and a vacuum of 200 mbar applied for infusion, unless specified otherwise.

The solvent and infusion setup with sealed laminate stack were equilibrated to the specified infusion temperature prior to infusion. The temperature during infusion was monitored by wire thermocouples (K-type, fresh wire ends were exposed for every infusion experiment to avoid effects of corrosion) positioned beneath the laminate stack, 5 mm from the edge of the laminate at both the inlet and outlet position. In contrast to SIP using IL, where partial dissolution is achieved by hot pressing, the laminate stack infused with NaOH/urea was placed in a 10 l cooling bath at -12 °C for the designated dissolution time. Dissolution was followed by the determination of solvent uptake. The laminate stack was then pressed at 1 MPa for 15 min

at 20 ± 2 °C, followed by regeneration, washing, and drying as described for IL in Section 3.2.

Specimens for SEM and tensile testing were cut with a sharp blade prior to drying. Tensile tests were performed on rectangular coupons with a length and width of 100 and 10 mm, respectively, at a gauge length of 40 mm.

5.2.2 *Optimisation of processing parameters*

The effects of the processing parameters infusion temperature, cooling during infusion and dissolution time were investigated and laminate performance optimised in three stages (Figure 45). Established dissolution procedures for cellulose in NaOH based solvents use temperatures of 20 °C [Isogai and Atalla, 1998], 0 °C [Qi et al., 2011] or -12 °C [Qin et al., 2012; Jin et al., 2007] when cellulose and solvent are mixed. Consequently, in Stage I the effect of infusion temperature was investigated by equilibrating the temperature of both the solvent and the sealed laminate stack to 20, 0 and -12 °C, respectively, prior to infusion. SIP was then performed at ambient conditions (20 ± 2 °C) and the infused setup placed in the cooling bath controlled at -12 °C for a dissolution time of 30 min (referred to as precooled/ambi-

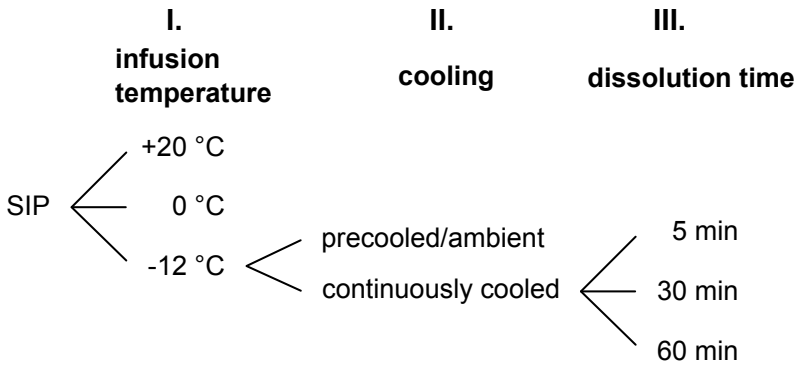

Figure 45: Schematic of the three stages of optimisation of the processing parameters for SIP using NaOH/urea.

ent SIP). In Stage II, the effect of continuous cooling during infusion was investigated by placing a flexible plastic bag ($200 \times 250\,mm^2$) filled with an aqueous ethylene glycol solution precooled to -12 °C over the top of the sealed laminate stack (referred to as continuously cooled SIP). In Stage III the influence of dissolution time was investigated by placing laminates infused at -12 °C with continuous cooling in the cooling bath for 5, 30 or 60 min, designated as SIP-5, SIP-30 and SIP-60, respectively.

5.2.3 *Solubility of rayon in aqueous sodium hydroxide/urea solution*

As a comparison to partial dissolution *via* SIP, the solubility of rayon fibres in NaOH/urea was determined in classical dissolution experiments carried out using the protocol of Qin et al. [2012]. The rayon fibres were cut into short fragments (~ 2 mm), dried at 90 °C in a vacuum oven for 12 h and their dry mass measured with a laboratory balance (ED2249, accuracy 0.1 mg, Sartorius AG, Göttingen, Germany). Prior to dissolution, the dry rayon was sealed in a glass container to prevent moisture uptake and precooled to -12 °C in a freezer. NaOH/urea was cooled to -12 °C in a cooling bath. 7 wt.% cellulose was added to the solvent and dissolution was carried out in a 200 ml glass beaker submerged in a 2 l cooling bath at a temperature of -12 °C. Maximum dissolution was achieved by stirring the solution with an overhead stirrer (Eurostar power-b, IKA-Werke, Staufen, Germany) at 2000 rpm for 5 min, as stated by Qin et al. [2012]. Subsequently, the cellulose-solvent mixture was divided into 4 equal parts and centrifuged at 3000 rpm for 10 min for degassing and separation of the dissolved and undissolved cellulose portions. The fully dissolved cellulose solutions were poured into individual Petri dishes and subsequently regenerated and washed in distilled water for 48 h, followed by drying under vacuum at 90 °C until mass

losses ceased. These cellulose samples provided 4 replicates for measuring the solubility of rayon in NaOH/urea.

The mass percentage of dissolved rayon $m_{dissolved}$ in the solution is given by

$$m_{dissolved} = \frac{m_{dry}}{m_{solution}} \times 100, \tag{8}$$

where m_{dry} is the mass of dissolved, centrifuged, regenerated and dried rayon and $m_{solution}$ the total mass of solution poured into a Petri dish after centrifugation. The solubility S is given by the ratio of dissolved rayon $m_{dissolved}$ to the dried rayon added initially $m_{initial}$,

$$S = \frac{m_{dissolved}}{m_{initial}} \times 100. \tag{9}$$

5.2.4 *Preparation of unreinforced cellulose films*

Unreinforced cellulose films were prepared as described in more detail in Section 3.3. Briefly, a 5 wt.% cellulose solution in NaOH/urea was obtained following the protocol of Qin et al. [2012] as described for the solubility experiments, cast into rectangular moulds of porous PTFE and regenerated in distilled water, followed by washing and drying. Tensile tests were performed on rectangular strips with a length and width of 30 and 4 mm, respectively, at a gauge length of 16 mm.

5.2.5 *Preparation of all-cellulose composite laminates by immersion*

Processing of ACC laminates *via* SIP was compared to a simple immersion routine. 150 g of NaOH/urea was precooled in a glass container in a cool-

ing bath at -12 °C. Two individual laminae were immersed in the solvent and a nylon mesh placed on top to ensure the textile was fully immersed throughout the dissolution time of 30 min. Subsequently, the wet laminae were aligned, stacked and pressed at 1 MPa for 15 min at 21 ± 2 °C, followed by the same routine of regeneration, washing, drying and specimen preparation as SIP samples.

5.3 RESULTS AND DISCUSSION

Thick and dimensionally stable ACC laminates were obtained by SIP using NaOH/urea as solvent. However, the microstructure and mechanical properties of the laminates processed with NaOH/urea varied substantially with processing conditions. Optimisation of the parameters infusion temperature, cooling during infusion and dissolution time resulted in overall shorter processing and dissolution times required to produce ACC laminates with higher mechanical properties when compared to using IL for SIP, as discussed in the following sections.

5.3.1 *Effect of infusion temperature*

When SIP was performed using NaOH/urea at 20 °C, swelling of the textile was observed immediately after coming in contact with the solvent. The textile swelled to such an extent, that further flow of the solvent was prevented. Thus, infusion was limited to the first 2 to 3 cm of the textile. In contrast, the laminate stack was thoroughly wetted when the infusion was carried out at 0 or -12 °C. The low viscosity of aqueous NaOH/urea solution resulted in

Table 5: Influence of the infusion temperature and external cooling of the laminate stack during infusion on tensile properties of ACC laminates. The dissolution time was 30 min for all laminates (# precooled/ambient, $*$ continuously cooled).

Infusion temperature	Young's modulus in GPa	Yield strength strength in MPa	Ultimate tensile strength in MPa	Strain at break in %
0 °C, #	3.2 ± 1.1	24.8 ± 5.1	85.3 ± 7.9	14.1 ± 1.1
-12 °C, #	6.0 ± 0.3	46.6 ± 4.9	97.3 ± 5.6	14.3 ± 2.2
-12 °C, $*$	6.8 ± 0.3	58.0 ± 2.7	107.2 ± 3.8	12.5 ± 2.0

rapid infusion of the textile, with infusion distances of ~ 100 mm achieved in less than 1 min, compared to more than 10 min when using the IL BmimAc.

The infusion temperature strongly influenced the microstructure of the ACC laminates. Large voids of ~ 10 µm width and more than 100 µm length appeared in the laminates infused at 0 °C and consolidation of individual fibres by matrix was limited (Figure 46). In contrast, ACCs infused at -12 °C exhibited an evenly consolidated cross section with fewer and smaller cracks than laminates infused at 0 °C (Figure 47a). Infusion at -12 °C created a 1 to 3 µm thick layer of regenerated cellulose matrix surrounding individual fibres, indicating successful partial dissolution (Figure 47c). However, some interlaminar voids (up to 300 µm long and 100 µm wide) were found and a few yarns seemed incompletely infused, resulting in unconsolidated fibres at the core of yarns (Figure 47b). There was no apparent difference in microstructure between cross sections parallel and perpendicular to the infusion direction.

A tensile strength of 85.3 ± 7.9 MPa and Young's modulus of 3.2 ± 1.1 GPa was measured for the laminate infused at 0 °C. Decreasing the infusion temperature to -12 °C increased the tensile strength and Young's modulus to 97.3 ± 5.6 MPa and 6.0 ± 0.3 GPa, respectively (Table 5).

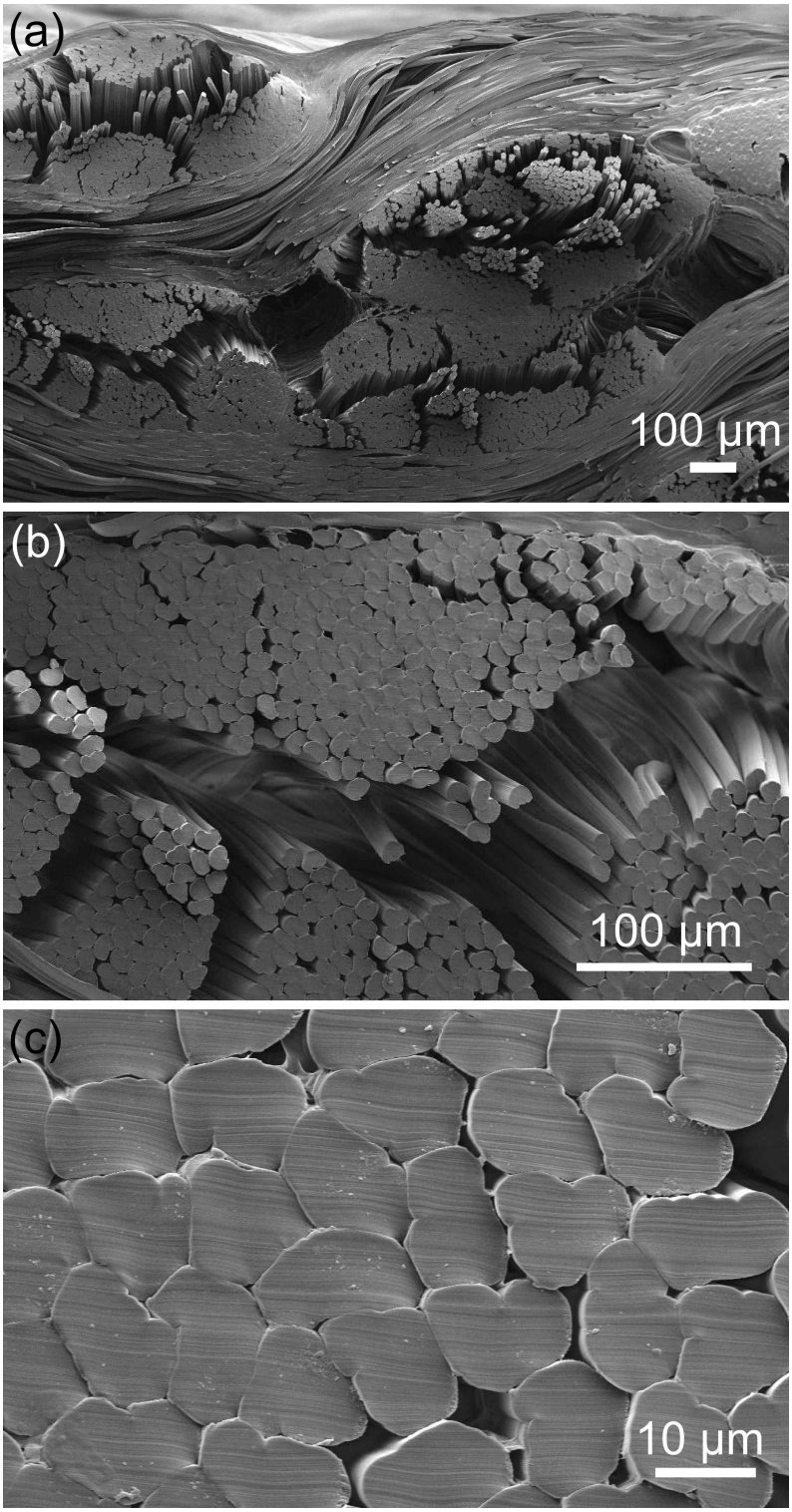

Figure 46: Scanning electron micrographs of the cross section of an ACC laminate prepared by SIP using NaOH/urea infused at 0 °C and dissolved for 30 min.

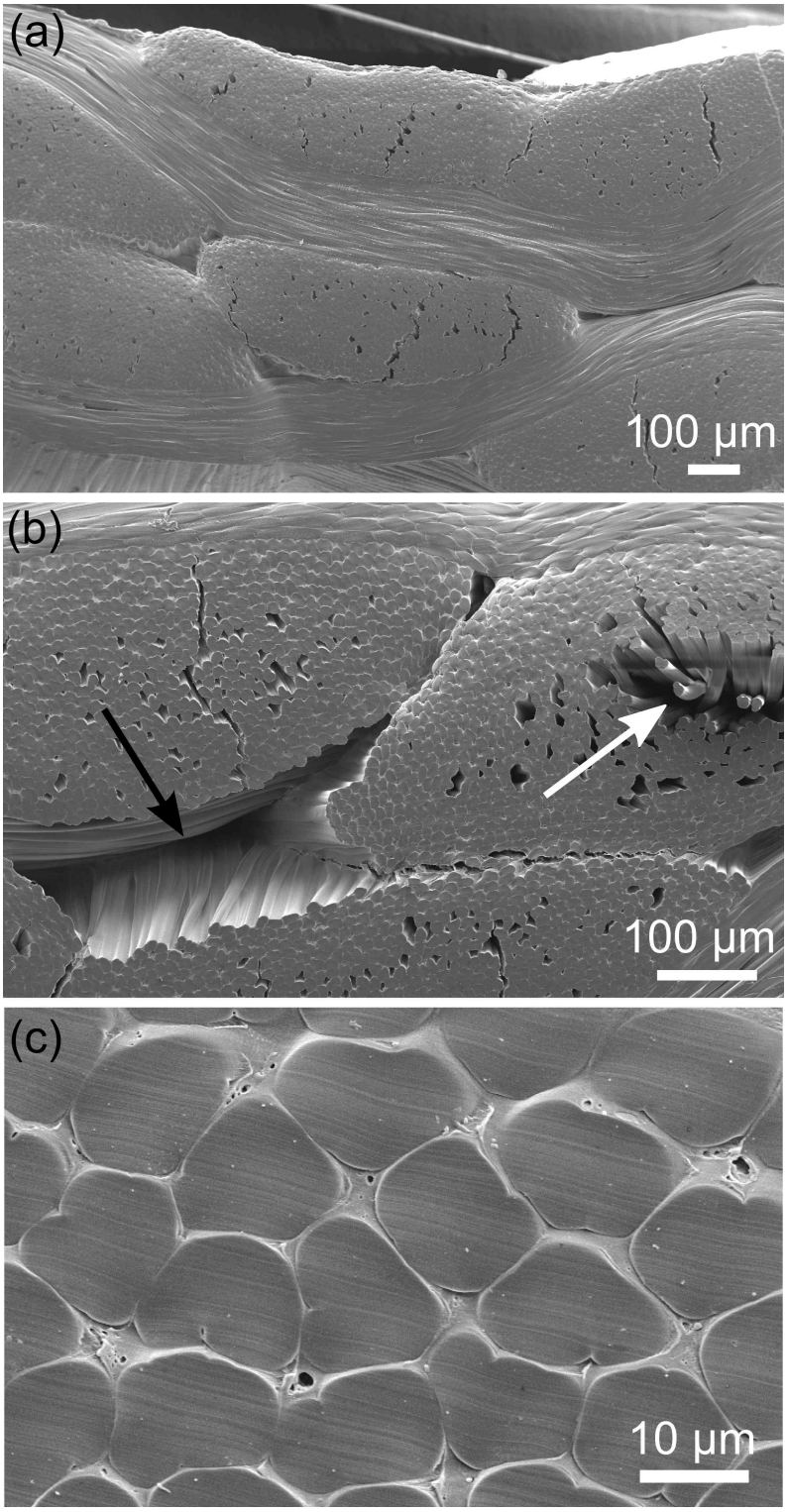

Figure 47: Scanning electron micrographs of the cross section of an ACC laminate prepared by SIP using NaOH/urea infused at -12 °C and dissolved for 30 min. An interlaminar void and an incompletely infused core of a yarn with loose fibres are indicated by a black and a white arrow, respectively, in (b).

Concluding from the results above, the 2-step procedure for dissolving cellulose in NaOH/urea described by Qi et al. [2011] may be adaptable to SIP as it is carried out at 0 °C. However, it is not deemed amenable for adaptation as a first infusion with NaOH-solution would have to be followed by a second infusion with urea-solution, which extends processing times and may result in washing out the NaOH-cellulose complex. The dissolution procedure described by Isogai and Atalla [1998] (dispersing cellulose in NaOH solution at room temperature and subsequently freezing the mixture for dissolution) does not translate to SIP, due to the excessive swelling of the textile at 20 °C. Hence, the strategy of SIP using IL, where the infusion is performed at temperatures at which the solvent has no or very low cellulose solubility and partial dissolution is achieved in a subsequent step [Huber et al., 2012a], cannot be followed when using NaOH/urea. Consequently, a direct dissolution procedure in the temperature range from 0 to -12 °C [Jin et al., 2007; Qi et al., 2008a; Qin et al., 2012] is identified as compatible with SIP. The more homogeneous microstructure, improved consolidation and higher mechanical properties of ACC laminates infused at -12 °C are attributed to the increase in cellulose solubility in NaOH/urea from 18 % at 0 °C to 100 % at -12 °C [Qi et al., 2008a]. However, performing SIP with NaOH/urea at low temperatures (0 and -12 °C) with immediate dissolution of the cellulose reinforcement has further implications on sample homogeneity that are discussed in the following section.

5.3.2 *Effect of continuous cooling during infusion*

The yield strength and Young's modulus of ACCs decreased with increasing distance from the inlet for laminates prepared by SIP performed precooled to 0 or -12 °C and infused in an ambient environment (precooled/ambient,

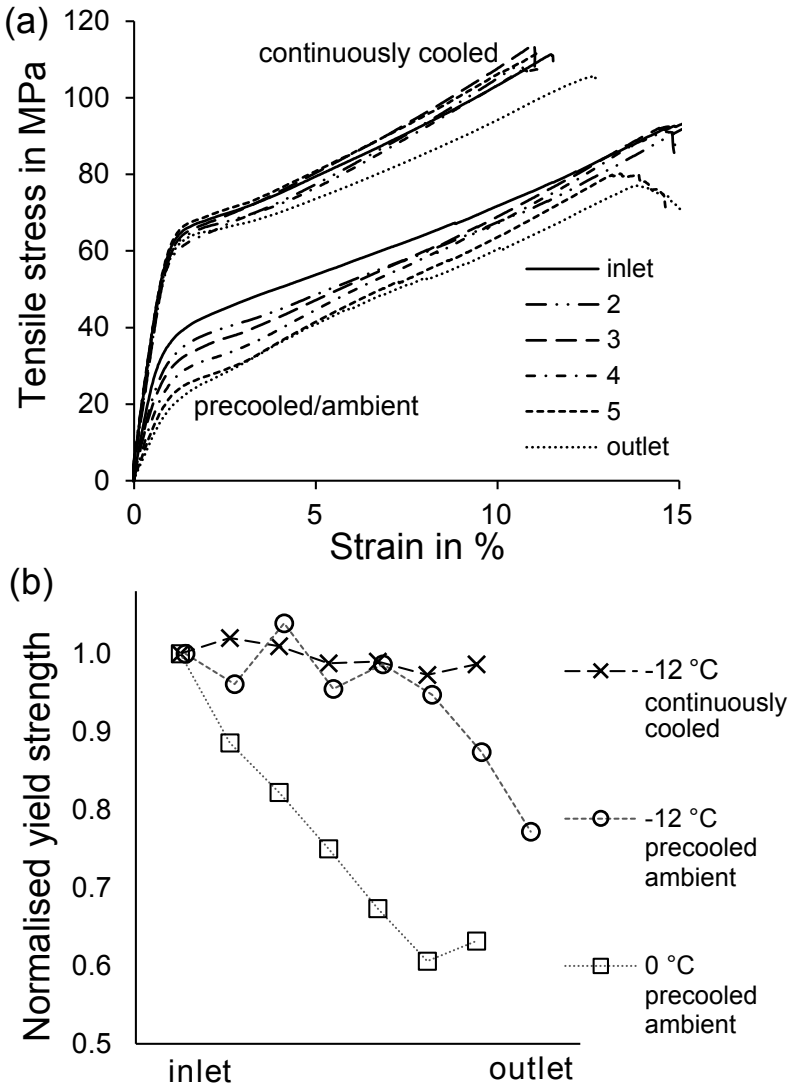

Figure 48: (a) Overlay of stress-strain curves as a function of distance from inlet to outlet of ACC laminates processed by 0 °C precooled/ambient SIP and -12 °C continuously cooled SIP, both prepared with a dissolution time of 30 min. (b) Normalised tensile yield strength as a function of distance from the inlet to outlet, for 0 °C and -12 °C precooled/ambient and -12 °C continuously cooled SIP with a dissolution time of 30 min (Results were normalised to the respective inlet value).

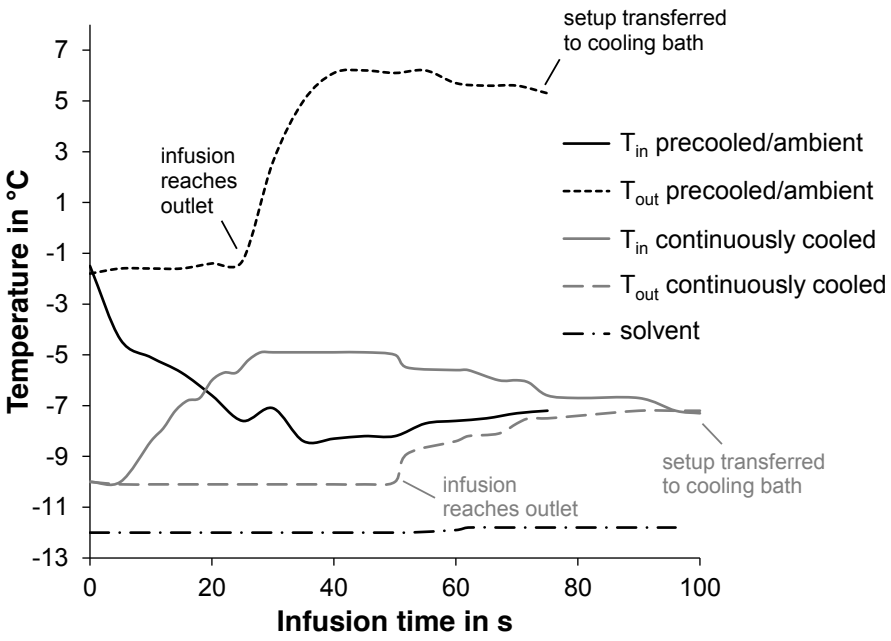

Figure 49: Temperature of the solvent and T_{in} and T_{out} as a function of infusion time during precooled/ambient (black) and continuously cooled SIP (grey).

Figure 48a). For 0 °C precooled/ambient SIP, the yield strength decreased linearly by 40 % from 33.4 MPa at the inlet to 20.3 MPa at the outlet (Figure 48b). This variation in mechanical properties was found to be caused by temperature variations in the laminate stack when comparing the temperature of the laminate stack at the inlet (T_{in}) and outlet (T_{out}) of the SIP setup (Figure 49). However, it was found that this variation in temperature could be minimised by continuously cooling the laminate stack during infusion, in order to maintain a constant temperature.

When performing -12 °C precooled/ambient SIP, the temperature of the precooled laminate stack increased from -12 °C to -2 °C within the approximately 3 min required to begin the infusion process after precooling (Figure 49). The solvent reached the outlet after 35 s, upon which the valves were closed and the setup was then transferred to the cooling bath for dissolution after 70 s. T_{in} decreased from -2 °C to -8 °C within the first 35 s of infusion, and then increased after the solvent flow was stopped, until the

setup was transferred to the cooling bath. T_{out} was constant at -2 °C for 35 s, followed by a rapid increase from -2 °C to +6 °C upon the solvent reaching the outlet (Figure 49).

In contrast, T_{in} and T_{out} remained at -10 °C until the beginning of the infusion process during continuously cooled SIP. Infusion reached the outlet end of the laminate stack after 45 s and the setup was transferred to the cooling bath after 95 s. T_{in} increased from -10 °C to -5 °C within the first 30 s of infusion followed by a decrease after 45 s when solvent flow was stopped. T_{out} remained constant at -10 °C for 45 s and increased to -7 °C upon the solvent reaching the outlet end of the laminate stack (Figure 49).

The increase in temperature during SIP is attributed to two factors: Warming from exposure to the ambient temperature and the exotherm that arises from dissolving cellulose in NaOH/urea [Wang, 2008]. In precooled/ambient SIP, ambient warming of the setup is significant before infusion, as evidenced by the increase in T_{in} and T_{out} from precooled -12 to -2 °C prior to starting infusion. However, ambient warming is assumed to be insignificant during infusion, since T_{out} remained constant in precooled/ambient SIP until the solvent reached the outlet (Figure 49).

The exotherm of cellulose dissolution appears to be significant, as in precooled/ambient SIP T_{in} decreases during infusion due to the flow of fresh, precooled solvent that has not been in contact with cellulose yet, but the solvent flow front warms by 18 °C over the length of the laminate stack from the precooled -12 °C to the +6 °C peak in T_{out}. In continuously cooled SIP the exotherm is also evidenced by the increase in temperature from precooled -12 °C to maximum temperatures of -5 and -7 °C in T_{in} and T_{out}, respectively. However, continuous cooling counteracts the exotherm due to cellulose dissolution and limits the warming to a difference of 7 °C between the

precooled -12 °C and the -5 °C peak in T_{in} in contrast to an increase of 18 °C in precooled/ambient SIP (Figure 49).

The decrease in mechanical properties and low repeatability of the stress-strain curve in laminates infused without cooling (Figure 48) are related to the increase in temperature of the aqueous NaOH/urea solution due to the exothermic dissolution of the cellulose reinforcement (Figure 49). The solubility of cellulose in aqueous NaOH/urea solution strongly depends on temperature. Qi et al. report that solubility is highest at the freezing point of -12.6 °C, is reduced to 50 % at -6 °C and to 18 % at 0 °C and almost no dissolution occurs at temperatures above 10 °C [Qi et al., 2008a]. As the temperature of the laminate stack during infusion without cooling varied from -8 °C at the inlet to up to +6 °C close to the outlet, the solubility consequently varied from high at the inlet to very limited at the outlet. Consequently, the amount of matrix created by partial dissolution also varied from high at the inlet to comparably low at the outlet.

The application of external cooling maintained the temperature below -5 °C (Figure 49), which kept the laminate stack within the temperature range that allows dissolution in NaOH/urea [Qi et al., 2008a]. Therefore, the cellulose textile was partially dissolved over the full length of the laminate stack. Consequently, a constant yield strength and repeatable stress-strain behaviour across the length of the laminate was achieved by continuously cooled SIP (Figure 48). Optimisation of the cooling setup to keep the laminate stack at the optimum dissolution temperature of -12.6 °C throughout the infusion process may lead to further improvements in structural homogeneity and mechanical properties. A potential setup is discussed in Chapter 8.

5.3.3 *Effect of dissolution time on the microstructure*

Image analysis revealed a trend of increasing matrix fraction (V_m) with increasing dissolution time from 3.8 ± 1.5 % in SIP-5 to 4.6 ± 1.2 % in SIP-60, although the results show relatively large scatter. The void fraction (V_v) as measured by image analysis was found to increase with increasing dissolution time from 0.8 ± 0.4 % to 4.5 ± 2.9 % in SIP-5 and SIP-60, respectively. V_v based on density was generally found to be higher when compared to image analysis and also increased from 4.2 ± 0.6 % to 6.6 ± 0.7 % for SIP-5 and SIP-60, respectively. Density decreased with increasing dissolution time from 1.457 ± 0.010 g cm^{-3} in SIP-5 to 1.420 ± 0.011 g cm^{-3} in SIP-60 (Table 6).

Qin et al. [2008] report that maximum cellulose solubility in 7 wt.% NaOH/ 12 wt.% urea is reached within 3 to 5 min when stirring. However, solubility depends on stirring efficiency and longer dissolution times of 10 min are necessary to reach maximum solubility at low stirring rates of 300 rpm when compared to high stirring rates of > 1700 rpm [Qin et al., 2008]. In the solubility experiments of the present study (-12 °C, stirring at 2000 rpm) a clear solution of fully dissolved rayon fibres in NaOH/urea was obtained within a dissolution time of 5 min.

Table 6: Variation of void and matrix fraction and density of ACC laminates with increasing dissolution time.

	V_m (image) in %	V_v (image) in %	V_v (density) in %	Density in g cm^{-3}
SIP-5	3.8 ± 1.5	0.8 ± 0.4	4.2 ± 0.6	1.457 ± 0.010
SIP-30	5.4 ± 2.5	3.2 ± 1.4	6.2 ± 0.3	1.426 ± 0.005
SIP-60	4.6 ± 1.2	4.5 ± 2.9	6.6 ± 0.7	1.420 ± 0.011

Table 7: Solubility of rayon fibre (Cordenka) in NaOH/urea aqueous solution.

Initial cellulose concentration	7 wt.%
Cellulose concentration in solution	5.7 ± 0.1 wt.%
Solubility of added cellulose	82.5 ± 1.1 %

The cellulose concentration in the solution was 5.7 wt.%, equalling a solubility of 82.5 % of the initial cellulose concentration of 7 wt.% (Table 7). The cellulose fraction in solution of 5.7 wt.% is comparable to values reported for dissolution of cotton linters in 7 wt.% NaOH/12 wt.% urea, which range from 4 wt.% reported by Qi et al. [2008a] to 5.4 wt.% and 6.5 wt.% reported by Jin et al. [2007] and Qin et al. [2008], respectively.

Cellulose solubility in NaOH/urea increases with decreasing degree of polymerisation and with decreasing crystallinity [Isogai and Atalla, 1998; Qi et al., 2008a; Jin et al., 2007]. Furthermore, a higher solubility of regenerated cellulose II is observed when compared to cellulose I and mercerised cellulose II of the same crystallinity [Isogai and Atalla, 1998]. The relatively high solubility of rayon (Cordenka) in this study can therefore be attributed to the cellulose II polymorph, comparatively low DP of 440 [Schuermann, 2014], and low crystallinity of 33 %.

SIP led to an average solvent uptake of 97.8 ± 13.7 %, resulting in a 1:1 ratio of cellulose to solvent in the infused laminate stack. Consequently, the maximum V_m of ACCs that can theoretically be achieved by partial dissolution is approximately equal to the 5.7 wt.% obtained in the solubility experiment. The maximum V_m in the ACC laminates was found to be 5.4 ± 2.5 % for SIP-30. Hence, a similarly high cellulose solubility is achieved by SIP and conventional dissolution in a beaker. However, a longer dissolution time of 30 min is necessary to reach the maximum in SIP, due to the fact that stirring is not possible within the vacuum setup.

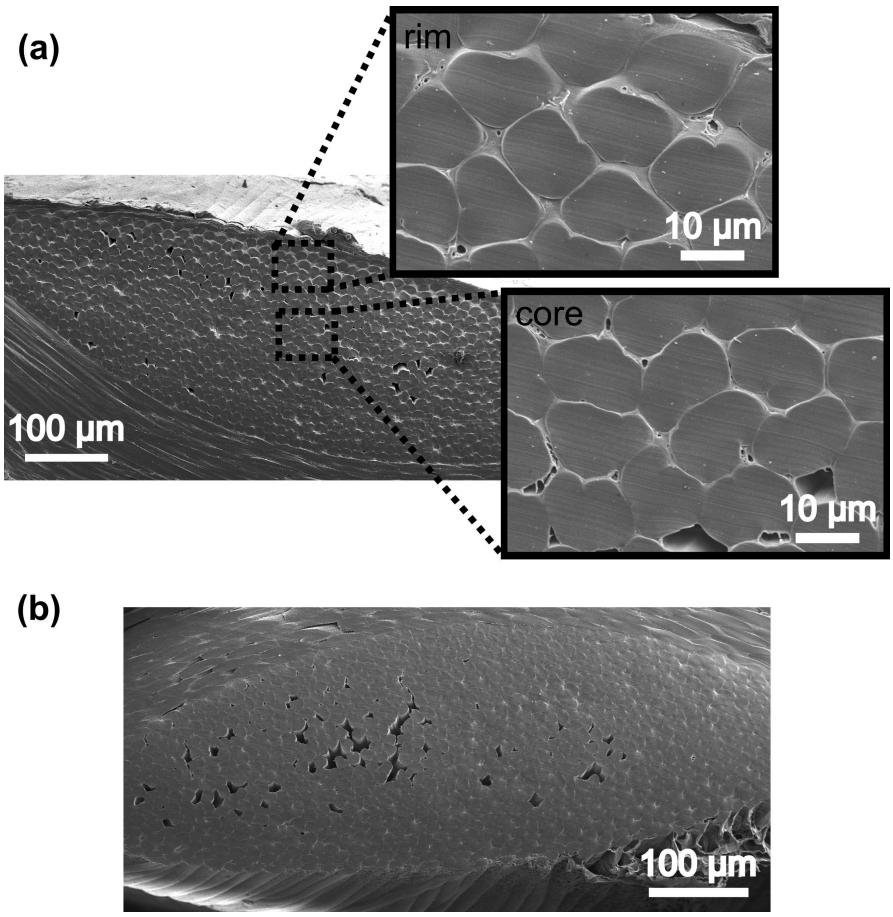

Figure 50: Scanning electron micrographs of ACC laminate cross sections. (a) Matrix content varied from high in the rim to low in the core of a yarn (SIP-5). (b) Voids were typically found in the core of a yarn (SIP-30).

A variation in V_m within the cross section of yarns was found. V_m was higher in the rim, when compared to the core of yarns (Figure 50). This variation is a consequence of the necessity to perform SIP at low temperatures that allow direct dissolution of cellulose in NaOH/urea, as discussed above. During infusion, the solvent flows along the surface of the textile and through gaps in the weave pattern initially and subsequently penetrates yarns. Interaction of the solvent with the fibres in the rim of a yarn will lead to local dissolution and swelling, impeding the flow of solvent into the core. The higher solvent uptake in the rim consequently results in a higher V_m when compared to the core of a yarn. The large scatter in the V_m results is

also due to this variation, as a collection of high magnification images from locations in both the rim and the core were analysed.

The increase of V_v and simultaneous decrease in density with increasing dissolution time may be due to a slow loss of vacuum pressure after the setup is disconnected from the vacuum pump and immersed in the cooling bath. The majority of voids was found in the core of yarns, probably due to small volumes of air that have not been replaced by solvent, being trapped in the core of yarns and expanding with the increase in pressure. The resulting gap between fibres cannot be bridged by the matrix, as the V_m of 3.8 to 5.4 % in ACCs is low when compared to composites with thermoplastic or thermoset matrices, where V_m is in the range of 30 to 50 % [Almeida and Neto, 1994; Madsen and Lilholt, 2003].

5.3.4 *Effect of dissolution time on the fine structure of cellulose*

As expected, the WAXD diffractograms of all samples produced diffraction peaks at 2θ of 12.3, 20, 22 and 35° (Figure 51a) that are assigned to the diffracting planes $(1\bar{1}0)$, (110), (020) and (004) of cellulose II [French, 2014]. The FTIR spectra also exhibited characteristics of cellulose II, with the typical peak of cellulose I at 1430 cm^{-1} shifted to 1420 cm^{-1} (CH_2 scissoring at C(6)), no appreciable band at 1110 cm^{-1} (ring asymmetric valence in cellulose I) and a strong band at 893 cm^{-1} (deformation at C(1) in cellulose II), as is typical for regenerated cellulose fibres (Figure 52) [Colom and Carrillo, 2002; Carrillo et al., 2004; Široký et al., 2010a]. It is concluded, that the cellulose II polymorph known for rayon fibres [Röder et al., 2009] remains unchanged with processing into ACC laminates.

The crystallinity of the ACC laminates was found to increase with increasing dissolution time, evident from the increasing height and sharpness of the

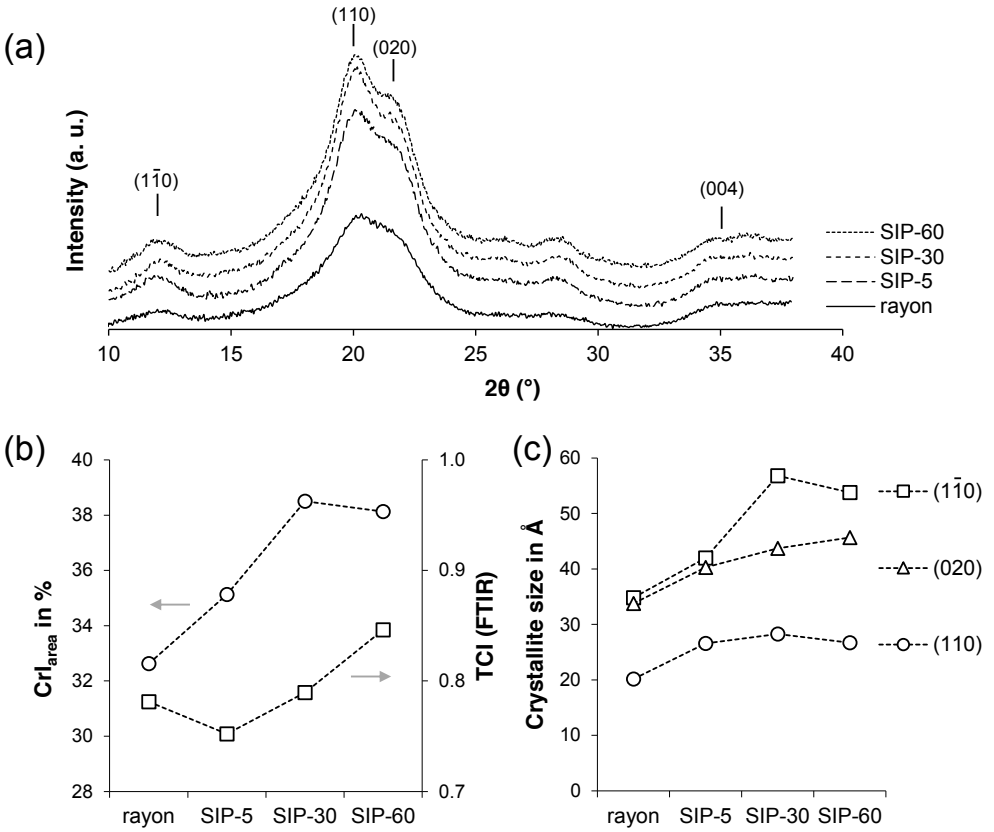

Figure 51: (a) Plots of WAXD intensity as a function of 2 θ for the as-received rayon textile and ACC laminates (diffractograms are vertically shifted for clarity). (b) Crystallinity determined by WAXD and TCI determined by FTIR as a function of dissolution time. (c) Crystallite size calculated from the WAXD diffractograms as a function of dissolution time.

diffraction peaks. The crystallinity increased from 32.6 % in the as-received rayon to 38.1 % in the ACC laminate SIP-60 (Figure 51b). A pronounced increase in crystallite size from 35.8 to 53.8 Å in the (1$\bar{1}$0) plane and from 33.8 to 45.7 Å in the (020) plane was observed for as-received rayon and SIP-60, respectively, while growth in the (110) plane was less pronounced (Figure 51c). The TCI calculated from FTIR spectra also increased from 0.78 for the as-received rayon to 0.85 for SIP-60 (Figure 51b), due to changes in the FTIR bands at 1372 cm^{-1} (C-H bending) and 2900 cm^{-1} (C-H and CH_2 stretching, Figure 52).

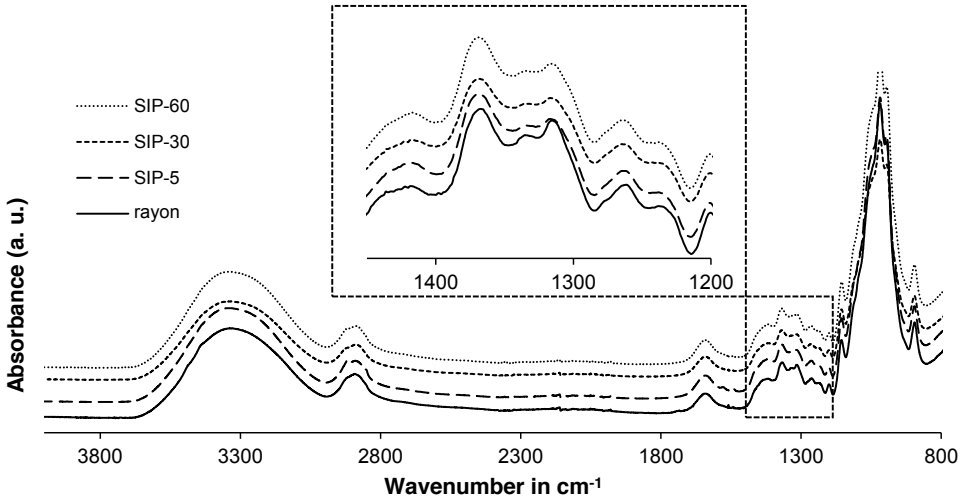

Figure 52: Area-normalised plots of FTIR spectra of the as-received rayon textile and ACC laminates (spectra are vertically shifted for clarity).

The finding of an increased crystallinity after processing fibres to ACCs (Figure 51b) is contrary to several studies in the literature [Nishino et al., 2004; Gindl-Altmutter et al., 2012; Soykeabkaew et al., 2008; Arévalo et al., 2010]. Gindl-Altmutter et al. [2012] found a decreased crystallinity in ACCs prepared from flax (78 % to 66 %) and from lyocell fibres (72 % to 63 %) following partial dissolution in the IL BmimCl. Soykeabkaew et al. [2008] observed a linear decrease of crystallinity with dissolution time of partially dissolved ramie fibres. Crystallinity was found to decrease by ca. 20 % in the first 2 h and dropped by ca. 50 % within 6 h of dissolution in LiCl/DMAc. Similarly, Arévalo et al. [2010] report a decrease in crystallinity of cotton fibres from 80.6 to 66.1, 41.4 and 22.2 % within dissolution times of 6, 12 and 18 h, respectively, in LiCl/DMAc.

It has to be noted that the rayon used in this work has a relatively low crystallinity (ca. 30 %) when compared to the cellulosic fibres used in other studies on ACCs prepared by partial dissolution (70 to 80 %). Therefore, the cellulose precursor contains a comparably large fraction of amorphous domains, which are more easily dissolved than crystalline domains and can

crystallise upon regeneration or directly recrystallise without having been dissolved due to swelling during washing and exposure to heat (60 °C) upon drying.

Firstly, the structure of cellulose can be altered by swelling in water or treatment with aqueous NaOH solutions and drying. Kouris et al. [1958] report that the crystallinity of dissolving grade softwood pulp with an initial crystallinity of 70 %, was restored to 50 % crystallinity by wetting in water for 24 h and drying at 105 °C after complete amorphisation to 0 % crystallinity by Wiley-milling. Ioelovich et al. [1983] also show that amorphised cellulose (CrI 15 %) recrystallises in the presence of a plasticiser, such as water, glycerol or ethylene glycol. Higher plasticiser contents and higher temperature result in more extensive recrystallisation. Wetting amorphous cellulose with water at 20 °C resulted in restoring a crystallinity of 40 % [Ioelovich et al., 1983]. Öztürk et al. [2008] report an increase in crystallinity of regenerated fibres (Lyocell) from 50.5 % to 56.9 % following immersion of the fibres in an aqueous 8 wt.% NaOH solution at room temperature for 2 h, washing in tap water and drying at 60 °C for 1 h. Several other studies also report crystallisation effects in regenerated cellulose fibres following immersion in water [Ibbett et al., 2007b] or swelling in aqueous NaOH solutions (6 to 12 wt.% NaOH at 20 °C) and washing with distilled water followed by drying [Colom and Carrillo, 2002; Ibbett et al., 2007a]. The increase in crystallinity is attributed to the mobilisation of cellulose molecules due to the disruption of hydrogen bonds upon swelling [Colom and Carrillo, 2002; Sreenivasan et al., 1988]. Furthermore, Öztürk et al. state that interfibrillar swelling pushes the fibrils closer to each other, which makes an increase in crystallite size and perfection possible. Additionally, short cellulose chains may interact and crystallise at the lateral surfaces of the $(1\bar{1}0)$ and (020) planes of the crystallites [Öztürk et al., 2008].

Secondly, dissolved cellulose can use crystalline fragments as nuclei for recrystallization. Polymer chains detached from a more disordered region are dispersed in the solution and follow a template growth mechanism to reassemble onto crystal surfaces [Fengel and Stoll, 1989; Paralikar and Aravindanath, 1988; Ibbett et al., 2008]. For example, Buleon et al. [1977] observed shish-kebab-like structures that consisted of regenerated cellulose II crystals that had nucleated on cellulose I crystals.

Following the second mechanism, the crystallites at the surface of the partially dissolved rayon fibres could serve as templates for crystal growth during regeneration of the dissolved portions. The enhanced growth of crystallites in the $(1\bar{1}0)$ plane with ACC processing agrees with the work of Buleon and Chanzy [1978], who discovered that the $(1\bar{1}0)$ plane is the growth face of single crystals of cellulose II. With extended dissolution time more cellulose is dissolved, while the surface area of the undissolved fibre portion acting as nucleation site remains almost constant. The further increase in crystallite size is consequently attributed to the first mechanism, interfibrillar swelling. Colom and Carrillo [2002] point out that recrystallisation due to swelling occurs independently from dissolution and can therefore affect the core of rayon fibres in ACCs while partial dissolution and nucleated recrystallisation during regeneration occur in the near surface region of the fibres. Longer dissolution times allow the solvent to penetrate the core of fibres, lead to swelling and allow its recrystallisation, preferentially in the $(1\bar{1}0)$ and (020) planes corresponding to the lateral crystallite thickness perpendicular to the fibre axis.

5.3.5 *Effect of dissolution time on the mechanical properties*

The changes in composite microstructure and cellulose fine structure are also reflected by a change in mechanical properties of ACC laminates with dissolution time. Tensile strength decreased with increasing dissolution time from 114 ± 1.9 MPa for 5 min to 97.3 ± 5.6 MPa for 60 min (Table 8 and Figure 54). Young's modulus and yield strength showed a similar trend with a decrease from 7.8 ± 0.5 GPa to 6.0 ± 0.3 GPa and from 63 ± 0.9 MPa to 46.6 ± 4.9 MPa for SIP-5 and SIP-60, respectively.

With longer dissolution times the matrix fraction of ACCs increased, meaning a larger fraction of the reinforcing rayon fibres was dissolved and transformed into the matrix phase. The matrix, tested individually as an unreinforced cellulose film, was significantly weaker than the laminates, hence a higher V_m is expected to result in a lower laminate strength. However, laminate strength decreased by 14.6 %, while V_m only increased by < 2 % (Table 8 and 6).

An additional loss of laminate strength might arise from the higher void fraction in SIP-30 and SIP-60. A higher V_v in composites is associated with lower strength due to a reduced load bearing volume and by introducing

Table 8: Influence of dissolution time on the mechanical properties of ACC laminates.

	Dissolution time in min	Young's modulus in GPa	Yield strength in MPa	Ultimate tensile strength in MPa	Strain at break in %
unreinf. cell. film	5	6.6 ± 0.5	56.2 ± 9.4	67.3 ± 7.9	2.0 ± 0.9
SIP-5	5	7.8 ± 0.5	63.0 ± 0.9	114.0 ± 1.9	12.9 ± 0.7
SIP-30	30	6.8 ± 0.3	58.0 ± 2.7	107.0 ± 3.8	12.5 ± 2.0
SIP-60	60	6.0 ± 0.3	46.6 ± 4.9	97.3 ± 5.6	14.3 ± 2.2

stress concentrations, as has been shown for flax-reinforced composites by Madsen and Lilholt [2003]. However, voids were not found to be detrimental to the ultimate tensile strength of ACC laminates, as they initiate transverse cracking and thereby contribute to the strengthening mechanism and positive size effect presented in Chapter 4.

It is proposed that the decrease in mechanical properties is linked to the fine structure of rayon fibres. Regenerated cellulose fibres have a semicrystalline character that is described by a parallel-series model, where crystalline domains are in series with amorphous domains, and an additional amorphous domain in parallel to the crystalline-amorphous chain (Figure 53a, Kong and Eichhorn, 2005). WAXD results show no change of the (004) peak with increasing dissolution time (Figure 51), indicating that longitudinal order is not affected by dissolution and that the strong crystalline parts of the crystalline-amorphous series structure remain intact. The increased crystallite thickness in the $(1\bar{1}0)$ and (020) planes (Figure 51c) suggests that amorphous domains have been dissolved and reassembled onto the lateral surfaces of neighbouring crystallites perpendicular to the fibre axis by a template growth mechanism, as discussed above (Section 5.3.4, Buleon et al. 1977; Buleon and Chanzy 1978; Fengel and Stoll 1989; Paralikar and Aravindanath 1988; Ibbett et al. 2008). Due to dissolution occurring preferentially in amorphous domains, which in regenerated fibres represent linkages between crystallites (Figure 53a, Kong and Eichhorn, 2005), these amorphous tie molecules may break down more extensively during prolonged dissolution times and lead to a weakening of the fibre structure.

Furthermore, Qi et al. [2011] report a small decrease in DP of cellulose from 570 as-received to 540 after dissolution in NaOH/urea. As chain scission occurs preferentially in amorphous domains of cellulose [Fleming et al., 2001], the amorphous tie molecules in between crystalline domains may be

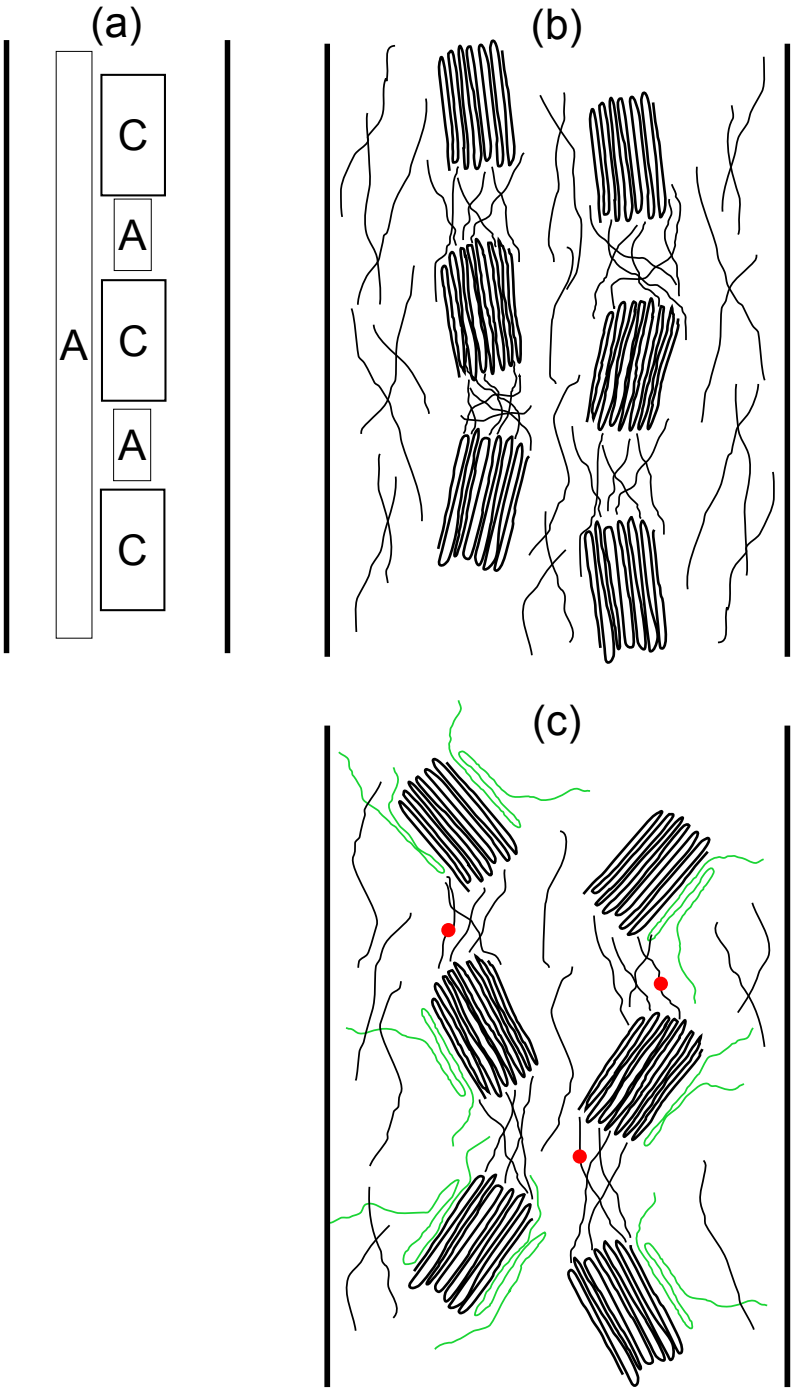

Figure 53: (a) Schematic of the parallel-series model of crystalline (C) and amorphous (A) domains in regenerated cellulose fibres (adapted from Kong and Eichhorn, 2005). (b,c) Schematics of the proposed molecular changes with processing of ACCs: (b) Initially highly oriented crystallites in as-received rayon connected by amorphous tie molecules. (c) Lateral increase in crystallite size (green), decreased orientation of crystallites and chain scission in amorphous tie molecules, caused by partial dissolution and swelling.

weakened by partial dissolution and act as breaking points of the fibres (Figure 53c).

Additionally, the decrease of Young's modulus and ultimate tensile strength of ACC laminates with increasing dissolution time may be the result of a decrease in the orientation of cellulose crystallites in the reinforcing fibres, as the highly preferred orientation induced by fibre extrusion (Figure 53b) is known to lead to the high mechanical properties of regenerated cellulose fibres [Loubinoux and Chaunis, 1987; Kreze and Malej, 2003; Kong and Eichhorn, 2005; Soykeabkaew et al., 2009a; Sun et al., 2015]. Soykeabkaew et al. report a decrease of the preferred crystallite orientation when preparing unidirectional ACCs by partial dissolution of regenerated cellulose fibres (Lyocell) in LiCl/DMAc. The preferred orientation of crystallites, and the Young's modulus and ultimate tensile strength of the ACC decrease with increasing dissolution time [Soykeabkaew et al., 2009a]. Therefore, partial dissolution in NaOH/urea is expected to create a matrix phase of lower crystallite orientation. Furthermore, swelling and plasticisation of the fibres may mobilise the cellulose crystallites at the fibre core, such that they reorient towards a more random distribution (Figure 53c), manifesting in a lower Young's modulus and ultimate tensile strength of the ACC laminates.

5.3.6 *Characteristic stress-strain behaviour*

The stress-strain curve of ACC laminates processed using NaOH/urea is characterised by three distinct stages: (i) linear elastic, (ii) stress plateau following yield and (iii) strain hardening at strains $>6\,\%$ (Figure 54). The laminates exhibit a high elongation at break of 12 to 14 %, typical for the reinforcing rayon fibres [Adusumali et al., 2006]. The unreinforced cellulose film exhibited linear elastic behaviour followed by fracture at a comparat-

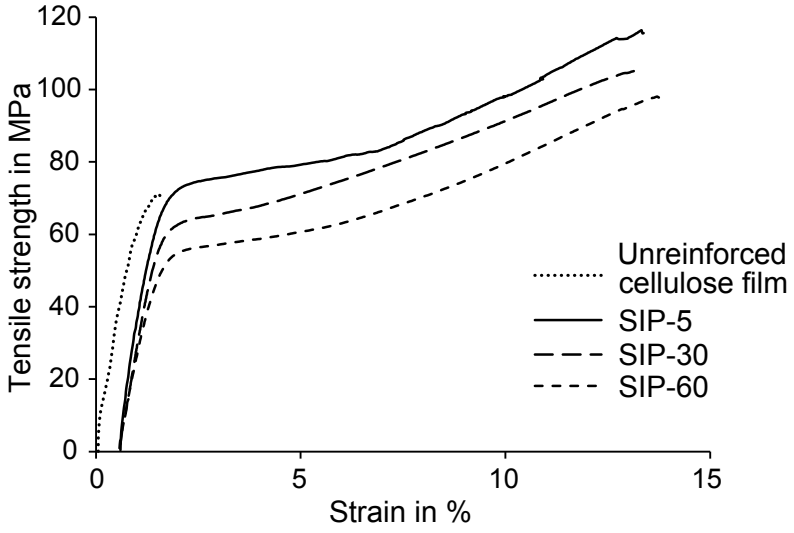

Figure 54: Overlay of typical stress-strain curves of the unreinforced cellulose film and ACC laminates with increasing dissolution time (Curves of ACCs have been shifted horizintally by 0.5 % for clarity).

ively low strain of 2.0 ± 0.9 % (Figure 54). The film strength of 67.3 ± 7.9 MPa is comparable to values in the range of 65 to 90 MPa reported by Zhang et al. [2005b] and Yang et al. [2011] while the same studies report higher elongations at break of 10 %. The difference in mechanical properties probably arises from the significant influence of cellulose source, dissolution and regeneration conditions [Zhang et al., 2005b].

Interestingly, the unreinforced cellulose film showed an almost identical behaviour as the laminate up to the yield point. However, the cellulose film broke at low strains, while the ACC laminates exhibited extensive elongation and strain hardening, due to the long-range cohesion of the fibres. In agreement with the results presented for ACC laminates prepared with IL as solvent in Chapter 4, the similarity of unreinforced film strength and laminate yield stress suggest that damage initiates with matrix failure at the yield point, although it needs to be considered that the structure and properties of the matrix phase in the ACCs might differ from the unreinforced film. The matrix is confined by the fibres, which may affect cellulose structure form-

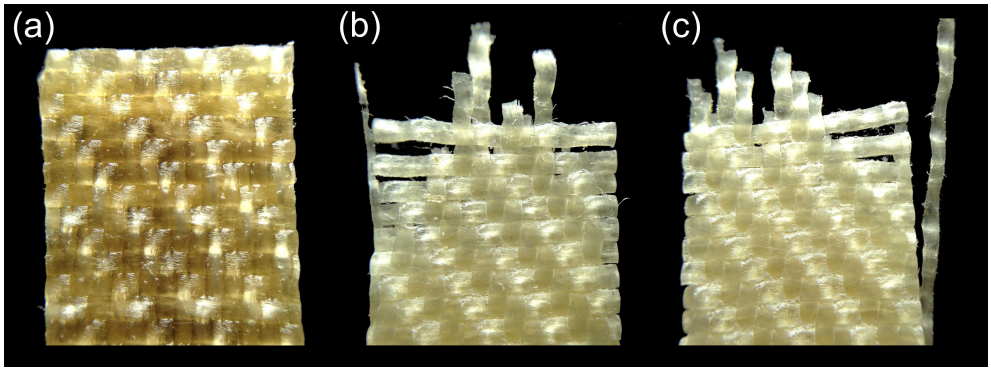

Figure 55: Photographs of (a) ACC laminate before tensile testing and (b & c) tensile tested ACCs at site of fracture with separated transverse and failed axial yarns. All specimens are 10 mm wide.

ation during regeneration by acting as nucleation sites, as discussed above. Furthermore, the matrix phase is only 1 to 3 µm thin, while the unreinforced film is 0.26 mm thick, hence tensile strength may be affected by size effects.

Accumulation of damage after yield is indicated by the tensile specimens turning more opaque and white in the gauge region after plastic deformation (Figure 55). The damage evolution of ACCs (Chapter 4) has shown that the fracture of the matrix leads to the separation of transverse and longitudinal yarns from each other, allowing the latter to straighten from the initial waviness implied by the weave. As soon as fibre slack is removed by additional strain, the straightening of longitudinal yarns in direction of the applied load is expected to result in a stiffening effect, which may account for the strain hardening observed at strains $> 6\,\%$ (Figure 54).

Such strain hardening is not seen in ACC laminates prepared by partial dissolution in IL, neither in thin nor thick laminates (Chapter 4). The difference in tensile characteristics is attributed to the higher void and lower matrix content in NaOH/urea ACCs (Table 6). The lower matrix content results in less cohesion of yarns and lower interlaminar strength, indicated by the separation of yarns and delamination upon failure of NaOH/urea ACCs (Figure 55), which is not seen in IL laminates (Figure 56). Consequently, the

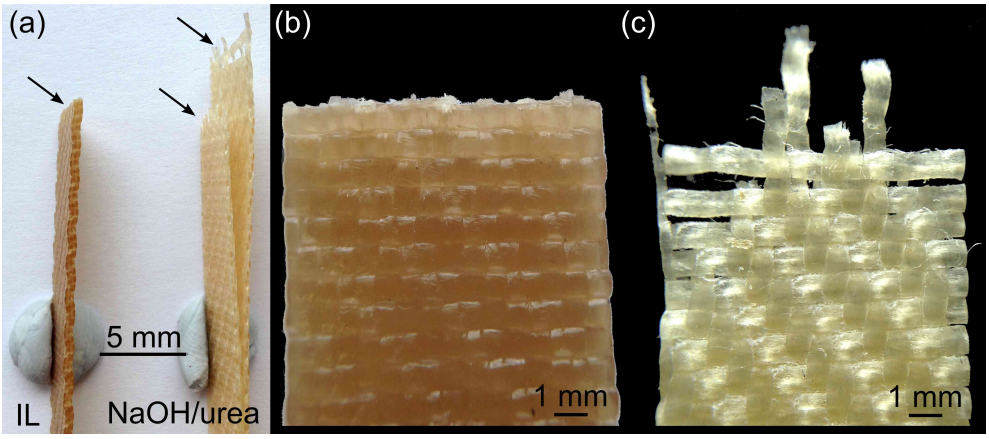

Figure 56: Photographs of fractured ACC laminates prepared by SIP using IL (a, left; b) and NaOH/urea (a right; c). Arrows in (a) indicate the sites of fracture.

separation of transverse and longitudinal yarns by matrix failure after yield in NaOH/urea laminates sets the longitudinal yarns free to straighten and stiffen, resulting in the observed strain hardening.

5.3.7 *Influence of increasing laminate thickness*

All results presented so far were obtained from ACCs with 2 laminae. In order to determine whether NaOH/urea also allows the processing of thicker laminates and to check for the existence of a thickness dependent size effect, ACCs with 4 laminae were manufactured by SIP, as well.

The infusion of 4-layered laminate stacks with NaOH/urea at -12 °C with continuous cooling proceeded with similar ease and speed as of 2 laminae. SIP resulted in well consolidated ACC laminates, i.e. the laminates felt stiff when bent and no signs of delamination were observed. The ACC laminate with four laminae exhibited an increased tensile strength of 123.4 ± 1.3 MPa compared to 114 ± 1.9 MPa (SIP-5) for two laminae (Table 9), in agreement with the size effect of increasing strength with increasing laminate thick-

Table 9: Tensile properties of ACCs with increasing number of laminae manufactured by SIP using NaOH/urea with a dissolution time of 5 min and continuously cooled infusion at -12 °C.

	Laminate thickness in mm	Young's modulus in GPa	Yield strength in MPa	Tensile strength in MPa	Strain at break in %
2 laminae	0.82	7.8 ± 0.5	63.0 ± 0.9	114.0 ± 1.9	12.9 ± 0.7
4 laminae	1.65	7.6 ± 0.9	57.1 ± 6.4	123.4 ± 1.3	12.5 ± 1.7

ness observed in ACC laminates processed using IL. It is argued that the same stress redistribution and strain delocalisation mechanism proposed for IL-laminates applies to NaOH-laminates, as damage accumulation is apparent from the increase in opacity with tensile strain and delamination and separation of transverse yarns from longitudinal yarns upon fracture of NaOH-laminates (Figures 55 and 56). The mechanism, that relies on transverse cracking, may even be enhanced by the increased presence of defects in NaOH-laminates (Table 6), as voids and microcracks are already present in the microstructure of unstrained NaOH-laminates (Figure 47).

Continuously cooled SIP at -12 °C resulted in homogeneous properties throughout the infused length of ACC laminates with 2 laminae (Figure 48). However, variations in the stress-strain curves of ACCs with 4 laminae were observed with increasing distance from the inlet (Figure 57), even though continuous cooling had been applied during SIP. Young's modulus and yield strength decreased by approximately 20 % from 8.2 GPa and 62.5 MPa at the inlet to 6.4 GPa and 49.5 MPa at the outlet, respectively (Figure 58).

The decrease in Young's modulus and yield strength indicates that the same phenomenon of increasing solvent temperature and hence decreasing cellulose solubility in NaOH/urea during infusion, as observed in pre-cooled/ambient SIP of ACCs with 2 laminae (Figures 48 and 49), occurs in

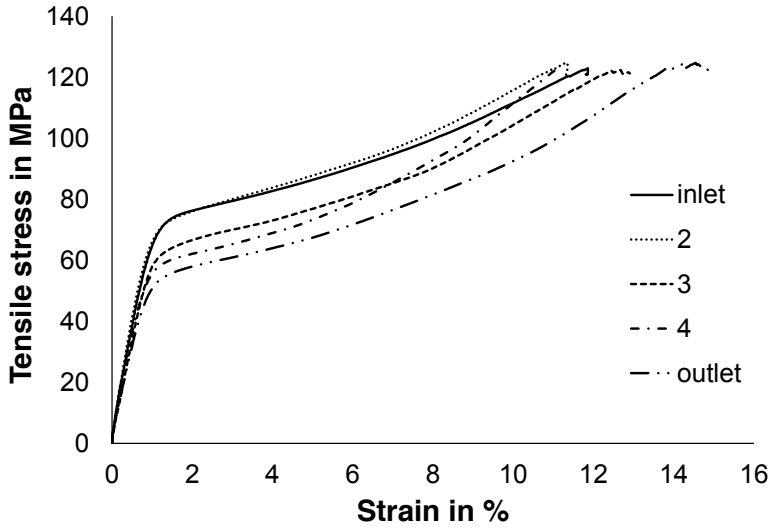

Figure 57: Overlay of stress-strain curves as a function of distance from inlet to outlet of a 4 layer laminate fabricated by -12 °C continuously cooled SIP.

continuously cooled SIP of a thicker laminate stack. The temperature within the laminate stack rises to a higher extent during the infusion of 4 laminae, due to the larger volume of cellulose being infused. The doubled volume of cellulose in 4 laminae sets free more heat by the exothermic dissolution process in NaOH/urea compared to 2 laminae, while only being cooled through the same surface area. Consequently, the temperature of the solvent increases as it infuses the textile, and due to the decrease in cellulose solubility of NaOH/urea by 82 % with an increase in temperature from -12 °C to 0 °C [Qi et al., 2008b], less matrix is created towards the outlet end of the laminate, resulting in a decrease of Young's modulus and yield strength (Figure 58). It is concluded, that in order to achieve homogeneous, high quality laminates on an industrial scale *via* SIP using NaOH/urea as cellulose solvent, cooling needs to be scaled up along with laminate thickness and infused length. An adaptation of the Quickstep process [Griffiths and Noble, 2004] might be a suitable solution for the cooling needs of SIP and is described in Chapter 8.

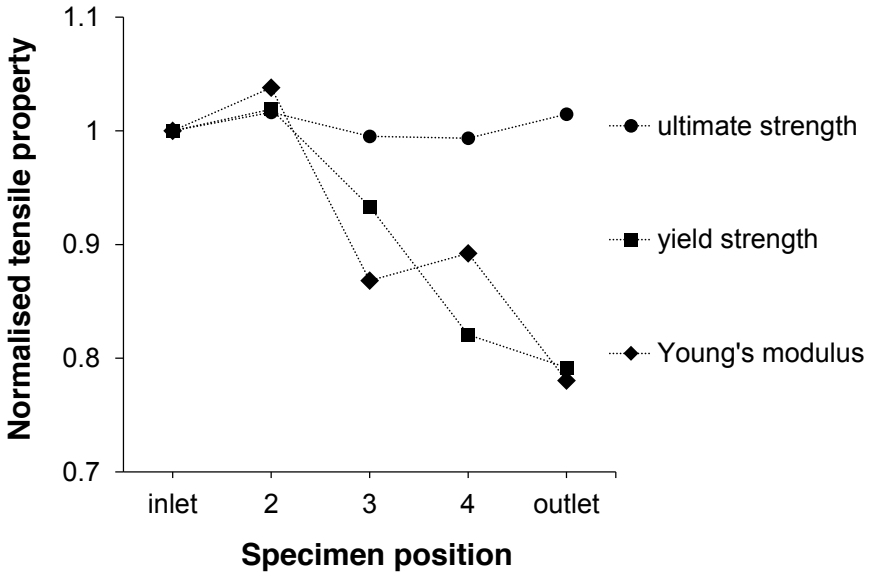

Figure 58: Variation of normalised tensile mechanical properties as a function of distance from inlet to outlet of a 4-layered ACC laminate fabricated by -12 °C continuously cooled SIP (Results were normalised by the respective inlet value).

In agreement with the findings for laminates composed of 2 laminae (Figure 48), only Young's modulus and yield strength of the 4 layered ACC laminate decreased with increasing distance from the inlet, while ultimate tensile strength remained constant (Figure 58). Furthermore, the laminate exhibited the highest tensile strength of all samples, in spite of insufficient cooling (Table 9). It is concluded that the ultimate tensile strength of ACC laminates is a fibre-dominated property, while Young's modulus and yield strength are matrix-dominated. Based on this finding it is suggested that the future optimisation of mechanical properties should focus on two aspects: Firstly, as composite strength is fibre-dominated, a stronger or weaker type of cellulose fibre should be chosen as precursor to reach a certain strength range adequate for the desired application. Secondly, the partial dissolution and regeneration conditions can be adjusted to tailor the Young's modulus and yield strength to the desired levels. A longer dissolution time leads to a

higher matrix content (Table 6) and the structure and properties of the matrix phase can be influenced by the regeneration conditions [Bang et al., 1999; Zhang et al., 2001; Mao et al., 2006; Yang et al., 2011].

5.3.8 *Effect of infusion pressure*

In the initial description of the solvent infusion process, Huber et al. [2012a] stress the importance of the application of pressure during dissolution. When using IL as the cellulose solvent, this is achieved by performing the infusion at a relatively low temperature (without cellulose dissolution) and placing the setup in a hot press at elevated temperatures for simultaneous compaction and dissolution (Huber et al. 2012a and Chapter 4). In contrast, infusion and dissolution cannot be divided into two consecutive stages when using NaOH/urea, due to the high extent of swelling when infusing at temperatures higher than 0 °C (Section 5.3.1). Consequently, the vacuum pressure applied for infusion may be a decisive parameter for achieving a high level of laminate compaction.

To investigate the influence of infusion pressure on ACC laminate properties, 4 layered laminate stacks were infused with NaOH/urea at an absolute pressure of 700 mbar ($ACC_{700mbar}$), a relatively low vacuum, and at 200 mbar ($ACC_{200mbar}$), a relatively high vacuum, that was also applied in all previously presented experiments. Continuously cooled SIP at -12 °C was performed.

ACC laminates infused at 700 mbar exhibited lower mechanical properties than those infused at 200 mbar (Table 10). The tensile strength and Young's modulus of the laminates decreased from 123.4 ± 1.3 MPa to 99.3 ± 2.2 MPa and from 7.6 ± 0.9 MPa to 6.2 ± 0.6 MPa in $ACC_{200mbar}$ and $ACC_{700mbar}$, respectively. The difference in infusion pressure resulted in a 14.5 % higher

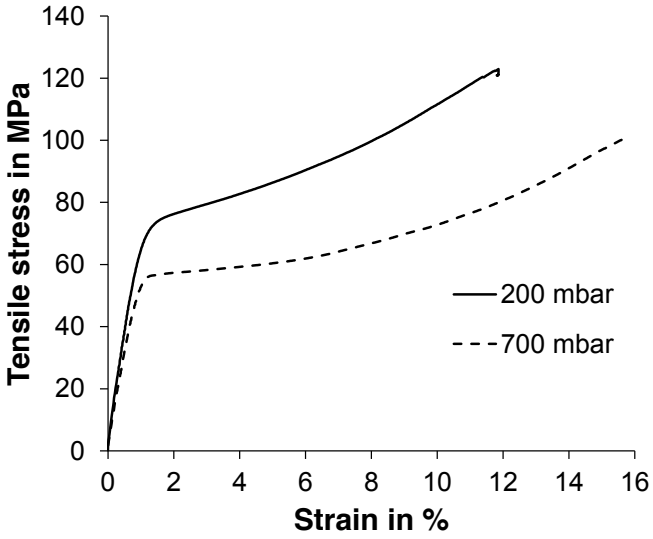

Figure 59: Representative stress-strain curves of ACC laminates infused at 200 mbar and 700 mbar.

thickness of 1.89 mm in $ACC_{700mbar}$ compared to 1.65 mm in $ACC_{200mbar}$. This difference in thickness was apparent even though both laminates were compacted at 1 MPa for 15 min after dissolution, a pressure that is 50 times greater than the infusion pressure of 200 mbar. A parallel decrease in density from 1.450 g mm^{-3} in $ACC_{200mbar}$ to 1.411 g mm^{-3} in $ACC_{700mbar}$ was measured, which equals an increase in void content from 4.6 to 7.1 vol.% (Table 10).

The increase in thickness equalled a change in cross-sectional area of 16.1 %, which accounts for most of the decrease in ultimate tensile strength of 19.5 %, due to the resulting decrease of reinforcement per unit area. The remaining difference in strength may be attributed to a higher matrix fraction, which is expected due to the 27 % higher solvent uptake of $ACC_{700mbar}$ (Table 10).

The comparison of $ACC_{700mbar}$ and $ACC_{200mbar}$ shows that the application of a high vacuum pressure during partial dissolution is of paramount importance to ACC processing *via* SIP using NaOH/urea. An adaptation of the Quickstep process to suit SIP using NaOH/urea, as discussed in Chapter 8,

Table 10: Comparison of mechanical (tensile) and physical properties of ACC laminates with 4 laminae infused at high (200 mbar) and low (700 mbar) vacuum pressure. Both laminates were processed by continuously cooled SIP at -12 °C with NaOH/urea and a dissolution time of 5 min.

	Tensile strength in MPa	Young's modulus in GPa	Strain at break in %	Yield stress in MPa	Density in g mm^{-3}	Void content in %	Solvent uptake in %
$ACC_{200mbar}$	123.4 ± 1.3	7.6 ± 0.9	12.5 ± 1.7	57.1 ± 6.4	1.450 ± 0.013	4.6	58
$ACC_{700mbar}$	99.3 ± 2.2	6.2 ± 0.6	16.8 ± 0.9	47.6 ± 3.7	1.411 ± 0.012	7.1	85

would be advantageous for adding (i) continuous cooling with precise temperature control and (ii) applying external pressure during infusion and dissolution to aid the compaction of the laminate stack.

Future investigations will have to determine the ideal balance between applied pressure and solvent uptake. On the one hand, a high pressure is required for compaction of the laminate stack to bring fibres into close proximity and achieve good bonding of fibres with the small amount of matrix generated by partial dissolution in NaOH/urea. On the other hand, solvent uptake decreases with increasing infusion pressure (Table 10), which reduces the amount of matrix that can be created by partial dissolution. The next objective would therefore be the determination of the solvent uptake required to create the minimum amount of matrix necessary to obtain a Young's modulus in the range of the top values found thus far (7 to 8 GPa). The minimal conversion of fibre to matrix will then result in ACCs with the highest obtainable strength for laminates with a high Young's modulus.

5.3.9 *Processing of all-cellulose composite laminates by immersion in aqueous sodium hydroxide/urea solution*

SIP is a straight forward processing technique and is based on VARTM, which is commonly applied in the composite industry [Mazumdar, 2001; Glancey, 2010]. However, the setup has a certain level of complexity. It necessitates expensive specialty equipment, like a vacuum pump and pressure gauge, and single-use consumables such as vacuum bag and sealing tape. Therefore, a simple immersion technique was trialled as an alternative manufacturing route to see if the more elaborate vacuum-assisted processing is necessary to achieve high mechanical properties of ACC laminates.

Microstructural analysis revealed many unconsolidated cores of yarns in immersion samples (Figure 60a). The occurrence of yarns with completely undissolved fibres in their core is higher in immersion samples than in SIP samples infused at -12 °C (Figure 47). In both SIP and immersion the NaOH/urea solution is used at -12 °C which causes immediate dissolution. Upon contact with the fibres in the rim of a yarn the solvent causes local swelling and dissolution, impeding the flow of solvent into the core, as seen in the inhomogeneous matrix distribution in the rim and core of yarns found in SIP samples (Figure 50). The penetration of yarns with solvent is slower in immersion when compared to being forced into the yarns with the aid of the applied vacuum in SIP. The higher extent of swelling caused by the slower solvent uptake in immersed samples subsequently prevents wetting and partial dissolution of the core.

The exposure of the textile to a large volume of solvent resulted in an increase in solvent uptake from 99 % in SIP-30 to 260 % by immersion (Table 11). The increase in solvent uptake resulted in enhanced dissolution of immersed samples, evident from a higher matrix content of 9.3 ± 2.7 vol. % compared

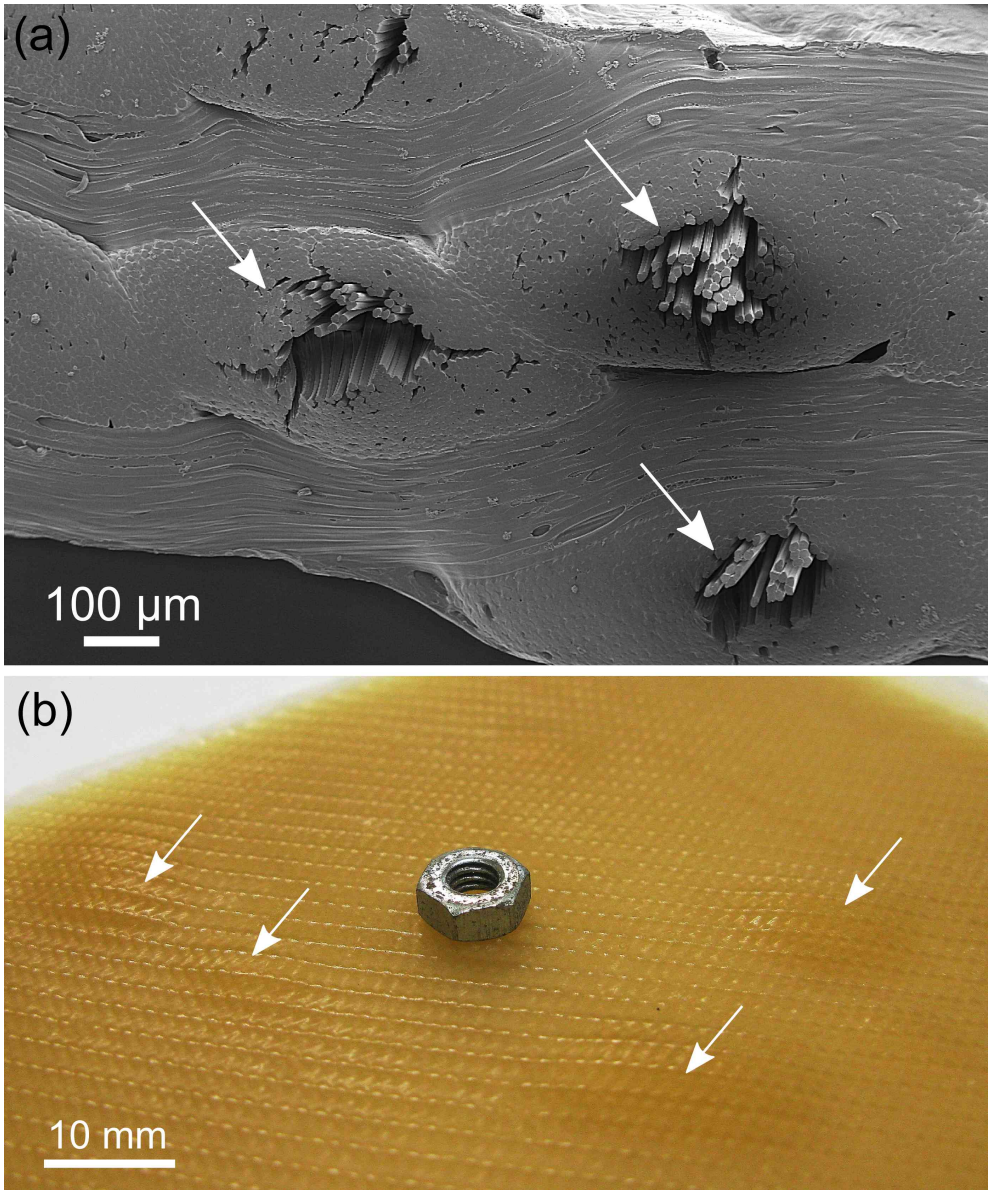

Figure 60: (a) Scanning electron micrograph of an ACC laminate processed by immersion. Arrows indicate unconsolidated fibres at the core of yarns. (b) Photograph of the same laminate with arrows indicating large interlaminar voids that appear as bubbles filled with water after regeneration (A nut with 8 mm diameter was placed on the ACC for size comparison).

Table 11: Comparison of ACC laminates processed by immersion and SIP using NaOH/urea at a dissolution time of 30 min.

	Tensile strength in MPa	Young's modulus in GPa	Strain at break in %	Yield stress in MPa	Matrix content in vol.%	Solvent uptake in %
SIP-30	107.2 ± 3.8	6.8 ± 0.3	12.5 ± 2	58.0 ± 2.7	5.4 ± 2.5	99
Immersion	78.3 ± 3.0	7.3 ± 0.7	6.7 ± 0.3	49.8 ± 4.1	9.3 ± 2.7	260

to 5.4 ± 2.5 vol. % in SIP-30 (Table 11). Furthermore, the partial dissolution of the textile surface creates a highly viscous layer and with stacking of laminae, air is easily entrapped between them. Entrapped air is not completely removed by pressing and results in large interlaminar voids which are filled with water during regeneration and washing. The voids swell to water-filled bubbles with a diameter ranging from 5 to 12 mm (Figure 60b). With drying, these bubbles turn into large interlaminar voids. The investigation of size effects (Chapter 4) has shown that microvoids with a diameter of 10 to 100 µm are not critical for failure of thick laminates. However, large voids with 3 to 10 mm diameter may cause premature failure. The influence of large voids on the strength of ACC laminates was not investigated and test coupons have been prepared from void-free laminate areas.

The immersion procedure with a dissolution time of 30 min resulted in a lower tensile strength of 78.3 ± 3.0 MPa compared to 107 ± 3.8 MPa of the SIP laminate using the same dissolution time (SIP-30). A similarly high Young's modulus of 7.3 ± 0.7 GPa was found for immersion when compared to 6.8 ± 0.3 GPa found for SIP-30 (Table 11). The stress-strain curve of the immersed ACC shows a lower strain at break of 6.7 ± 0.3 % and misses the characteristic plateau with strain hardening of SIP laminates at strains above 6 % (Figure 61). Furthermore, the immersed laminate fractured without delamination, whereas the SIP laminate delaminated and transverse yarns were de-

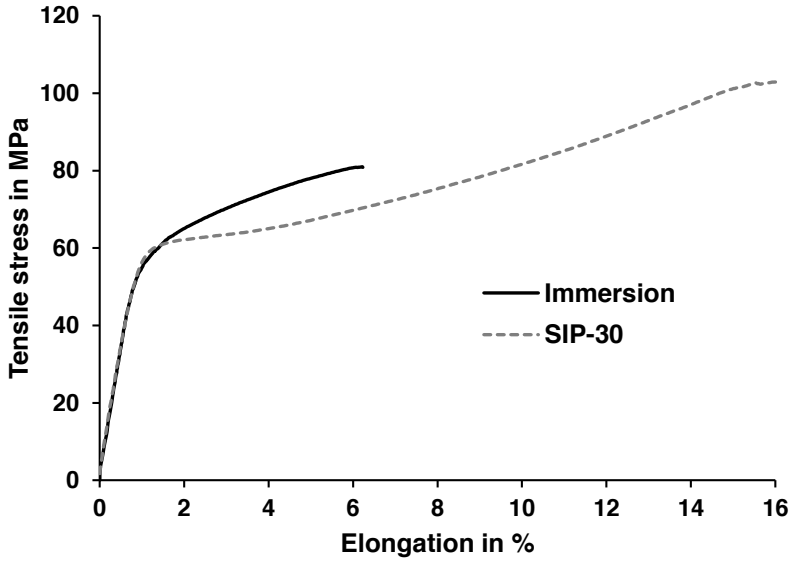

Figure 61: Typical stress-strain curves of ACC laminates prepared *via* immersion and SIP using NaOH/urea, both with a dissolution time of 30 min.

tached (Figure 62a). Fractured immersion laminates did not separate at the site of fracture. The two ends of the specimens were held together by the unconsolidated fibres at the core of yarns (Figure 62b), to which no load had been transferred due to the lack of matrix.

The differences in tensile behaviour between ACCs prepared by SIP and immersion are attributed to the almost doubled V_m of 9.3 vol. % in immersed samples in comparison to 5.4 vol. % in SIP samples. Immersed NaOH/urea laminates exhibit tensile and fracture behaviour similar to that of laminates prepared by SIP using IL, which also have a V_m of approximately 10 vol. %. The increased cohesion due to the comparably high V_m prevents the detaching of transverse yarns in immersed NaOH/urea-laminates. The separation of longitudinal from transverse yarns accounts for the high elongation at break and strain hardening at strains above 6 % seen in NaOH/urea-SIP laminates.

Consequently, the lower strength of immersed laminates is attributed to the prevented straightening of longitudinal yarns, the reduction in reinfor-

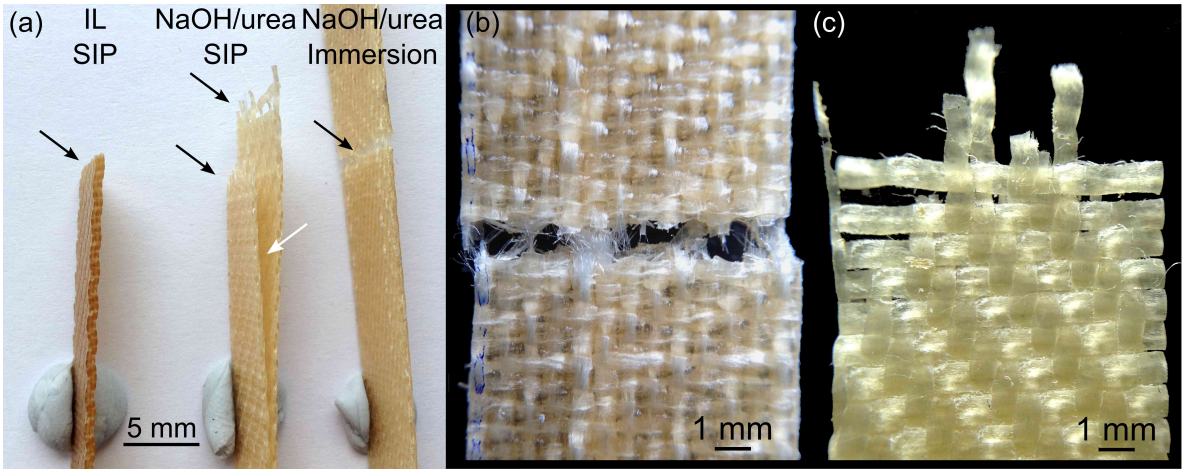

Figure 62: Photographs of fractured ACC laminates. (a) Comparison of laminates prepared by SIP using IL or NaOH/urea and by immersion in NaOH/urea, arrows indicate the site of fracture. (b) Macro of the fracture of an ACC laminate prepared by immersion in NaOH/urea. (c) Macro of the fracture of an ACC laminate prepared by SIP using NaOH/urea.

cing fibre volume associated with the higher V_m, as well as the weakening of fibres by solvent interaction, as discussed above (Figure 53). Additionally, the lack of matrix in unconsolidated cores of yarns impedes stress transfer, hence a substantial volume of reinforcement cannot contribute to the strength of ACCs prepared by immersion.

Interestingly, no substantial increase in Young's modulus was observed with the approximately two-fold increase in V_m, which indicates that only a low V_m is necessary to reach the maximum Young's modulus observed in ACC laminates in the range of 7 to 8 GPa (Table 8).

In summary, vacuum assisted SIP is found to be beneficial to the homogeneity of the microstructure of ACC laminates and results in higher mechanical properties.

5.3.10 *Comparison between ionic liquids and aqueous sodium hydroxide/urea solution for solvent infusion processing*

Replacing IL with NaOH/urea as solvent for SIP led to an increase in tensile strength of ACC laminates by 28 % to 123 MPa using NaOH/urea in continuously cooled SIP at -12 °C (Table 9), compared to 96 MPa (Table 4), and 91 MPa [Huber et al., 2012a], using the IL BmimAc (all values for ACCs with 4 laminae). The higher strength is attributed to the lower solubility of cellulose in NaOH/urea (6.5 wt.%, Qin et al., 2008) when compared to IL (> 20 wt.%, Swatloski et al., 2002), which leads to less transformation of fibre to matrix during partial dissolution for similar solvent uptake. Furthermore, the lower matrix and higher void fraction in NaOH/urea-laminates when compared to IL-laminates also increases the initiation of transverse cracks and delamination. The accumulation of such damage releases the longitudinal yarns from the constraints of the matrix and results in the stress plateau extending to elongations in excess of 10 % and the strain hardening observed only in ACC laminates processed by SIP using NaOH/urea.

In addition to higher tensile strength, using NaOH/urea for SIP has several other benefits: Processing times are reduced by the shorter dissolution time (5 min compared to 60 min) and quicker infusion. The low viscosity of aqueous NaOH/urea solution allows infusion of a 100 mm laminate stack in less than 1 min, compared to more than 10 min using the more viscous IL BmimAc. Furthermore, the thermal energy consumption is lower for NaOH/urea since the setup needs to be cooled to -12 °C compared to heating to 100 °C for dissolution of cellulose in IL [Swatloski et al., 2002; Huber et al., 2012a].

An additional advantage is that NaOH/urea is available at 3 % of the price of the IL BmimAc, resulting in a dramatic reduction of solvent costs by 97 %.

It is also worth noting that NaOH/urea has a lower environmental impact, since imidazolium-based ILs are toxic and non-biodegradable [Ranke et al., 2004; Bernot et al., 2005; Zhao et al., 2007; Jastorff et al., 2005; Matzke et al., 2007] and their potential release to the environment in industrial manufacture of ACCs poses a risk factor. NaOH and urea, on the other hand, are naturally occurring substances of low toxicity [Reece et al., 2013; ATSDR, 2014].

5.4 SUMMARY

Infusion with NaOH/urea needs to be performed with the setup and solvent precooled to -12 °C to prevent excessive swelling of the cellulose precursor. Performing SIP at the optimum dissolution temperature of NaOH/ urea necessitates continuous cooling during the infusion to minimise the increase in temperature of the solvent and laminate stack due to the exotherm of cellulose dissolution in NaOH/urea, as an increase in temperature is associated with a decrease in cellulose solubility of NaOH/urea. The application of continuous cooling facilitates homogeneous mechanical properties throughout the infused length of the composite (100 mm). A high vacuum pressure during infusion and dissolution was necessary to achieve the optimum mechanical properties. A simple immersion technique was found unsatisfactory for processing ACC laminates by partial dissolution in NaOH/urea. The processing times required for SIP are reduced in comparison to the use of IL, due to the lower viscosity of NaOH/urea that allows quicker infusion and the rapid partial dissolution achieved within 5 min.

In comparison to ACC laminates prepared using IL, the NaOH/urea laminates have a lower matrix content of 4 to 5 vol. %, attributed to the lower

solubility of NaOH/urea. A similar Young's modulus of 7.6 GPa and a 28 % higher tensile strength of 123 MPa was found when compared to IL-laminates of equal thickness (4 laminae). It is concluded that the minimal conversion of fibre to matrix by partial dissolution in NaOH/urea creates a sufficiently high matrix content to facilitate stress transfer from matrix to fibre resulting in a comparable Young's modulus, while most of the volume of reinforcing fibres remains that results in the superior strength compared to IL-laminates.

The cellulose crystallinity was found to increase from 32.6 % in the as-received rayon textile to 35.1 % upon partial dissolution for 5 min and a further increase to 38.1 % was found with increasing the dissolution time to 60 min. A parallel decrease in ultimate tensile strength of 14.6 % was found with the increase in dissolution time, that exceeds the increase in matrix volume fraction from 3.8 ± 1.5 % to 4.6 ± 1.2 %. It is concluded that the core of reinforcing fibres is affected by solvent interaction. Crystallite growth in the $(1\bar{1}0)$ and (020) planes was observed, which is attributed to lateral recrystallisation of amorphous domains. A weakening of the amorphous domains, which are in series with crystalline domains and act as tie molecules, and a reduction in crystallite orientation are proposed as the cause of the reduction in tensile strength.

Overall, NaOH/urea is a promising solvent for the manufacture of ACC laminates *via* SIP that facilitates rapid infusion and partial dissolution in 5 min. It has been established that NaOH/urea can replace ILs as a more cost-effective cellulose solvent of lower environmental impact, although it presents new challenges due to the low temperatures required for processing.

6

REMOVAL OF SOLVENT FROM ALL-CELLULOSE COMPOSITE LAMINATES

6.1 INTRODUCTION

In contrast to many other polymers, cellulose in its non-derivatised form is not thermoplastic. Accordingly, cellulose solvents need to be used in order to shape cellulosic products, such as regenerated fibres and ACCs [Klemm et al., 2005; Wertz et al., 2010; Huber et al., 2012b]. Dissolved cellulose regenerates when it comes into contact with a non-solvent and the exchange of solvent and non-solvent relies on diffusion. Consequently enough time and a sufficient concentration gradient between the solvent in the regenerating cellulose and the washing bath are required to fully remove the solvent [Jiang et al., 2011; Mao et al., 2006].

Complete removal of the cellulose solvent from ACCs is important for several reasons. Firstly, the solvent needs to be recovered to allow its recycling and reuse. Especially when using expensive solvents, such as ILs, the reuse is paramount for financial reasons. Recovery of solvents is also required to minimise the environmental impact of cellulose processing, as the release of contaminated washing baths may lead to the accumulation of non-biodegradable and toxic ILs in aquatic ecosystems [Romero et al., 2008; Jastorff et al., 2005; Matzke et al., 2007]. Secondly, solvent residues are un-

desirable in the final cellulose product, as they may be disadvantageous or even harmful in applications such as toys or biomedical products.

Furthermore, the cellulose structure and mechanical properties of ACCs may be affected by residual solvent. Even small amounts of entrapped IL lead to a decrease in the crystallinity of regenerated cellulose. Mahadeva and Kim [2012] observed a decrease in crystallinity of regenerated cellulose films (prepared from cotton pulp) from 29 % to 16 % with increasing nitrogen content (evidence of residual IL) from 0.84 wt. % to 2.67 wt. %, respectively. Additionally, ILs are known to act as plasticisers of cellulose. Ou et al. [2014] show that untreated poplar wood does not show thermal softening up to temperatures in excess of 200 °C, whereas the addition of 6 wt. %, 18 wt. % and 36 wt. % IL (EmimCl) lowers the thermal softening temperature to 135 °C, 91 °C and 68 °C, respectively.

Similarly, the high Young's modulus and tensile strength of ACCs would be lost at high residual solvent contents, as Wu et al. [2014] observed a Young's modulus and tensile strength of only 0.2 GPa and 8.3 MPa, respectively, for an IL content of 30 wt. % in IL-plasticised MCC processed by compression moulding. It is argued that the decrease in mechanical properties and loss of order are caused by the formation of hydrogen bonds between cellulose and the residual IL and a decrease of the strong inter- and intramolecular hydrogen bonds found in crystalline cellulose [Mahadeva and Kim, 2012; Wu et al., 2014; Ou et al., 2014].

Furthermore, the excellent biodegradability of ACCs shown by Kalka et al. [2014] may be negatively affected by residual solvent due to the toxicity of IL and the basic (alkaline) character of NaOH/urea.

However, the removal of solvent following cellulose processing has received little attention in the field of ACCs. It is generally stated that ACCs were regenerated and washed for a given period of time, but the solvent con-

centration in the washing bath was not monitored and the final ACCs have not been analysed for traces of residual solvent [Nishino et al., 2004; Gindl and Keckes, 2005; Soykeabkaew et al., 2008; Arévalo et al., 2010; Pullawan et al., 2010; Huber et al., 2012a]. Haverhals et al. are the only authors stating that removal of solvent, in this case IL used for processing ACCs by partial dissolution, was confirmed by FTIR analysis. However, this finding is not presented and discussed in detail, but limited to a single statement. Furthermore, FTIR was performed using an ATR setup and only the surface of samples was analysed with an estimated IR penetration depth of 2 µm [Haverhals et al., 2010, 2012]. It is therefore deemed necessary to investigate the solvent removal from ACCs in more detail, especially due to the increase in ACC thickness with SIP and the chance of solvent being trapped in the core of thick laminates.

FTIR spectroscopy and elemental analysis have been shown to be suitable methods for analysing the residual solvent content in regenerated cellulose. The chemical composition of cellulose $(C_6H_{10}O_5)_n$ differs from the imidazolium ($C_3H_5N_2$) cation in IL and NaOH/urea (CH_4N_2O). FTIR spectra consequently exhibit different peaks attributed to the C-N (imidazolium and urea) and C=N (imidazolium) bond vibrations (Figure 63) exclusive to the solvents [Mahadeva and Kim, 2012; Wu et al., 2014]. Elemental analysis (EA) reveals the mass fraction of C, H and N present in a sample and as N is only present in the solvents and not in the cellulose it represents a direct measure of solvent content. Mahadeva and Kim [2012] established a correlation between the integrated area of a peak in FTIR spectra attributed to IL and the nitrogen content determined by EA for cellulose regenerated from EmimAc solutions. Shibata et al. used FTIR spectroscopy to show that the IL BmimCl was removed by Soxhlet extraction after processing wood

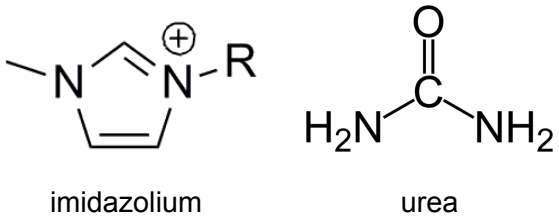

Figure 63: Structure of the imidazolium cation in the IL EmimAc and urea.

flour [Shibata et al., 2013b], cotton fabric and wood [Shibata et al., 2013a] to all-cellulose and all-wood composites by partial dissolution.

In addition to FTIR and EA, which are relatively time-consuming, single-measurement techniques that can be applied to the final cellulose product, a means of constantly measuring the solvent content in the washing bath is required. A continuous measurement of the washing bath would facilitate the determination of the required washing time for complete solvent removal. Conductivity is expected to be a suitable parameter, due to the ionic nature of NaOH and IL, that may also be applicable to other cellulose solvents, such as DMAc/LiCl, DMSO/TBAF and phosphoric acid solutions. In addition, the OH^- set free by the dissociation of NaOH in water is expected to lead to an increase in pH of the washing bath.

This chapter investigates the effectiveness of pH and conductivity measurements for routine control of solvent content in the washing bath of ACC laminates. Washing of ACC laminates is followed by FTIR and EA to determine whether IL and NaOH/urea have been completely removed. The aim of the chapter is to establish that a simple washing routine in distilled water leads to full solvent removal to obtain ACCs that are safe for future applications.

6.2 EXPERIMENTAL PROCEDURES

6.2.1 *Conductivity and pH measurements*

ACC laminates with 4 layers were prepared *via* SIP using the IL EmimAc and NaOH/urea, as described previously in Sections 3.2 and 5.2, respectively (Infusion pressure 200 mbar, dissolution times of 60 min for EmimAc and 5 min with continuously cooled infusion for NaOH/urea, pressed at 1 MPa for 15 min). Rectangles of ca. $10 \times 20\,mm^2$ with a mass of 1.2 g were cut from the infused and partially dissolved laminates using a razor blade. Three samples of the IL and the NaOH/urea laminate were placed in separate plastic containers filled with 100 ml of distilled water. Three pieces of as-received rayon textile of equal mass (1.2 g) were prepared accordingly as reference samples. The containers were closed and kept at ambient temperature (15 to 18 °C). The pH and conductivity of the water were measured every 12 h using a portable multiparameter meter (HQ40d, HACH LANGE GmbH, Düsseldorf, Germany) followed by replacing the washing bath with fresh distilled water.

In an additional experiment the sensitivity of conductivity measurements to the presence of solvents was analysed. Therefore, the conductivity of a mixture of distilled water and solvent was measured for an increasing mass fraction of added NaOH or EmimAc.

6.2.2 *Fourier transformed infrared spectroscopy*

The solvents (liquid EmimAc dried for five days in a vacuum-oven at 95 °C; NaOH and urea crushed to fine powders using a pestle and mortar) and

washed ACCs were characterised by FTIR with an attenuated total reflectance (ATR) equipped spectrometer (Alpha, Bruker, Billerica, MA, USA). Thin slices were cut from the cross section of the ACC laminates with a razor blade to ensure that the full thickness including the core and not only the surface of samples was analysed. Three specimens of each sample were analysed by averaging 64 scans in the wavenumber range 4000 to 650 cm^{-1} at a resolution of 2 cm^{-1}.

In order to check for a potential increase in residual IL content with increasing laminate thickness an ACC with 8 laminae (processed by SIP using BmimAc, partially dissolved at 95 °C for 60 min at a pressure of 1 MPa, regenerated and washed in distilled water until no further increase in conductivity was measured) was cut into 80 µm thin sections using a sliding microtome, followed by FTIR analysis.

6.2.3 *Elemental analysis*

Total carbon, hydrogen and nitrogen (C, H, N) content was determined by elemental analysis (EA) carried out by the Campbell Microanalytical Laboratory of Otago University in Dunedin, NZ (www.otago.ac.nz, 13.08.2015). The samples were precisely weighed on a microbalance (UMT2, accuracy 0.1 µg, Mettler Toledo, Greifensee, Switzerland) into lightweight tin capsules and analysed by combustion in an elemental analyser (EA 1108, Carlo-Erba, Milan Italy) with a detection limit below 0.3 wt.%.

6.3 RESULTS AND DISCUSSION

6.3.1 *Monitoring of solvent removal by washing in distilled water*

Removal of the solvents from the ACC laminates led to a substantial increase in conductivity of the washing bath from 6.05 µS cm^{-1} in distilled water to 740 ± 44 µS cm^{-1} and 2340 ± 10 µS cm^{-1} for EmimAc and NaOH/urea , respectively, after the first 12 h washing cycle. Subsequently, the conductivity decreased exponentially within the next 24 h and reached the same order of magnitude as distilled water after a total of 36 h in three washing cycles (Figure 64a).

The pH of the washing bath of the EmimAc laminate decreased slightly from 6.47 ± 0.14 measured in distilled water to 6.13 ± 0.03 in the first 12 h, reached a similar value of 6.48 ± 0.04 after the next washing cycle and remained stable thereafter (Figure 64b). The initial decrease may be due to the potential presence of acetic acid. An increase in pH from 6.47 ± 0.14 in distilled water to 11.94 ± 0.02 after 12 h followed by a decrease to 11.03 ± 0.03 after 24 h was observed in the washing bath of the NaOH/urea laminate. A neutral pH of 6.94 ± 0.18 was measured after 36 h of washing (Figure 64b).

Washing of the as-received rayon textile did not affect the pH of the washing bath, but resulted in an increase in conductivity from 6.05 ± 0.61 µS cm^{-1} in distilled water to 27.25 ± 0.06 µS cm^{-1} (Figure 64), which may be due to residues from the fibre spinning process. It is however noted that the increase in conductivity is small. From a practical point of view it may also be the result of the textile having been handled for shipping and storage prior to the experiment, as dipping a fingertip into 100 ml of distilled water resulted in a similar increase in conductivity.

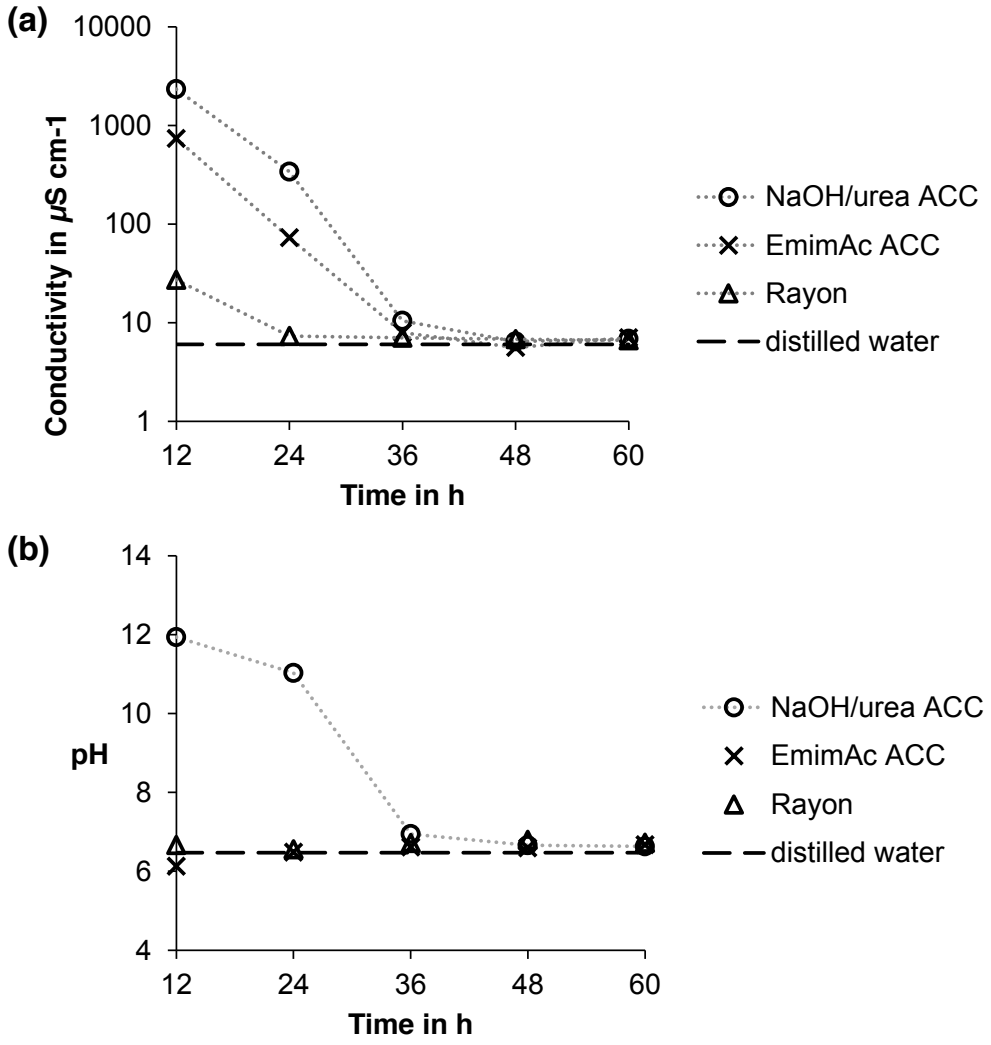

Figure 64: (a) Conductivity and (b) pH as a function of washing time of ACC laminates and as-received rayon in distilled water (Standard deviations are smaller than the markers).

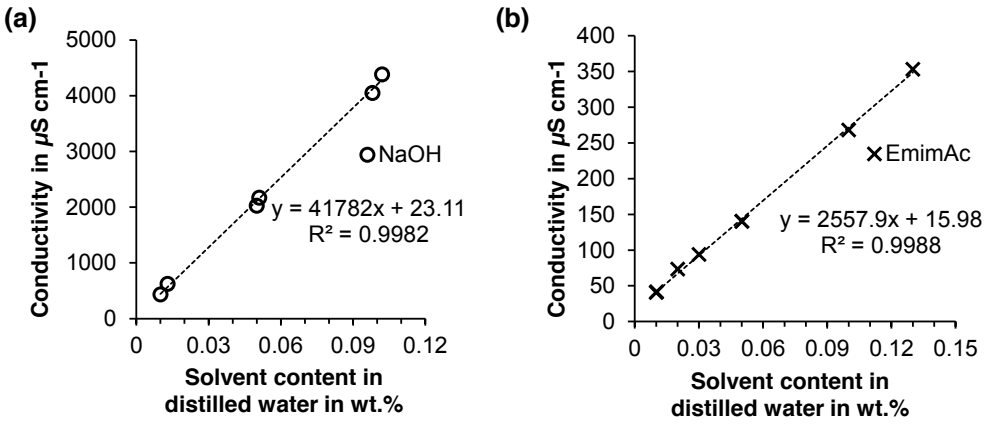

Figure 65: Conductivity of the washing bath as a function of solvent content for (a) NaOH and (b) EmimAc.

In summary, the conductivity and pH measurements of the washing bath indicate that no further solvent was released from the laminates after 36 to 48 h corresponding to three and four washing cycles (Figure 64).

Regarding the methodology, conductivity measurements were found to be advantageous over pH as a means for monitoring the solvent content in the washing bath. Measuring conductivity is a rapid method with stable measurements obtained within 5 to 10 s and a high sensitivity for both solvent systems (Figure 65). The presence of NaOH leads to a strong increase in conductivity already at low concentrations, e.g. a 100-fold increase from the conductivity of 6 µS cm^{-1} in distilled water to 620 µS cm^{-1} at a NaOH concentration of 0.013 wt. % was observed (Figure 65a). Conductivity increases less with the addition of EmimAc, due to the lower atomic mass of NaOH and consequently larger number of ions per added mass of solvent. However, conductivity is still a sensitive measure for EmimAc with a 6-fold increase from distilled water to 40.8 µS cm^{-1} observed for 0.01 wt. % EmimAc (Figure 65b).

Measuring pH, on the contrary, is a less favourable indicator, as it does not allow an estimate of IL content due to the very low change in pH ob-

served even at relatively high IL concentrations in the first washing cycles (Figure 64b). Additionally, measurements are comparably slow with up to 5 min necessary to reach equilibrium and prone to inaccuracies, particularly in high purity water, where measures need to be taken to avoid the influence of carbon dioxide intrusion in the water and static buildup in the sensor [Hach, 2012].

6.3.2 *Analysis of solvent removal by Fourier-transformed infrared spectroscopy*

FTIR spectra of the washed EmimAc and NaOH/urea laminates exhibited only the typical peaks of cellulose II, such as measured for the rayon used as cellulose precursor (Figure 66). The characteristic peaks of the IL EmimAc found at 3095, 1562 and 1463 cm^{-1}, which are attributed to stretching vibrations of C-H, C-N and C=C bonds in the imidazolium cation, respectively [Mahadeva and Kim, 2012; Wu et al., 2014], are not found in the spectrum of the EmimAc ACC laminate (Figure 66a). Similarly, the characteristic peaks of NaOH at 3600 and 1450 cm^{-1}, assigned to O-H stretching of the OH^- group and C-O stretching of the sodium carbonate $NaCO_3$ formed by the reaction of NaOH with CO_2 in air, respectively [Nyquist and Kagel, 1971], and of urea at 3369, 1668, 1562 and 1471 cm^{-1} assigned to vibrations of symmetric N-H stretching, symmetric NH_2 deformation, C-N stretching and antisymmetric C=O stretching, respectively [Grdadolnik and Maréchal, 2002; Madhurambal et al., 2010], are absent from the spectrum of the washed NaOH/urea ACC laminate (Figure 66b).

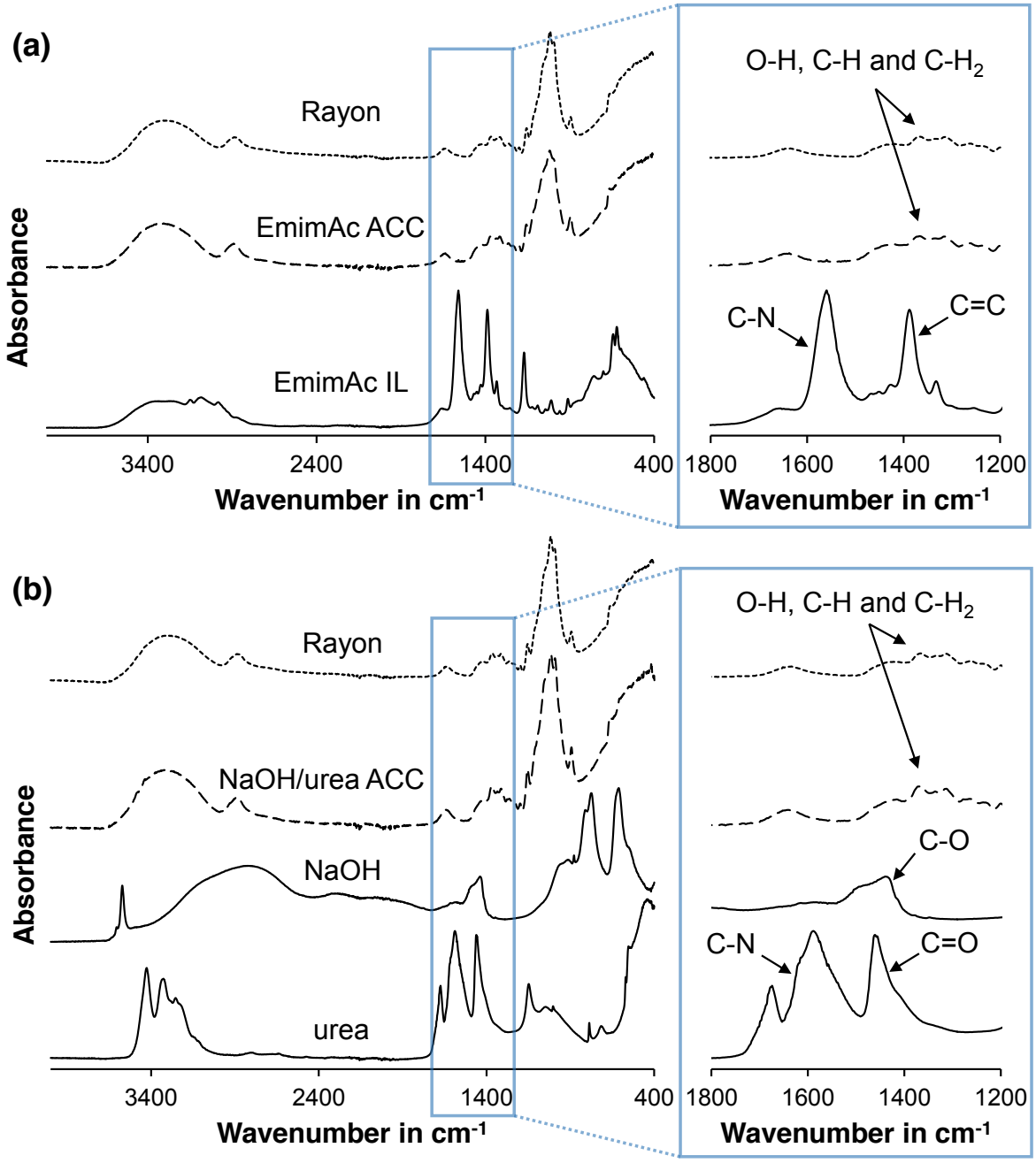

Figure 66: FTIR spectra of rayon, ACCs washed for 60 h and corresponding solvents used for processing, (a) EmimAc and (b) NaOH/urea. The magnified views on the right indicate characteristic peaks of cellulose II and the solvents and their assigned bonds.

Table 12: Carbon, hydrogen and nitrogen (C, H, N) content of as-received rayon and ACC laminates washed for 60 h determined by elemental analysis.

		C in wt. %	H in wt. %	N in wt. %
Rayon	Run 1	42.59	6.64	< 0.3
	Run 2	42.20	6.62	< 0.3
EmimAc ACC	Run 1	40.58	6.58	<0.3
	Run 2	40.63	6.64	<0.3
NaOH/urea ACC	Run 1	40.16	6.27	<0.3
	Run 2	39.99	6.31	<0.3

6.3.3 *Analysis of solvent removal by elemental analysis*

EA revealed a C content of 42.4 wt. % of the as-received rayon and 40.6 wt. % and 40.1 wt. % for EmimAc and NaOH/urea laminates after 60 h of washing, respectively. A low N content of < 0.3 wt. % was found for as-received rayon and all washed ACC laminates (Table 12).

The C content of 42.4 wt. % found for as-received rayon is similar to values observed in other experimental studies of viscose rayon, such as ca. 40 wt. % [Ko et al., 2001] and 40.42 wt. % to 42.52 wt. % [Özgüney et al., 2006]. Similarly, Trejo-O'Reilly et al. [1997] report 43.09 wt. % and 41.44 wt. % C for a commercial microcrystalline cellulose (Avicel, DP 130) and a cellulose fibre regenerated from NMMO, respectively. Brendel et al. [2000] found a C content of 42.56 ± 1.91 wt. % in purified pine wood.

However, the experimentally found C contents of 40 to 42 wt. % are substantially lower than the theoretically expected 44.45 % for pure cellulose (Table 13). The overall lower values in the literature and of rayon in the present study may result from residues of other wood components after cellulose purification, as e.g. the relative C content of lignin is ca. 37 wt.%

and its presence would therefore lower the relative C content of a cellulose sample [Brendel et al., 2000]. A decrease in cellulose chain length also results in a lower C content [Brendel et al., 2000], hence the low DP of 440 of the Cordenka rayon contributes to the low C content found experimentally. Furthermore, other substances may be present from the manufacturing process of rayon. For instance, Özgüney et al. [2006] have found that 12 out of 17 viscose rayon samples contain sulphur, although only small sulphur fractions of 0.064 wt.% were present.

While the relatively low C content of rayon in comparison to the theoretically expected C content of cellulose may be attributed to a general deviation of theoretical and experimental results, low DP and impurities in the sample from fibre processing, the decrease in C content from 42.4 wt. % in as-received rayon to 40.6 wt. % and 40.1 wt. % in ACC laminates (Table 12) requires further discussion. The decrease in C content with ACC processing may be caused by several factors: (i) a decrease in the DP of cellulose, (ii) the presence of other elements, and (iii) varying amounts of water present in the samples prior to EA.

Brendel et al. [2000] argue that a decrease in cellulose chain length results in a C content lower than theoretically expected. The cellulose chain is formed by condensation polymerisation of anhydroglucose units ($C_6H_{12}O_6$) and the separation of -OH and -H as H_2O during polymerisation results in the molecular formula $C_6H_{10}O_5$ for a cellulose chain of infinite length. With decreasing chain length, i.e. decreasing DP, -OH and -H are added to the respective ends of the new, shortened cellulose chains. Therefore, low DP cellulose will have a lower relative C content.

However, calculations based on the atomic mass ratios of cellulose with varying chain length result only in a minor decrease in theoretical C content from 44.45 wt. % to 44.37 wt. % for a reduction in DP from 5000 to 500. A fur-

Table 13: Theoretical elemental composition of pure cellulose, the solvents EmimAc and NaOH/urea, pure water, and their mixtures.

	C	H	N	O	Na
	in wt. %	in wt. %	in wt. %	in wt. %	in wt. %
EmimAc ($C_8H_{14}N_2O_2$)	56.45	8.29	16.46	18.78	-
NaOH/urea (CH_4N_2O)	14.40	5.54	33.60	30.38	16.08
Water (H_2O)	-	11.19	-	88.81	-
Cellulose ($C_6H_{10}O_5$)	44.45	6.22	-	49.34	-
Cellulose + 1 wt. % EmimAc	44.57	6.24	0.16	49.03	-
Cellulose + 5 wt. % EmimAc	45.05	6.32	0.82	47.81	-
Cellulose + 1 wt. % NaOH/urea	44.15	6.21	0.34	49.15	0.16
Cellulose + 5 wt. % NaOH/urea	42.94	6.18	1.68	48.39	0.80
Cellulose + 1 wt. % water	44.00	6.27	-	49.73	-
Cellulose + 5 wt. % water	42.22	6.47	-	51.31	-

ther reduction to a DP of 10 lowers the theoretical C content to 43.96 wt. % and results in an overall decrease in C of ca. 0.5 wt. %. Consequently, a decrease in DP only results in a significant change in C content for massive reductions in chain length.

The dissolution and regeneration of rayon in the IL EmimAc results in a decrease in DP from 440 as received, to 360 after regeneration [Schuermann, 2014], which in turn equals a theoretical decrease in C content of only 0.0025 wt.%. Cellulose chain degradation during partial dissolution can therefore be regarded as a minimal contribution to the change in elemental mass fractions and other factors need to be taken into account, as the EA results deviate by ca. 2 wt. % C.

Based on the elemental composition of each compound, the presence of either solvent would change the proportions of C, H and N from those typical for cellulose. In the case of EmimAc, C content would increase with IL

residues, due to its high C fraction of 56.45 wt. %. Simultaneously, H and N content would increase (Table 13). NaOH/urea residues, on the other hand, would lead to a decrease in C content, due to the addition of relatively heavy N and Na atoms, and a low C content of 14.40 wt. % in the elemental composition of NaOH/urea (Table 13).

The experimentally observed decrease in C content by 1.8 wt. % for the EmimAc ACC is opposite to the theoretically expected increase for a mixture of cellulose and the IL (Table 13). Consequently, IL residues can not be responsible for the change in C content of the EmimAc ACC. On the other hand, the experimentally observed decrease in C content by 2.3 wt. % for the NaOH/urea ACC matches the theoretically expected trend for a mixture of cellulose and NaOH/urea. However, relatively large fractions of NaOH/urea of >5 wt. % in the mixture with cellulose are necessary to achieve a decrease in C content of >1.5 wt. %. Such a high NaOH/urea content would simultaneously result in a significant increase in N content to >1.7 wt. %, that would be well detectable by EA (Table 13). In the experiments no change in N content was observed (Table 12), indicating that relatively high levels of NaOH/urea are also an unlikely cause for the change in C content.

The third factor to consider is the presence of water in the samples, as additional H_2O would lead to a decrease in C fraction due to the relatively heavy O atoms. The presence of water has a strong influence on the elemental composition of cellulose, with a decrease in C content of 0.45 wt. % per 1 wt. % water (Table 13). Therefore, an increase in moisture content of approximately 4 wt. % and 4.5 wt. % in EmimAc and NaOH/urea ACCs would result in the experimentally observed decrease in C content.

All samples were dried prior to performing EA, in order to avoid artefacts due to moisture. However, the moisture adsorption in cellulose from vapour

occurs at high rates with e.g. 15 wt. % water adsorbed within 4 min reported by Stamm [1956] for a regenerated cellulose film (cellophane) at 84 % RH and 26.7 °C.

Even though the RH of ambient air may be lower than 84 %[1], it appears possible that the samples adsorbed 4 to 5 wt. % water during preparation. Considering that the ACCs are harder to cut than the rayon fibres, it is likely that their preparation was more time-consuming, resulting in longer exposure to ambient air and hence higher moisture content.

In summary, the difference in C content between as-received rayon and ACCs is best explained by a difference in moisture content of the samples. Small amounts of additional water result in a comparably strong decrease in C content without increasing the N content, whereas solvent residues would have led to an increase in C content in the case of EmimAc, and to a simultaneous increase in N content in case of NaOH/urea, both of which were not observed in EA.

The absence of the characteristic peaks of the solvents in the FTIR spectra of washed ACCs (Figure 66) and no increase in the N content determined by EA (Table 12) indicates that virtually all of the solvent has been removed from the laminates. However, it cannot be ruled out that traces of solvent remain in the ACCs, due to the relatively low sensitivity of EA ($\pm$ 0.3 wt. %) at concentrations close to 0 wt. %. The presence of 1 wt. % EimAc in an ACC laminate results in a N content of only 0.16 wt. %, which is too low to be detected by EA. The relatively dark appearance of ACCs prepared using ILs, especially multi-layered laminates (Figure 67), hence poses the question, whether the colour change from white rayon to brown ACCs is due to remaining IL.

1 The average RH in Dunedin, NZ, where EA was performed at Otago University, in August is ca. 70 % (www.weather-and-climate.com, 8.9.2015).

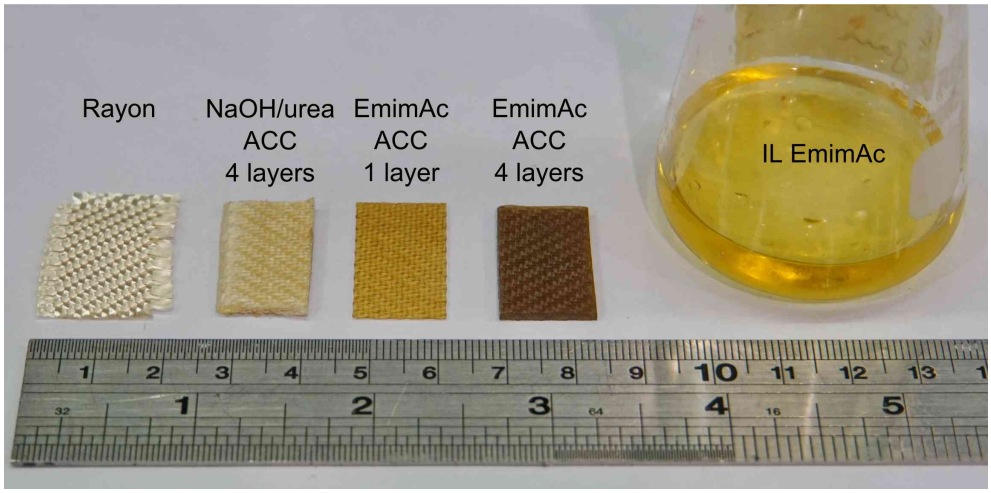

Figure 67: Photograph as received rayon, ACC laminates and the solvent EmimAc.

FTIR analysis of sections from a thick ACC with 8 laminae cut from the skin to the core revealed no traces of the IL with increasing thickness (Figure 68). The absence of typical solvent-related vibrations is indicative of complete solvent removal, as the detection of impurities in solids with concentrations down to the part per million range (0.0001 wt.%) is possible by means of FTIR, which is frequently used in e.g. forensic, pharmaceutical and food sciences [Chan and Kazarian, 2006; Mauer et al., 2009; Gonzalvez et al., 2011]. The Beer-Lambert law states that the absorbance intensity is proportional to the concentration of a compound, hence a higher intensity radiation (e.g. synchrotron beam) results in a higher sensitivity of FTIR [Chan and Kazarian, 2006]. Furthermore, for heterogeneously distributed substances the limit of detection can be lowered by measuring a smaller area, in which the local concentration of the substance in question is higher [Chan and Kazarian, 2006]. Synchrotron-based FTIR-microspectroscopy (beam spot size 5 µm) of the matrix phase, which is expected to contain the highest concentration of residual solvent, also reveals no typical IL peaks (results presented in Chapter 7, Figure 81), confirming the results obtained by macro ATR-FTIR.

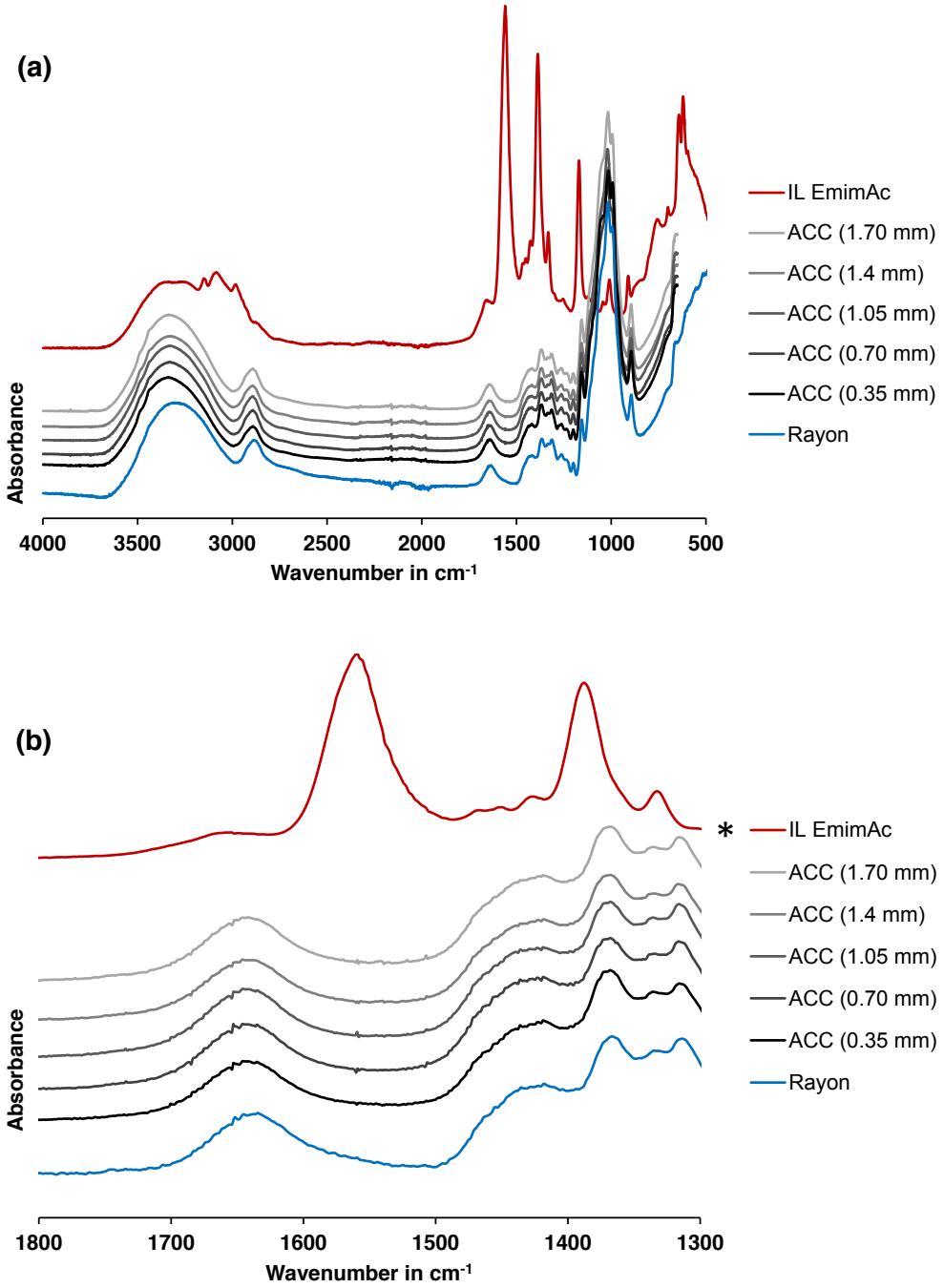

Figure 68: (a) FTIR spectra of an ACC with 8 laminae as a function of thickness from the skin (0.35 mm) to the core (1.70 mm). (b) Magnification of the wavenumber region 1300 to 1800 cm^{-1} with C-N (1562 cm^{-1}) and C=C (1463 cm^{-1}) vibrations typical for the imidazolium (* The intensity of the IL spectrum was decreased by a factor of 0.4 to fit the y-axis).

The absence of peaks typical for IL in the FTIR spectra indicates that the colour change is likely due to the other reasons, such as cellulose degradation. Rayon textile dried at 95 °C, the temperature used for partial dissolution, exhibits the same colour as the as-received rayon, indicating that no cellulose decomposition occurs. Meine et al. [2010] found the ILs EmimCl and BmimCl to be thermally stable at 100 °C with the onset of degradation observed at 140 °C, suggesting that neither the cellulose nor the IL on their own degrade at the temperature used for partial dissolution (95 °C).

However, the presence of IL has been observed to lead to more rapid decomposition of cellulose [Swatloski et al., 2002]. Firstly, ILs lead to a reduction in DP of cellulose during dissolution [Zhang et al., 2005a; De Silva et al., 2015], and secondly act as catalysts in the pyrolysis of cellulose, thereby lowering the onset temperature of cellulose decomposition [Kudo et al., 2011]. A change in colour of IL from yellow as-received to brown after recovery from cellulose pyrolysis at 250 °C is reported by Kudo et al. [2011] and attributed to the presence of levoglucosenone. Levoglucosenone is formed from levoglucosan, an anhydroglucose that is formed in the first step of cellulose pyrolysis [Lin et al., 2009]. Similarly, the change in colour of the ACCs may be the result of the onset of cellulose pyrolysis catalysed by the IL during partial dissolution.

NaOH/urea laminates also show a slight change in colour when compared to as-received rayon (Figure 67). The higher fraction of N in NaOH/urea means that EA is more sensitive to residual NaOH/urea when compared to EmimAc. However, NaOH/urea contents below 1 wt. % might still go unnoticed, as the fraction of N (0.34 wt. %, Table 13) approaches the limit of detectability ($\pm$ 0.3 wt. %). However, no traces of NaOH/urea were detected by FTIR (Figure 66). Furthermore, a low residual NaOH/urea content would not prohibit the use of ACCs in e.g. biomedical applications, as NaOH and

urea are substances of low toxicity that occur naturally in mammals. Na^+ ions are, for example, part of the nervous system and urea is a product of protein metabolism and excreted by the kidney [Reece et al., 2013].

Removal of solvent from ACCs in an industrial context

For industrial/commercial processing of ACCs a shorter washing time than 36 to 60 h will likely be required. Overall, the diffusion rate of solvent from ACC laminates will increase and consequently the total washing time will decrease with (i) increasing concentration gradient between solvent in the regenerated material and the washing bath, and (ii) increasing temperature of the washing bath [Bang et al., 1999; Jiang et al., 2011]. The washing cycles of 12 h were relatively long, resulting in an extensive total washing time. It can be assumed that more frequent water exchanges or a countercurrent washing setup, such as is used in Viscose fibre production [Woodings, 2001], and an elevated temperature of the washing bath will result in greatly enhanced washing efficiency. For example, the diffusion coefficient of IL in water increases by almost threefold from 2 to $5.5 \times 10^{-7} cm^2\ s^{-1}$ when the temperature increases from 15 to 75 °C and almost doubles from 1.24 to $2.26 \times 10^{-7} cm^2\ s^{-1}$ when decreasing the IL content in the washing bath from 20 to 0 wt. %, respectively [Jiang et al., 2011]. Consequently, reduced total washing times of less than 12 h appear feasible and measuring the conductivity of the washing bath is an easily implemented pathway for continuously monitoring the solvent content and determining the completion of solvent removal, also on an industrial scale.

However, a reduction of washing times will give rise to certain drawbacks. Firstly, the washing efficiency is in direct competition with the efficiency of solvent recovery. If a higher concentration gradient will be achieved by

exposing the regenerating ACC to larger volumes of water, the solvent concentration will be lower in the washing bath. Consequently, larger volumes of water need to be evaporated or filtered to regain the solvent for recycling, which is important for financial and environmental reasons. Secondly, the diffusion rate of the solvent is linked to the structure and properties of the regenerated cellulose. It has been reported that a higher diffusion rate leads to the formation of larger pores and lower strength of regenerated cellulose films [Bang et al., 1999; Mao et al., 2006]. Therefore, future investigations need to address whether reduced washing times can be achieved without compromising solvent recycling and mechanical properties of ACC laminates.

6.4 SUMMARY

Conductivity measurements were established as a sensitive method for routine control of solvent content in the washing bath. Completion of solvent removal was indicated by no further increase in conductivity of the washing bath after a total washing time of 48 h in four washing cycles. Complete removal of EmimAc and NaOH/urea by washing ACC laminates in distilled water is indicated by the absence of characteristic peaks of the solvents in FTIR spectra and no observed increase in nitrogen content determined by elemental analysis.

It is concluded that the conductivity of the washing bath is a good indicator for determining the necessary washing times of ACCs, can be used to monitor solvent content during recovery and recycling, and is a good indication of the safe character of ACCs for use in general applications.

7

INDIVIDUAL CHARACTERISATION OF THE FIBRE AND MATRIX PHASES IN ALL-CELLULOSE COMPOSITE LAMINATES

7.1 INTRODUCTION

When processing ACCs *via* the 1-step method, a portion of the cellulose reinforcement is reshaped into the matrix phase by dissolution and regeneration. It is well known that the dissolution and regeneration of cellulose has an effect on cellulose structure. The inter- and intramolecular hydrogen bonding network, van der Waals forces and hydrophobic interactions of cellulose are disrupted by solvent interaction and upon regeneration the DP, polymorph and crystallinity may differ from the original cellulose [O'Sullivan, 1997; Lindman et al., 2010; Yamane et al., 2015; De Silva et al., 2015].

As a consequence of the dissolution and regeneration process, the cellulose matrix of an ACC will exhibit a different fine structure than the cellulose precursor. In general, a lower crystallinity of ACCs are observed when compared to the precursor. For instance, Nishino et al. [2004] report a decrease in crystallinity from 82 % in as-received ramie fibres to 65 % in partially dissolved and regenerated ACCs. Similar decreases in crystallinity have been observed for e.g. cotton, flax and lyocell fibres upon processing to ACCs [Gindl-Altmutter et al., 2012; Soykeabkaew et al., 2008; Arévalo et al., 2010].

In spite of the relevance of understanding the complex interplay of changes in cellulose structure induced by processing (with a variety of influential parameters such as solvent system, dissolution time, regeneration rate and medium, and drying conditions) and the mechanical properties of the final ACCs, a combined analysis of the structure and mechanical properties of the individual phases is missing in the literature.

Duchemin et al. investigated the structural changes during partial dissolution in detail and observed that the matrix in ACCs prepared from microcrystalline cellulose consists of a mixture of poorly crystalline and amorphous cellulose that is best described as paracrystalline [Duchemin et al., 2007, 2009b]. Furthermore, the structure of the cellulose matrix depends on the regeneration and drying conditions. A slow regeneration rate by vapour precipitation under exposure to ambient air results in ACCs with a 10 to 14 % higher crystallinity and significantly improved mechanical properties when compared to fast regeneration by water spraying and immersion [Duchemin et al., 2009b]. Although the structure of the ACCs was analysed in detail, the mechanical analysis was limited to the bulk properties and not extended to the individual phases.

An individual mechanical characterisation of the cellulose fibre and regenerated cellulose matrix in an ACC was carried out by Gindl et al. [2006c]. ACCs were prepared by partial dissolution of beech pulp in LiCl/DMAc and the individual phases characterised by nanoindentation and compared to an epoxy-matrix composite using the same pulp fibres as reinforcement. The elastic modulus of the cellulose fibres increased from ca. 10 GPa embedded in epoxy to 20 GPa in the ACC. The regenerated cellulose matrix exhibited an elastic modulus equal to the undissolved fibres. Gindl et al. [2006c] argue that the increase of fibre modulus results from partial dissolution not only at the surface but also within the cell wall of the fibres. Hence, a regenerated

matrix phase is formed in between fibres and between cellulose I microfibrils within the cell walls, resulting in an increased indentation modulus of the fibres.

The hypothesis of partial dissolution affecting the core of cellulose fibres proposed by Gindl et al. [2006c] appears likely to be true, considering the inhomogeneous dissolution of natural fibres where the S2 cell wall layer at the core dissolves prior to the primary cell wall at the surface [Cuissinat and Navard, 2006; Le Moigne et al., 2008, 2010]. However, Gindl et al. [2006c] only analysed the cellulose structure of the bulk ACCs by WAXD, which revealed a shift of diffraction peaks, indicating the formation of cellulose II with ACC processing. Unfortunately, the structural differences between cellulose fibre and matrix are not evident from these results.

Even though the structural and mechanical properties of ACCs have been reported in substantial detail, a combined analysis of the individual phases within a given ACC system (the variety of cellulose precursors, solvents and processing procedures make comparisons between studies complicated) has thus far not been published. A challenge in this topic is the small volume fraction of matrix of only ca. 3 to 10 vol. % in ACCs (Chapters 4 and 5). The matrix layer in between fibres ranges from barely measurable between contacting fibres to a thickness of 2 to 5 µm (Figures 47 and 50). Consequently, characterisation methods with a high spatial resolution are required. Nanoindentation, atomic force microscopy (AFM), FTIR-microspectroscopy and transmission electron microscopy (TEM) have been identified as suitable methods for an *in-situ* analysis of the mechanical (nanoindentation, AFM) and structural (FTIR, TEM) properties of the fibre and matrix phases in ACC laminates.

Nanoindentation is a sensitive tool for determination of mechanical properties at small length scales [Schuh, 2006]. Nanoindentation has been estab-

lished as a useful technique for determining the local elastic properties of cellulosic materials, such as the cell walls of pine wood [Tze et al., 2007] and bamboo [Wang et al., 2012], as well as regenerated cellulose fibres [Gindl et al., 2006a; Ganser et al., 2015], and of fibre and matrix in polymer matrix composites [Gregory and Spearing, 2005; Hardiman et al., 2014], and bio-based composites [Wang et al., 2006]. Similarly, AFM phase imaging facilitates mapping of qualitative differences in viscoleastic properties in a sample with nanoscale resolution [Magonov et al., 1997; García and Perez, 2002] and has been utilised for the characterisation of fibre and matrix phases in composites [Wang and Hahn, 2007; Gao and Mäder, 2002; Downing et al., 2000; Lee et al., 2009; Wang et al., 2010b; Nair et al., 2013].

FTIR has been established as a tool for characterising cellulose structure for decades [O'Connor et al., 1957, 1958; Nelson and O'Connor, 1964; Röder et al., 2006; Široký et al., 2010b]. FTIR microspectroscopy combines the extraction of structural information from a sample by FTIR with the imaging capability of optical microscopy. When using standard laboratory FTIR microscopes the signal to noise ratio decreases with decreasing IR beam spot size, due to the low brightness of the infrared source [Carr, 2001]. Preliminary experiments conducted on ACC laminates using a laboratory FTIR microscope (Frontier, Perkin Elmer, Waltham, MA, USA) revealed that in the case of ACCs, an aperture of $100 \times 100\,\mu m^2$ resulted in a clear spectrum, at $50 \times 50\,\mu m^2$ noise increased substantially but typical features were still apparent (Figure 69). When setting the aperture to $25 \times 25\,\mu m^2$ a critical noise level was reached that obscured the spectrum and at $5 \times 5\,\mu m^2$, the spot size required for investigating individual fibre and matrix locations, only noise was measured (Figure 69).

A higher spatial resolution is possible when using the high brightness of synchrotron radiation for FTIR microspectroscopy. A synchrotron IR beam

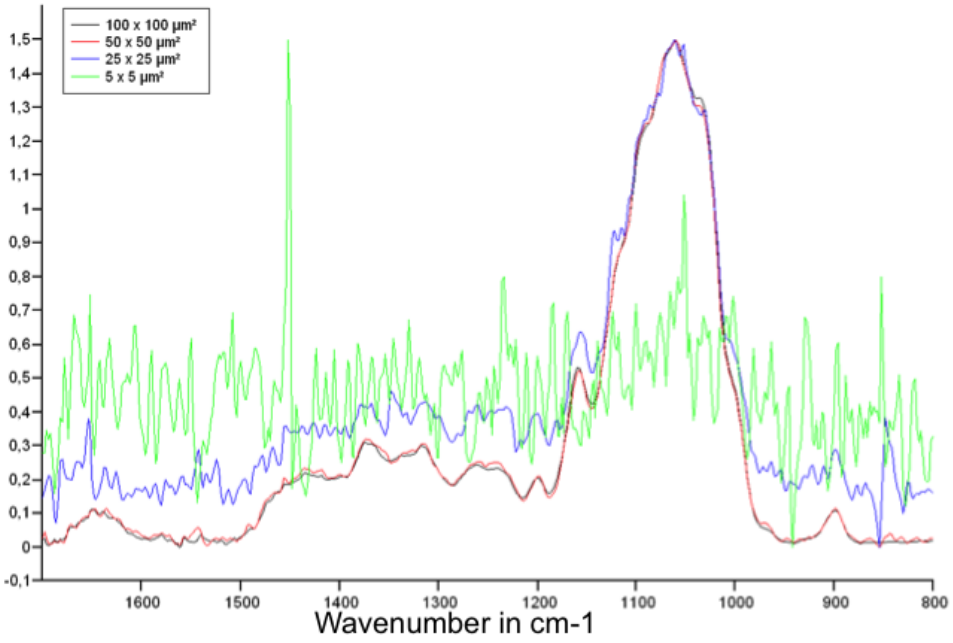

Figure 69: Decreasing signal to noise ratio with decreasing aperture in FTIR microspectroscopy of ACCs using a standard laboratory light source (Frontier, Perkin Elmer, Waltham, MA, USA).

can be set to diffraction limited spot sizes with apertures similar to the wavelength of the beam [Carr, 2001], which is down to 2 µm in the mid-IR range used for characterising cellulose [Nelson and O'Connor, 1964]. At the IR beamline of the Australian Synchrotron in Melbourne a spatial resolution of 3 to 5 µm is achieved in the mid-IR range at 3000 to 1500 cm^{-1} (www.synchrotron.org.au, 21.09.2015).

A further method that allows the characterisation of cellulose at high spatial resolution is TEM. The microstructure of cellulose samples can be analysed in TEM micrographs that resolve features on the nanoscale [Hanley et al., 1997; Rous et al., 2006]. Furthermore, electron diffraction facilitates analysis of the fine structure of cellulose [Aravindanath et al., 1982; Chaudhuri et al., 1983; Sugiyama et al., 1991] and diffraction patterns can be obtained with a beam spot size of 1 $µm^2$ [Müller et al., 2000].

This chapter investigates the structure-property relationship in 1-step processed ACCs through a combined structural and mechanical analysis of ACC laminates and their individual phases. The influence of the processing parameters dissolution time and regeneration medium on the fibre and matrix phases in ACCs were determined, by subjecting the ACCs to a complete structural and mechanical characterisation. The bulk ACC laminates were characterised by tensile testing, WAXD and FTIR. The individual fibre and matrix phases were characterised by nanoindentation, AFM, synchrotron-based FTIR-microspectroscopy and TEM.

7.2 EXPERIMENTAL PROCEDURES

7.2.1 *Sample preparation*

IL (EmimAc) was used as solvent to ensure a sufficiently high matrix fraction of approximately 10 vol. % in ACC laminates for characterisation of the matrix phase. ACCs with 2 laminae were prepared by SIP using an infusion pressure of 200 mbar. Dissolution was carried out in a hot press at 95 °C and 1 MPa. The effect of dissolution time on the structure and properties of ACC laminates and their individual phases was investigated by hot pressing the samples for either a short or long time of 15 min and 6 h, respectively (Table 14). The effect of the regeneration medium was investigated by regenerating in distilled water or acetone. The samples regenerated in acetone were kept in an acetone bath for 72 h with two acetone exchanges daily. Subsequently, the samples were transferred to a distilled water bath. All samples were washed in water until no further increase in conductivity was measured to ensure complete solvent removal. Specimens for SEM and tensile testing

Table 14: Processing parameters for the ACCs subjected to individual phase analysis.

Sample	Solvent	Dissolution time	Regeneration medium
IL_15min_H_2O	EmimAc	15 min	distilled water
IL_6h_H_2O	EmimAc	6 h	distilled water
IL_6h_acetone	EmimAc	6 h	acetone

were cut with a sharp blade prior to drying. Tensile tests were performed on rectangular coupons with a length and width of 100 and 10 mm, respectively, at a gauge length of 40 mm.

Unreinforced cellulose films were prepared as described in Section 3.3 with the same processing parameters as for the ACC laminates (Table 14). Tensile tests were performed on rectangular strips with a length and width of 30 and 4 mm, respectively, at a gauge length of 16 mm.

7.2.2 *Synchrotron-based Fourier-transformed infrared microspectroscopy*

FTIR microspectroscopy was performed at the IR-beamline of the Australian Synchrotron in Melbourne. FTIR spectra were obtained using a V80v FT-IR spectrometer and Hyperion 2000 IR Microscope (Bruker, Billerica, MA, USA) in transmission and ATR mode (www.synchrotron.org.au, 29.09.2015).

For acquisition of transmission spectra, sections of 4 µm thickness were cut from ACCs using a sliding microtome following softening by immersion in distilled water for 30 min. The sections were collected on glass slides, covered by a cover slip and air-dried at ambient conditions (20 ± 2 °C, 30 to 50 % RH). The sections were mounted in a sample holder with IR-transparent diamond windows and slightly compressed to ensure contact between the sample and diamond surfaces.

Transmission spectra were obtained by averaging 64 scans in the wavenumber range 4000 to 700 cm^{-1} at a resolution of 4 cm^{-1}. The IR-beam was limited by the aperture to a spot size of $5 \times 5\,\mu m^2$. A small portion of potassium bromide (KBr) was placed in the diamond compression cell next to the ACC samples for background measurements. The background measurement was repeated every 8 measurements.

ATR spectra were acquired by automatically lowering the ATR crystal onto microtomed surfaces of the ACCs. The aperture was set to $20 \times 20\,\mu m^2$, which was reduced to a beam spot size of $5 \times 5\,\mu m^2$ on the sample, due to the refractive index of the Germanium ATR crystal. 128 scans in the wavenumber range 4000 to 700 cm^{-1} were averaged to obtain ATR spectra at a resolution of 4 cm^{-1}.

7.2.3 *Analysis of Fourier-transformed infrared spectra*

FTIR spectra were analysed using Opus 7.2 (Bruker, Billerica, MA, USA). The FTIR based cellulose crystallinity indices TCI (I_{2900}/I_{1372}) and LOI (I_{1420}/I_{890}) were calculated according to Nelson and O'Connor [1964] and O'Connor et al. [1958]. I_{2900} is measured from a horizontal baseline drawn from the minimum at 2990 cm^{-1}. The baselines for I_{1420} and I_{890} are drawn between the neighbouring minima and for I_{1372} between the minima at 1400 and 1280 cm^{-1} (Figure 70). The determination of peak intensities was automated by programming a protocol using the integration tool of Opus 7.2, to ensure repeatability of the measurements.

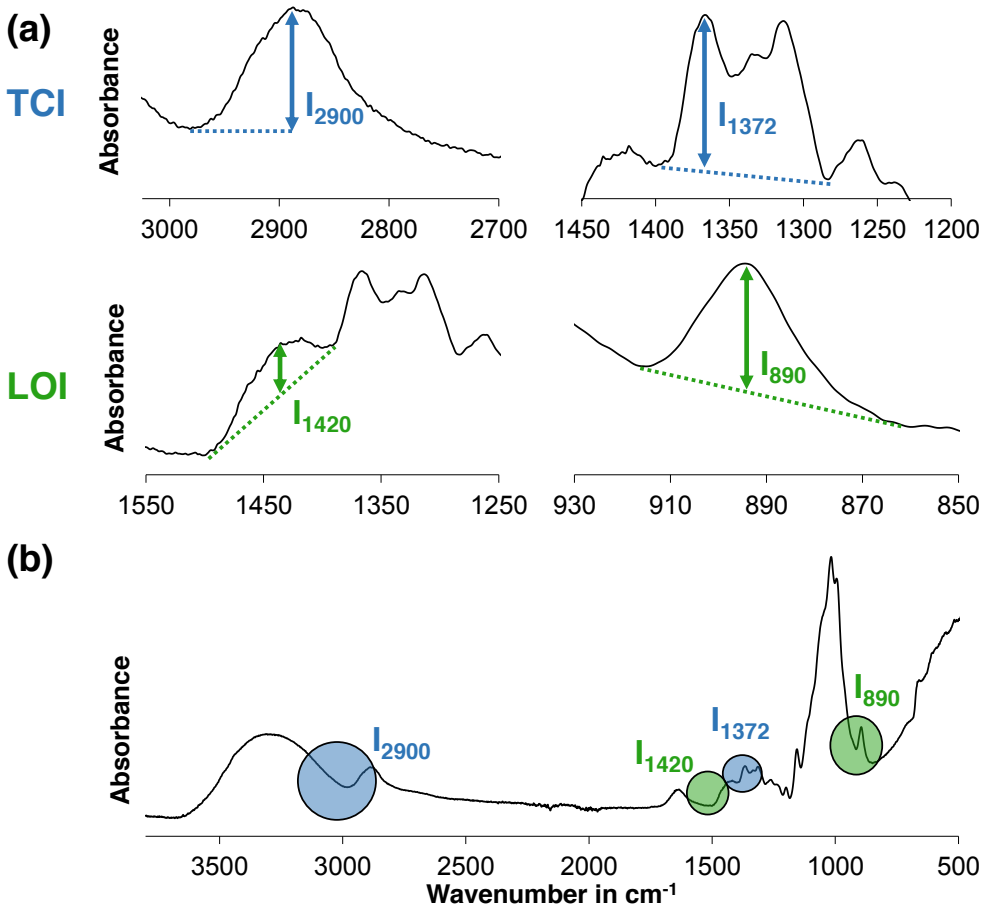

Figure 70: (a) The baselines for determining the intensity (b) and the position of the respective wavenumbers in the spectrum of cellulose II for the FTIR intensity ratios TCI (I_{2900}/I_{1372}) and LOI (I_{1420}/I_{890}) according to Nelson and O'Connor [1964] and O'Connor et al. [1958].

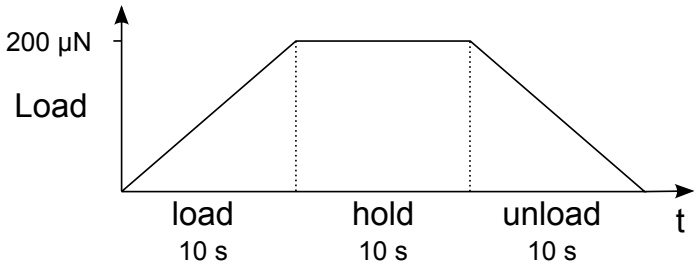

Figure 71: Load function for quasi-static nanoindentation.

7.2.4 *Nanoindentation*

Quasi-static nanoindentation experiments were conducted on a Triboindenter TI-950 using a Berkovich diamond indenter tip and the data was analysed in Triboviewer V. 5.1.5.0 (Hysitron Inc., Minneapolis, MN, USA). The contact area of the diamond tip was calibrated by indenting a quartz of known elastic modulus. A load function similar to that described by Gindl et al. [2006a] for nanoindentation of regenerated cellulose fibres was applied. Load controlled indentation was performed with a maximum load of 200 µN, which was loaded, held and unloaded in 10 s intervals (Figure 71), resulting in a loading and unloading speed of 20 µN s^{-1}. All residual indents were checked for regularity of shape and placement by scanning the topography of the sample after indentation.

Specimen surfaces were prepared by means of an ultramicrotome equipped with a glass knife (Ultracut UCT, Leica Microsystems GmbH, Wetzlar, Germany). An arithmetic average surface roughness R_a of 10 to 20 nm was achieved. The indentation depth at the maximum load of 200 µN was in the range of 150 to 190 nm. Hence, a compromise was achieved between an indentation depth of 10 to 20 times of the surface roughness required to avoid data scatter from variations in contact area [Fischer-Cripps, 2002] and yet relatively small indents that allowed close spacing of neighbouring

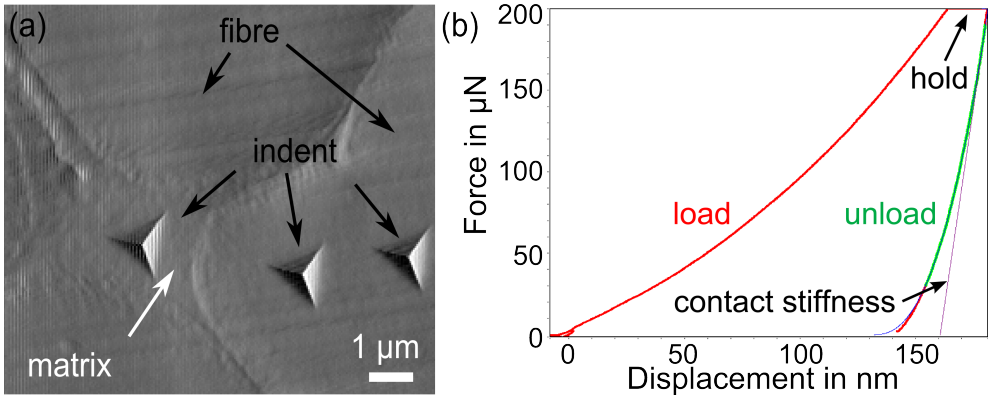

Figure 72: (a) Topography scan of residual indents on the fibre and matrix phases in an ACC laminate. (b) Typical force-displacement curve for nanoindentation of ACCs.

indents. The indentations were placed on the fibre and matrix phases, with their centres spaced at a minimum distance of 3 µm to exclude overlap of the plastic deformation zones (Figure 72a). Nanoindentation was performed at ambient conditions (24 ± 2 °C and 40 to 50 % RH). A minimum of 17 indentations were performed on each phase.

The contact stiffness, derived from the initial slope of the unloading segment of nanoindentation force-displacement curves (Figure 72b), and reduced modulus were calculated by applying the Oliver-Pharr method [Oliver and Pharr, 1992]. The reduced modulus (E_r) includes the elastic deformation of both sample and the indenter tip (therefore reduced), and can be converted to the elastic modulus by the following equation

$$\frac{1}{E_r} = \frac{(1-\nu^2)}{E} + \frac{1-\nu_i^2)}{E_i} \tag{10}$$

where E is the elastic modulus and ν the Poisson's ratio of the sample and ν_i and E_i the same quantities of the indenter, respectively. However, this formula only holds true for isotropic materials [Fischer-Cripps, 2002; Gindl et al., 2006a]. Regenerated cellulose fibres are anisotropic with a preferred

crystallite orientation parallel to the fibre axis and a gradient in crystallite orientation from skin to core [Müller et al., 2000] and a gradient in the porosity from skin to core of rayon [Rous et al., 2006]. Furthermore, Lee et al. [2007] found a difference in E_r of 50 % when performing nanoindentation of lyocell fibres in longitudinal (13.2 GPa) and transverse (6.7 GPa) direction. Therefore, no conversion was carried out in this work and E_r is reported. Gindl et al. [2006a] argue that due to $E_{diamond} \gg E_{rayon}$ the deviation of E_r from the elastic modulus is small when investigating cellulosic fibres and ACCs.

7.2.5 *Atomic force microscopy*

Phase and topography images of ACCs were obtained by tapping mode atomic force microscopy (Dimension 3100 AFM, Veeco, Plainview, NY, USA). Standard monolithic silicon tapping mode tips with an approximate resonant frequency of 300 kHz, a spring constant of 40 N m^{-1} and a tip radius $<$ 10 nm were used. Images were analysed using Nanoscope V1.4 (Bruker, Billerica, MA, USA). Specimen surfaces were prepared by means of an ultramicrotome equipped with a glass knife (Ultracut UCT, Leica Microsystems GmbH, Wetzlar, Germany).

Background: Phase imaging in atomic force microscopy

The simplest imaging mode of AFM is contact mode, where the tip of the cantilever is in continuous contact with the surface. The deflection of the cantilever, i.e. the force exerted by the tip pressing on the surface (tip-to-surface force), is kept constant by adjusting the height of the cantilever in a feedback loop of the piezo drive that controls the cantilever movement. An image of the topography is obtained by using the height movements of the

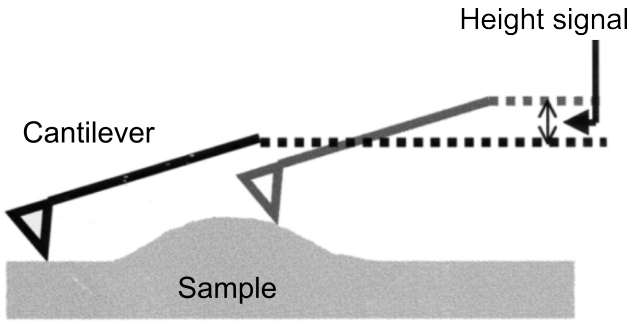

Figure 73: Schematic of contact mode AFM (reproduced from Reich et al., 2001; with kind permission of Elsevier).

cantilever as signal [Reich et al., 2001; Vancso and Schönherr, 2010]. A drawback of contact mode AFM is that the image is limited to the topography and furthermore the tip-to-surface force may deform the sample and further artefacts can arise from particles adhering to the tip, and tip wear (blunting) which reduces resolution [Vancso and Schönherr, 2010].

Intermittent contact or tapping mode is an AFM imaging method employed to reduce the tip-to-surface forces and inelastic surface deformation [Magonov et al., 1997]. Additionally, tapping mode yields information beyond topography, such as variations in the surface adhesion, friction coefficient and (visco)elastic properties of the sample [García and Perez, 2002]. In tapping mode, the AFM cantilever is oscillated at or near its resonance frequency while scanning the sample surface and hence only periodic, intermittent contact between tip and sample occurs. The tip-to-sample force is generally found to be lower than in contact mode [García and Perez, 2002] and is controlled by the ratio of the free oscillating amplitude A_0 and the setpoint amplitude A_{sp} [Magonov et al., 1997]. The amplitude of the oscillation is used as feedback signal to image the surface topography [García and Perez, 2002].

In addition to the amplitude, the phase shift between the cantilever oscillation and the external driving force can be monitored in tapping mode

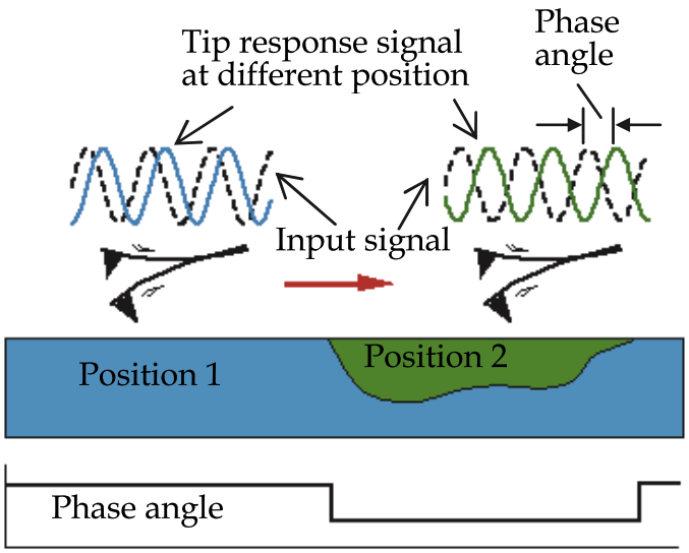

Figure 74: Schematic of tapping mode AFM illustrating a variation in the phase angle depending on the sample composition, where the green phase at Position 2 is stiffer in comparison to Position 1 [Xu et al., 2011].

(Figure 74). Magonov et al. describe the interaction between an oscillating tip and the sample surface upon contact and show the correlation between the phase shift and the modulus of a sample. A variation in modulus results in the generation of contrast in the phase image, with stiffer regions exhibiting a positive phase shift that appears brighter in phase images obtained at moderate tapping conditions (A_{sp}/A_0 = 0.4 to 0.7) [Magonov et al., 1997].

Phase lag is also sensitive to sudden changes in topography [García and Perez, 2002]. The ultramicrotomed surfaces of ACC laminates exhibited a low average arithmetic surface roughness R_a of 10 to 20 nm and gentle slopes between spots of different height were observed, thus limiting the influence of topography on the phase signal to a minimum. Under the assumption that the adhesive surface forces acting on the cantilever tip are similar for the fibre and matrix phases in ACC laminates, a difference in the phase signal can be interpreted as a qualitative difference in the viscoelastic properties.

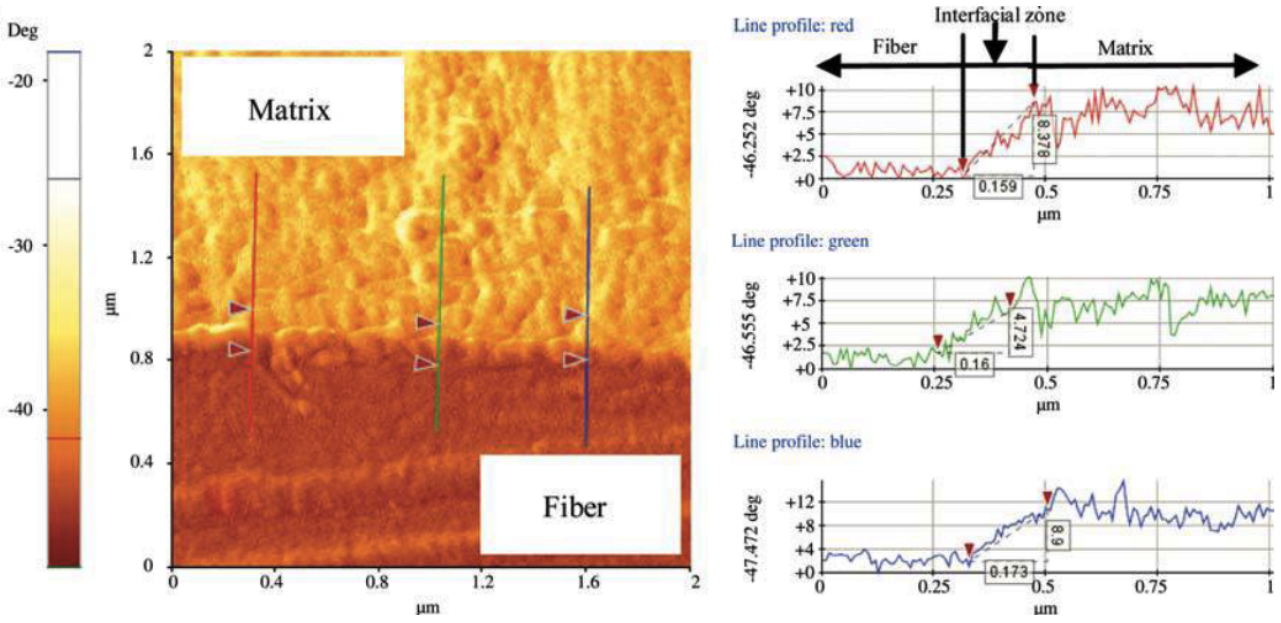

Figure 75: Example of AFM phase imaging to distinguish the fibre, matrix and interphase in a regenerated cellulose fibre-reinforced polypropylene composite [Lee et al., 2009].

AFM phase imaging has been used as a tool to determine qualitative differences between the fibre and matrix phase of composites (Figure 75), such as carbon fibre-reinforced epoxy [Wang and Hahn, 2007], glass fibre-reinforced epoxy [Gao and Mäder, 2002; Downing et al., 2000], and regenerated cellulose fibre-reinforced polypropylene [Lee et al., 2009; Wang et al., 2010b; Nair et al., 2013].

7.2.6 *Transmission electron microscopy*

ACC laminate samples were embedded in Spurr resin and sections with a thickness of 100 nm were prepared using an ultramicrotome equipped with a diamond knife (Ultracut UCT, Leica Microsystems GmbH, Wetzlar, Germany). The sections were collected on copper grids (G200-Cu, Electron Microscopy Sciences, Hatfield, PA, USA) and air-dried.

Transmission electron micrographs were obtained using a 200 kV JEOL 2010 FEG transmission electron microscope (JEOL, Peabody, USA) fitted with a double tilt sample holder (tilt ±42°). Bright field low dose images of the utramicrotomed sections of ACC laminates were recorded using a bottom-mounted 1k SIS Keenview CCD camera (Olympus Soft Imaging Solutions GmbH, Münster, Germany).

7.3 RESULTS AND DISCUSSION

7.3.1 *Microstructure*

The microstructure of the ACC laminates was found to be very similar despite the differences in processing parameters. All laminates were found well consolidated with a thin layer of matrix between fibres (Figures 76, 77 and 78). A similar matrix fraction (V_m) of 9.9 ± vol. 3.1 % was found for IL_15min_H_2O when compared to the laminates dissolved for 6 h with a V_m of 11.4 ± 3.3 vol. % for IL_6h_H_2O and 8.4 ± 1.1 % for IL_6h_acetone. This finding indicates that a comparably short dissolution time of 15 min is sufficient to reach a high cellulose concentration in the infused IL, which does not increase substantially by extending the dissolution time to 6 h, although a 12 % higher solvent uptake may have aided the high V_m in IL_15min_H_2O (Table 15).

SEM observations revealed a higher occurrence of interlaminar voids with a diameter of approximately 100 µm in IL_6h_acetone when compared to IL_15min_H_2O and IL_6h_H_2O, which is reflected in the higher void fraction based on density of 3.0 ± 0.3 vol. % compared to 2.0 ± 0.4 vol. % and 2.3 ± 0.5 vol. %, respectively. A very low void content of 0.11 ± 0.13 vol. % or

Table 15: Density, void fraction (V_v) and matrix fraction (V_m) of ACC laminates. (Void fraction was determined based on the actual and theoretical density of the ACCs (density of rayon 1.52 g cm^{-3}) and by image analysis).

	Density in g cm^{-3}	V_v (density) in %	V_v (image) in %	V_m (image) in %	Solvent uptake in %
IL_15min_H_2O	1.489 ± 0.007	2.0 ± 0.4	0.02 ± 0.01	9.9 ± 3.1	72
IL_6h_H_2O	1.485 ± 0.007	2.3 ± 0.5	0.03 ± 0.01	11.4 ± 3.3	60
IL_6h_acetone	1.474 ± 0.004	3.0 ± 0.3	0.11 ± 0.13	8.4 ± 1.1	57

less was measured by image analysis. This is due to the requirement of analysing high magnification images of a yarn, which excludes the larger interlaminar voids. The low V_v measured by image analysis shows that SIP using IL effectively joins all fibres in a yarn with few microdefects, although it is a localised measure that will not represent the full microstructure. Therefore, the V_v based on density is regarded as the more reliable measure of voids in ACC laminates.

7.3.2 *Effect of ACC processing on cellulose structure*

The cellulose structure was observed to change with partial dissolution (Figure 79). An increase in cellulose crystallinity (CrI_{area}) from 32.6 % in as-received rayon to 35.3 % in IL_15min_H_2O was found by WAXD of the bulk laminates (Figure 80). A smaller increase to 34.2 % was found for a dissolution time of 6 h in IL_6h_H_2O. A similar crystallinity of 34.5 % was observed for regeneration in acetone (Figure 80).

Overall, a stronger increase in CrI_{Segal} from 26.5 % to 33.9 % was found in comparison to CrI_{area} (Figure 80). The more pronounced effect on CrI_{Segal} originates from a reduced intensity of the shoulder at 15 to 18 ° 2 θ (Figure 79), which increases the peak based ratio CrI_{Segal} but lowers the area based ratio

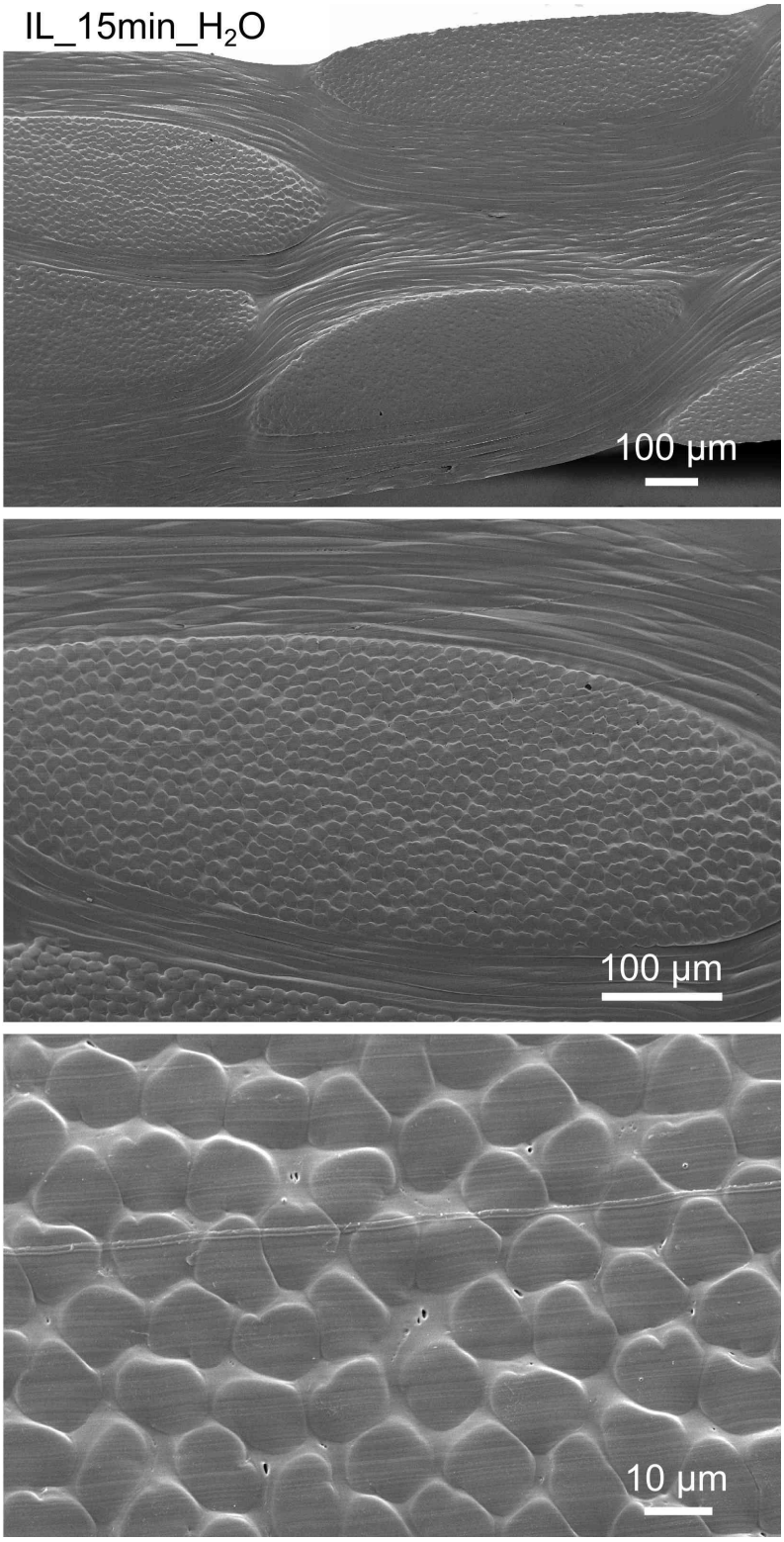

Figure 76: SEM micrographs of the ACC laminate IL_15min_H_2O at increasing magnification.

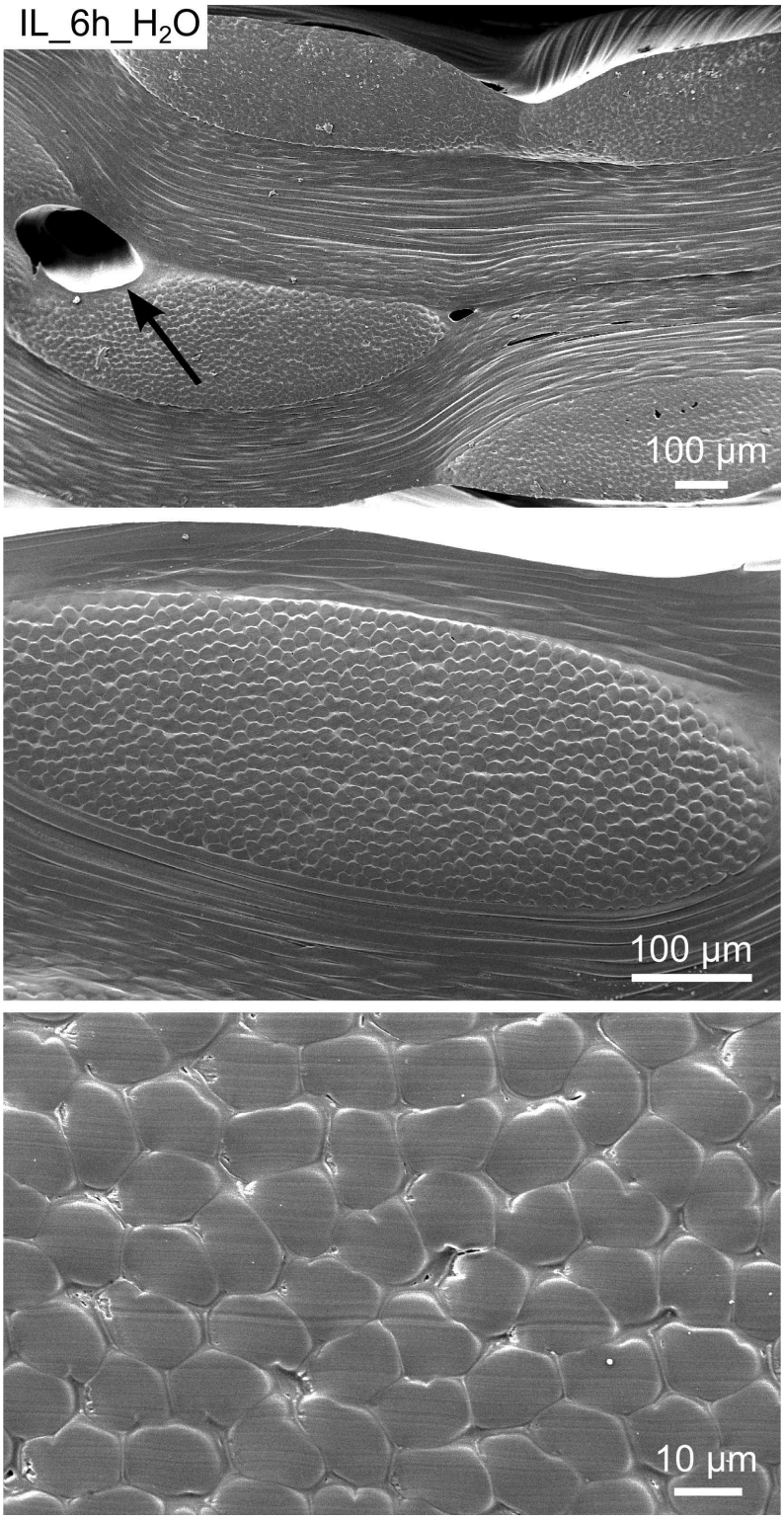

Figure 77: SEM micrographs of the ACC laminate IL_6h_H_2O at increasing magnification. An interlaminar void is indicated by a black arrow.

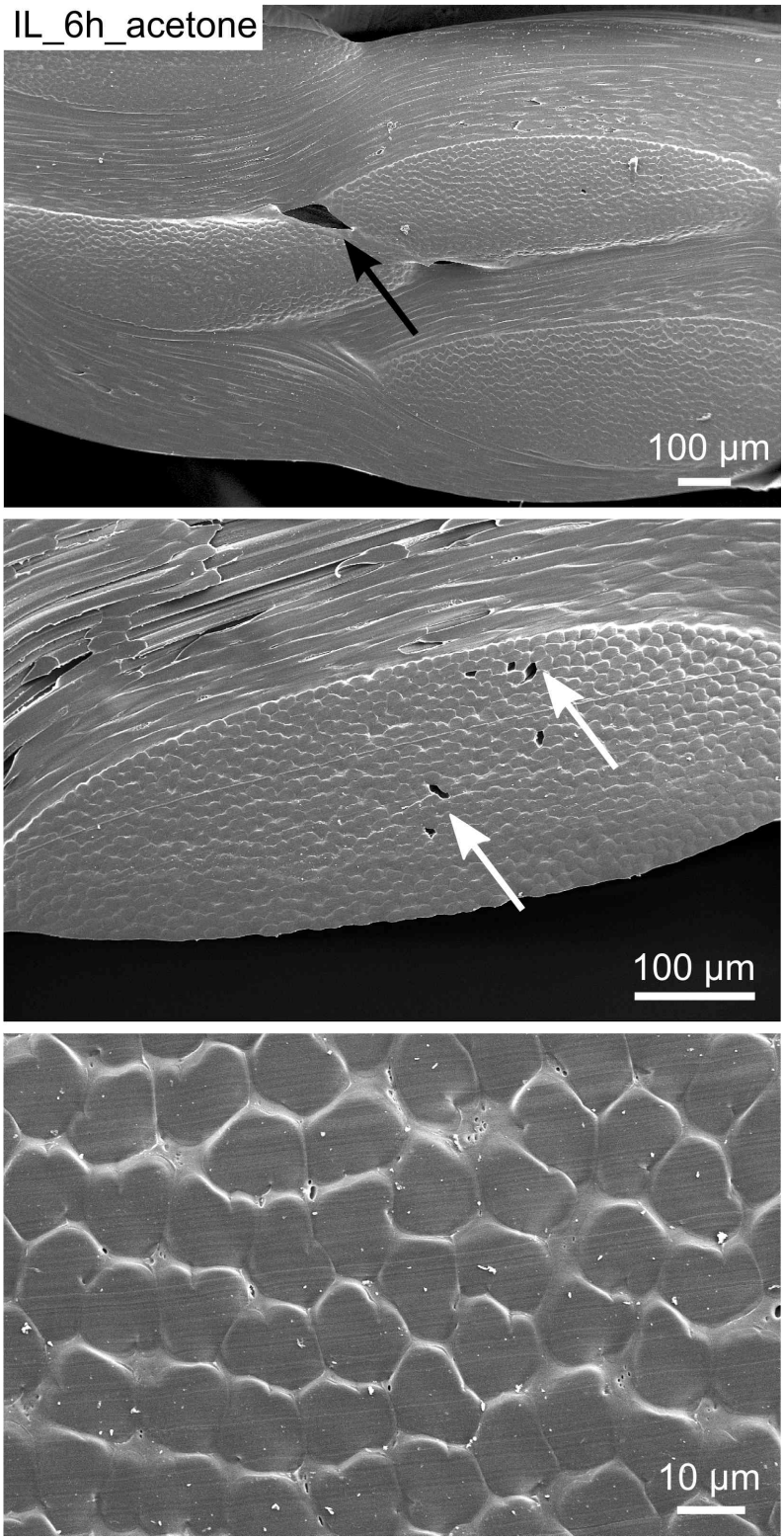

Figure 78: SEM micrographs of the ACC laminate IL_6h_acetone at increasing magnification. Interlaminar and intrayarn microvoids are indicated by black and white arrows, respectively.

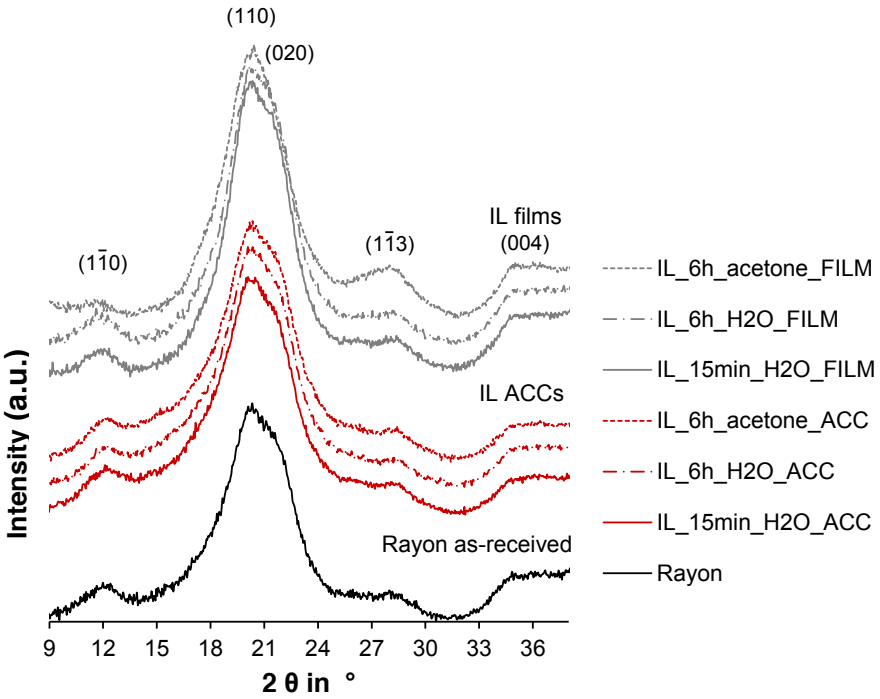

Figure 79: X-ray diffractograms of the ACC laminates and unreinforced cellulose films. Diffractograms were shifted vertically for clarity.

CrI_{area}. The shoulder is attributed to the scattering of amorphous cellulose that exhibits a hump at 15 to 20 ° 2 θ [Segal et al., 1959; Ciolacu et al., 2011] and may be reduced by preferential dissolution of amorphous domains. Furthermore, CrI_{Segal} increases with increasing crystallite size, which increases with ACC processing (Table 16), and is known to underestimate the amorphous fraction when analysing cellulose II due to crystalline peaks overlapping the intensity from amorphous scattering [French and Cintrón, 2012; Nam et al., 2016], both of which contributes to the higher crystallinity estimated by CrI_{Segal}.

The increase in crystallinity with processing of ACCs is contrary to the findings of other studies that report a lower crystallinity of ACCs when compared to the cellulose precursor [Nishino et al., 2004; Gindl-Altmutter et al., 2012; Soykeabkaew et al., 2008; Arévalo et al., 2010]. The increase in

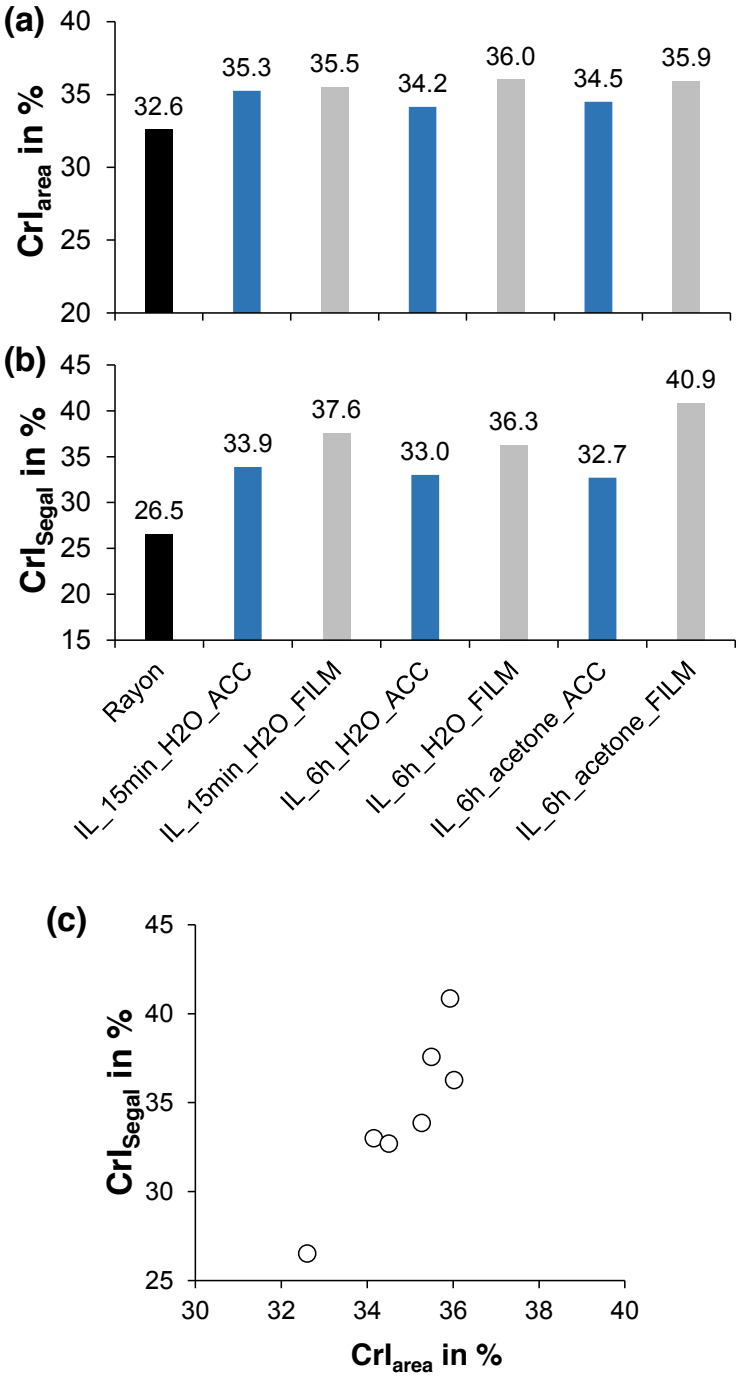

Figure 80: Crystallinity of ACC laminates and unreinforced cellulose films determined by XRD as (a) CrI_{area} and (b) CrI_{Segal}. (c) Correlation graph of CrI_{Segal} as a function of CrI_{area}.

Table 16: Crystallite size of rayon and ACC laminates in the crystal planes $(1\bar{1}0)$, (110) and (020) at 12, 20.1 and 21.8 ° 2 θ, respectively.

	$(1\bar{1}0)$	(110)	(020)
Rayon	23.5 Å	20.7 Å	27.4 Å
IL_15min_H_2O	27.0 Å	20.2 Å	28.9 Å
IL_6h_H_2O	33.4 Å	20.6 Å	28.2 Å
IL_6h_acetone	30.4 Å	20.5 Å	23.6 Å

crystallinity in the present work is attributed to the low initial crystallinity (ca. 30 %) of the rayon used as precursor, whereas in the other studies mentioned above cellulose precursors with a crystallinity in the range of 70 to 80 % were used. The crystallisation is attributed to the mechanisms described for processing ACC laminates using NaOH/urea (Chapter 5): Firstly, dissolved cellulose chains crystallise onto remaining crystals, e.g. at the surface of partially dissolved fibres. Such a template growth mechanism is suggested by the strongest increase in crystallite size found in the $(1\bar{1}0)$ plane, which is the growth face of cellulose II single crystals [Buleon and Chanzy, 1978]. Furthermore, amorphous cellulose is known to recrystallise in the presence of a plasticiser, such as water, and exposure to heat, due to the disruption of hydrogen bonds and mobilisation of cellulose molecules upon swelling [Kouris et al., 1958; Ioelovich et al., 1983; Sreenivasan et al., 1988]. Consequently, amorphous domains of the matrix and within the fibres of ACCs may recrystallise during the washing and drying steps of ACC processing.

The higher increase in crystallinity when processing ACCs using NaOH/urea (+ 17 %, Figure 51) when compared to using IL (+ 8 %) is attributed to the differences in solvent character. ILs are known as direct cellulose solvents in a wide temperature range with an increasing solubility with increasing temperature [Swatloski et al., 2002; Zhu et al., 2006; Gibril et al., 2012a],

whereas NaOH/urea changes from a direct solvent at temperatures < 0 °C to a strong swelling agent at > 0 °C that also facilitates polymorph transformation of cellulose crystals [Sobue et al., 1939; Qi et al., 2008b; Navard et al., 2012]. It is therefore argued, that the stronger swelling in NaOH/urea and its ability to modify cellulose crystals even at non-dissolution temperatures facilitates a higher degree of recrystallisation.

The regeneration in acetone was expected to lead to an ACC of lower crystallinity, due to the inhibition of an ordered alignment of cellulose molecules by hydrophobic stacking in media with low dielectric constants [Miyamoto et al., 2009; Cao et al., 2014]. However, IL_6h_H_2O and IL_6h_acetone exhibited very similar diffractograms and crystallinities of 34.2 and 34.5 %, respectively (Figure 79). The small difference in crystallinity is thought to be due to the relatively small contribution of the regenerated matrix phase (8 vol. %, Table 15) in comparison to the full volume of the ACC. Additionally, the ACC laminate IL_6h_acetone had to be washed in distilled water after regeneration in acetone due to the low solubility of EmimAc in acetone. The washing/swelling in distilled water and drying at 60 °C may have reversed the amorphisation caused by regeneration in acetone.

However, the WAXD measurements were performed on the bulk laminates and the contribution of the individual phases to the increase in crystallinity can therefore not be determined.

One possible approach is the characterisation of regenerated cellulose films as a representation of the matrix phase, which has been performed in several studies on ACCs [Nishino et al., 2004; Pullawan et al., 2010; Soykeabkaew et al., 2008]. In the present study, unreinforced cellulose films of fully dissolved rayon exhibited a 1 to 2 % higher CrI_{area} and 3 to 8 % higher CrI_{Segal} than the respective ACCs, for equal dissolution temperature, time and regeneration medium (Figure 80).

The higher crystallinity is likely to result from different regeneration conditions of the films. Firstly, the cellulose solution of the films were cast into porous moulds, which were then submersed for regeneration. The porosity of the mould allowed only a slow exchange of solvent and coagulant, resulting in a slow regeneration rate, which is known to enhance the crystallisation of regenerated cellulose [Bang et al., 1999; Duchemin et al., 2009b] Secondly, based on the solvent uptake of 60 to 70 % and V_m of ca. 10 vol. % in ACCs, the cellulose concentration in the IL of infused and partially dissolved laminates was ca. 14 %, which is high in comparison to the 5 wt. % cellulose in the solution used for casting the films. Hence, the lower viscosity due to the lower cellulose content supposedly results in less entanglement and allows the cellulose chains in the films to regenerate into ordered crystalline domains.

Furthermore, it needs to be considered that the confinement of the cellulose solution in the micron-sized gaps between fibres may affect structure formation upon regeneration and separately prepared cellulose films cannot be considered a reliable representation of the matrix phase in ACCs. Consequently, the question arises where the crystallisation occurs, in the fibre or matrix or both? Therefore, an *in-situ* characterisation of the individual phases is required.

7.3.3 *Synchrotron-based Fourier-transformed infrared microspectroscopy*

Analysis in transmission

The microstructure of the ACCs was clearly visible in the optical microscope (Figure 81a). The IR beam was positioned at desired locations on fibre and matrix and spectra with typical cellulose peaks were obtained. However, the

spectra also exhibited distortions. The curves appeared to be composed of a typical cellulose spectrum overlayed by a sinusoidal wave (Figure 81b).

Sinusoidal distortions in FTIR spectra obtained in transmission experiments are known as "interference fringes" [Faggin and Hines, 2004; Ibrahim et al., 2013; Konevskikh et al., 2015]. In the case of light passing through a thin sample with plane-parallel sides, the sample may act as a Fabry-Pérot etalon, manifesting in multiple internal reflections [Faggin and Hines, 2004]. These reflections can occur within the sample film, within the holder or in between the sample and holder, and cause additional interferences between the two infrared beams of an FTIR spectrometer [Konevskikh et al., 2015]. In addition to the main interference, referred to as the centre burst, the reflections cause additional spikes, so called side bursts. These side bursts are subsequently also Fourier transformed and result in sinusoidal waves, the fringes, that overlay the spectrum [Ibrahim et al., 2013]. Furthermore, variations in sample thickness lead to a difference in the effective optical path length, which also influences the interference in the spectrometer [Konevskikh et al., 2015].

Fringes present a challenge in the interpretation of FTIR spectra, as they change relative peak heights or obscure weak absorptions, hence prohibiting the accurate measurement of absorbance intensities [Faggin and Hines, 2004; Konevskikh et al., 2015]. In the case of ACCs, where cellulose structure is to be analysed by the infrared ratios TCI (I_{2900}/I_{1372}), and LOI (I_{1430}/I_{890}) (Figure 70), a dramatic influence of the fringes on the relevant peak intensities was observed. When comparing spectra measured along a line from the core of a fibre to the matrix of the ACC IL_15min_H_2O, both peaks relevant for calculating the TCI are distorted in a different manner depending on the measurement position (Figure 81c,d). Similarly, the peak at 1420 cm^{-1} required for the calculation of the LOI shows irregular variations (Figure 81d).

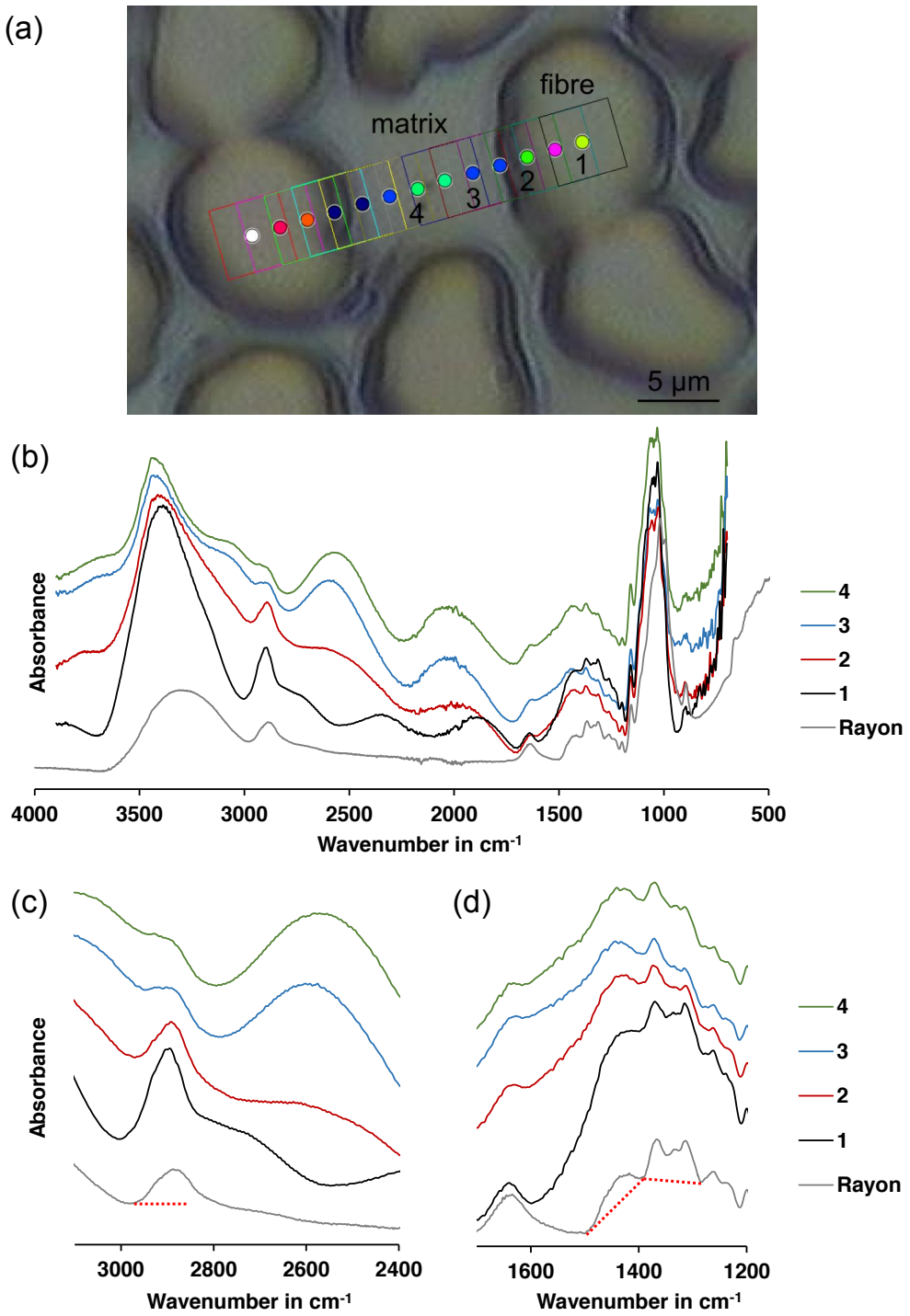

Figure 81: (a) Optical transmission microscope image of the ACC microstructure with IR beam positions on fibre and matrix. The squares indicate the beam spot size. (b) Transmission-FTIR spectra of fibre and matrix in the ACC IL_15min_H2O at positions 1 to 4 indicated in (a) distorted by fringes. For comparison, an undistorted ATR-FTIR spectrum of as-received rayon is shown. (c,d) Details of the peaks at 2900, 1430 and 1372 cm^{-1} with baselines for peak intensity determination.

In order to improve the quality of distorted spectra, methods for the suppression of interference fringes have been established (Figure 82, Faggin and Hines 2004; Ibrahim et al. 2013; Konevskikh et al. 2015). Suppression methods can be divided into two groups: (i) interferogram editing and (ii) signal processing techniques. In interferogram editing the side bursts caused by the interferences are located in the interferogram and corrected, e.g. by replacing with zeros, a straight line interpolation or a polynomial fit. Subsequently, the spectrum is recalculated by Fourier transformation. In the signal processing approach, the spectrum including the fringes is fitted by a polynomial function. The fringe frequency, amplitude and phase are estimated and the spectrum refitted to obtain a corrected model of the original spectrum [Ibrahim et al., 2013].

Ibrahim et al. [2013] have shown that the signal processing approach results in significantly higher quality and consistency of the corrected spectrum when compared to interferogram editing. A drawback of the interferogram editing approach is the significant reduction of line intensities, whereas signal processing results in spectra with differences in line intensities of only 3 %, which is within the experimentally expected range of uncertainty of 2 to 3 % [Ibrahim et al., 2013].

However, signal processing requires a narrow spectral range (5 to 10 cm^{-1}) in order to obtain a good quality fit, which makes the procedure laborious for suppressing fringes in a wide range, such as necessary in the present results from 600 to 4000 cm^{-1}. Furthermore, the method was developed for high frequency interferential fringing in the order of 1 fringe per 1 cm^{-1}. The frequency of fringes in ACC spectra is in the order of 1 fringe per 500 cm^{-1} and there is only a comparably narrow gap in the spectrum between 2700 and 1700 cm^{-1} that is free of typical cellulose peaks. Additionally, the amplitude of the fringes in cellulose spectra is of similar magnitude as the peak height

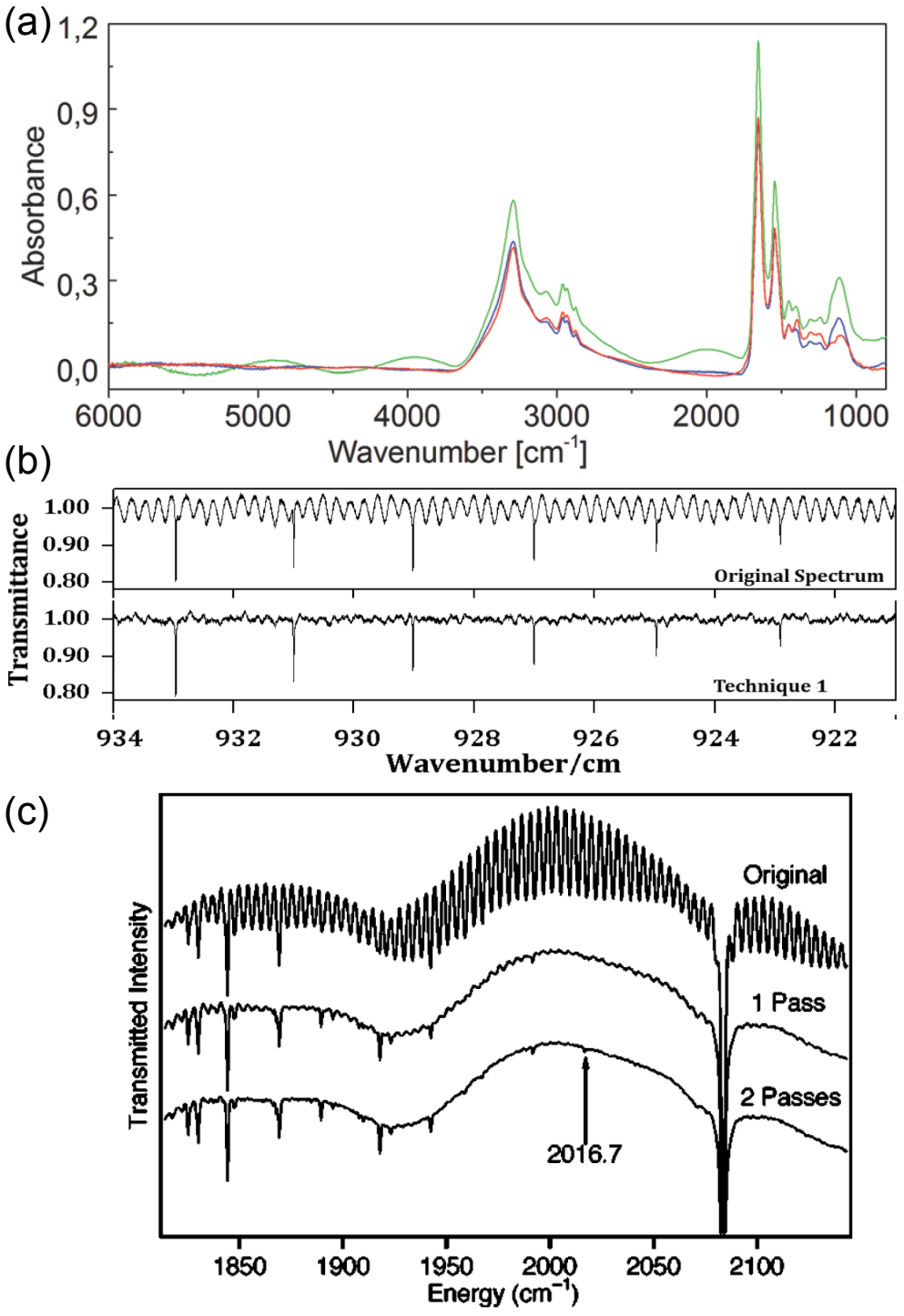

Figure 82: Examples of methods for the suppression of fringes in transmission spectra. (a) Correction *via* signal processing: fringed spectrum in green, corrected spectrum in blue, reference spectrum in red Konevskikh et al., 2015). (b and c) Correction *via* interferogram editing (b, Ibrahim et al., 2013 ; c, Faggin and Hines, 2004).

of I_{2900} and is greater than the peak height of I_{1430} and I_{1372} (Figure 81). Consequently, the accurate determination of frequency, amplitude and phase of the fringes in cellulose spectra is problematic, making the procedure infeasible for the present results.

Another signal processing pathway to remove fringes from spectra is extended multiplicative signal correction described by Konevskikh et al. [2015]. This method is based on the observation that chemical variations lead to reproducible, but small changes in the spectrum. Major visual differences, i.e. fringes, are caused by physical parameters, such as variations in effective optical path length. Furthermore, it has been shown, that for IR spectroscopy of thin biological films the fringes and the original spectrum can be treated as additive in good approximation. Consequently, the function of fringes can be calculated based on the refractive index and film thickness of the sample, which is then subtracted from the distorted spectrum [Konevskikh et al., 2015].

Unfortunately, this technique is also not applicable to ACCs due to variations in film thickness after air-drying. The differential shrinkage of fibre and matrix in ACCs [Duchemin et al., 2009b] led to an inconsistent film thickness with a thinner matrix phase in comparison to the fibres. This deviation in thickness is reflected in a high variability of the FTIR spectra, evident from the different appearance of the fibre spectra 1 and 2 when compared to the matrix spectra 3 and 4 in Figure 81, especially in the wavenumber region 3000 to 1700 cm^{-1}.

In summary, the fringes prohibit the use of transmission spectra for analysis of cellulose structural features due to distortion of relevant spectral features. As a consequence of the similar amplitude of the fringes to cellulose peaks, as well as the high variability of the fringes with measurement position, suppression of the fringes is infeasible. Thus, the analysis of cel-

lulose structure by synchrotron-based FTIR was therefore limited to results obtained by ATR microspectroscopy.

Analysis by attenuated total reflectance

In contrast to transmission mode, the spectra obtained by ATR-microspectroscopy only show the typical peaks of cellulose and no sign of fringes (Figure 83). Spectra of the fibre and matrix phase of the ACCs IL_15min_H_2O and IL_6h_H_2O were obtained and the TCI determined. A decrease in TCI from as-received rayon to the fibres in IL_15min_H_2O was found, followed by an increasing TCI of the fibres in IL_6h_H_2O and IL_6h_acetone (Figure 84a). The TCI, which is established to increase with increasing crystallinity as measured by WAXD [Nelson and O'Connor, 1964], suggests a lower crystallinity of the matrix when compared to the fibres of the ACCs IL_15min_H_2O and IL_6h_H_2O ACC. However, no statistically significant differences were found (Figure 84a).

A drawback of ATR mode in comparison to transmission is the lower optical quality (Figures 81 and 83), and no suitable spot for measuring the matrix phase in IL_6h_acetone was found. The spectra also show a generally lower absorbance intensity which further decreases with decreasing wavenumber due to diffraction effects caused by the aperture set to dimensions similar to the wavelength of the IR beam [Carr, 2001]. In the wavenumber-region below 1000 cm^{-1} the signal to noise ratio decreases such that the peak at 890 cm^{-1} is obscured (Figure 83c). The disappearance of the peak at 890 cm^{-1} consequently impedes the determination of the LOI as a second measure for cellulose crystallinity.

The wavenumber region 1350 to 1200 cm^{-1} features peaks at 1336, 1316, 1278 and 1227 cm^{-1}, which are typical for crystalline cellulose II and show a

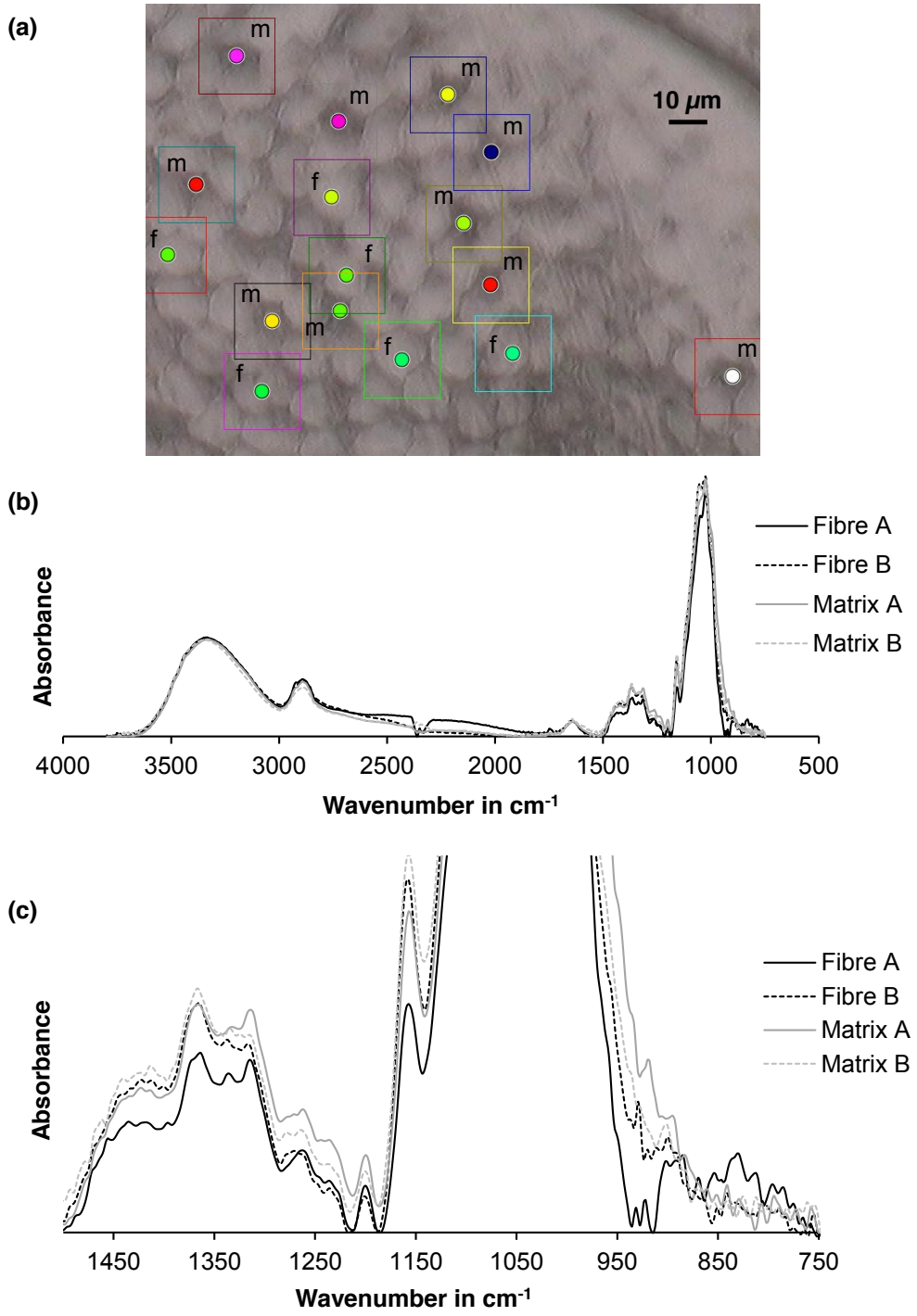

Figure 83: (a) Optical reflection microscope image of the ACC microstructure with synchrotron ATR-FTIR beam positions on fibre (f) and matrix (m). Circles indicate the beam position, the square resembles the aperture, which is reduced by a factor of 4 due to refraction of the ATR crystal to form the beam spot size. (b) Representative synchrotron ATR-FTIR spectra of fibre and matrix of the ACC IL_6h_H_2O. (c) Detail of the 1500 to 750 cm^{-1} wavenumber region. Note the scatter at low wavenumbers obscuring the expected peak at 890 cm^{-1}.

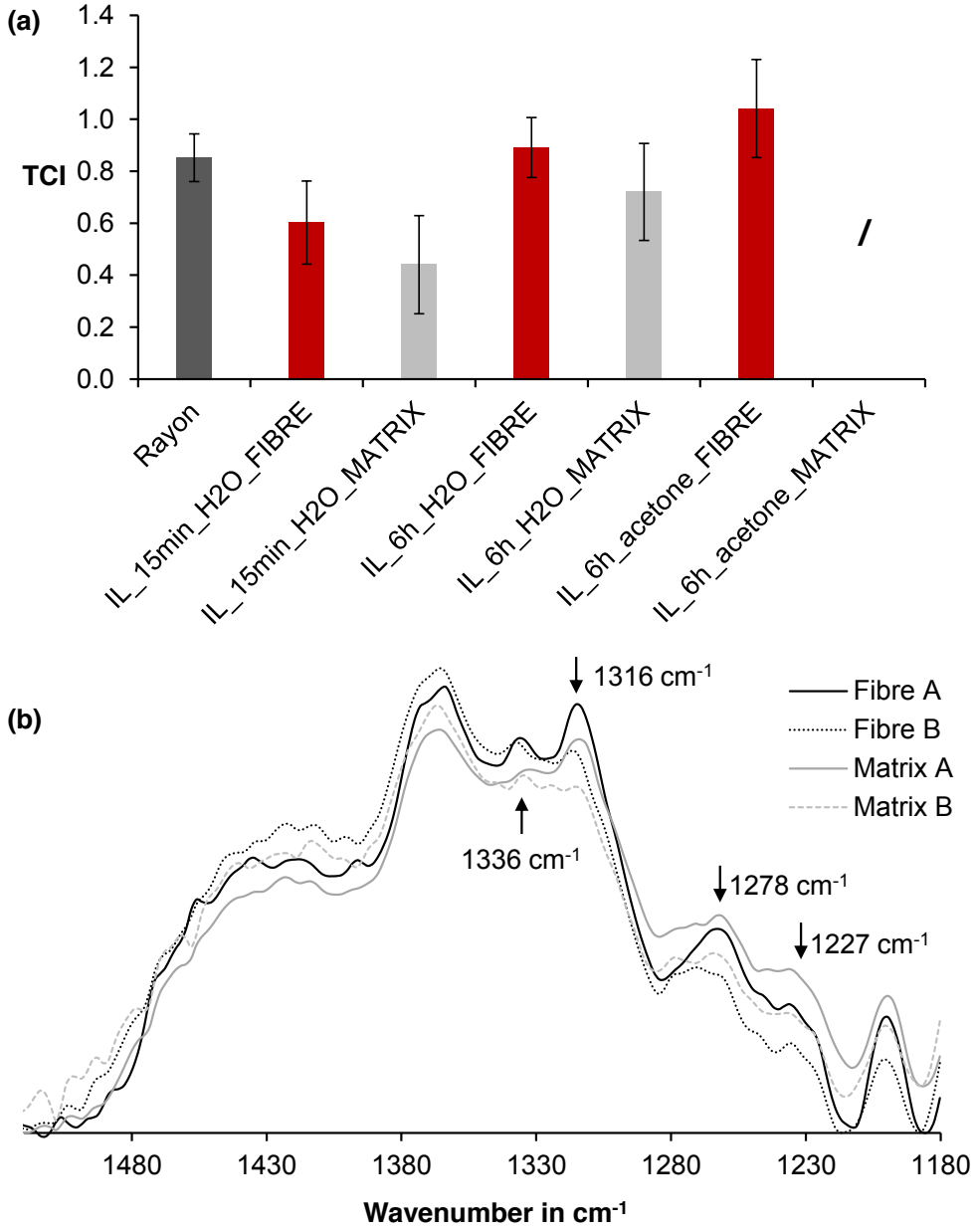

Figure 84: (a) TCI determined from fibre and matrix of ACCs *via* synchrotron-based ATR-FTIR microspectroscopy. No suitable matrix rich areas were found in the ACC IL_6h_acetone. No statistically significant difference was found between the TCI of fibre and matrix of IL_15min_H_2O and IL_6h_H_2O. (b) Baseline corrected and normalised plots of synchrotron ATR-FTIR spectra comparing the fibre and matrix of the ACC IL_6h_$H_{text2}O$. The wavenumbers at 1336, 1278 and 1227 cm^{-1} typical for crystalline cellulose II [Nelson and O'Connor, 1964; Colom and Carrillo, 2002] are indicated by arrows.

low intensity in amorphous cellulose [Nelson and O'Connor, 1964; Colom and Carrillo, 2002; Kondo and Sawatari, 1996]. A comparative analysis of the spectra measured for fibre and matrix of the ACC IL_6h_H_2O, revealed variations in the intensity of the peaks at 1316 and 1278 cm^{-1}. However, some spectra of the matrix contain relatively intense peaks and some fibre spectra contain weak peaks (Figure 84b). This ambiguity of more crystalline or more amorphous features in the spectra, as well as the non-significant differences in TCI found for fibre and matrix may be the result of the relatively low magnification in the reflection microscope, which leads to an uncertainty in placing the measuring points. Considering the small dimensions of the matrix pockets, the matrix measurements may include a portion of the fibre.

The TCI of both fibre and matrix of IL_15min_H_2O was found to be lower than that of as-received rayon, indicating a lower crystallinity, which is contrary to the WAXD results of a higher crystallinity in the ACC laminate. In order to determine the sensitivity of the TCI for determining differences in cellulose crystallinity, macro ATR-FTIR spectra of the bulk ACC laminates were obtained using a standard laboratory FTIR spectrometer. The correlation of TCI with CrI_{Segal} and CrI_{area} determined from WAXD results does not show the expected linear trend (Figure 85a). The imperceptible correlation between macro-FTIR-TCI and WAXD-CrI is attributed to the narrow range of crystallinities observed in the ACCs (CrI_{Segal}: 26.5 to 40.9 %, CrI_{area}: 32.6 to 36.0 %). In the same crystallinity range, the data presented by Nelson and O'Connor [1964] also shows considerable deviations from the linear correlation found for the full range from 0 to 100 % crystallinity (Figure 85b).

Röder et al. [2006] have shown that TCI from FTIR data obtained in transmission correlates better ($R^2 = 94.3$) with WAXD crystallinity than ATR-FTIR data ($R^2 = 80.9$, Figure 85c), indicating that ATR-FTIR is not the ideal method

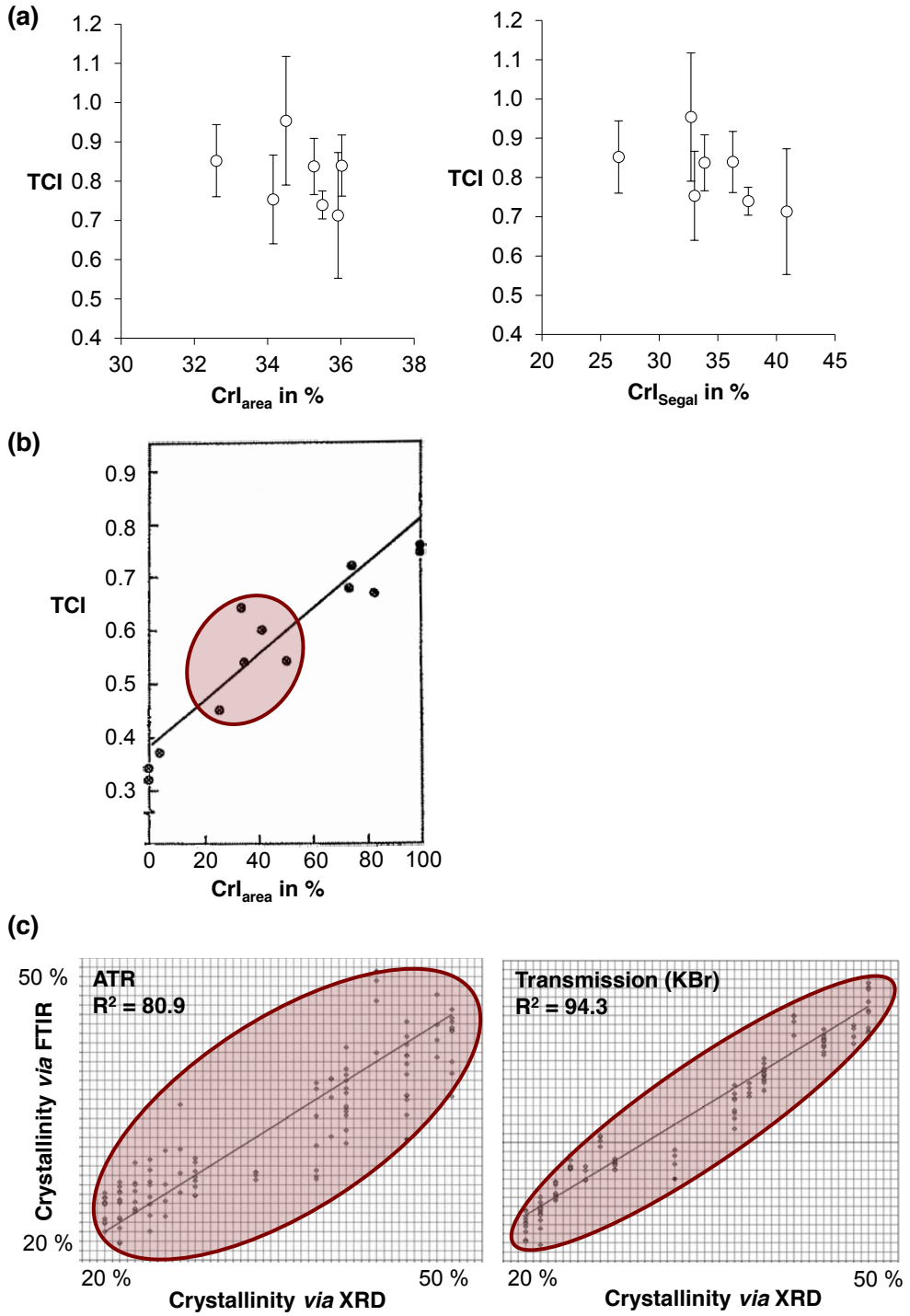

Figure 85: (a) Correlation of crystallinity of ACC laminates and unreinforced films determined from WAXD and Macro-ATR-FTIR performed on the bulk materials using a standard laboratory spectrometer (independent of localised synchrotron experiments, which are not directly comparable to the bulk WAXD results). (b) Correlation of TCI with CrI_{area}, adapted from the TCI defining study of Nelson and O'Connor [1964]. (c) Correlation of TCI determined from FTIR experiments in ATR and transmission mode (adapted from Röder et al., 2006).

for analysing samples with small differences in crystallinity, such as the individual phases in the ACCs under investigation here.

Transmission electron microscopy

The microstructure of the ACC can be clearly observed from a difference in contrast between fibre and matrix phase in TEM bright field micrographs of IL_15min_H_2O, with the matrix appearing brighter (Figure 86). The fibres are found to exhibit the typical skin-core structure of viscose rayon with pores at the core [Rous et al., 2006], indicating that the microstructure of yarns remains similar after partial dissolution. The skin of fibres appears void-free, as can be expected, whereas the matrix features microvoids, often clustered in the centre of a matrix pocket (Figure 86).

The porosity of rayon is not evident from SEM, probably due to smearing during sample preparation by manual cutting with a razor blade. However, the microvoids in the matrix are observed (Figure 87). These microvoids may arise from drying, as they are often found at the median line in the space between neighbouring fibres where the largest drying-induced deformation is expected. However, they might also be the result of air inclusions introduced during solvent infusion, as they were found in random locations throughout the matrix phase and are too large in comparison to the matrix phase to be solely attributable to shrinkage (Figure 87).

The contrast in TEM bright field micrographs is composed of diffraction contrast and mass-thickness contrast, such that a higher crystallinity, higher density and larger thickness result in a darker image [Williams and Carter, 2009]. Consequently, the brighter appearance of the matrix phase may be attributed to a more amorphous structure, and lower density arising from the 5 to 6 % higher density of crystalline cellulose [Woodings, 2001; Hermans

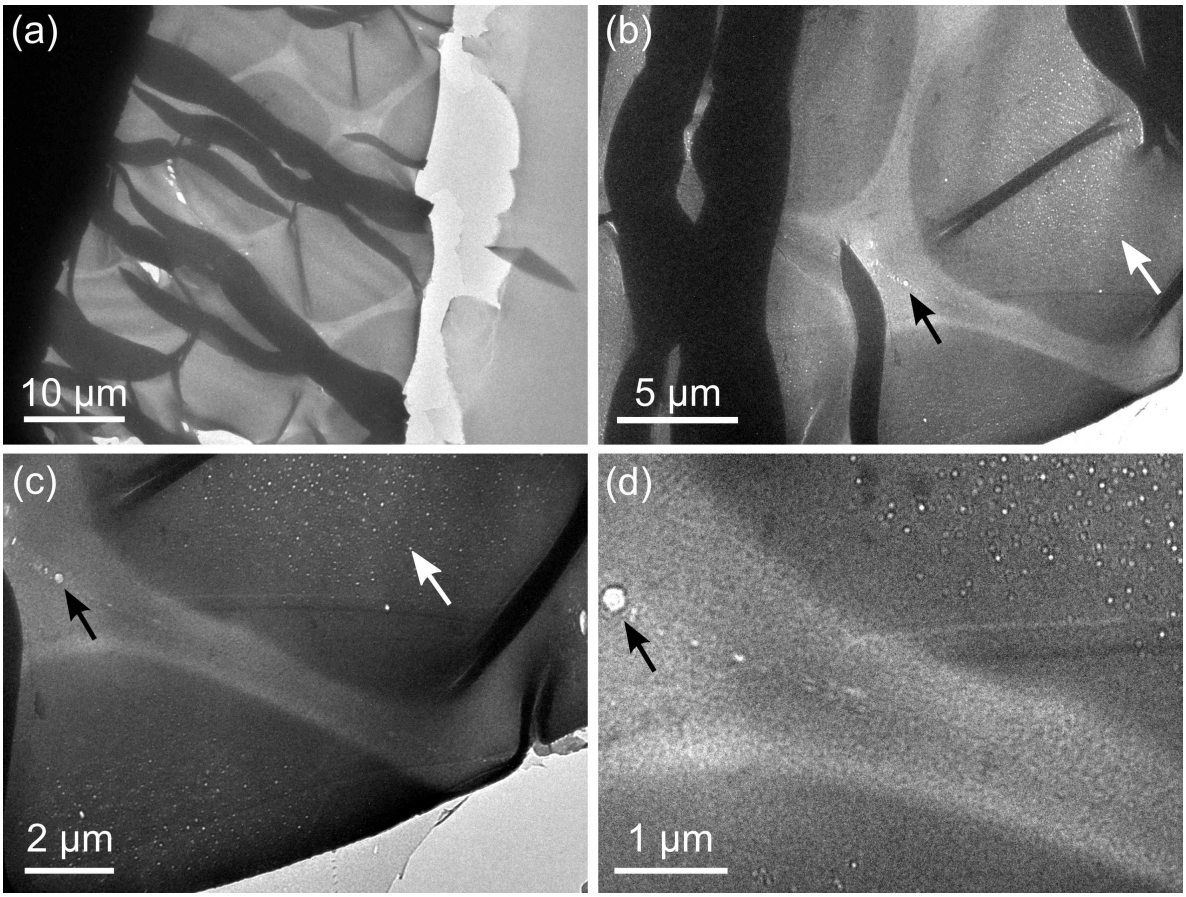

Figure 86: TEM bright-field micrographs of the ACC IL_15min_H_2O showing the overall microstructure of fibre and matrix (a,b) and details of the matrix layer in between two fibres (c,d). Voids at the core of fibres and in the matrix are indicated by white and black arrows, respectively.

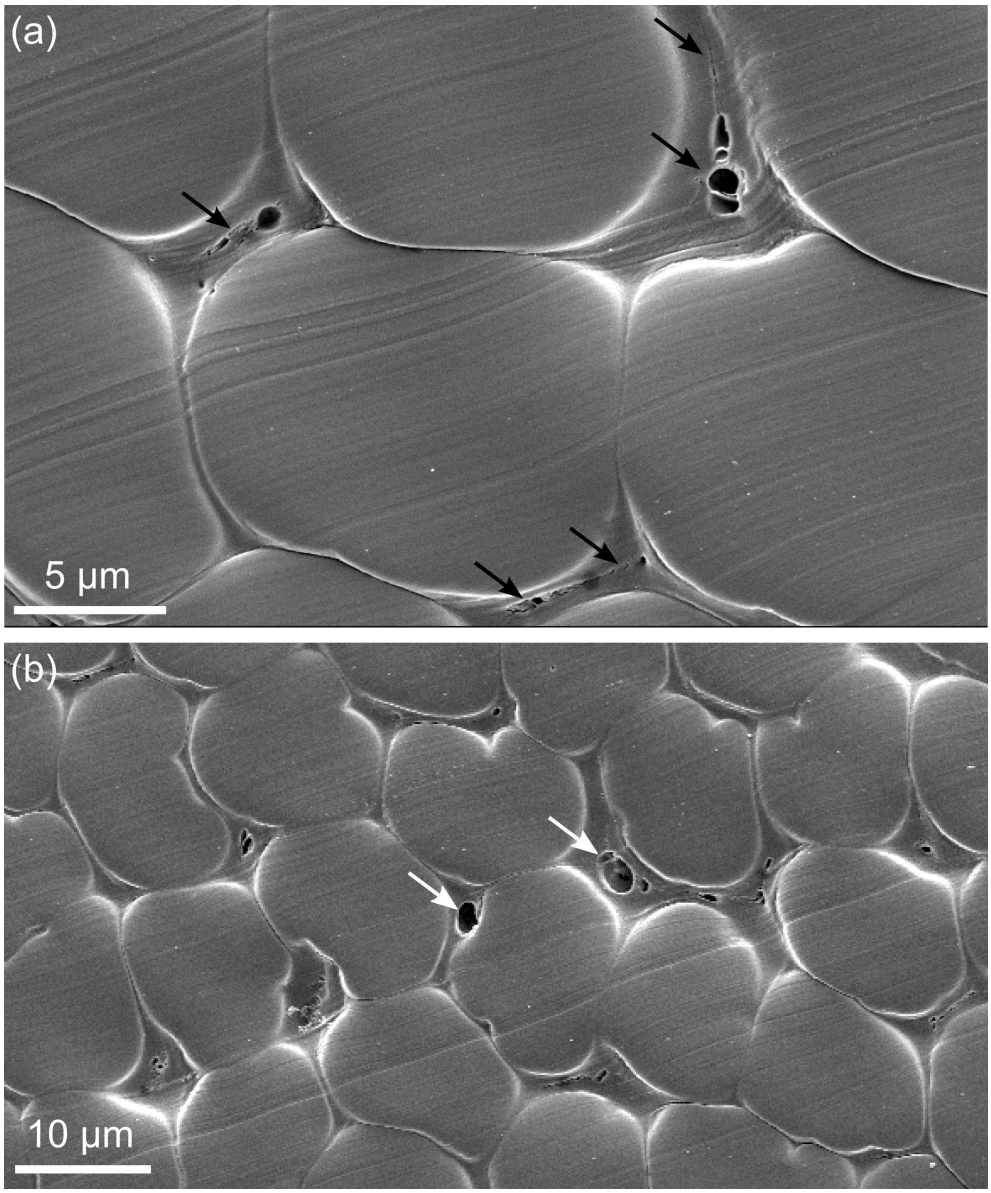

Figure 87: SEM micrograph of (a) microvoids and fine cracks in the matrix (black arrows), predominantly occurring along the median line between fibres, where the largest deformation during drying is expected. (b) Larger voids (white arrows) arising from air inclusions introduced by solvent infusion.

and Vermaas, 1946; Ishikawa et al., 1997], in comparison to the fibre. The skin of the fibre, which is the region most likely to increase in crystallinity due to partial dissolution, regeneration and swelling, appears darkest and therefore more crystalline.

However, it needs to be considered that a potential difference in thickness due to the differential shrinkage of fibre and matrix may result in the same contrast. The 100 nm thin sections for TEM were ultramicrotomed off a dry specimen which is expected to result in an even thickness, but had to be collected in a water reservoir behind the knife edge and air-dried on copper grids. A thinner matrix phase due to stronger shrinkage can therefore not be ruled out.

An extension of the qualitative characterisation of the individual phases by TEM based on contrast in BF images, are electron diffraction patterns of fibre and matrix. Unfortunately, cellulose in general and cellulose II in particular, is highly susceptible to damage by electron radiation. Artefacts arising from beam damage occur in images at high magnification and samples rapidly degrade in diffraction experiments, due to the very low lethal dosage of 4 electrons $Å^{-2}$ shown by Chanzy for cellulose microfibrils from *Valonia* [Kaushik et al., 2015]. Cooling the specimen can extend the lethal electron dose by a factor of 3 [Kaushik et al., 2015]. However, a cryo-stage was not available for the present experiments and no diffraction patterns could be obtained.

7.3.4 *Nanoindentation*

No significant difference in E_r of the skin and core of as-received rayon fibres was found by nanoindentation (Figure 88), in spite of the differences in crystallite orientation and porosity of skin and core [Müller et al., 2000; Rous

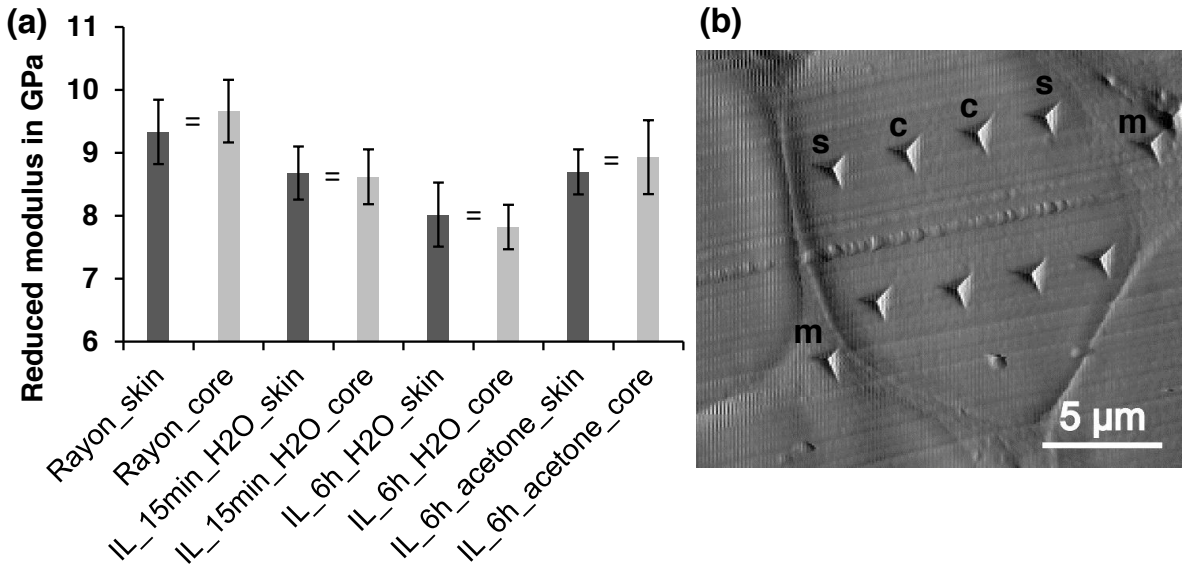

Figure 88: (a) Comparison of the reduced modulus at skin and core of as-received rayon and fibres in ACC laminates. No statistically significant differences were found between skin and core results (marked by =). (b) Surface contact scanning image of the topography of an ACC laminate exhibiting residual indents at fibre skin (s), core (c) and matrix (m).

et al., 2006], which is in agreement with the nanoindentation study of rayon by Gindl et al. [2006a]. Similarly, no significant differences in E_r were found when comparing the skin and core of fibres in ACC laminates, indicating that partial dissolution did not have a selective effect on the elastic properties of skin and core (Figure 88; results of skin and core were subsequently pooled for comparisons between as-received fibres and the individual fibre and matrix phases in ACCs).

On the other hand, a significant decrease in E_r of up to 15 % was found from as-received rayon with an E_r of 9.4 ± 0.8 GPa to the fibres in ACCs, with an E_r in the range of 7.9 ± 0.5 GPa to 8.9 ± 0.5 GPa (Figure 89). The effect of extending the dissolution time from 15 min to 6 h on the fibres was ambiguous; for regeneration in water a lower E_r, for regeneration in acetone an equal E_r was found, when compared to that of IL_15min_H_2O (Figure 89).

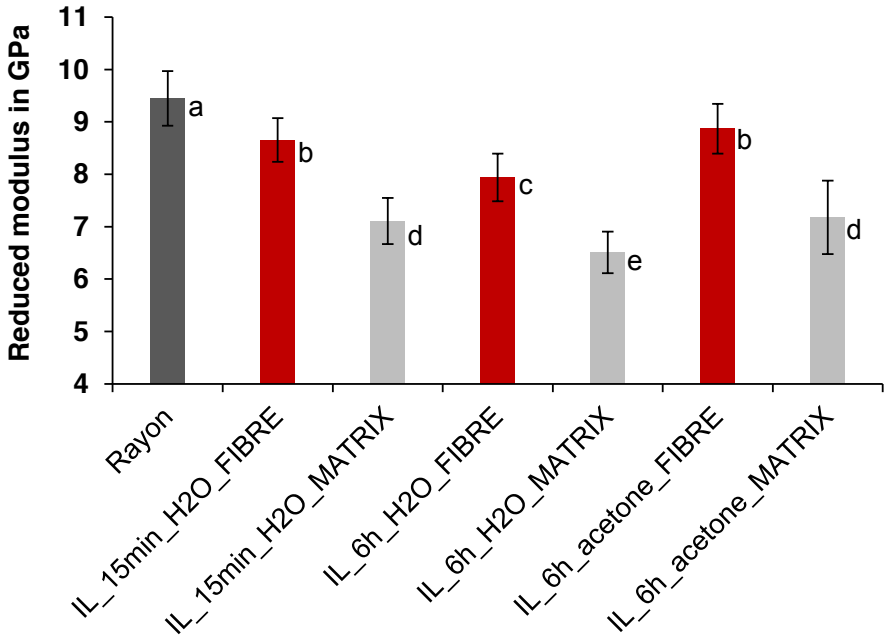

Figure 89: Reduced modulus of as-received rayon and fibre and matrix in ACCs determined by nanoindentation. Statistically significant differences were found between the as-received rayon and fibres in the laminates, as well as between the fibres and the matrix in all ACCs (Statistically significant differences (α = 0.05) are indicated by different letters.).

E_r of the matrix phase in the ACC laminates was found to be lower than that of the fibres in all ACC laminates (Figure 89). The effect of extending the dissolution time on the matrix phase was ambiguous. An equal E_r was found for the matrix in IL_15min_H_2O and IL_6h_acetone, whereas a lower E_r was found for the matrix in IL_6h_H_2O (Figure 89).

The nanoindentation results for E_r of rayon and the fibre and matrix phase of ACCs are in agreement with values reported for regenerated cellulose fibres in the literature in the range of 9 to 12 GPa for viscose rayon and lyocell [Lee et al., 2007; Gindl et al., 2006a]. It should however be noted, that the results obtained by quasi-static nanoindentation from polymers such as cellulose generally need to be interpreted with care, as viscoelasticity introduces artefacts due to creep during the indentation [VanLandingham et al., 2001]. Although, a negligible effect of creep in nanoindentation experiments

of regenerated cellulose fibres at unloading rates similar to those used in the present work were found by Lee et al. [2007], derived from no significant differences in E_r when comparing continuous stiffness measurements and unloading at the final indentation depth. However, the values reported here should still not be regarded as definite measures of the modulus, but mainly as a relative comparison between the individual samples of the system under investigation.

In addition to the lower E_r of the matrix found by nanoindentation, a relative difference between the modulus of fibre and matrix phase is evident from AFM phase imaging. A decrease in the phase signal, a qualitative measure for local variations in the modulus of a sample surface [Lee et al., 2009; Wang et al., 2010b,a; Nair et al., 2013], was observed for the matrix when scanning the surface of ACCs in tapping mode AFM (Figure 90d). The brighter appearance of the fibres in the phase image of IL_15min_H_2O (Figure 90b) indicates a local increase in stiffness [Magonov et al., 1997], in agreement with the nanoindentation results. The influence of topography on the phase signal is regarded as negligible, as the ultramicrotomed surface exhibits a very low roughness R_a of 6.6 nm and there are no steep edges in the height profile when moving from the fibre to the matrix (Figure 90c).

The generally lower E_r of either phase in ACCs in comparison to the as-received rayon could arise from residual IL, which is known to act as a plasticiser of cellulose [Mahadeva and Kim, 2012; Shibata et al., 2013a]. However, the influence of residual IL is regarded as negligible, due to the absence of typical peaks from localised FTIR spectra (Figure 83), indicating complete removal of solvent from the ACCs, as shown in Chapter 6. Therefore, the decrease in E_r with ACC processing is attributed to changes in cellulose fine structure.

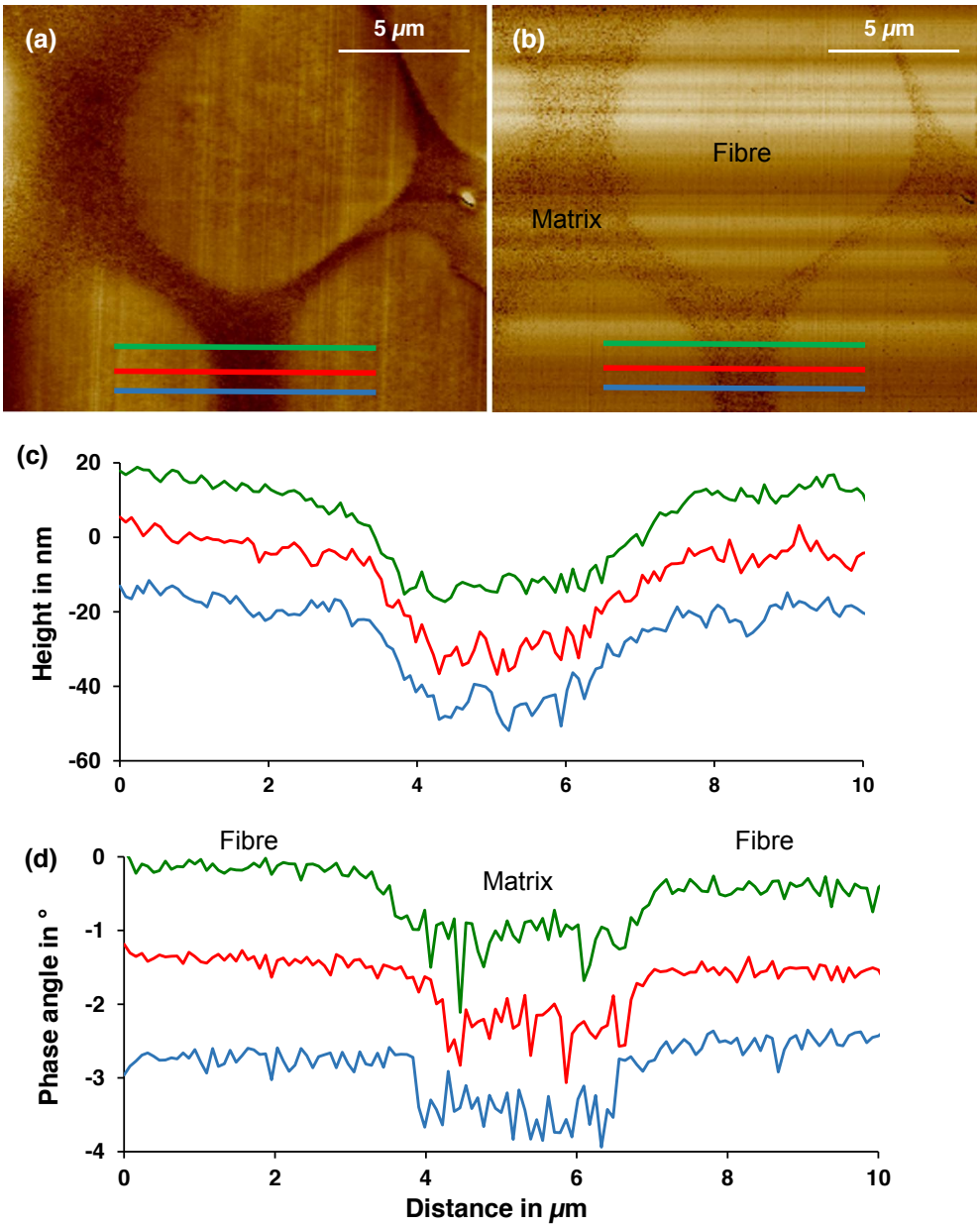

Figure 90: Height (a) and phase image (b) of ACC IL_15min_H_2O obtained in tapping mode AFM. (c) Plots of height and phase angle over distance indicated by the lines of equal colour in (a) and (b). Height profiles have been shifted by 15 nm and phase profiles by 1 ° for clarity.

Firstly, the lower E_r of the matrix in comparison to the fibres in ACCs (Figure 89) may be due to a more amorphous matrix, as suggested by the TEM and ATR-FTIR results. Amorphous cellulose generally exhibits an elastic modulus that is an order of magnitude lower than for crystalline cellulose [Ishikawa et al., 1997] and furthermore amorphous cellulose is more accessible to moisture regain [Nelson and O'Connor, 1964]. Hence, a more amorphous matrix is expected to equilibrate at a higher moisture content at any given RH. A more amorphous structure of the matrix could therefore account for the lower E_r in comparison to the fibres, as Ganser et al. [2015] report a decrease in E_r for pulp fibres with increasing moisture content. However, it needs to be considered that TEM results could not be quantified by diffraction and no significant differences were found in the TCI of fibre and matrix.

Secondly, regenerated cellulose fibres are known to exhibit a decreasing Young's modulus and tensile strength with a decreasing degree of orientation of the cellulose crystallites in regard to the long fibre axis [Loubinoux and Chaunis, 1987; Kreze and Malej, 2003; Kong and Eichhorn, 2005; Perepelkin, 2007; Soykeabkaew et al., 2009a; Sun et al., 2015]. A decrease in crystallite orientation accompanied by a decrease in Young's modulus and tensile strength was reported by Soykeabkaew et al. [2009a] with partial dissolution of regenerated cellulose fibres in LiCl/DMAc. A similar loss of preferred orientation in the conversion from fibre to matrix by dissolution and regeneration of rayon in IL can serve as explanation for the lower E_r of the matrix in comparison to the fibres (Figure 89). The crystallites in the core volume of fibres may also be mobilised by swelling and plasticisation in the solvent-water mixture during regeneration and washing, leading to a randomised reorientation from the preferred orientation they were forced into by stretching during the fibre formation process [Woodings, 2001; Sun

et al., 2015]. Such a reduction of crystallite orientation may account for the decrease in E_r observed when comparing as-received rayon fibres and fibres in ACC-laminates (Figure 89).

However, the change in crystallite orientation could not be calculated from the linear WAXD diffractograms obtained on bulk laminates. Localised electron diffraction patterns of the matrix and fibres could not be acquired by TEM, as a liquid nitrogen cooled sample stage was not available and the ACC sections degraded too quickly in the electron beam.

As no definite conclusion on crystallinity and crystallite orientation can be drawn, the impact of changes in cellulose structure with processing on the mechanical properties of the individual phases requires further investigation. An outline of suggested techniques for future experiments is given in Chapter 8.

7.3.5 *Influence of the individual phases on the laminate properties*

The highest ultimate tensile strength and Young's modulus of 100.7 ± 4.4 MPa and 8.7 ± 0.6 GPa, respectively, were found for the ACC laminate with a short dissolution time, IL_15min_H_2O, which also exhibited a high E_r of fibre and matrix (Figure 91). Increasing the dissolution time to 6 h resulted in a decrease in ultimate tensile strength and Young's modulus by 17 and 22 %, respectively, when comparing IL_15min_H_2O and IL_6h_H_2O.

The decrease in Young's modulus of the laminate with increasing dissolution time is also reflected in a lower E_r of fibre and matrix in IL_6h_H_2O (Figure 91b).

However, no influence of the regeneration medium on the Young's modulus was found on the laminate scale, whereas nanoindentation showed a higher E_r for the individual fibre and matrix phase when regenerating in

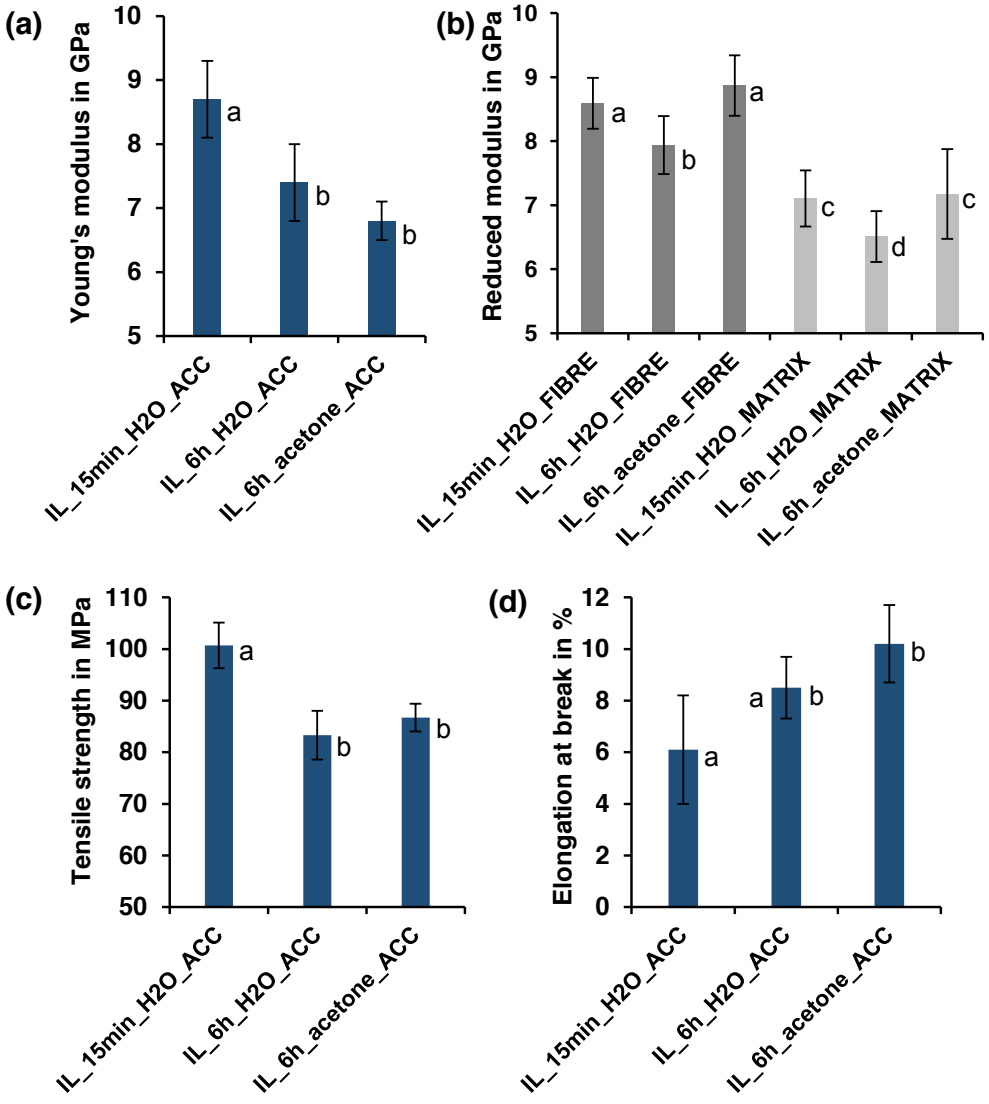

Figure 91: (a) Comparison of the Young's modulus of ACC laminates determined in tensile tests and reduced modulus determined by nanoindentation of the individual phases. (b) Ultimate tensile strength and (c) elongation at break determined in tensile tests of ACC laminates. Statistically significant differences ($\alpha = 0.05$) are marked by different letters.

acetone (Figures 91 and 89). It was found that the E_r of the individual phases has no clear effect on the Young's modulus of ACC laminates. IL_6h_acetone exhibits the lowest tensile Young's modulus of all laminates, in spite of a significantly higher E_r of both phases in comparison to IL_6h_H_2O (Figure 91). It is therefore concluded that with the limited number of processing conditions and ambiguous results of the individual characterisation no clear correlation between the elastic properties of the individual phases and the laminates can be established.

However, by combining the results of Chapter 5 and the current chapter, correlations between the matrix (V_m), void (V_v) and fibre (V_f) fraction (100 - V_m - V_v) and the mechanical properties of ACC laminates were derived (Figure 92). Although the two solvents NaOH/urea and IL have substantial differences in processing conditions and cellulose interactions, a comparison is deemed valuable for understanding the influence of each constituent on the mechanical properties of ACC laminates.

Ultimate tensile strength clearly decreases with increasing V_m. The strength of NaOH/urea-laminates with a low V_m of 4 to 5 vol. % exceeds that of IL-laminates with a comparably high V_m of 8 to 11 vol. % (Figure 92a). An important finding is that laminate strength decreases with increasing dissolution time in both solvents, in spite of no further conversion of fibre volume to matrix, as V_m was not found to increase with extended dissolution times in IL (Table 15) and only marginally in NaOH/urea (Table 6). This finding suggests that extended partial dissolution and solvent interaction in both solvents have a detrimental effect on the remaining fibre core. Supposedly, amorphous linkages in the crystalline-amorphous chain structure are weakened by dissolution, as DP is known to decrease with dissolution, marginally in NaOH/urea [Qi et al., 2011] and substantially in IL [De Silva et al., 2015]. Furthermore, crystallites are probably reorientating ran-

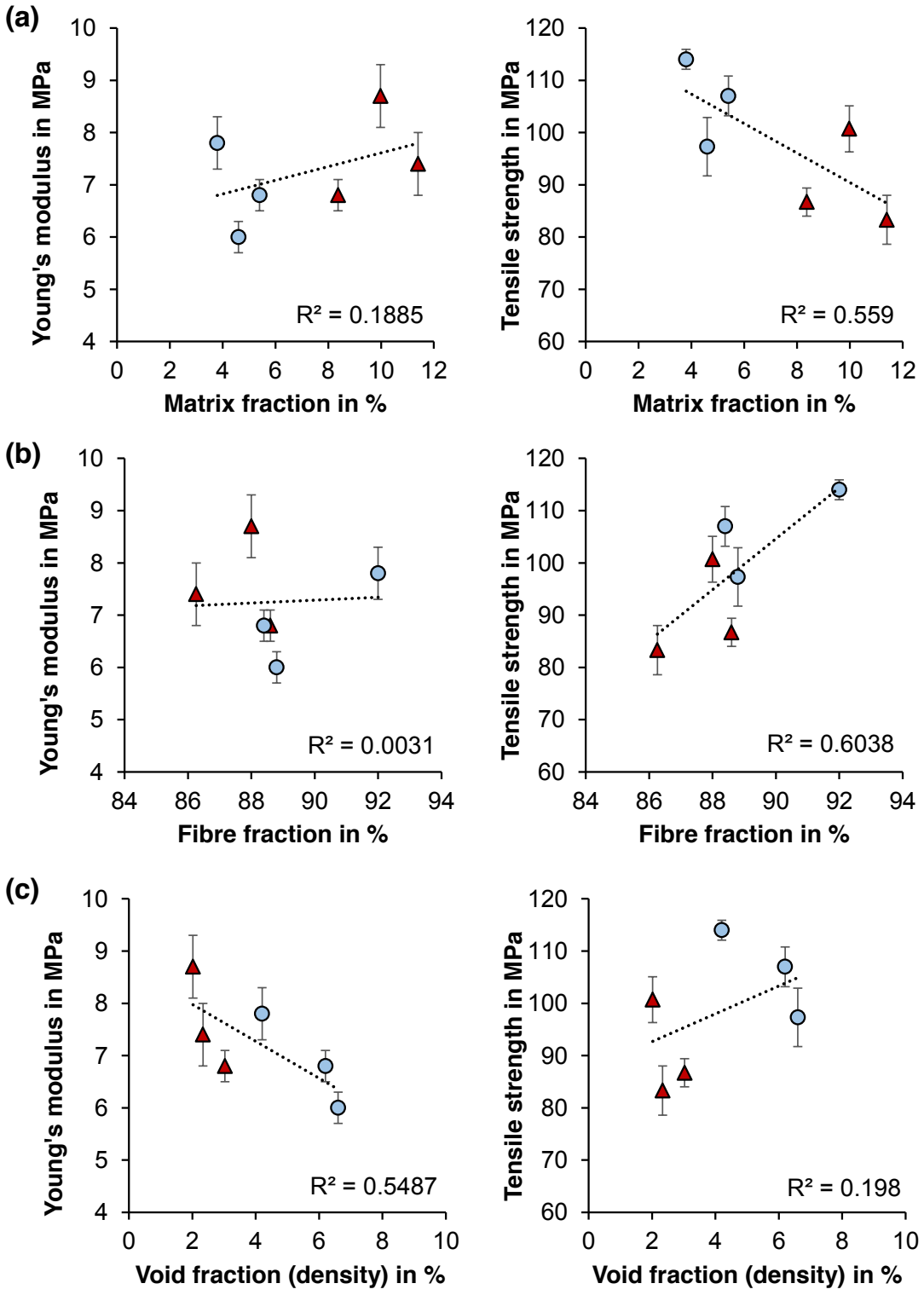

Figure 92: Correlations of Young's modulus and ultimate tensile strength of ACC laminates with (a) matrix, (b) fibre, (c) void fraction. Data of 2-layered ACCs prepared by SIP using IL (red △; IL_6h_H_2O, IL_15min_H_2O, IL_6h_acetone,) and NaOH/urea (blue ◯; SIP-5, SIP-30, SIP-60).

domly from their highly preferred orientation to the fibre axis upon partial dissolution and swelling (Figure 53), leading to a decrease in strength and modulus as reported by Soykeabkaew et al. [2009a].

Tensile strength also depends on V_f with a larger V_f leading to higher strength (Table 15b), as can be expected for higher reinforcement content.

The high V_v of NaOH/urea laminates reveal that voids are not detrimental to tensile strength, as the highest stresses were observed for the highest V_v of 5 to 6 vol. % (Figure 92c).

Young's modulus does not depend strongly on V_m (Figure 92a). NaOH/urea laminates with 4 vol. % can exceed the Young's modulus of IL-laminates with 11 vol. % matrix. On the other hand, a clear correlation of increasing Young's modulus with decreasing V_v is found (Figure 92c). It is concluded that a minimal matrix fraction of ca. 4 vol. % can suffice to achieve stress transfer to the majority of reinforcing fibres, if high laminate compaction, i.e. a low void content is achieved. At matrix fractions greater than this required minimum of matrix, reinforcing fibre volume is lost in the conversion to matrix and continuing solvent interaction weakens fibres, hence Young's modulus and ultimate tensile strength decrease with prolonged dissolution times.

7.4 SUMMARY

Nanoindentation and AFM show a difference in viscoelastic properties when comparing the fibre and matrix phase of ACC laminates. A 17 to 19 % lower E_r was found in the matrix, when compared to the fibres in the respective ACC. This decrease in mechanical properties is thought to arise from structural changes induced by ACC processing. However, the fine structure of the individual phases was not characterised unambiguously. TEM suggests

a more amorphous matrix in comparison to the fibres in ACCs, although this conclusion is only based on qualitative differences in BF image contrast. TCI determined *via* FTIR microspectroscopy also suggests a more amorphous matrix. However, no significant differences were found, which is attributed to the low sensitivity of FTIR in the narrow range of crystallinities of the ACCs under investigation and potential inclusion of fibre portions when measuring matrix areas similar in size to the FTIR beam. In order to relate the lower elastic properties of the matrix to changes in cellulose structure, further investigations, ideally synchrotron-based X-ray microdiffraction experiments, with higher resolution and sensitivity are required.

Nanoindentation revealed a 15 % decrease in E_r from as-received rayon fibre to the fibres in ACCs. Notably, no difference in the E_r of the skin and core of fibres in the ACCs was found. It is thus concluded that all of the reinforcing volume is affected by 1-step processing of ACCs, and not only the surface.

However, the correlation of the E_r of the individual phases with the tensile Young's modulus of the ACC laminates was ambiguous. It is concluded that future studies aiming at optimising and modelling of ACCs for upscaled industrial manufacturing should not rely on a rule of mixtures approach based on the individual properties of fibre and matrix. It has to be taken into account that solvent interaction and other steps in partial dissolution processing of ACCs affect the fibre properties and any variation in the processing parameters need to be investigated and modelled. For example, a correction factor will be required to estimate the decrease of fibre modulus and strength with processing, particularly for long dissolution times.

Correlations of the matrix, void and fibre content with the mechanical properties of ACC laminates led to the conclusion that in order to manufacture ACC laminates of high Young's modulus and maximum tensile strength

for a given precursor, only a small amount of matrix of ca. 4 vol.% will be required to achieve a high level of stress transfer from matrix to fibre. Short dissolution times of 5 min in NaOH/urea seem adequate to achieve such matrix fractions while limiting solvent interaction with the core of the reinforcement, thereby resulting in little fibre degradation by ACC processing.

8

DISCUSSION OF METHODOLOGY AND FUTURE WORK

8.1 SPECIMEN PREPARATION FOR MICROSCOPY

A clean surface finish is required for microstructural analysis of ACCs by optical and scanning electron microscopy. Resin embedding, grinding and diamond polishing procedures similar to those commonly applied to metals have worked favourably for ACCs prepared *via* SIP using IL [Huber et al., 2012a]. However, when embedding and polishing ACCs prepared using NaOH/urea with a comparably low matrix and a high void fraction the procedure introduced artefacts, particularly of samples infused at 0 and 20 °C where a very limited amount of matrix was formed. Embedding resin infiltrates porosities in the ACCs and formed a "secondary matrix phase", that could easily be misinterpreted as regenerated cellulose (Figure 93). The true microstructure, characterised by voids and cracks, was only revealed by cutting a wet laminate with a razor blade and performing SEM without prior embedding in a resin (Figure 94).

The mechanical interaction during grinding and polishing also affected the microstructure of ACCs. Cracks and ruptures were introduced, especially transverse fibres running parallel to the polishing surface are pulled out and protrude from the surface. Furthermore, even a fine diamond polish down to a particle size of 1 µm left scratches in the surface of ACCs

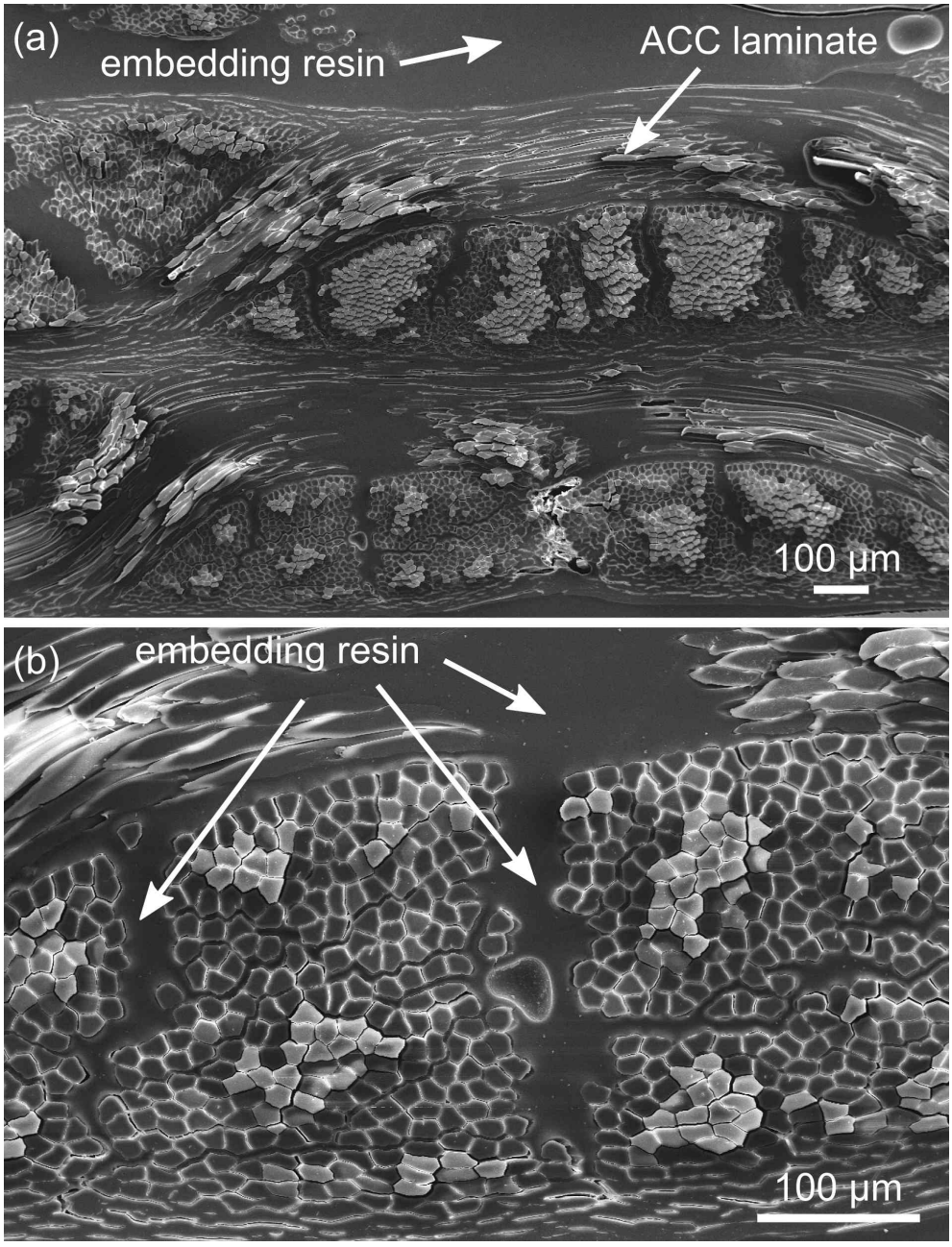

Figure 93: SEM micrographs of an ACC laminate prepared *via* SIP using NaOH/urea at 0 °C embedded in epoxy resin, ground and polished with diamond suspension. Arrows indicate the embedding resin surrounding the ACC laminate (a) and infiltrating voids and cracks within the ACC laminate (b).

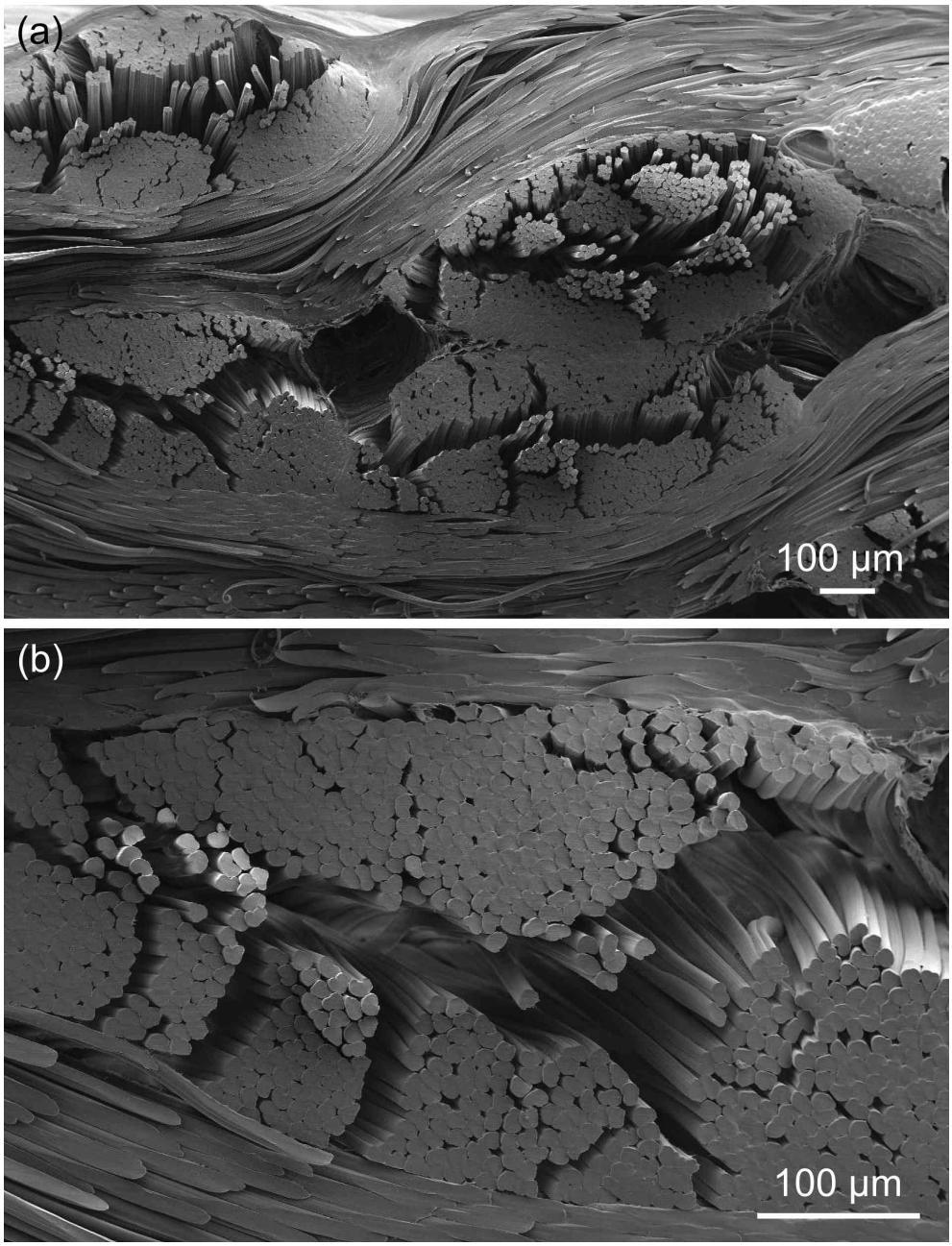

Figure 94: SEM micrographs of an ACC laminate prepared *via* SIP using NaOH/urea at 0 °C cut with a razor blade prior to drying, without embedding in a resin.

and particle residues were often found on the surface in spite of ultrasonic cleaning (Figure 95).

In contrast, smooth surfaces of ACCs with little artefacts were prepared following a procedure described by Exley et al. [1974] for wood samples. One face of a small block of an ACC laminate (edge length of 5 to 10 mm) is carefully cut with a razor blade by hand. Care needs to be taken to cut in a single, smooth motion while only cutting a thin slice off the surface and a fresh part of the blade has to be used for every cut. Cutting requires cellulosic samples to be softened in water [Exley et al., 1974]. For ACCs the ideal timing for sample preparation is therefore between regeneration and drying. However, samples can also be immersed in distilled water for 30 min, as e.g. in the case of damage analysis of dried and tensile tested specimens (Chapter 4). No changes in the microstructure of ACC laminates were observed upon drying, softening and re-drying.

A careful cut resulted in a high quality surface finish that could be inspected by SEM after drying and sputtering with gold. The surface featured lines in the direction of the cut and is otherwise free of microstructural artefacts (Figure 95). However, it is to be noted that the differential shrinkage of fibre and matrix resulted in the fibres protruding from the matrix, which shrinks to a larger extent during drying. This effect is of little practical concern in SEM due the large depth of field, but is apparent in optical microscopy. However, it has has to be taken into account for characterisation methods that necessitate contact of the surface, such as nanoindentation and ATR-FTIR microscopy.

Similarly smooth surfaces were obtained using a sliding microtome, but only when ACCs were softened in water. Hence, the same effect of a receding matrix was found. The use of an ultramicrotome allows sectioning and planing of dry ACCs. The effect of protruding fibres was hardly observed

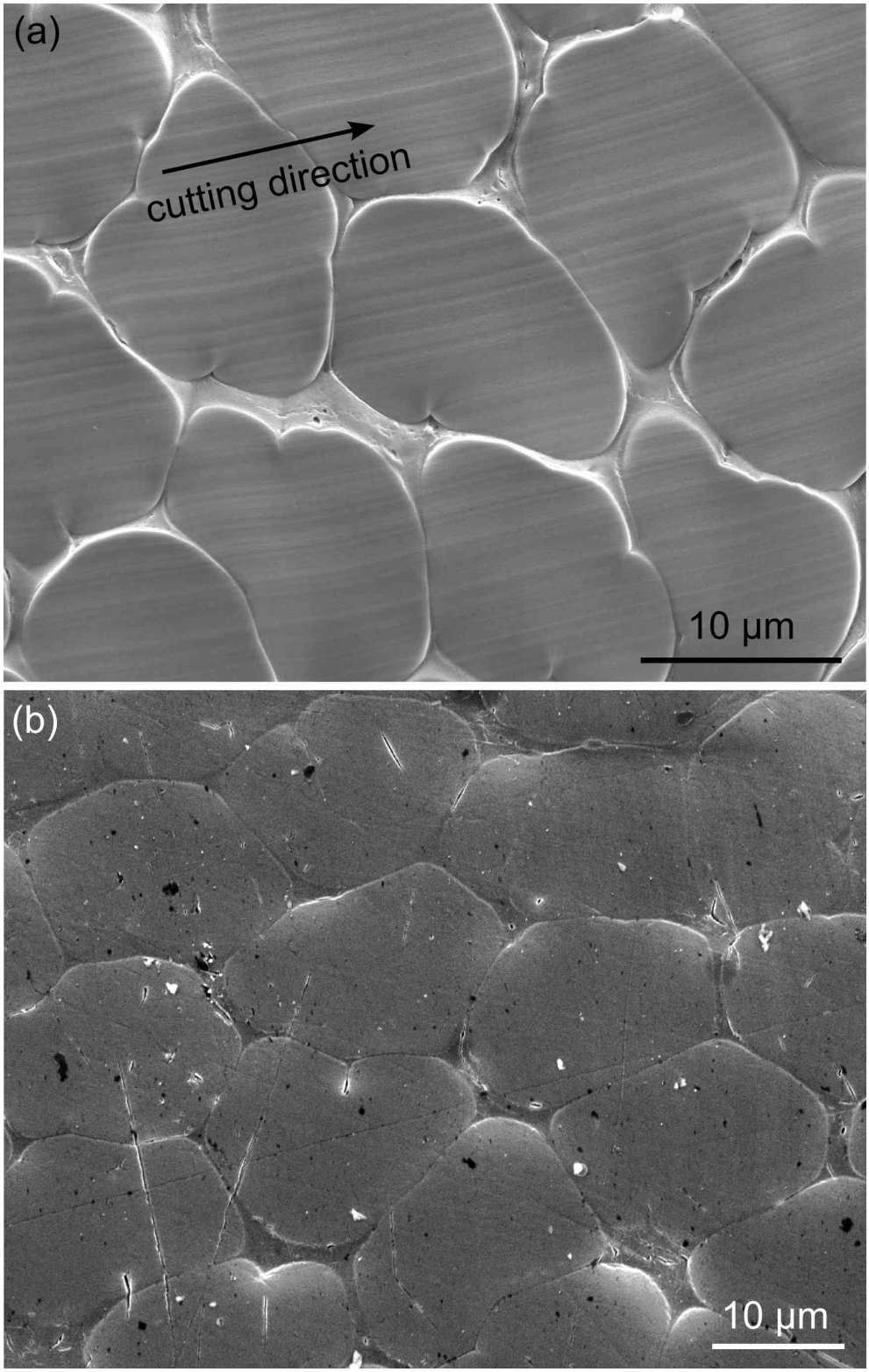

Figure 95: High magnification SEM micrographs of ACC laminates with surfaces prepared by (a) cutting with a razor blade and (b) diamond polishing.

in ultramicrotomed surfaces used for nanoindentation. However, a variation in temperature and RH between the environment in which the surface is ultramicrotomed and the characterisation (e.g. nanoindentation or ATR-FTIR microscopy) may lead to a similar effect.

In summary, cutting a softened ACC with a fresh razor blade is a straight forward preparation method for SEM, that yields a high quality surface finish with minimal time and effort when compared to grinding and polishing. Smooth and plane-parallel surfaces for AFM, nanoindentation and FTIR microspectroscopy in ATR mode can be prepared by ultramicrotoming.

8.2 DETERMINATION OF VOID AND MATRIX FRACTIONS

The mass or volume fraction of the individual constituents of a composite can be determined by several methods. ASTM-D3171 describes procedures relying on the removal of the matrix phase by ignition, melting or chemical digestion. Following such treatments, the individual constituent fractions are calculated based on the initial mass of the composite, the mass of the residual reinforcement and the densities of the matrix and reinforcement.

However, this approach is not applicable to ACCs, and other single polymer composites for that matter, as both phases consist of the same material and the matrix cannot be selectively removed. When analysing ACCs, it is therefore inevitable to rely on a microscopy-based approach [Soykeabkaew et al., 2008; Huber, 2012].

As outlined by Aström, images of a carefully prepared cross section of a composite are obtained using a microscope. Subsequently, the area fraction is determined from images and can be assumed equal to the volume fraction,

in the case of continuous, parallel fibres that are sectioned perpendicular to their long axis [Aström, 1997].

While images of carbon and glass fibre-reinforced composites often exhibit sufficient contrast to rely on semi-automatised phase recognition using image manipulation software, such as ImageJ, the low contrast of ACCs requires arduous manual delineation of the matrix phase to enhance contrast (see experimental section 3.4.4). Furthermore, only small areas are analysed, that may not be representative of the complete sample volume [Aström, 1997].

ACC laminates exhibit a substantial variability of matrix fraction even within a single yarn, probably due to local variations in solvent uptake (Figures 96 and 50). Consequently, the analysis of multiple images from several locations is required, making the determination of matrix and void fractions a laborious and time-consuming task. This can however not be avoided, as image analysis is the only suitable method for characterising the matrix fraction in ACCs.

In the case of void fraction, a density-based approach can also be applied to ACCs. A comparison reveals that a higher void content is found when relying on density measurements (Tables 6 and 15). This is due to the relatively high magnification necessary in micrographs to allow the identification of voids. Determination of void content by image analysis was limited to yarn scale (Figure 27). Hence, large interlaminar voids (~ 100 µm), as well as microvoids in the matrix (< 1 µm) are not accounted for (Figure 97). While the volume of microvoids can be regarded as negligible compared to the full void fraction, the omission of larger voids introduces a significant error and void contents below 1 % have to be considered as a local estimate that is not representative of the laminate volume. Void volume fractions in the

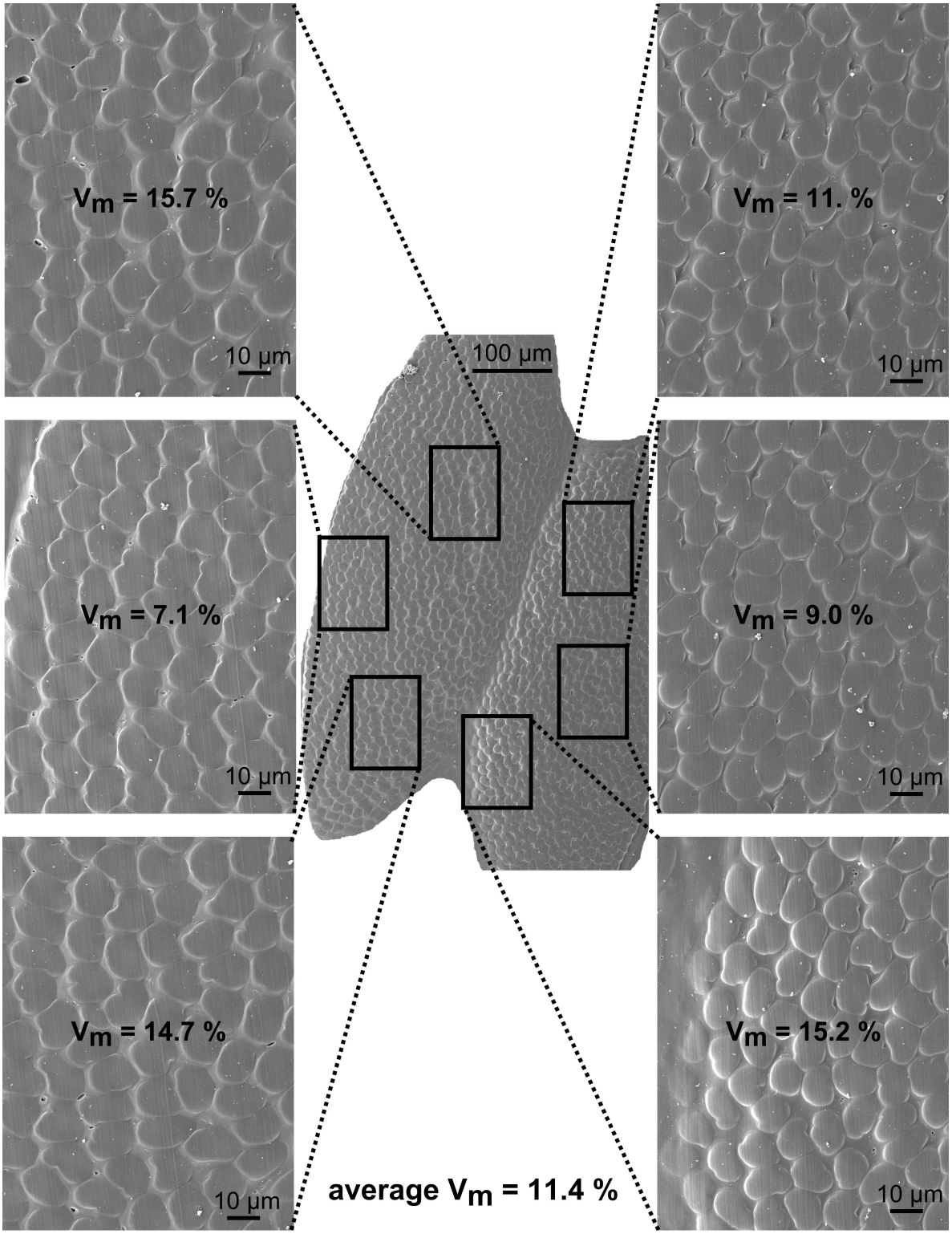

Figure 96: Variation of matrix fraction (V_m) in an ACC (EmimAc, dissolution time 6 h at 95 °C) as determined by image analysis.

order of 5 % as determined based on density measurements are considered representative of the full composite volume (Tables 6 and 15).

8.3 UPSCALED COOLING SETUP FOR SOLVENT INFUSION PROCESSING USING AQUEOUS SODIUM HYDROXIDE/ UREA SOLUTION

The processing of ACC laminates *via* SIP using NaOH/urea requires a temperature of -12 °C to be maintained throughout the infusion in order to obtain homogeneous material properties across the infused length of the laminate (Chapter 5). An adaptation of the Quickstep process for manufacturing advanced composites may be suitable for the required cooling of the SIP setup.

The Quickstep process was developed as an alternative to autoclaving for processing high-end composite parts [Griffiths and Noble, 2004]. The process relies on a liquid instead of the air in an autoclave to apply pressure and transfer heat into and away from the composite. The Quickstep setup consists of a pressure chamber lined with flexible bladders on top and bottom. A vacuum bagged laminate is then placed between the flexible bladders and the pressure chamber closed. The flexible bladders are filled with a heating/cooling liquid that is connected to three storage tanks held at three different temperature levels, to allow rapid temperature changes during the cure cycle [Griffiths and Noble, 2004].

Replacing the gas used in an autoclave to apply heat and pressure with a liquid has the advantage of a higher thermal conductivity, thus allowing more rapid temperature changes in cure cycles when comparing Quickstep to autoclaving, resulting in reduced cure cycle times of up to 95 % [Silcock

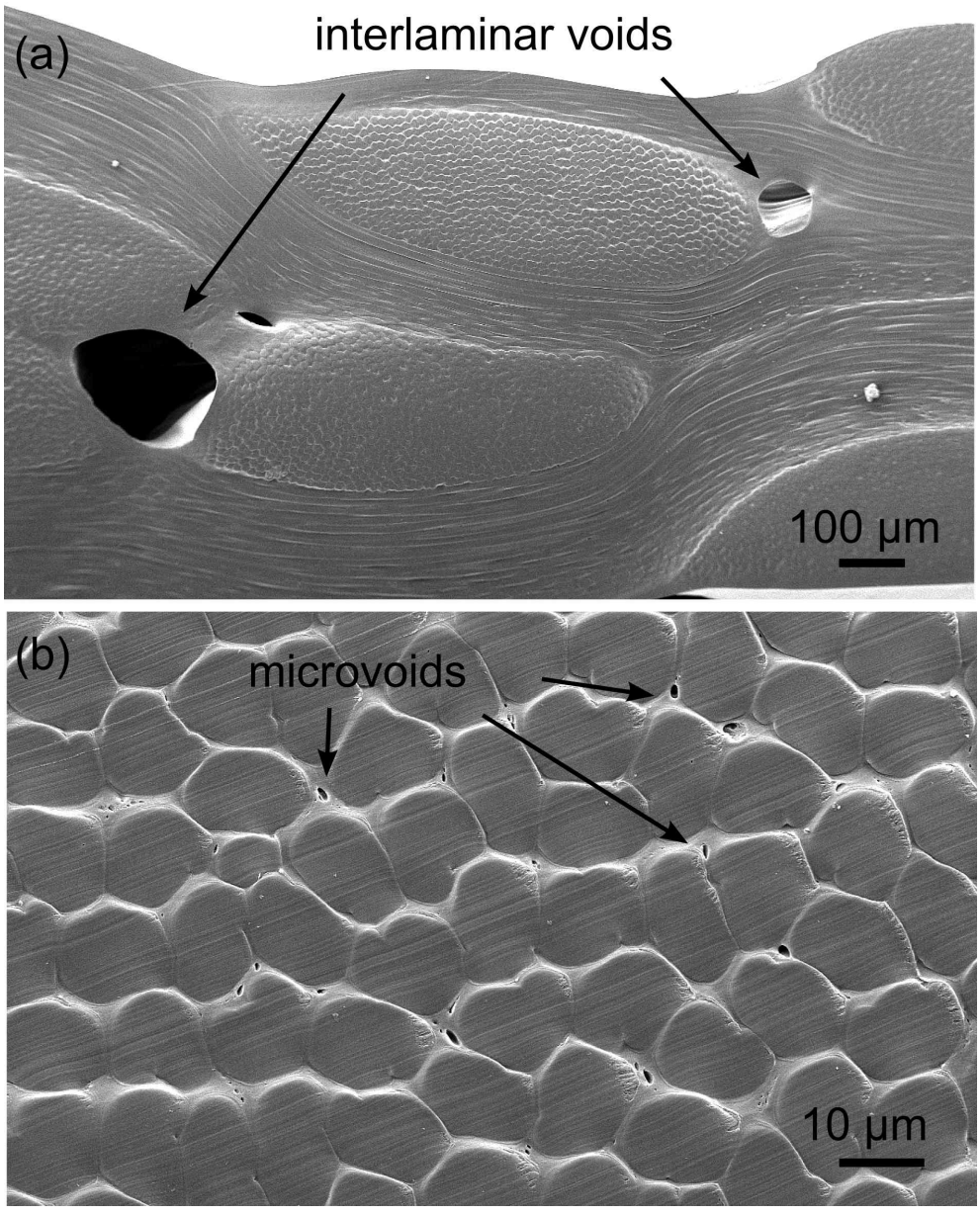

Figure 97: SEM micrographs of (a) interlaminar voids and (b) microvoids within the matrix of ACC laminates.

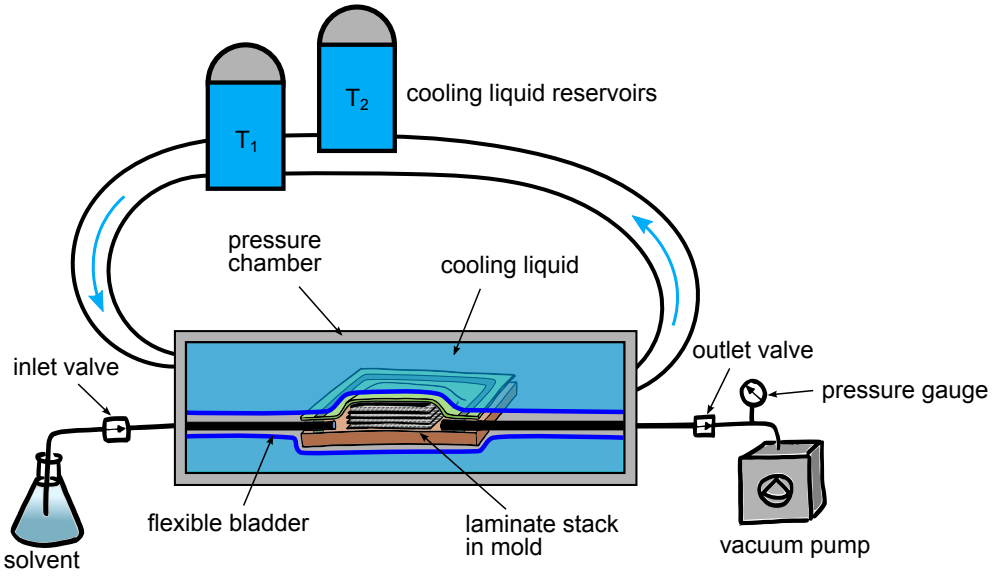

Figure 98: Schematic of the Quickstep process adapted to SIP using NaOH/urea by using a cooling liquid. The temperature of the SIP setup within the pressure chamber is controlled by the flow of cooling liquid from the reservoirs at T_1 below and T_2 above the target temperature of -12.6 °C.

et al., 2007]. Furthermore, Quickstep allows to quickly take away heat from a laminate generated by an exotherm of the resin being cured. Quickstep has been used to cure pre-preg materials and can be applied to resin infusion [Griffiths and Noble, 2004].

SIP using NaOH/urea has thus far been performed in a simplified version of the Quickstep process by placing a flexible cooling bag over the setup during infusion and immersing the setup in a cooling bath for dissolution. Performing SIP in the Quickstep pressure chamber and replacing the heating liquid by a cooling liquid (Figure 98) would allow simultaneous dissolution and application of pressure while precisely controlling the temperature during infusion. A temperature controlled flow of cooling liquid around the SIP setup would take away the heat generated by the exotherm of cellulose dissolution in NaOH/urea. The temperature of the cooling liquid would then have to be optimised and adjusted for variations in the

infused cellulose volume and the corresponding amount of heat generated by the exotherm to keep the laminate stack at the desired temperature of -12.6 °C for optimum dissolution of cellulose in NaOH/urea [Qi et al., 2008a; Qin et al., 2012].

8.4 ALTERNATIVE METHODS FOR THE CHARACTERISATION OF THE INDIVIDUAL FIBRE AND MATRIX PHASES

In order to clarify the ambiguous result of 1-step processing on the structure of the fibre and matrix phases in ACC laminates (Chapter 7), experiments with a higher spatial resolution and higher sensitivity are required. Furthermore, future experiments should focus on changes in the crystallite orientation with ACC processing.

Raman spectroscopy is a well established technique for the structural characterisation of cellulose [Schenzel and Fischer, 2001; Rusli and Eichhorn, 2008; Schenzel et al., 2009; Pullawan et al., 2014]. In their comparison of experimental methods for determining the crystallinity of cellulose II samples, Röder et al. [2006] come to the conclusion that FT-Raman spectroscopy is the ideal method for facile and quick characterisation. FT-Raman micro-spectroscopy is also available, sometimes called nano-spectroscopy, as spot sizes in the range of 400 to 500 nm are possible [Richter et al., 2011; Kotera et al., 2012]. Confocal FT-Raman micro-spectroscopy has for example been used to study the local fractions of cellulose, pectin and lignin in the plant cell wall of *Phormium tenax* (Harakeke, New Zealand flax) by Richter et al. [2011]. FT-Raman micro-spectroscopy has also been used for characterising the microstructure of a single-polymer composite based on polyethylene [Kotera et al., 2012].

An interesting combination of methods for characterising the individual phases in ACCs are coupled AFM and FT-Raman microscopes, which are commercially available (e.g. by Renishaw and Witec, 14.10.2015). The combination of AFM phase imaging and FT-Raman micro-spectroscopy would facilitate the simultaneous characterisation of the local mechanical and structural properties in ACCs at high spatial resolution. However, both FT-Raman and FTIR are vibrational spectroscopy methods [Sathyanarayana, 2004], and FT-Raman may not offer the required sensitivity for characterising the small changes in crystallinity in ACCs.

An alternative approach are diffraction based methods. Electron as well as X-ray diffraction offer high resolution and facilitate the determination of crystallinity, crystallite size and crystallite orientation of cellulose [Segal et al., 1959; Paralikar and Betrabet, 1977; Müller et al., 2000]. While TEM offers excellent magnification and electron diffraction can be performed at an area of 1 µm in diameter, the high susceptibility of cellulose to electron beam damage is problematic [Müller et al., 2000]. Although methods to minimise damage have been proposed [Paralikar and Betrabet, 1977; Hagege, 1980], the problem remains that electron diffraction patterns of cellulose are of low intensity and Müller et al. [2000] report that differences between skin and core of rayon fibres are apparent, but analysis is limited to qualitative conclusions.

Müller et al. [2000] compare the use of electron diffraction and X-ray microbeam diffraction for structural analysis of rayon fibres and come to the conclusion that X-ray diffraction using a microbeam is the better technique. In contrast to the low intensity patterns obtained by electron diffraction, it was possible to radially integrate the X-ray microdiffraction patterns and crystallinity, crystallite size and crystallite orientation were quantified [Müller et al., 2000]. However, restricting the X-rays to a microbeam re-

quires synchrotron radiation to achieve the necessary beam intensity and for example the X-ray microbeamline of the Australian Synchrotron is limited to a beam size of $25 \times 15\,\mu m^2$ (www.synchrotron.org.au, 14.10.2015). Consequently, the experiments would have to be carried out overseas at e.g. the P03 micro- and nanofocus X-ray scattering beamline at PETRA III (DESY, Hamburg, Germany) or the ID13 microfocus XRD beamline of the European Synchrotron Radiation Facility (ESRF, Grenoble, France) which operates down to a beam size of $100 \times 100\,nm^2$ (www.esrf.eu, 14.10.2015) and was used by Müller et al. [2000] for microdiffraction of rayon.

In order to fully understand the changes occurring with partial dissolution, diffraction experiments should aim at determining local variations in crystallinity, crystallite size and crystallite orientation. Additionally, nanoindentation should be extended to longitudinal sections of fibres in order to determine axial and radial changes in E_r.

9

CONCLUSIONS AND OUTLOOK

9.1 CONCLUDING REMARKS

Cellulose is an abundant natural resource and all-cellulose composites are a promising class of sustainable and biodegradable materials. Solvent infusion processing (SIP) has been developed by Huber et al. [2012a] as a viable pathway to facilitate the upscaled manufacturing of all-cellulose composites in the form of thick laminates. The present work demonstrates that increasing the thickness of ACC laminates processed by SIP is not detrimental to their mechanical properties. Quite the contrary, ACC laminates based on a woven rayon textile exhibit a *positive* size effect of increasing strength with increasing laminate thickness. In the proposed strengthening mechanism of thick laminates (4 and 8 laminae), longitudinal yarns act as crack arresters and facilitate the accumulation of damage in the form of cracked transverse yarns and local delamination. The accumulation of damage results in strain delocalisation and detached longitudinal yarns are free to straighten from the undulated shape imposed by the weave. A plateau in the stress-strain curve develops and manifests in a transition from failure of thin laminates (1 and 2 laminae) at comparatively low strains and stresses to a macroscopically ductile behaviour of thick laminates (4 and 8 laminae) with failure at higher stress and strain levels and a six-fold increase in work to fracture. In addition to the positive strength size effect, the increase in laminate thickness is

accompanied by scale effects of an increasing void content and an increased crystallinity at the core, of which the latter is due to decelerated regeneration. The observation of a positive size effect establishes that woven textile-based ACC laminates manufactured by SIP can be upscaled to a thickness that is likely to allow a wide range of applications without compromising their mechanical properties.

The toxicity and high costs associated with ionic liquids give an impetus to find alternative cellulose solvents for upscaled manufacturing of ACC laminates. An aqueous solution of 7 wt.% NaOH/12 wt.% urea (NaOH/urea) was established as an alternative solvent of low toxicity and low cost for SIP. The optimum processing conditions were found to be continuously cooled solvent infusion at -12 °C, where a vacuum pressure of 200 mbar was applied. The application of pressure *during* infusion and dissolution was found paramount to achieve the optimum mechanical properties, and cannot be replaced by applying a 50 × higher pressure *after* infusion and dissolution. A short dissolution time of 5 min was found sufficient to create a matrix fraction of approximately 4 vol. %. Extended dissolution times of 30 or 60 min resulted in a reduction of Young's modulus and ultimate tensile strength. Using an aqueous NaOH/urea solution as cellulose solvent facilitates the manufacture of ACC laminates exhibiting a comparable Young's modulus in the range of 7 to 8 GPa and a 28 % higher ultimate tensile strength of 123 MPa, while offering a dramatic reduction of solvent-related costs by 97 %, when compared to ionic liquids.

Continuous cooling was required during infusion with NaOH/urea precooled to -12 °C in order to achieve a homogeneous Young's modulus and yield strength of the ACC laminates. A decrease in Young's modulus and yield strength with increasing distance from the solvent inlet in uncooled infusion was observed and attributed to an increase in solvent temperat-

ure caused by the exothermic dissolution of cellulose in NaOH/urea. The solubility of cellulose in NaOH/urea decreases with increasing temperature [Qi et al., 2008b; Qin et al., 2012]. Consequently, solvent infusion resulted in immediate partial dissolution by the precooled solvent at the inlet region, whereas the warmed up solvent reaching the outlet region had a decreased solubility and little matrix phase was created. From the decrease of Young's modulus and yield strength by up to 40 % when comparing the inlet to the outlet region of laminates it is concluded that the Young's modulus and yield strength of ACC laminates based on a woven rayon textile are matrix-dependent properties. Ultimate tensile strength was not found to be influenced by variations in temperature during infusion and is therefore considered a fibre-dependent property.

Based on these findings, the future optimisation of the mechanical properties should include two aspects: Firstly, ultimate tensile strength is a fibre-dominated property, hence the choice of cellulose precursor facilitates adjusting ACC strength to the desired range for a given application. Secondly, Young's modulus and yield strength can be tailored by variations in partial dissolution and regeneration conditions. Overall, it was found that a comparably low matrix fraction below 5 vol. % in NaOH/urea-ACC laminates was sufficient to reach a Young's modulus in the range of 7 to 8 GPa, similar to the maximum of 8.7 GPa reached when using an ionic liquid to prepare ACC laminates with a matrix fraction of 10 vol. %. It is concluded that the optimisation needs to aim at the minimum matrix fraction required to achieve full stress transfer between matrix and fibres. Furthermore, a low void fraction was found important to achieve a high Young's modulus. NaOH/urea therefore seems a highly promising solvent to manufacture ACC laminates of high Young's modulus and maximum strength, due to short dissolution times of 5 min required to achieve sufficient partial dissolution while limit-

ing solvent interaction, which was found detrimental to fibre strength. The development of a Quickstep-like SIP setup providing adequate cooling and compaction to the laminate tack would facilitate upscalable ACC laminate processing, using NaOH/urea as a rapid, environmentally friendly and cost effective solvent.

The complete removal of solvents from ACC laminates of up to 3.4 mm thickness by washing in distilled water was confirmed by Fourier-transformed infrared spectroscopy (FTIR) and elemental analysis. The absence of solvent-associated peaks in FTIR spectra in ACCs and no variation in the elemental composition with processing indicates that ACC laminates can be classified as safe from a consumer and environmental point of view. Measuring the conductivity of the washing bath has been established as an indicator of the solvent content. Monitoring the conductivity is a useful and easily implemented method for determining the required washing times for solvent removal from ACCs.

A distinctive difference is apparent in the influence of processing on the fine structure of ACCs, depending on the use of highly crystalline or predominantly amorphous cellulose precursors. For cellulose precursors with a crystallinity in the range of 70 to 80 % a decrease in crystallinity with partial dissolution is reported [Nishino et al., 2004; Gindl-Altmutter et al., 2012; Soykeabkaew et al., 2008; Arévalo et al., 2010]. In the present work the opposite was found when processing rayon of relatively low crystallinity to ACCs by partial dissolution. The crystallinity increased from 32.6 % in the rayon precursor to 38.1 % in ACCs prepared by partial dissolution in NaOH/urea for 60 min and to 35.3 % when using ionic liquid as cellulose solvent and a dissolution time of 15 min. The increase in crystallinity is attributed to the crystallisation of dissolved cellulose onto remaining crystalline domains of

the reinforcement following a template-growth mechanism and to the recrystallisation of amorphous domains with swelling and drying.

The mechanical characterisation of the individual phases by nanoindentation revealed a lower modulus of the matrix phase in comparison to the fibres in ACC laminates. The decrease in modulus may be attributed to structural changes with partial dissolution and regeneration. Transmission electron microscopy suggests a more amorphous matrix and on average a lower crystallinity of the matrix was determined by FTIR-microspectroscopy, although the differences were not significant. The low sensitivity of FTIR to changes in crystallinity within the narrow range present in ACC laminates impedes a clear conclusion on the matter. Electron or X-ray microbeam diffraction experiments are required to determine with certainty how partial dissolution affects the crystallinity, crystallite size and crystallite orientation upon the transformation of fibrous cellulose precursor to matrix phase.

Processing results in a decrease in nanoindentation modulus from as-received rayon fibres to the fibres in ACC laminates. Thus, 1-step processing affects the core of reinforcing fibres and not only the surface of the rayon fibres used as cellulose precursor by solvent interaction. The term "surface-selective dissolution", which is frequently used in the context of ACCs, is therefore a misleading description as it implies that the core of the reinforcement remains unaffected. "Partial dissolution" is suggested as a more appropriate and generally applicable description of 1-step processing of ACCs. In spite of the core not being dissolved, its properties are affected by processing. A decrease in nanoindentation modulus with processing was found on the individual fibre level and extended dissolution times result in a decrease of the ultimate tensile strength, which is more pronounced than the percentage of fibre converted to matrix, thus indicating that solvent interac-

tion decreases the strength of the remaining core volume, probably due to a decrease in crystallite orientation.

9.2 OUTLOOK

Potential applications

ACC laminates match the mechanical properties of petrochemically-derived polymers [Ashby et al., 1995; Shah, 2014] and could substitute them in many applications. However, they should ideally be used for products with a relatively short life-span to make the most of their main advantage - biodegradability. Dicker et al. [2014] summarise the attributes of green composites and identify consumer electronics, like smart phones, and sporting equipment as suitable applications. The low density and high damping properties of flax fibre-reinforced bio-based composites when compared to glass and carbon fibre-reinforced composites [Duc et al., 2014] make their use attractive in e.g. tennis rackets and golf clubs [Peters, 2014]. These properties could also be utilised in flax-based ACCs and the high impact resistance of ACC laminates based on rayon [Huber et al., 2013] suggests their use in lightweight helmets.

Other areas of interest include the biomedical sector with applications like tissue engineering. It has been shown that all-cellulose nanocomposites allow human cell-proliferation and stimulate directed cell growth, which is important in scaffolds used for artificial blood vessels and nerves [He et al., 2014]. Mathew et al. [2012] showed that all-cellulose nanocomposites prepared by partial dissolution exhibit mechanical properties similar to natural tendon and ligament when tested in simulated body conditions. Further-

more, cytocompatibility of the nano-ACCs was demonstrated, indicating the potential use of ACCs in medical applications [Mathew et al., 2012].

Regenerated cellulose films have also been discovered as a smart material termed electroactive paper, that can serve as an actuator or biosensor [Kim et al., 2006]. ACCs widen the range of achievable properties and their optical transparency makes it possible to use them as flexible, writeable electronics [Xiong et al., 2014].

Biodegradability and recycling of all-cellulose composites

A key attribute of ACCs is their biodegradability. Many commonly used biopolymers, such as poly-lactic acid (PLA), need elevated composting temperatures of ca. 60 °C for effective biodegradation [Kunioka et al., 2006; Mathew et al., 2005]. In contrast, cellulose and regenerated cellulose films readily biodegrade in the temperature range of 20 to 30 °C [Zhang et al., 1996, 1999]. This is reflected in the excellent biodegradability of ACC laminates based on rayon in soil burial experiments with a mass loss of up to 73 % in 70 days [Kalka et al., 2014].

In contrast to ACCs, SPCs based on thermoplastics cannot be composted; however, ultimate recyclability *via* remelting is claimed as a sustainable feature [Matabola et al., 2009; Fakirov, 2013; Karger-Kocsis and Bárány, 2014]. The recycling of ACCs is unexplored as of yet, although the outlook is promising. Due to large volumes of cellulose used in the paper and cardboard industry and the high recycling rate, cellulose is the most extensively recycled polymer [Baldwin, 1995]. Recent studies at the VTT research institute in Finland show that textile waste of e.g. cotton fabrics can be recycled by dissolution in IL and extruded into regenerated fibres with performance similar to commercially available Lyocell [Asaadi et al., 2015]. Similarly, at the end

of their product lifetime, ACCs could serve as high purity cellulose starting material for regenerated fibres, which can in turn be used for manufacturing ACCs. The depolymerisation associated with dissolution and regeneration of cellulose can be minimal [Ciolacu et al., 2011] and the fine structure and mechanical properties of regenerated fibres can be tailored during processing [Ingersoll, 1946; Woodings, 2001; Adusumali et al., 2006]. Hence, the recycling of ACCs into fibres of equivalent quality for textile applications or reprocessing into composites seems feasible.

Another perspective is the chemical recycling of ACCs by pyrolitic conversion into chiral building blocks. Levoglucosenone is a highly functionalised chiral structure that can be gained from cellulose and is used as building block in a variety of natural and synthetic compounds [Corne et al., 2013]. ACCs in general and especially those prepared from regenerated fibres are purified cellulose and their chemical recycling may be a promising alternative.

Remaining challenges

Even though promising mechanical properties and feasible processing pathways of ACCs have been reported, some challenges remain.

The intrinsic hydrophilicity of cellulose limits the field of applications and modifications or surface treatments will be required to protect ACCs from moisture ingress. Manifold chemical and physical methods ranging from oiling or varnishing to sophisticated grafting or vapour deposition procedures have been reported to make cellulose hydrophobic [Cunha and Gandini, 2010; Samyn et al., 2013; Song and Rojas, 2013; Kalia et al., 2013]. Yousefi et al. [2013] applied a silane coupling treatment to ACCs and report a decrease in moisture absorption and an increase in the water contact angle from ca. 50 °

to >90 °, which is in the range of water-repellent polymers such as polyethylene. Furthermore, an increase in the tensile mechanical properties with treatment was observed in dried and conditioned (65 % RH) composites [Yousefi et al., 2013]. More studies of this kind will need to be conducted in order to establish that long-term hydrophobicity of ACCs can be achieved. It should also be considered that modifying treatments have to be environmentally-friendly, in order to maintain the green character of ACCs throughout the manufacturing process.

The swelling and shrinkage that is connected to the hydrophilicity of cellulose also adds to the complexity of processing ACCs. In the development of upscaled manufacturing of ACCs the differential shrinkage of fibre and matrix [Duchemin et al., 2009b] is expected to lead to warpage. Particularly when manufacturing three-dimensional objects of increased dimensions, models will need to be developed to precisely predict the final shape in order to meet the narrow tolerances demanded by the polymer and composite industries.

The influence of the cellulose precursor also deserves further attention. A comparative study of a broad selection of natural and man-made cellulose fibres using the same manufacturing pathway and solvent would be a very valuable screening of the achievable range of mechanical properties of ACCs. Furthermore, the type of weave in textiles could be used as a tool to tailor the properties of ACCs to specific needs and turning innovative textile products into ACCs should be explored, such as ACCs based on three-dimensional braids reported by Huber [2012].

From an ecological and economical point of view the recycling of solvents still needs further attention and more research is also necessary to facilitate the use of financially attractive raw cellulose sources without purification. It also needs to be said that efforts are necessary to clarify and guarantee

that ACCs are actually green. In this light, the cellulose source, solvent, and energy usage during manufacture need to be taken into account.

Even though the high level of interfacial bonding is often referred to as an explanation for the good mechanical properties of ACCs, there is still a lack of in depth studies of the interfacial region. ACCs have been described as "interfaceless" composites [Nishino et al., 2004] due to the chemical compatibility of the matrix and reinforcement. However, interfacial effects in single polymer composites cannot be ignored as Karger-Kocsis and Bárány [2014] point out in their review. Capiati and Porter [1975] describe the formation of a transcrystalline layer at the interface of all-polyethylene composites. Also in ACCs the differential shrinkage between fibre and matrix, and changes in cellulose polymorph and crystallinity impede the formation of a truly interfaceless composite [Duchemin et al., 2009b; Huber et al., 2013]. Several aspects, like the bonding between different polymorphs, e.g. at a cellulose I/ cellulose II interface in partially dissolved ACCs based on natural fibres, or the crystallisation effects seen when regenerating a cellulose solution mixed with highly crystalline cellulose nanowhiskers [Pullawan et al., 2010] have not yet been investigated. Sinko and Keten [2015] performed atomistic simulations of the interfacial interaction between nanocrystals of cellulose Iβ. Hydrogen bonded crystal interfaces were found to have a greater tensile strength than those governed by weaker interactions. Simulations of shearing intersheet interfaces led to a stick-slip phenomenon due to the molecular roughness of this interface, whereas a continuous sliding and rebonding mechanism was found for hydrogen bonded interfaces [Sinko and Keten, 2015]. The extension of such a study to the interactions between cellulose I and cellulose II crystals, as well as between crystalline and amorphous cellulose has great promise for the development of ACCs. The fundamental

understanding of such interfacial phenomena will set the basis for further improvements of the mechanical properties of ACCs in the future.

BIBLIOGRAPHY

Abbott, A. and Bismarck, A. (**2010**): Self-reinforced cellulose nanocomposites, Cellulose, Vol. 17, No. 4 pp. 779–791. (Cited on page 8.)

Adusumali, R.; Reifferscheid, M.; Weber, H.; Roeder, T. and Sixta, H. (**2006**): Mechanical properties of regenerated cellulose fibres for composites, Macromolecular Symposia, Vol. 244, No. 1 pp. 119–125. (Cited on pages xiv, 54, 60, 61, 103, 134, and 248.)

Agarwal, U.; Reiner, R. and Ralph, S. (**2009**): Determination of cellulose I crystallinity by FT-Raman spectroscopy, in Proceedings of the 15th International Symposium on Wood, Fiber and Pulping Chemistry, Oslo, Norway, pp. 1–5. (Cited on page 30.)

Almeida, S. and Neto, Z. (**1994**): Effect of void content on the strength of composite laminates, Composite Structures, Vol. 28, No. 2 pp. 139–148. (Cited on pages 101 and 126.)

Alves, L.; Medronho, B. F.; Antunes, F. E.; Romano, A.; Miguel, M. G. and Lindman, B. (**2015**): On the role of hydrophobic interactions in cellulose dissolution and regeneration: Colloidal aggregates and molecular solutions, Colloids and Surfaces A: Physicochemical and Engineering Aspects, Vol. 483 pp. 257–263. (Cited on pages 31 and 39.)

Araki, J.; Wada, M.; Kuga, S. and Okano, T. (**1998**): Flow properties of microcrystalline cellulose suspension prepared by acid treatment of native cellulose, Colloids and Surfaces A: Physicochemical and Engineering Aspects, Vol. 142 pp. 75–82. (Cited on page 26.)

Aravindanath, S.; Paralikar, K.; Betrabet, S. and Chaudhuri, N. (**1982**): Structural study of cellophane, Polymer, Vol. 23 pp. 823–828. (Cited on page 179.)

Arévalo, R.; Picot, O.; Wilson, R. M.; Soykeabkaew, N. and Peijs, T. (**2010**): All-cellulose composites by partial dissolution of cotton fibres, Journal of Biobased Materials and Bioenergy, Vol. 4 pp. 129–138. (Cited on pages xxiii, 53, 128, 155, 175, 195, and 244.)

Argon, A. S. and Cohen, R. E. (**2003**): Toughenability of polymers, Polymer, Vol. 44, No. 19 pp. 6013–6032. (Cited on pages 101 and 102.)

Asaadi, S.; Hummel, M.; Härkäsalmi, T. and Sixta, H. (**2015**): High Tenacity Regenerated Cellulose Fibres From Recycled Cotton in Design Driven Value Chains in the World of Cellulose, technical report, Aalto University. (Cited on page 247.)

Ashby, M. F.; Gibson, L. J.; Wegst, U. and Olive, R. (**1995**): The mechanical properties of natural materials. I. Material property charts, Proceedings of the Royal Society of London, Vol. 450, No. 1938 pp. 123–140. (Cited on page 246.)

ASTM-D2734 (**2009**): Standard Test Methods for Void Content of Reinforced Plastics. (Cited on page 72.)

ASTM-D3171 (**2015**): Standard Test Methods for Constituent Content of Composite Materials. (Cited on page 232.)

ASTM-D792 (**2013**): Standard Test Methods for Density and Specific Gravity (Relative Density) of Plastics by Displacement. (Cited on page 71.)

Aström, B. T. (**1997**): Manufacturing of Polymer Composites, Chapman & Hall, Cheltenham, UK. (Cited on pages 232 and 233.)

ATSDR (**2014**): Sodium Hydroxide (NaOH), technical report, Agency for Toxic Substances and Disease Registry, Atlanta, USA. (Cited on pages 108 and 150.)

Azubuike, C. P.; Rodríguez, H.; Okhamafe, A. O. and Rogers, R. D. (**2012**): Physicochemical properties of maize cob cellulose powders reconstituted from ionic liquid solution, Cellulose, Vol. 19, No. 2 pp. 425–433. (Cited on page 74.)

Baldwin, S. D. (**1995**): Cellulose and Paper Recycling: A Pragmatic View, in **Rader, C. P.; Baldwin, S. D.; Cornell, D. D.; Sadler, G. D. and Stockel, R. F.** (Ed.), Plastics, Rubber and Paper Recycling, ACS Symposium Series Vol. 609, chapter 23, pp. 274–285. (Cited on page 247.)

Bang, Y. H.; Lee, S.; Park, J. B. and Cho, H. H. (**1999**): Effect of coagulation conditions on fine structure of regenerated cellulosic films made from cellulose/N-methylmorpholine-N-oxide/H2O systems, Journal of Applied Polymer Science, Vol. 73, No. 13 pp. 2681–2690. (Cited on pages 45, 92, 93, 94, 141, 172, 173, and 199.)

Bažant, Z.; Daniel, I. and Li, Z. (**1996**): Size effect and fracture characteristics of composite laminates, Journal of Engineering Materials and Technology, Vol. 118, No. 3 pp. 317–324. (Cited on pages 18, 77, 78, 96, 98, and 99.)

Bažant, Z.; Kim, J.; Daniel, I.; Becq-Giraudon, E. and Zi, G. (**1999**): Size effect on compression strength of fiber composites failing by kink band propagation, International Journal of Fracture, Vol. 95 pp. 103–141. (Cited on page 98.)

Bažant, Z. P. (**1999**): Size Effect on Structural Strength: A Review, Archive of Applied Mechanics, Vol. 69, No. 9-10 pp. 703–725. (Cited on page 78.)

Bažant, Z. P. and Chen, E.-P. (**1997**): Scaling of Structural Failure, Applied Mechanics Reviews, Vol. 50, No. 10 pp. 593–627. (Cited on pages 78 and 101.)

Bažant, Z. P. and Guo, Z. (**2002**): Size Effect on Strength of Floating Sea Ice under Vertical Line Load, Journal of Engineering Mechanics, Vol. 128, No. 3 pp. 254–263. (Cited on page 101.)

Bažant, Z. P.; Lee, S.-G. and Pfeiffer, P. a. (**1987**): Size effect tests and fracture characteristics of aluminum, Engineering Fracture Mechanics, Vol. 26, No. 1 pp. 45–57. (Cited on page 101.)

Bergenstrahle, M.; Wohlert, J.; Himmel, M. E. and Brady, J. W. (**2010**): Simulation studies of the insolubility of cellulose, Carbohydrate Research, Vol. 345, No. 14 pp. 2060–2066. (Cited on pages xiii, 39, 41, and 279.)

Bernot, R.; Brueseke, M. A.; Evans-White, M. and Lamberti, G. (**2005**): Acute and chronic toxicity of imidazolium-based ionic liquids on Daphnia magna, Environmental Toxicology and Chemistry, Vol. 24, No. 1 pp. 87–92. (Cited on pages 19, 107, and 150.)

Bhama Iyer, P.; Sreenivasan, S.; Chidambareswaran, P. and Patil, N. (**1984**): Crystallization of Amorphous Cellulose, Textile Research Journal, Vol. 54, No. 11 pp. 732–735. (Cited on page 30.)

Biganska, O. and Navard, P. (**2003**): Phase diagram of a cellulose solvent: N-methylmorpholine-N-oxide-water mixtures, Polymer, Vol. 44, No. 4 pp. 1035–1039. (Cited on pages xii, 33, and 34.)

Bledzki, A.; Faruk, O. and Sperber, V. (**2006**): Cars from Bio Fibres, Macromolecular Materials and Engineering, Vol. 291, No. 5 pp. 449–457. (Cited on pages xii, 3, and 279.)

Bledzki, A. K. and Gassan, J. (**1999**): Composites reinforced with cellulose based fibres, Progress in Polymer Science (Oxford), Vol. 24, No. 2 pp. 221–274. (Cited on pages xiv, 2, 4, 17, 50, 51, and 52.)

Boerstoel, H.; Maatman, H.; Westerink, J. B. and Koenders, B. M. (**2001**): Liquid crystalline solutions of cellulose in phosphoric acid, Polymer, Vol. 42, No. 17 pp. 7371–7379. (Cited on page 57.)

Brandenberger, J. E. (**1918**): Composite cellulose film. US Patent 1266766. (Cited on page 6.)

Brendel, O.; Iannetta, P. P. M. and Stewart, D. (**2000**): A rapid and simple method to isolate pure alpha-cellulose, Phytochemical Analysis, Vol. 11, No. 1 pp. 7–10. (Cited on pages 164 and 165.)

Brown, W. F. (**1999**): Vulcanized Fibre - An Old Material With A New Relevancy, in Electrical Insulation Conference and Electrical Manufacturing and Coil Winding Conference Proceedings, pp. 309–312. (Cited on page 6.)

Buleon, A. and Chanzy, H. (**1978**): Single crystals of cellulose II, Journal of Polymer Science, Polymer Physics Edition, Vol. 16, No. 5 pp. 833–839. (Cited on pages 130, 132, and 197.)

Buleon, A.; Chanzy, H. and Roche, E. (**1977**): Shish kebab-like structures of cellulose, Journal of Polymer Science, Polymer Letters Edition, Vol. 15, No. 5 pp. 265–270. (Cited on pages 130 and 132.)

Cai, J. and Zhang, L. (**2005**): Rapid dissolution of cellulose in LiOH/urea and NaOH/urea aqueous solutions, Macromolecular Bioscience, Vol. 5, No. 6 pp. 539–48. (Cited on pages xiii, 10, 19, 38, 39, 40, 109, and 279.)

Cao, X.; Peng, X.; Sun, S.; Zhong, L.; Wang, S.; Lu, F. and Sun, R. (**2014**): Impact of regeneration process on the crystalline structure and enzymatic hydrolysis of cellulose obtained from ionic liquid., Carbohydrate polymers, Vol. 111 pp. 400–3. (Cited on page 198.)

Capiati, N. and Porter, R. (**1975**): The concept of one polymer composites modelled with high density polyethylene, Journal of materials science, Vol. 10, No. 10 pp. 1671–1677. (Cited on pages 5, 6, and 250.)

Carr, G. L. (**2001**): Resolution limits for infrared microspectroscopy explored with synchrotron radiation, Review of Scientific Instruments, Vol. 72, No. 3 pp. 1613–1619. (Cited on pages 178, 179, and 205.)

Carrillo, F.; Colom, X.; Suñol, J. and Saurina, J. (**2004**): Structural FTIR analysis and thermal characterisation of lyocell and viscose-type fibres, European Polymer Journal, Vol. 40, No. 9 pp. 2229–2234. (Cited on page 126.)

Cartier, N.; Escaffre, P.; Mathevet, F.; Chanzy, H. and Vuong, R. (**1994**): Structure and recycling of vegetable parchment, Tappi Journal, Vol. 77 pp. 95–101. (Cited on page 6.)

Chan, K. L. A. and Kazarian, S. G. (**2006**): Detection of trace materials with Fourier transform infrared spectroscopy using a multi-channel detector, Analyst, Vol. 131, No. 1 pp. 126–131. (Cited on page 169.)

Chaudemanche, C. and Navard, P. (**2011**): Swelling and dissolution mechanisms of regenerated Lyocell cellulose fibers, Cellulose, Vol. 18, No. 7635 pp. 1–15. (Cited on page 62.)

Chaudhuri, N.; Aravindanath, S. and Betrabet, S. (**1983**): Electron Diffraction Study of Regenerated Cellulose Fibers, Textile Research Journal, Vol. 53 pp. 701–705. (Cited on pages 59 and 179.)

Chen, X.; Burger, C.; Wan, F.; Zhang, J.; Rong, L.; Hsiao, B. S.; Chu, B.; Cai, J. and Zhang, L. (**2007**): Structure study of cellulose fibers wet-spun from environmentally friendly NaOH/urea aqueous solutions, Biomacromolecules, Vol. 8, No. 6 pp. 1918–1926. (Cited on page 31.)

Ciolacu, D.; Ciolacu, F. and Popa, V. (**2011**): Amorphous cellulose - structure and characterization, Cellulose Chemistry and Technology, Vol. 45, No. 1 pp. 13–21. (Cited on pages 29, 74, 195, and 248.)

Colom, X. and Carrillo, F. (**2002**): Crystallinity changes in lyocell and viscose-type fibres by caustic treatment, European Polymer Journal, Vol. 38, No. 11 pp. 2225–2230. (Cited on pages xx, 126, 129, 130, 207, and 208.)

Cordenka (**2009**): Cordenka 700, technical report. (Cited on pages xxiii and 66.)

Corne, V.; Botta, M. C.; Giordano, E. D. V.; Giri, G. F.; Llompart, D. F.; Biava, H. D.; Sarotti, A. M.; Mangione, M. I.; Mata, E. G.; Suárez, A. G. and Spanevello, R. A. (**2013**): Cellulose recycling as a source of raw chirality, Pure Applied Chemistry, Vol. 85, No. 8 pp. 1683–1692. (Cited on page 248.)

Cross, C. F.; Bevan, E. T. and Beadle, C. (**1893**): Thiokohlensäureester der Zellulose, Berichte der Deutschen Chemischen Gesellschaft, Vol. 26, No. 1 pp. 1090–1097. (Cited on pages 32 and 55.)

Cuissinat, C. and Navard, P. (**2006**): Swelling and Dissolution of Cellulose Part II: Free Floating Cotton and Wood Fibres in NaOH Water Additives Systems, Macromolecular Symposia, Vol. 244, No. 1 pp. 19–30. (Cited on pages 61, 62, and 177.)

Cunha, A. G. and Gandini, A. (**2010**): Turning polysaccharides into hydrophobic materials: a critical review. Part 1. Cellulose, Cellulose, Vol. 17, No. 5 pp. 875–889. (Cited on page 248.)

Davidson, G. F. (**1934**): The Dissolution of Chemically Modified Cellulose in Alkaline Solutions. Part I - In Solutions of Sodium Hydroxide, Particularly at Temperatures Below the Normal, Journal of the Textile Institute Transactions, Vol. 25, No. 5 pp. T174–T196. (Cited on pages xii, 10, 36, and 37.)

Davidson, G. F. (**1936**): The Dissolution of Chemically Modified Cellulose in Alkaline Solutions. Part II - A Comparison of the Solvent Action of Solutions of Lithium, Sodium, Potassium and Tetramethylammonium Hydroxides, Journal of the Textile Institute Transactions, Vol. 27, No. 4 pp. T112–130. (Cited on page 36.)

Davidson, G. F. (**1937**): The Dissolution of Chemically Modified Cellulose in Alkaline Solutions. Part III - In Solutions of Sodium and Potassium Hydroxide Containing Dissolved Zinc, Beryllium and Aluminium Oxides, Journal of the Textile Institute Transactions, Vol. 28, No. 2 pp. T27–44. (Cited on page 36.)

De Silva, R.; Vongsanga, K.; Wang, X. and Byrne, N. (**2015**): Cellulose regeneration in ionic liquids: factors controlling the degree of polymerisation, Cellulose, Vol. 22, No. 5 pp. 2845–2849. (Cited on pages 20, 171, 175, and 221.)

Dicker, M. P. M.; Duckworth, P. F.; Baker, A. B.; Francois, G.; Hazzard, M. K. and Weaver, P. M. (**2014**): Green composites: A review of material attributes and complementary applications, Composites Part A: Applied Science and Manufacturing, Vol. 56 pp. 280–289. (Cited on page 246.)

Dieke, S.; Allen, G. S. and Richter, C. P. (**1947**): The acute toxicity of thioureas and related compounds to wild and domestic norway rats, The Journal of Pharmacology and Experimental Therapeutics, Vol. 90, No. 3 pp. 260–270. (Cited on page 108.)

Dong, X. M.; Revol, J.-F. and Gray, D. G. (**1998**): Effect of microcrystallite preparation conditions on the formation of colloid crystals of cellulose, Cellulose, Vol. 5, No. 1 pp. 19–32. (Cited on page 26.)

Downing, T. D.; Kumar, R.; Cross, W. M.; Kjerengtroen, L. and Kellar, J. J. (**2000**): Determining the interphase thickness and properties in polymer matrix composites using phase imaging atomic force microscopy and nanoindentation, Journal

of Adhesion Science and Technology, Vol. 14, No. 14 pp. 1801–1812. (Cited on pages 178 and 189.)

Duc, F.; Bourban, P. E.; Plummer, C. J. G. and Manson, J. A. E. (**2014**): Damping of thermoset and thermoplastic flax fibre composites, Composites Part A: Applied Science and Manufacturing, Vol. 64 pp. 115–123. (Cited on page 246.)

Duchemin, B. (**2015**): Mercerisation of cellulose in aqueous NaOH at low concentrations, Green Chemistry, Vol. 17, No. 7 pp. 3941–3947. (Cited on page 36.)

Duchemin, B.; Newman, R. H. and Staiger, M. P. (**2007**): Phase transformations in microcrystalline cellulose due to partial dissolution, Cellulose, Vol. 14, No. 4 pp. 311–320. (Cited on pages 9, 20, and 176.)

Duchemin, B.; Thuault, A. and Vicente, A. (**2012**): Ultrastructure of cellulose crystallites in flax textile fibres, Cellulose, Vol. 19, No. 6 pp. 1837–1854. (Cited on page 74.)

Duchemin, B. J. C.; Mathew, A. P. and Oksman, K. (**2009**a): All-cellulose composites by partial dissolution in the ionic liquid 1-butyl-3-methylimidazolium chloride, Composites Part A: Applied Science and Manufacturing, Vol. 40, No. 12 pp. 2031–2037. (Cited on pages 8, 10, and 44.)

Duchemin, B. J. C.; Newman, R. H. and Staiger, M. P. (**2009**b): Structure-property relationship of all-cellulose composites, Composites Science and Technology, Vol. 69, No. 7 pp. 1225–1230. (Cited on pages 9, 11, 14, 20, 49, 92, 94, 176, 199, 204, 249, and 250.)

Egal, M.; Budtova, T. and Navard, P. (**2007**): Structure of aqueous solutions of microcrystalline cellulose/sodium hydroxide below 0 degrees C and the limit of cellulose dissolution., Biomacromolecules, Vol. 8, No. 7 pp. 2282–2287. (Cited on pages 36 and 38.)

Egal, M.; Budtova, T. and Navard, P. (**2008**): The dissolution of microcrystalline cellulose in sodium hydroxide-urea aqueous solutions, Cellulose, Vol. 15, No. 3 pp. 361–370. (Cited on page 19.)

Eichhorn, S. J.; Young, R. J. and Yeh, W.-Y. (**2001**): Deformation Processes in Regenerated Cellulose Fibers, Textile Research Journal, Vol. 71, No. 2 pp. 121–129. (Cited on page 103.)

Endres, H.-J. and Habermann, C. (**2013**): The Project: Sustainability Racing - The Vision: Mobility of the Future, in **Wellnitz, J.; Subic, A. and Trufin, R.** (Ed.), Sustainable Automotive Technologies 2013 - Lecture Notes in Mobility, Springer International Publishing, pp. 269–275. (Cited on page 4.)

Exley, R. R.; Butterfield, B. G. and Meylan, B. A. (**1974**): Preparation of wood specimens for the scanning electron microscope, Journal of Microscopy, Vol. 101, No. 1 pp. 21–30. (Cited on page 230.)

Faggin, M. F. and Hines, M. (**2004**): Improved algorithm for the suppression of interference fringe in absorption spectroscopy, Review of Scientific Instruments, Vol. 75, No. 11 pp. 4547–4553. (Cited on pages xix, 200, 202, and 203.)

Fakirov, S. (**2013**): Nano- and microfibrillar single-polymer composites: A review, Macromolecular Materials and Engineering, Vol. 298, No. 1 pp. 9–32. (Cited on pages 5 and 247.)

Fan, J.; Nassiopoulos, E.; Brighton, J.; Larminat, A. D. and Njuguna, J. (**2011**): New Structural Bio Composites for Car Applications, in Society of Plastics Engineers - EUROTEC 2011, Barcelona, Spain, pp. 1–5. (Cited on page 4.)

Faruk, O.; Bledzki, A. K.; Fink, H. P. and Sain, M. (**2012**): Biocomposites Reinforced with Natural Fibers: 2000-2010, Progress in Polymer Science, Vol. 37, No. 11 pp. 1552–1596. (Cited on pages 2, 4, 17, and 50.)

Feng, L. and Chen, Z. L. (**2008**): Research progress on dissolution and functional modification of cellulose in ionic liquids, Journal of Molecular Liquids, Vol. 142, No. 1 pp. 1–5. (Cited on pages xiii, 41, 42, and 43.)

Fengel, D. and Stoll, M. (**1989**): Crystals of cellulose grown from TFA solution, Wood Science and Technology, Vol. 23, No. 1 pp. 85–94. (Cited on pages 130 and 132.)

Fink, H. P.; Hofmann, D. and Philipp, B. (**1995**): Some aspects of lateral chain order in cellulosics from X-ray scattering, Cellulose, Vol. 2, No. 1 pp. 51–70. (Cited on pages xii, 26, 27, 75, and 279.)

Fink, H.-P.; Philipp, B.; Paul, D.; Serimaa, R. and Paakkari, T. (**1987**): The structure of amorphous cellulose as revealed by wide-angle X-ray scattering, Polymer, Vol. 28, No. 8 pp. 1265–1270. (Cited on page 29.)

Fink, H. P.; Weigel, P.; Purz, H. J. and Ganster, J. (**2001**): Structure formation of regenerated cellulose materials from NMMO-solutions, Progress in Polymer Science, Vol. 26, No. 9 pp. 1473–1524. (Cited on page 9.)

Fischer-Cripps, A. C. (**2002**): Nanoindentation, Springer, New York. (Cited on pages 184 and 185.)

Fleming, K.; Gray, D. G. and Matthews, S. (**2001**): Cellulose crystallites, Chemistry - A European Journal, Vol. 7, No. 9 pp. 1831–1835. (Cited on pages 26 and 132.)

Franck, R. R. (**2005**): Bast and other plant fibres, Woodhead Publishing Limited, Cambridge, UK. (Cited on pages xxiii, 50, 52, 53, and 60.)

French, A. (**2014**): Idealized powder diffraction patterns for cellulose polymorphs, Cellulose, Vol. 21 pp. 885–896. (Cited on pages 76, 92, and 126.)

French, A. D. and Cintrón, M. S. (**2012**): Cellulose polymorphy, crystallite size, and the Segal Crystallinity Index, Cellulose, Vol. 20, No. 1 pp. 583–588. (Cited on pages 74 and 195.)

Ganser, C.; Kreiml, P.; Morak, R.; Weber, F.; Paris, O.; Schennach, R. and Teichert, C. (**2015**): The effects of water uptake on mechanical properties of viscose fibers, Cellulose, Vol. 22, No. 4 pp. 2777–2786. (Cited on pages 178 and 218.)

Ganster, J. and Fink, H.-p. (**2006**): Novel cellulose fibre reinforced thermoplastic materials pp. 271–280. (Cited on pages xxiii and 66.)

Gao, S. L. and Mäder, E. (**2002**): Characterisation of interphase nanoscale property variations in glass fibre reinforced polypropylene and epoxy resin composites, Composites Part A: Applied Science and Manufacturing, Vol. 33, No. 4 pp. 559–576. (Cited on pages 178 and 189.)

García, R. and Perez, R. (**2002**): Dynamic atomic force microscopy methods, Surface Science Reports, Vol. 47 pp. 197–301. (Cited on pages 178, 187, and 188.)

George, J.; Sreekala, M. S. and Thomas, S. (**2001**): A review on interface modification and characterization of natural fiber reinforced plastic composites, Polymer Engineering & Science, Vol. 41, No. 9 pp. 1471–1485. (Cited on page 4.)

Gibril, M. E.; Yue, Z.; Xin da, L.; Huan, L.; Xuan, Z.; Feng, L. H. and Muhuo, Y. (**2012**a): Current status of applications of ionic liquids for cellulose dissolution and modifications: Review, International Journal of Engineering Science and Technology, Vol. 4, No. 7 pp. 3556–3571. (Cited on page 197.)

Gibril, M. E.; Zhang, Y.; X, L.; H, L.; Zhong, X.; Feng, L. H. and M, Y. (**2012**b): Current status of applications of ionic liquids for cellulose dissolution and modifications: Review, International Journal of Engineering Science, Vol. 4, No. 7 pp. 3556–3571. (Cited on page 41.)

Gindl, W. and Keckes, J. (**2005**): All-cellulose nanocomposite, Polymer, Vol. 46, No. 23 pp. 10221–10225. (Cited on pages 7, 8, 9, and 155.)

Gindl, W.; Konnerth, J. and Schöberl, T. (**2006**a): Nanoindentation of regenerated cellulose fibres, Cellulose, Vol. 13 pp. 1–7. (Cited on pages 59, 178, 184, 185, 186, 214, and 215.)

Gindl, W.; Martinschitz, K. J.; Boesecke, P. and Keckes, J. (**2006**b): Changes in the molecular orientation and tensile properties of uniaxially drawn cellulose films, Biomacromolecules, Vol. 7, No. 11 pp. 3146–3150. (Cited on page 12.)

Gindl, W.; Reifferscheid, M.; Martinschitz, K. J.; Boesecke, P. and Keckes, J. (**2008**): Reorientation of crystalline and noncrystalline regions in regenerated cellulose fibers and films tested in uniaxial tension, Journal of Polymer Science Part B: Polymer Physics, Vol. 46, No. 3 pp. 297–304. (Cited on page 103.)

Gindl, W.; Schöberl, T. and Keckes, J. (**2006**c): Structure and properties of a pulp fibre-reinforced composite with regenerated cellulose matrix, Applied Physics A, Vol. 83, No. 1 pp. 19–22. (Cited on pages 8, 176, and 177.)

Gindl-Altmutter, W.; Keckes, J.; Plackner, J.; Liebner, F.; Englund, K. and Laborie, M.-P. (**2012**): All-cellulose composites prepared from flax and lyocell fibres compared to epoxy matrix composites, Composites Science and Technology, Vol. 72, No. 11 pp. 1304–1309. (Cited on pages xxiii, 9, 53, 62, 128, 175, 195, and 244.)

Glancey, J. L. (**2010**): Vacuum-Assisted Resin Transfer Molding, in **Schwartz, M.** (Ed.), Innovations in Materials Manufacturing, Fabrication, and Environmental Safety, CRC Press, chapter 18, pp. 531–544. (Cited on pages 15 and 144.)

Gonzalvez, A.; Garrigues, S.; de la Guardia, M. and Armenta, S. (**2011**): The ways to the trace level analysis in infrared spectroscopy, Analytical Methods, Vol. 3, No. 1 pp. 43–52. (Cited on page 169.)

Graenacher, C. (**1934**): Cellulose solution, US Patent 1943176. (Cited on page 41.)

Graenacher, C. and Sallmann, R. (**1939**): Cellulose Solutions and Process of Making Same, US Patent, 2179181. (Cited on page 33.)

Grdadolnik, J. and Maréchal, Y. (**2002**): Urea and urea-water solutions - An infrared study, Journal of Molecular Structure, Vol. 615 pp. 177–189. (Cited on page 162.)

Gregory, J. R. and Spearing, S. M. (**2005**): Nanoindentation of neat and in situ polymers in polymer-matrix composites, Composites Science and Technology, Vol. 65 pp. 595–607. (Cited on page 178.)

Griffiths, B. and Noble, N. (**2004**): Process and tooling for low cost, rapid curing of composites structures, SAMPE, Vol. 40, No. 1 pp. 41–46. (Cited on pages 139, 235, and 237.)

Gurvich, M. and Pipes, R. (**1995**): Strength size effect of laminated composites, Composites Science and Technology, Vol. 55 pp. 93–105. (Cited on page 99.)

Hach (**2012**): pH measurement in high purity and low ionic strength water, technical report, Hach Lange GmbH, Düsseldorf, Germany. (Cited on page 162.)

Hagege, R. (**1980**): Electron diffraction and dark field on ultrathin sections of textile fibres, in **French, A. and Gardner, K. C. H.** (Ed.), Fiber diffraction methods, ACS Symposium Series Vol. 141; American Chemical Society, chapter 17, pp. 279–301. (Cited on page 239.)

Halonen, H.; Larsson, P. T.; Iversen, T.; Tomas, P.; Iversen, T.; Larsson, P. T.; Iversen, T. and Tomas, P. (**2012**): Mercerized cellulose biocomposites: a study of influence of mercerization on cellulose supramolecular structure, water retention value and tensile properties, Cellulose, Vol. 20, No. 1 pp. 57–65. (Cited on pages xii and 13.)

Hämmerle, F. M. (**2011**): The Cellulose Gap (the Future of Cellulose Fibres), Lenzinger Berichte, Vol. 89 pp. 12–21. (Cited on page 53.)

Han, D. and Yan, L. (**2010**): Preparation of all-cellulose composite by selective dissolving of cellulose surface in PEG/NaOH aqueous solution, Carbohydrate Poly-

mers, Vol. 79, No. 3 pp. 614–619. (Cited on page 11.)

Hanley, S.; Revol, J.-F.; Godbout, L. and Gray, D. (**1997**): Atomic force microscopy and transmission electron microscopy of cellulose from Micrasterias denticulata; evidence for a chiral helical microfibril twist, Cellulose, Vol. 4 pp. 209–220. (Cited on page 179.)

Hardiman, M.; Vaughan, T. and McCarthy, C. (**2014**): Fibrous composite matrix characterisation using nanoindentation: The effect of fibre constraint and the evolution from bulk to in-situ matrix properties, Composites Part A: Applied Science and Manufacturing, Vol. 68 pp. 296–303. (Cited on page 178.)

Haverhals, L. M.; Reichert, W. M.; De Long, H. C. and Trulove, P. C. (**2010**): Natural fiber welding, Macromolecular Materials and Engineering, Vol. 295 pp. 425–430. (Cited on pages 7, 10, 44, and 155.)

Haverhals, L. M.; Sulpizio, H. M.; Fayos, Z. A.; Trulove, M. A.; Reichert, W. M.; Foley, M. P.; De Long, H. C. and Trulove, P. C. (**2012**): Process variables that control natural fiber welding: Time, temperature, and amount of ionic liquid, Cellulose, Vol. 19 pp. 13–22. (Cited on pages 10, 44, and 155.)

He, X.; Xiao, Q.; Lu, C.; Wang, Y.; Zhang, X.; Zhao, J.; Zhang, W.; Zhang, X. and Deng, Y. (**2014**): Uniaxially aligned electrospun all-cellulose nanocomposite nanofibers reinforced with cellulose nanocrystals: Scaffold for tissue engineering, Biomacromolecules, Vol. 15, No. 2 pp. 618–627. (Cited on page 246.)

Hearle, J. W. S. and Peters, R. H. (**1963**): Fibre Structure, The Textile Institute Butterworths, Manchester & London. (Cited on page 26.)

Heinze, T.; Schwikal, K. and Barthel, S. (**2005**): Ionic liquids as reaction medium in cellulose functionalization, Macromolecular Bioscience, Vol. 5 pp. 520–525. (Cited on page 43.)

Hermans, P. H. (**1941**): The analogy between the mechanism of deformation of cellulose and that of rubber, Journal of Physical Chemistry, Vol. 45, No. 5 pp. 827–836. (Cited on page 58.)

Hermans, P. H.; Hermans, J. J. and Vermaas, D. (**1946**): Density of Cellulose Fibers. III. Density and Refractivity of Natural Fibers and Rayon, Journal of Polymer Science, Vol. 1, No. 3 pp. 162–171. (Cited on page 94.)

Hermans, P. H. and Vermaas, D. (**1946**): Density of Cellulose Fibers. I. Introduction and Experiments, Journal of Polymer Science Part A, Vol. 1, No. 3 pp. 149–155. (Cited on page 210.)

Herzog, R. O.; Jancke, W. and Polanyi, M. (**1923**): Zur Struktur der Cellulose- und Seidenfasern, Zeitschrift für Phsik, Vol. 8 p. 413. (Cited on page 26.)

a.M. Hindeleh and Johnson, D. (**1974**): Crystallinity and crystallite size measurement in cellulose fibres: 2. Viscose rayon, Polymer, Vol. 15, No. 11 pp. 697–705. (Cited on page 65.)

Hindeleh, A. M. (**1980**): X-Ray Characterization of Viscose Rayon and the Significance of Crystallinity on Tensile Properties, Textile Research Journal, Vol. 50 pp. 581–589. (Cited on pages 59 and 65.)

Howsmon, J. A. and Sisson, W. A. (**1954**): Cellulose and cellulose derivatives Part 1, in **Ott, E.; Spurlin, M. and Grafflin, M. W.** (Ed.), Cellulose and cellulose derivatives, Wiley Intercience, 2 edition, p. 278ff. (Cited on pages xii and 26.)

Huber, T. (**2012**): Processing of All Cellulose Composites via an Ionic Liquid Route, PhD Thesis, Mechanical Engineering, University of Canterbury, Christchurch, NZ,. (Cited on pages 232 and 249.)

Huber, T.; Bickerton, S.; Müssig, J.; Pang, S. and Staiger, M. P. (**2012**a): Solvent infusion processing of all-cellulose composite materials, Carbohydrate Polymers,

Vol. 90, No. 1 pp. 730–733. (Cited on pages xii, xiv, 7, 9, 10, 13, 15, 16, 17, 18, 44, 67, 68, 79, 107, 109, 118, 141, 149, 155, 227, and 241.)

Huber, T.; Bickerton, S.; Müssig, J.; Pang, S. and Staiger, M. P. (**2013**): Flexural and impact properties of all-cellulose composite laminates, Composites Science and Technology, Vol. 88 pp. 92–98. (Cited on pages 16, 246, and 250.)

Huber, T.; Müssig, J.; Curnow, O.; Pang, S.; Bickerton, S. and Staiger, M. P. (**2012**b): A critical review of all-cellulose composites, Journal of Materials Science, Vol. 47, No. 3 pp. 1171–1186. (Cited on pages xii, 8, 12, 13, 17, 32, 33, 34, 35, and 153.)

Huber, T.; Pang, S. and Staiger, M. P. (**2012**c): All-cellulose composite laminates, Composites Part A: Applied Science and Manufacturing, Vol. 43, No. 10 pp. 1738–1745. (Cited on pages xii and 8.)

Huber, T.; Pang, S. and Staiger, M. P. (**2012**d): All-cellulose composite laminates, Composites Part A: Applied Science and Manufacturing, Vol. 43, No. 10 pp. 1738–1745. (Cited on pages 9, 10, 15, 44, and 63.)

Hull, D. and Clyne, T. (**1996**): An Introduction to Composite Materials, Cambridge University Press, Cambridge, UK, 2 edition. (Cited on pages 1, 7, 102, and 103.)

Ibbett, R.; Taylor, J.; Schuster, K. C. and Cox, M. (**2007**a): Interpretation of relaxation and swelling phenomena in lyocell regenerated cellulosic fibres and textiles associated with the uptake of solutions of sodium hydroxide, Cellulose, Vol. 15, No. 3 pp. 393–406. (Cited on page 129.)

Ibbett, R. N.; Domvoglou, D. and Fasching, M. (**2007**b): Characterisation of the supramolecular structure of chemically and physically modified regenerated cellulosic fibres by means of high-resolution Carbon-13 solid-state NMR, Polymer, Vol. 48, No. 5 pp. 1287–1296. (Cited on page 129.)

Ibbett, R. N.; Domvoglou, D. and Phillips, D. a. S. (**2008**): The hydrolysis and recrystallisation of lyocell and comparative cellulosic fibres in solutions of mineral acid, Cellulose, Vol. 15, No. 2 pp. 241–254. (Cited on pages 130 and 132.)

Ibrahim, A.; Predoi-Cross, A. and Povey, C. (**2013**): Handling techniques for channel spectra in synchrotron-based Fourier transform spectra1., Canadian Journal of Physics, Vol. 91, No. 11 pp. 910–923. (Cited on pages xix, 200, 202, and 203.)

Imai, T.; Boisset, C.; Samejima, M.; Igarashi, K. and Sugiyama, J. (**1998**): Unidirectional processive action of cellobiohydrolase Cel7A on Valonia cellulose microcrystals, FEBS Letters, Vol. 432, No. 3 pp. 113–116. (Cited on page 26.)

Ingersoll, H. G. (**1946**): Fine Structure of Viscose Rayon, Journal of Applied Physics, Vol. 17 pp. 924–939. (Cited on pages 26, 58, and 248.)

Ioelovich, M. Y.; Kaimin, I. F. and Veveris, G. P. (**1983**): Crystallization of Amorphized Cellulose., Polymer science USSR, Vol. 24, No. 6 pp. 1382–1387. (Cited on pages 129 and 197.)

Ishikawa, A.; Okano, T. and Sugiyama, J. (**1997**): Fine structure and tensile properties of ramie fibres in the crystalline form of cellulose I, II, IIII and IVI, Polymer, Vol. 38, No. 2 pp. 463–468. (Cited on pages 94, 213, and 218.)

Isobe, N.; Kimura, S.; Wada, M. and Kuga, S. (**2012**): Mechanism of cellulose gelation from aqueous alkali-urea solution, Carbohydrate Polymers, Vol. 89, No. 4 pp. 1298–1300. (Cited on page 45.)

Isogai, A. and Atalla, R. H. (**1998**): Dissolution of cellulose in aqueous NaOH solutions, Cellulose, Vol. 5, No. 4 pp. 309–319. (Cited on pages xxiii, 38, 39, 62, 108, 111, 118, and 124.)

Jastorff, B.; Mölter, K.; Behrend, P.; Bottin-Weber, U.; Filser, J.; Heimers, A.; Ondruschka, B.; Ranke, J.; Schaefer, M.; Schröder, H.; Stark, A.; Stepnowski, P.; Stock, F.; Störmann, R.; Stolte, S.; Welz-Biermann, U.; Ziegert, S. and Thöming,

J. (**2005**): Progress in evaluation of risk potential of ionic liquids - basis for an eco-design of sustainable products, Green Chemistry, Vol. 7, No. 5 p. 362. (Cited on pages 19, 107, 150, and 153.)

Jiang, G.; Huang, W.; Zhu, T.; Zhang, C.; Kumi, A. K.; Zhang, Y.; Wang, H. and Hu, L. (**2011**): Diffusion dynamics of 1-Butyl-3-methylimidazolium chloride from cellulose filament during coagulation process, Cellulose, Vol. 18, No. 4 pp. 921–928. (Cited on pages 45, 93, 153, and 172.)

Jin, H.; Zha, C. and Gu, L. (**2007**): Direct dissolution of cellulose in NaOH/thiourea/urea aqueous solution., Carbohydrate research, Vol. 342, No. 6 pp. 851–8. (Cited on pages xxiii, 19, 31, 38, 39, 108, 111, 118, and 124.)

John, M. and Thomas, S. (**2008**): Biofibres and biocomposites, Carbohydrate Polymers, Vol. 71, No. 3 pp. 343–364. (Cited on pages 2 and 50.)

Joshi, S. V.; Drzal, L. T.; Mohanty, A. K. and Arora, S. (**2004**): Are natural fiber composites environmentally superior to glass fiber reinforced composites?, Composites Part A, Vol. 35 pp. 371–376. (Cited on pages 2 and 51.)

Judd, C. W. and Wright, W. (**1978**): Voids and their effects on the mechanical properties of composites - an appraisal, SAMPE Journal, Vol. 14 pp. 10–14. (Cited on page 101.)

Kalia, S.; Thakur, K.; Celli, A.; Kiechel, M. A. and Schauer, C. L. (**2013**): Surface modification of plant fibers using environment friendly methods for their application in polymer composites, textile industry and antimicrobial activities: A review, Journal of Environmental Chemical Engineering, Vol. 1, No. 3 pp. 97–112. (Cited on pages 4 and 248.)

Kalka, S.; Huber, T.; Steinberg, J.; Baronian, K.; Müssig, J. and Staiger, M. P. (**2014**): Biodegradability of all-cellulose composite laminates, Composites Part A, Vol. 59 pp. 37–44. (Cited on pages 154 and 247.)

Karger-Kocsis, J. and Bárány, T. (**2014**): Single-polymer composites (SPCs): Status and future trends, Composites Science and Technology, Vol. 92 pp. 77–94. (Cited on pages 5, 6, 247, and 250.)

Karus, M.; Ortmann, S.; Vogt, D. and Müssig, J. (**2005**): Naturfaserverstärkte Kunststoffe, Fachagentur Nachwachsende Rohstoffe, Gülzow, Germany. (Cited on page 3.)

Kaushik, M.; Fraschini, C.; Chauve, G.; Putaux, J.-l. and Moores, A. (**2015**): Transmission Electron Microscopy for the Characterization of Cellulose Nanocrystals, in **Maaz, K.** (Ed.), The Transmission Electron Microscope - Theory and Applications, Intech Open, chapter 6, pp. 129–163. (Cited on page 213.)

Keijsers, E. R. P.; Yilmaz, G. and van Dam, J. E. G. (**2013**): The cellulose resource matrix, Carbohydrate Polymers, Vol. 93, No. 1 pp. 9–21. (Cited on page 24.)

Keller, a.; Leupin, M.; Mediavilla, V. and Wintermantel, E. (**2001**): Influence of the growth stage of industrial hemp on chemical and physical properties of the fibres, Industrial Crops and Products, Vol. 13 pp. 35–48. (Cited on page 51.)

Kim, J.; Yun, S. and Ounaies, Z. (**2006**): Discovery of Cellulose as a Smart Material, Macromolecules, Vol. 39 pp. 4202–4206. (Cited on page 247.)

Klemm, D.; Heublein, B.; Fink, H.-P. and Bohn, A. (**2005**): Cellulose: fascinating biopolymer and sustainable raw material, Angewandte Chemie International Edition, Vol. 44, No. 22 pp. 3358–3393. (Cited on pages xiv, xxiii, 23, 24, 25, 30, 51, 52, 53, 56, 57, 58, 62, and 153.)

Kmetty, A.; Bárány, T. and Karger-Kocsis, J. (**2010**): Self-reinforced polymeric materials: A review, Progress in Polymer Science, Vol. 35, No. 10 pp. 1288–1310. (Cited on pages 5 and 6.)

Ko, Y. G.; Choi, U. S.; Ahn, D. J.; Kim, J. S. and Kim, T. Y. (**2001**): Physicochemical and thermal studies of viscose rayon borate fiber and its carbon fiber, Journal of Polymer Science, Part A: Polymer Chemistry, Vol. 39, No. 22 pp. 3875–3883. (Cited on page 164.)

Kolpak, F. J. and Blackwell, J. (**1976**): Determination of the Structure of Cellulose II, Macromolecules, Vol. 9, No. 2 pp. 273–278. (Cited on page 28.)

Kondo, T. and Sawatari, C. (**1996**): A fourier transform infra-red spectroscopic analysis of the character of hydrogen bonds in amorphous cellulose, Polymer, Vol. 37, No. 3 pp. 393–399. (Cited on pages 30 and 208.)

Konevskikh, T.; Ponossov, A.; Blümel, R.; Lukacs, R. and Kohler, A. (**2015**): Fringes in FTIR spectroscopy revisited: understanding and modelling fringes in infrared spectroscopy of thin films, The Analyst, Vol. 140, No. 12 pp. 3969–3980. (Cited on pages xix, 200, 202, 203, and 204.)

Kong, K. and Eichhorn, S. (**2005**): Crystalline and amorphous deformation of process-controlled cellulose-II fibres, Polymer, Vol. 46, No. 17 pp. 6380–6390. (Cited on pages xvii, 132, 133, 134, and 218.)

Kosan, B.; Michels, C. and Meister, F. (**2007**): Dissolution and forming of cellulose with ionic liquids, Cellulose, Vol. 15, No. 1 pp. 59–66. (Cited on page 43.)

Kotera, M.; Urushihara, Y.; Izumo, D. and Nishino, T. (**2012**): Interfacial structure of all-polyethylene laminate using scanning thermal microscope and nano-Raman spectroscope, Polymer, Vol. 53, No. 9 pp. 1966–1971. (Cited on page 238.)

Kouris, M.; Ruck, H. and Mason, S. G. (**1958**): The Effect of Water Removal on the Crystallinity of Cellulose, Canadian Journal of Chemistry, Vol. 36 pp. 931–948. (Cited on pages 129 and 197.)

Kreze, T. and Malej, S. (**2003**): Structural Characteristics of New and Conventional Regenerated Cellulosic Fibers, Textile Research Journal, Vol. 73 pp. 675–684. (Cited on pages 58, 59, 134, and 218.)

Kudo, S.; Zhou, Z.; Norinaga, K. and Hayashi, J.-i. (**2011**): Efficient levoglucosenone production by catalytic pyrolysis of cellulose mixed with ionic liquid, Green Chemistry, Vol. 13, No. 11 p. 3306. (Cited on page 171.)

Kunioka, M.; Ninomiya, F. and Funabashi, M. (**2006**): Biodegradation of poly(lactic acid) powders proposed as reference test materials for international standard of biodegradation evaluation method, Journal of Polymer Degradation and Stability, Vol. 91, No. 9 pp. 1919–1928. (Cited on page 247.)

Langford, J. (**1978**): A rapid method for analysing the breadths of diffraction and spectral lines using the Voigt function, Journal of Applied Crystallography, Vol. 11, No. 1 pp. 10–14. (Cited on page 75.)

Larsson, P. A.; Berglund, L. A. and Wagberg, L. (**2014**): Ductile All-Cellulose Nanocomposite Films Fabricated from Core-Shell Structured Cellulose Nanofibrils, Biomacromolecules, Vol. 15 pp. 2218–2223. (Cited on pages xii and 13.)

Le Moigne, N.; Bikard, J. and Navard, P. (**2010**): Rotation and contraction of native and regenerated cellulose fibers upon swelling and dissolution: The role of morphological and stress unbalances, Cellulose, Vol. 17 pp. 507–519. (Cited on pages 61, 62, and 177.)

Le Moigne, N.; Montes, E.; Pannetier, C.; Höfte, H. and Navard, P. (**2008**): Gradient in dissolution capacity of successively deposited cell wall layers in cotton fibres, Macromolecular Symposia, Vol. 262 pp. 65–71. (Cited on pages 61, 62, and 177.)

Lee, S.-H.; Wang, S.; Endo, T. and Kim, N. H. (**2009**): Visualization of interfacial zones in lyocell fiber-reinforced polypropylene composite by AFM contrast imaging based on phase and thermal conductivity measurements, Holzforschung,

Vol. 63, No. 2 pp. 240–247. (Cited on pages xix, 178, 189, and 216.)

Lee, S.-H.; Wang, S.; Pharr, G. M.; Kant, M. and Penumadu, D. (**2007**): Mechanical properties and creep behavior of lyocell fibers by nanoindentation and nanotensile testing, Holzforschung, Vol. 61 pp. 254–260. (Cited on pages 186, 215, and 216.)

Li, D.; Liu, Z.; Al-Haik, M.; Tehrani, M.; Murray, F.; Tannenbaum, R. and Garmestani, H. (**2010**): Magnetic alignment of cellulose nanowhiskers in an all-cellulose composite, Polymer bulletin, Vol. 65, No. 6 pp. 635–642. (Cited on page 12.)

Li, Y.; Li, Q. and Ma, H. (**2015**): The voids formation mechanisms and their effects on the mechanical properties of flax fiber reinforced epoxy composites, Composites Part A: Applied Science and Manufacturing, Vol. 72 pp. 40–48. (Cited on page 101.)

Liebert, T. (**2009**): Cellulose Solvents - Remarkable History, Bright Future, in Cellulose Solvents: For Analysis, Shaping and Chemical Modification, ACS Symposium Series; American Chemical Society, pp. 3–54. (Cited on pages 9 and 35.)

Lin, Y. C.; Cho, J.; Tompsett, G. a.; Westmoreland, P. R. and Huber, G. W. (**2009**): Kinetics and mechanism of cellulose pyrolysis, Journal of Physical Chemistry C, Vol. 113, No. 46 pp. 20097–20107. (Cited on page 171.)

Lindman, B.; Karlström, G. and Stigsson, L. (**2010**): On the mechanism of dissolution of cellulose, Journal of Molecular Liquids, Vol. 156, No. 1 pp. 76–81. (Cited on pages 31 and 175.)

Lomov, S.; Ivanov, D.; Truong, T.; Verpoest, I.; Baudry, F.; Vanden Bosche, K. and Xie, H. (**2008**): Experimental methodology of study of damage initiation and development in textile composites in uniaxial tensile test, Composites Science and Technology, Vol. 68, No. 12 pp. 2340–2349. (Cited on page 81.)

Loubinoux, D. and Chaunis, S. (**1987**): An Experimental Approach to Spinning New Cellulose Fibers with N-Methylmorpholine-Oxide as a Solvent, Textile Research Journal, Vol. 57 pp. 61–65. (Cited on pages 9, 58, 134, and 218.)

Lu, X.; Zhang, M. Q.; Rong, M. Z.; Shi, G. and Yang, G. C. (**2002**): All-Plant Fiber Composites. I: Unidirectional Sisal Fiber Reinforced Benzylated Wood, Journal of Polymer Composites, Vol. 23, No. 4 pp. 624–633. (Cited on pages 7 and 8.)

Lu, X.; Zhang, M. Q.; Rong, M. Z.; Shi, G. and Yang, G. C. (**2003**): Self-reinforced melt processable composites of sisal, Composites Science and Technology, Vol. 63 pp. 177–186. (Cited on page 7.)

Ma, H.; Zhou, B.; Li, H.-S.; Li, Y.-Q. and Ou, S.-Y. (**2011**): Green composite films composed of nanocrystalline cellulose and a cellulose matrix regenerated from functionalized ionic liquid solution, Carbohydrate Polymers, Vol. 84, No. 1 pp. 383–389. (Cited on pages 10 and 44.)

Madhurambal, G.; Mariappan, M. and Mojumdar, S. C. (**2010**): Thermal, UV and FTIR spectral studies of urea-thiourea zinc chloride single crystal, Journal of Thermal Analysis and Calorimetry, Vol. 100 pp. 763–768. (Cited on page 162.)

Madsen, B. and Lilholt, H. (**2003**): Physical and mechanical properties of unidirectional plant fibre composites - an evaluation of the influence of porosity, Composites Science and Technology, Vol. 63 pp. 1265–1272. (Cited on pages 126 and 132.)

Magonov, S.; Elings, V. and Whangbo, M.-H. (**1997**): Phase imaging and stiffness in tapping-mode atomic force microscopy, Surface Science Letters, Vol. 375, No. 2-3 pp. L385–L391. (Cited on pages 178, 187, 188, and 216.)

Mahadeva, S. K. and Kim, J. (**2012**): Influence of Residual Ionic Liquid on the Thermal Stability and Electromechanical Behavior of Cellulose Regenerated from 1-Ethyl-3-Methylimidazolium Acetate, Fibers and Polymers, Vol. 13, No. 3 pp.

289–294. (Cited on pages 20, 154, 155, 162, and 216.)

Mao, Y.; Zhou, J.; Cai, J. and Zhang, L. (**2006**): Effects of coagulants on porous structure of membranes prepared from cellulose in NaOH/urea aqueous solution, Journal of Membrane Science, Vol. 279 pp. 246–255. (Cited on pages 20, 48, 141, 153, and 173.)

Matabola, K. P.; De Vries, A. R.; Moolman, F. S. and Luyt, A. S. (**2009**): Single polymer composites: a review, Journal of materials science, Vol. 44, No. 23 pp. 6213–6222. (Cited on pages 5, 6, and 247.)

Mathew, A. P.; Oksman, K.; Pierron, D. and Harmand, M.-F. (**2012**): Fibrous cellulose nanocomposite scaffolds prepared by partial dissolution for potential use as ligament or tendon substitutes, Carbohydrate Polymers, Vol. 87, No. 3 pp. 2291–2298. (Cited on pages 246 and 247.)

Mathew, A. P.; Oksman, K. and Sain, M. (**2005**): Mechanical properties of biodegradable composites from poly lactic acid (PLA) and microcrystalline cellulose (MCC), Journal of Applied Polymer Science, Vol. 97, No. 5 pp. 2014–2025. (Cited on page 247.)

Matsumura, H.; Sugiyama, J. and Glasser, W. G. (**2000**): Cellulosic nanocomposites. I. Thermally deformable cellulose hexanoates from heterogeneous reaction, Journal of Applied Polymer Science, Vol. 78 pp. 2242–2253. (Cited on page 7.)

Matzke, M.; Stolte, S.; Thiele, K.; Juffernholz, T.; Arning, J.; Ranke, J.; Welz-Biermann, U. and Jastorff, B. (**2007**): The influence of anion species on the toxicity of 1-alkyl-3-methylimidazolium ionic liquids observed in an (eco)toxicological test battery, Green Chemistry, Vol. 9, No. 11 p. 1198. (Cited on pages 19, 107, 150, and 153.)

Mauer, L. J.; Chernyshova, A. A.; Hiatt, A.; Deering, A. and Davis, R. (**2009**): Melamine Detection in Infant Formula Powder Using Near- and Mid-Infrared Spectroscopy, Journal of Agricultural and Food Cemistry, Vol. 57, No. 10 pp. 3974–3980. (Cited on page 169.)

Mazumdar, S. K. (**2001**): Composites Manufacturing: Materials, Product, and Process Engineering, CRC Press, Boca Raton, FL, USA. (Cited on pages 15 and 144.)

McCann, J.; Choi, E.; Yamasaki, E. and Ames, B. N. (**1975**): Detection of carcinogens as mutagens in the Samonella/microsome test: Assay of 300 chemicals, Proceedings of the National Academy of Sciences of the United States of America, Vol. 72, No. 12 pp. 5135–5139. (Cited on page 108.)

Medronho, B. and Lindman, B. (**2014**a): Brief overview on cellulose dissolution/regeneration interactions and mechanisms, Advances in Colloid and Interface Science, Vol. 222 pp. 502–508. (Cited on pages 31 and 39.)

Medronho, B. and Lindman, B. (**2014**b): Competing forces during cellulose dissolution: From solvents to mechanisms, Current Opinion in Colloid and Interface Science, Vol. 19, No. 1 pp. 32–40. (Cited on pages xiii, 31, 39, and 41.)

Medronho, B.; Romano, A.; Miguel, M. G.; Stigsson, L. and Lindman, B. (**2012**): Rationalizing cellulose (in)solubility: Reviewing basic physicochemical aspects and role of hydrophobic interactions, Cellulose, Vol. 19 pp. 581–587. (Cited on pages 31 and 39.)

Meine, N.; Benedito, F. and Rinaldi, R. (**2010**): Thermal stability of ionic liquids assessed by potentiometric titration, Green Chemistry, Vol. 12, No. 10 pp. 1711–1714. (Cited on page 171.)

de Menezes, A. J.; Pasquini, D.; Curvelo, A. A. d. S. and Gandini, A. (**2009**a): Self-reinforced composites obtained by the partial oxypropylation of cellulose fibers. 1. Characterization of the materials obtained with different types of fibers,

Carbohydrate Polymers, Vol. 76, No. 3 pp. 437–442. (Cited on page 7.)

de Menezes, A. J.; Pasquini, D.; Curvelo, A. A. D. S. and Gandini, A. (**2009**b): Self-reinforced composites obtained by the partial oxypropylation of cellulose fibers. 2. Effect of catalyst on the mechanical and dynamic mechanical properties, Cellulose, Vol. 16, No. 2 pp. 239–246. (Cited on page 7.)

Miyamoto, H.; Umemura, M.; Aoyagi, T.; Yamane, C.; Ueda, K. and Takahashi, K. (**2009**): Structural reorganization of molecular sheets derived from cellulose II by molecular dynamics simulations, Carbohydrate Research, Vol. 344, No. 9 pp. 1085–1094. (Cited on pages xiii, 44, 45, 46, 47, 198, and 279.)

Mohanty, A. K.; Misra, M. and Drzal, L. T. (**2001**): Surface modifications of natural fibers and performance of the resulting biocomposites: An overview, Composite Interfaces, Vol. 8, No. 5 pp. 313–343. (Cited on page 4.)

Mohanty, A. K.; Misra, M. and Drzal, L. T. (**2002**): Sustainable Bio-Composites from renewable resources: Opportunities and challenges in the green materials world, Journal of Polymers and the Environment, Vol. 10, No. 1 pp. 19–26. (Cited on pages 2 and 50.)

Morehead, F. F. and Sisson, W. A. (**1945**): Skin Effect in Viscose Rayon, Textile Research Journal, Vol. 15, No. 12 pp. 443–450. (Cited on page 59.)

Müller, M.; Riekel, C.; Vuong, R. and Chanzy, H. (**2000**): Skin / core microstructure in viscose rayon fibres analysed by X-ray microbeam and electron diffraction mapping, Polymer, Vol. 41 pp. 2627–2632. (Cited on pages 59, 179, 186, 213, 239, and 240.)

Müssig, J. (Ed.) (**2010**): Industrial applications of natural fibres: structure, properties and technical applications, John Wiley & Sons, Hoboken, NJ, USA. (Cited on pages xiii, 2, 49, 50, 51, and 60.)

Mwaikambo, L. Y. and Ansell, M. P. (**1999**): The effect of chemical treatment on the properties of hemp, sisal, jute and kapok for composite reinforcement, Die Angewandte Makromolekulare Chemie, Vol. 272, No. 1 pp. 108–116. (Cited on pages xxiii and 53.)

Nair, S. S.; Hurley, D. C.; Wang, S. and Young, T. M. (**2013**): Nanoscale Characterization of Interphase Properties in Maleated Polypropylene-Treated Natural Fiber-Reinforced Polymer Composites, Polymer Science and Engineering, Vol. 53, No. 4 pp. 888–896. (Cited on pages 178, 189, and 216.)

Nam, S.; French, A. D.; Condon, B. D. and Concha, M. (**2016**): Segal crystallinity index revisited by the simulation of X-ray diffraction patterns of cotton cellulose Iβ and cellulose II, Carbohydrate Polymers, Vol. 135 pp. 1–9. (Cited on pages 74 and 195.)

Navard, P.; Wendler, F.; Meister, F.; Bercea, M. and Budtova, T. (**2012**): Preparation and Properties of Cellulose Solutions, in **Navard, P.** (Ed.), The European Polysaccharide Network of Excellence, Springer, Wien, chapter 5, pp. 91–152. (Cited on pages xii, xiii, 9, 31, 32, 33, 34, 36, 37, and 198.)

Nelson, M. L. and O'Connor, R. T. (**1964**): Relation of Certain Infrared Bands to Cellulose Crystallinity and Crystal Lattice Type. Part II. A New Infrared Ratio for Estimation of Crystallinity in Celluloses I and II, Journal of Polymer Science, Vol. 8 pp. 1325–1341. (Cited on pages xviii, xx, 29, 74, 75, 76, 178, 179, 182, 183, 205, 207, 208, 209, 218, and 276.)

Nishino, T.; Matsuda, I. and Hirao, K. (**2004**): All-cellulose composite, Macromolecules, Vol. 37, No. 20 pp. 7683–7687. (Cited on pages 6, 8, 9, 11, 17, 20, 35, 128, 155, 175, 195, 198, 244, and 250.)

Northolt, M. G.; Boerstoel, H.; Maatman, H.; Huisman, R.; Veurink, J. and Elzerman, H. (**2001**): The structure and properties of cellulose fibres spun from an anisotropic phosphoric acid solution, Polymer, Vol. 42 pp. 8249–8264. (Cited on page 57.)

Northolt, M. G. and Vries, H. D. (**1985**): Tensile Deformation of Regenerated and Native Cellulose Fibres, Die Angewandte Makromolekulare Chemie, Vol. 133, No. 2148 pp. 183–203. (Cited on page 103.)

Nyquist, R. A. and Kagel, R. (**1971**): Infrared spectra of inorganic compounds, Academic Press, New York. (Cited on page 162.)

O'Brien, K. T. and Salpekar, S. A. (**1993**): Scale Effects on the Transverse Tensile Strength of Graphite/Epoxy Composites, Composite Materials: Testing and Design, Vol. 11 pp. 23–52. (Cited on page 78.)

O'Connor, R.; DuPré, E. and Mitcham, D. (**1958**): Applications of infrared absorption spectroscopy to investigations of cotton and modified cottons Part I: physical and crystalline modifications and oxidation, Textile Research Journal, Vol. 28 pp. 382–392. (Cited on pages xviii, 30, 178, 182, 183, and 276.)

O'Connor, R. T.; DuPre, E. F. and McCall, E. R. (**1957**): Infrared Spectrophotometric Procedure for Analysis of Cellulose and Modified Cellulose, Analytical Chemistry, Vol. 29 pp. 998–1005. (Cited on page 178.)

Odom, E. M. and Adams, D. F. (**1992**): Specimen size effect during tensile testing of an unreinforced polymer, Journal of Material Science, Vol. 27 pp. 1767–1771. (Cited on pages 77 and 101.)

Okano, T. and Sarko, A. (**1985**): Mercerization of cellulose. II. Alkali-cellulose intermediates and a possible mercerization mechanism, Journal of Applied Polymer Science, Vol. 30, No. 1 pp. 325–332. (Cited on page 28.)

Oliver, W. and Pharr, G. (**1992**): An improved technique for determining hardness and elastic modulus using load and displacement sensing indentation experiments, Journal of Materials Research, Vol. 7, No. 6 pp. 1564–1583. (Cited on page 185.)

Olsson, C. and Wesman, G. (**2013**): Direct dissolution of cellulose: background, means and applications, in **van den Ven, T. and Godbout, L.** (Ed.), Cellulose - fundamental aspects, INTECH, chapter 6, pp. 143–178. (Cited on pages xii, xiii, 9, 31, 32, 33, 34, 35, 38, 42, and 43.)

O'Sullivan, A. (**1997**): Cellulose: the structure slowly unravels, Cellulose, Vol. 4 pp. 173–207. (Cited on pages xii, 27, 28, 29, and 175.)

Ou, R.; Xie, Y.; Wang, Q.; Sui, S. and Wolcott, M. P. (**2014**): Thermoplastic deformation of poplar wood plasticized by ionic liquids measured by a nonisothermal compression technique, Holzforschung, Vol. 68, No. 5 pp. 555–566. (Cited on page 154.)

Ouajai, S. and Shanks, R. A. (**2009**): Preparation, structure and mechanical properties of all-hemp cellulose biocomposites, Composites Science and Technology, Vol. 69, No. 13 pp. 2119–2126. (Cited on pages 9 and 34.)

Özgüney, A. T.; Körlü, A.; Bahtiari, I. and Bahar, M. (**2006**): A novel approach for sulphur test on viscose based materials, Journal of Textile and Apparel Technology and Management, Vol. 5, No. 2 pp. 1–8. (Cited on pages 164 and 165.)

Öztürk, H. B.; Potthast, A.; Rosenau, T.; Abu-Rous, M.; MacNaughtan, B.; Schuster, K. C.; Mitchell, J. R. and Bechtold, T. (**2008**): Changes in the intra- and inter-fibrillar structure of lyocell (TENCEL) fibers caused by NaOH treatment, Cellulose, Vol. 16, No. 1 pp. 37–52. (Cited on page 129.)

Paralikar, K. M. and Aravindanath, S. (**1988**): Crystallization of Cellulose, Journal of Applied Polymer Science, Vol. 35 pp. 2085–2089. (Cited on pages 130 and 132.)

Paralikar, K. M. and Betrabet, S. M. (**1977**): Electron Diffraction Technique for the Determination of Cellulose Crystallinity, Journal of Applied Polymer Science, Vol. 21 pp. 899–903. (Cited on page 239.)

Parameswaran, N. and Liese, W. (**1976**): On the fine structure of bamboo fibres, Wood Science and Technology, Vol. 10 pp. 231–246. (Cited on page 25.)

Perepelkin, K. E. (**2007**): Lyocell fibres based on direct dissolution of cellulose in N-methylmorpholine N-oxide: Development and prospects, Fibre Chemistry, Vol. 39, No. 2 pp. 163–172. (Cited on pages 58 and 218.)

Peters, S. (**2014**): Material Revolution 2: New Sustainable and Multi-Purpose Materials for Design and Architecture, Walter de Gruyter, Berlin, Germany. (Cited on page 246.)

Pinkert, A.; Marsh, K. N. and Pang, S. (**2010**): Reflections on the Solubility of Cellulose, Industrial & engineering chemistry research, Vol. 49 pp. 11121–11130. (Cited on pages xii and 24.)

Pinkert, A.; Marsh, K. N.; Pang, S. and Staiger, M. P. (**2009**): Ionic liquids and their interaction with cellulose, Chemical reviews, Vol. 109, No. 12 pp. 6712–6728. (Cited on pages 19, 41, 42, and 43.)

Pullawan, T.; Wilkinson, A. and Eichhorn, S. (**2010**): Discrimination of matrix-fibre interactions in all-cellulose nanocomposites, Composites Science and Technology, Vol. 70, No. 16 pp. 2325–2330. (Cited on pages 155, 198, and 250.)

Pullawan, T.; Wilkinson, A. N. and Eichhorn, S. J. (**2012**): Influence of magnetic field alignment of cellulose whiskers on the mechanics of all-cellulose nanocomposites., Biomacromolecules, Vol. 13, No. 8 pp. 2528–36. (Cited on page 12.)

Pullawan, T.; Wilkinson, A. N. and Eichhorn, S. J. (**2013**): Orientation and deformation of wet-stretched all-cellulose nanocomposites, Journal of Materials Science, Vol. 48, No. 22 pp. 7847–7855. (Cited on pages 8, 9, and 12.)

Pullawan, T.; Wilkinson, A. N.; Zhang, L. N. and Eichhorn, S. J. (**2014**): Deformation micromechanics of all-cellulose nanocomposites: Comparing matrix and reinforcing components, Carbohydrate Polymers, Vol. 100 pp. 31–39. (Cited on pages 11, 19, 40, 109, and 238.)

Qi, H.; Cai, J.; Zhang, L. and Kuga, S. (**2009**): Properties of films composed of cellulose nanowhiskers and a cellulose matrix regenerated from alkali/urea solution., Biomacromolecules, Vol. 10, No. 6 pp. 1597–602. (Cited on pages 11, 19, 40, and 109.)

Qi, H.; Chang, C. and Zhang, L. (**2008**a): Effects of temperature and molecular weight on dissolution of cellulose in NaOH/urea aqueous solution, Cellulose, Vol. 15, No. 6 pp. 779–787. (Cited on pages 10, 19, 38, 108, 109, 118, 122, 124, and 238.)

Qi, H.; Chang, C. and Zhang, L. (**2008**b): Effects of temperature and molecular weight on dissolution of cellulose in NaOH/urea aqueous solution, Cellulose, Vol. 15, No. 6 pp. 779–787. (Cited on pages 139, 198, and 243.)

Qi, H.; Yang, Q.; Zhang, L.; Liebert, T. and Heinze, T. (**2011**): The dissolution of cellulose in NaOH-based aqueous system by two-step process, Cellulose, Vol. 18, No. 2 pp. 237–245. (Cited on pages 31, 108, 111, 118, 132, and 221.)

Qin, C.; Soykeabkaew, N.; Xiuyuan, N. and Peijs, T. (**2008**): The effect of fibre volume fraction and mercerization on the properties of all-cellulose composites, Carbohydrate Polymers, Vol. 71, No. 3 pp. 458–467. (Cited on pages 6, 8, 9, 123, 124, and 149.)

Qin, X.; Lu, A. and Zhang, L. (**2012**): Effects of Stirring Conditions on Cellulose Dissolution in NaOH/urea Aqueous Solution at Low Temperature, Journal of Applied Polymer Science, Vol. 126 pp. E469–E476. (Cited on pages xxiii, 38, 39, 108, 111, 112, 113, 118, 238, and 243.)

R Core Team (**2013**): R: A Language and Environment for Statistical Computing, R Foundation for Statistical Computing, Vienna, Austria. ISBN 3-900051-07-0, URL http://www.R-project.org/. (Cited on page 76.)

Ranke, J.; Mölter, K.; Stock, F.; Bottin-Weber, U.; Poczobutt, J.; Hoffmann, J.; Ondruschka, B.; Filser, J. and Jastorff, B. (**2004**): Biological effects of imidazolium ionic liquids with varying chain lengths in acute Vibrio fischeri and WST-1 cell viability assays, Ecotoxicology and Environmental Safety, Vol. 58, No. 3 pp. 396–404. (Cited on pages 19, 107, and 150.)

Reddy, M. M.; Vivekanandhan, S.; Misra, M.; Bhatia, S. K. and Mohanty, A. K. (**2013**): Biobased plastics and bionanocomposites: Current status and future opportunities, Progress in Polymer Science, Vol. 38, No. 10-11 pp. 1653–1689. (Cited on page 4.)

Reddy, N. and Yang, Y. (**2005**): Structure and properties of high quality natural cellulose fibers from cornstalks, Polymer, Vol. 46, No. 15 pp. 5494–5500. (Cited on page 75.)

Reece, J.; Urry, L.; Cain, M.; Wassermann, S.; Minorsky, P. and Jackson, R. (**2013**): Biology, Benjamin Cummings, 10 edition. (Cited on pages 107, 150, and 172.)

Reich, Z.; Kapon, R.; Nevo, R.; Pilpel, Y.; Zmora, S. and Scolnik, Y. (**2001**): Scanning force microscopy in the applied biological sciences., Biotechnology advances, Vol. 19, No. 6 pp. 451–85. (Cited on pages xviii, 187, and 279.)

Ren, X. (**2000**): Development of environmental performance indicators for textile process and product, Journal of Cleaner Production, Vol. 8, No. 6 pp. 473–481. (Cited on page 40.)

Revol, J. F.; Dietrich, a. and Goring, D. a. I. (**1987**): Effect of mercerization on the crystallite size and crystallinity index in cellulose from different sources, Canadian Journal of Chemistry, Vol. 65, No. 8 pp. 1724–1725. (Cited on page 74.)

Richter, S.; Müssig, J. and Gierlinger, N. (**2011**): Functional plant cell wall design revealed by the Raman imaging approach., Planta, Vol. 233, No. 4 pp. 763–72. (Cited on page 238.)

Röder, T.; Moosbauer, J.; Fasching, M.; Bohn, A.; Baldinger, T. and Sixta, H. (**2006**): Crystallinity determination of man-made cellulose fibres - comparison of analytical methods, Lenzinger Berichte, Vol. 86 pp. 132–136. (Cited on pages xx, 30, 65, 178, 208, 209, and 238.)

Röder, T.; Moosbauer, J.; Kliba, G.; Schlader, S.; Zuckerstatter, G. and Sixta, H. (**2009**): Comparative characterisation of man-made regenerated cellulose fibres, Lenzinger Berichte, Vol. 87 pp. 98–105. (Cited on pages 92 and 126.)

Romero, A.; Santos, A.; Tojo, J. and Rodriguez, A. (**2008**): Toxicity and biodegradability of imidazolium ionic liquids, Journal of Hazardous Materials, Vol. 151 pp. 268–273. (Cited on pages 107 and 153.)

Rosato, D. V. and Rosato, D. V. (**1995**): Injection molding handbook, Chapman & Hall, 2 edition. (Cited on page 14.)

Rosenau, T.; Potthast, A.; Adorjan, I.; Hofinger, A.; Firgo, H. and Kosma, P. (**2002**): Cellulose solutions in N-methylmorpholine-N-Oxide (NMMO) - degradation processes and stabilizers, Cellulose, Vol. 9 pp. 283–291. (Cited on pages 9 and 34.)

Rous, M. A.; Ingolic, E. and Schuster, K. C. (**2006**): Visualisation of the fibrillar and pore morphology of cellulosic fibres applying transmission electron microscopy,

Cellulose, Vol. 13, No. 4 pp. 411–419. (Cited on pages 179, 186, 210, and 213.)

Rusli, R. and Eichhorn, S. J. (**2008**): Determination of the stiffness of cellulose nanowhiskers and the fiber-matrix interface in a nanocomposite using Raman spectroscopy, Applied Physics Letters, Vol. 93, No. 3 pp. 0331111–0331113. (Cited on page 238.)

Samyn, P.; Schoukens, G.; Stanssens, D.; Vonck, L. and Van den Abbeele, H. (**2013**): Hydrophobic waterborne coating for cellulose containing hybrid organic nanoparticle pigments with vegetable oils, Cellulose, Vol. 20, No. 5 pp. 2625–2646. (Cited on page 248.)

Sathyanarayana, D. N. (**2004**): Vibrational Spectroscopy - Theory and Application, New Age International Ltd., New Delhi, 1 edition. (Cited on page 239.)

Schenzel, K.; Almlof, H. and Germgard, U. (**2009**): Quantitative analysis of the transformation process of cellulose I to cellulose II using NIR FT Raman spectroscopy and chemometric methods, Cellulose, Vol. 16, No. 3 pp. 407–415. (Cited on page 238.)

Schenzel, K. and Fischer, S. (**2001**): NIR FT Raman spectroscopy - a rapid analytical tool for detecting the transformation of cellulose polymorphs, Cellulose, Vol. 8 pp. 49–57. (Cited on page 238.)

Scherrer, P. (**1918**): Bestimmung der Größe und der inneren Struktur von Kolloidteilchen mittels Röntgenstrahlen, Nachrichten von der Gesellschaft der Wissenschaften zu Göttingen, Mathematisch-Physikalische Klasse, Vol. 26 pp. 98–100. (Cited on page 75.)

Schuermann, J. (**2014**): Novel Processing Pathways for All-Cellulose Composites, Phd, University of Canterbury, Christchurch, New Zealand. (Cited on pages 65, 124, and 166.)

Schuh, C. (**2006**): Nanoindentation studies of materials, Materials Today, Vol. 9, No. 5 pp. 32–40. (Cited on page 177.)

Segal, L.; Creely, J.; a.E. Martin and Conrad, C. (**1959**): An Empirical Method for Estimating the Degree of Crystallinity of Native Cellulose Using the X-Ray Diffractometer, Textile Research Journal, Vol. 29, No. 10 pp. 786–794. (Cited on pages 30, 74, 195, and 239.)

Seoud, O. a. E.; Koschella, A.; Fidale, L. C.; Dorn, S. and Heinze, T. (**2007**): Applications of Ionic Liquids in Carbohydrate Chemistry: A Window of Opportunities, Biomacromolecules, Vol. 8, No. 9 pp. 2629–2647. (Cited on pages 41 and 43.)

Seurin, M. J. and Sixou, P. (**1987**): Behavior of Hydroxypropylcellulose Solutions in the Presence of an Inorganic Salt, European Polymer Journal, Vol. 23, No. 1 pp. 77–87. (Cited on page 35.)

Shah, D. U. (**2014**): Natural fibre composites: Comprehensive Ashby-type materials selection charts, Materials & Design, Vol. 62 pp. 21–31. (Cited on page 246.)

Shaikh, T.; Chaudhari, S. and Varma, A. (**2012**): Viscose Rayon : A Legendary Development in the Manmade Textile, International Journal of Engineering Research and Applications (IJERA), Vol. 2, No. 5 pp. 675–680. (Cited on page 54.)

Shen, L.; Worrell, E. and Patel, M. K. (**2010**): Environmental impact assessment of man-made cellulose fibres, Resources, Conservation and Recycling, Vol. 55, No. 2 pp. 260–274. (Cited on pages 63 and 64.)

Shibata, M.; Teramoto, N.; Nakamura, T. and Saitoh, Y. (**2013**a): All-cellulose and all-wood composites by partial dissolution of cotton fabric and wood in ionic liquid., Carbohydrate polymers, Vol. 98, No. 2 pp. 1532–1539. (Cited on pages xii, 10, 13, 44, 156, and 216.)

Shibata, M.; Yamazoe, K.; Kuribayashi, M. and Okuyama, Y. (**2013**b): All-wood biocomposites by partial dissolution of wood flour in 1-butyl-3-methylimidazolium chloride, Journal of Applied Polymer Science, Vol. 127 pp. 4802–4808. (Cited on pages xii, 10, 13, 44, 155, and 156.)

Silcock, M. D.; Garschke, C.; Hall, W. and Fox, B. L. (**2007**): Rapid Composite Tube Manufacture Utilizing the QuickstepTM Process, Journal of Composite Materials, Vol. 41, No. 8 pp. 965–978. (Cited on page 235.)

Sinko, R. and Keten, S. (**2015**): Traction-separation laws and stick-slip shear phenomenon of interfaces between cellulose nanocrystals, Journal of the Mechanics and Physics of Solids, Vol. 78 pp. 526–539. (Cited on page 250.)

Sobue, H.; Kiessig, H. and Hess, K. (**1939**): The cellulose-sodium hydroxide-water system as a function of temperature (Das System Cellulose-Natriumhydroxid-Wasser in Abhängigkeit von der Temperatur), Journal of Physical Chemistry B, Vol. 43 pp. 309–328. (Cited on pages xiii, 10, 36, 37, and 198.)

Song, H.; Niu, Y.; Yu, J.; Zhang, J.; Wang, Z. and He, J. (**2013**): Preparation and morphology of different types of cellulose spherulites from concentrated cellulose ionic liquid solutions, Soft Matter, Vol. 9 pp. 3013–3020. (Cited on pages 48, 49, and 94.)

Song, J. and Rojas, O. J. (**2013**): Approaching super-hydrophobicity from cellulosic materials : A Review, Nordic Pulp and Paper Research Journal, Vol. 28, No. 2 pp. 216–238. (Cited on page 248.)

Soykeabkaew, N.; Arimoto, N.; Nishino, T. and Peijs, T. (**2008**): All-cellulose composites by surface selective dissolution of aligned ligno-cellulosic fibres, Composites Science and Technology, Vol. 68, No. 10-11 pp. 2201–2207. (Cited on pages 7, 9, 11, 63, 84, 128, 155, 175, 195, 198, 232, and 244.)

Soykeabkaew, N.; Nishino, T. and Peijs, T. (**2009**a): All-cellulose composites of regenerated cellulose fibres by surface selective dissolution, Composites Part A: Applied Science and Manufacturing, Vol. 40, No. 4 pp. 321–328. (Cited on pages 6, 7, 9, 36, 58, 134, 218, and 223.)

Soykeabkaew, N.; Sian, C.; Gea, S.; Nishino, T. and Peijs, T. (**2009**b): All-cellulose nanocomposites by surface selective dissolution of bacterial cellulose, Cellulose, Vol. 16, No. 3 pp. 435–444. (Cited on page 8.)

Sreenivasan, S.; Krishna Iyer, K. R.; Chidambareswaran, P. and Patil, N. (**1988**): X-Ray Orientation of Equatorial Planes in Swollen and Stretched Cellulosic Fibers, Textile Research Journal, Vol. 58, No. 5 pp. 299–301. (Cited on pages 129 and 197.)

Stamm, A. J. (**1956**): Diffusion of Water into Uncoated Cellophane I. From Rates of Water Adsorption and Liquid Water Absorption, Journal of Physical Chemistry, Vol. 60, No. 2 pp. 72–86. (Cited on page 168.)

Staudinger, H. (**1930**): Über hochpolymere Verbindungen. 46. Mittleilung. Organische Chemie und Kolloidchemie., Colloid & Polymer Science, Vol. 53, No. 1 pp. 19–32. (Cited on page 26.)

Sugiyama, J.; Vuong, R. and Chanzy, H. (**1991**): Electron-Diffraction Study on the 2 Crystalline Phases Occurring in Native Cellulose From an Algal Cell-Wall, Macromolecules, Vol. 24 pp. 4168–4175. (Cited on pages 27 and 179.)

Sun, L.; Chen, J. Y.; Jiang, W. and Lynch, V. (**2015**): Crystalline characteristics of cellulose fiber and film regenerated from ionic liquid solution., Carbohydrate polymers, Vol. 118 pp. 150–5. (Cited on pages 58, 134, and 218.)

Sutherland, L.; Shenoi, R. and Lewis, S. (**1999**a): Size and scale effects in composites: I. Literature review, Composites Science and Technology, Vol. 59 pp. 209–220. (Cited on pages xiv, xvi, 18, 77, 78, 98, 99, and 100.)

Sutherland, L.; Shenoi, R. and Lewis, S. (**1999**b): Size and scale effects in composites: III. Woven-roving laminates, Composites Science and Technology, Vol. 59 pp. 235–251. (Cited on pages 78 and 104.)

Swatloski, R. P.; Spear, S. K.; Holbrey, J. D. and Rogers, R. D. (**2002**): Dissolution of cellulose with ionic liquids., Journal of the American Chemical Society, Vol. 124 pp. 4974–4975. (Cited on pages 9, 18, 41, 43, 149, 171, and 197.)

Tabiei, A. and Sun, J. (**2000**): Analytical simulation of strength size effect in composite materials, Composites Part B: Engineering, Vol. 31 pp. 133–139. (Cited on pages 77 and 99.)

Tang, T.; Shah, S. P. and Ouyang, C. (**1992**): Fracture Mechanics and Size Effect of Concrete in Tension, Journal of Structural Engineering, Vol. 118, No. 11 pp. 3169–3185. (Cited on page 101.)

Trejo-O'Reilly, J.; Cavaille, J. and Gandini, A. (**1997**): The surface chemical modification of cellulosic fibres in view of their use in composite materials, Cellulose, Vol. 4, No. 4 pp. 305–320. (Cited on page 164.)

Turbak, A. F.; El-Kafrawy; Snyder, F. W. and Auerbach, A. B. (**1981**): Patent 4,402,252. (Cited on page 35.)

Tze, W.; Wang, S.; Rials, T.; Pharr, G. and Kelley, S. (**2007**): Nanoindentation of wood cell walls: Continuous stiffness and hardness measurements, Composites Part A: Applied Science and Manufacturing, Vol. 38 pp. 945–953. (Cited on page 178.)

Vancso, G. J. and Schönherr, H. (**2010**): Scanning Force Microscopy of Polymers, Springer. (Cited on page 187.)

VanderHart, D. L. and Atalla, R. H. (**1984**): Studies of microstructure in native celluloses using solid-state carbon-13 NMR, Macromolecules, Vol. 17 pp. 1465–1472. (Cited on page 27.)

VanLandingham, M. R.; Villarubia, J. S.; Guthrie, W. F. and Meyers, G. F. (**2001**): Nanoindentation of polymers: An overview, Macromolecular Symposia, Vol. 167 pp. 15–43. (Cited on page 215.)

Volkmann, E.; Einsiedel, R. and Müssig, J. (**2012**): Cellulose Fiber Reinforcement for Impact-Stressed Components, Kunststoffe international, Vol. 6 pp. 22–27. (Cited on pages xxiii and 66.)

Široký, J.; Blackburn, R. S.; Bechtold, T.; Taylor, J. and White, P. (**2010**a): Attenuated total reflectance Fourier-transform Infrared spectroscopy analysis of crystallinity changes in lyocell following continuous treatment with sodium hydroxide, Cellulose, Vol. 17, No. 1 pp. 103–115. (Cited on page 126.)

Široký, J.; Blackburn, R. S.; Bechtold, T.; Taylor, J. and White, P. (**2010**b): Attenuated total reflectance Fourier-transform Infrared spectroscopy analysis of crystallinity changes in lyocell following continuous treatment with sodium hydroxide, Cellulose, Vol. 17, No. 1 pp. 103–115. (Cited on page 178.)

Wagner, H. D. (**1989**): Stochastic concepts in the study of size effects in the mechanical strength of highly oriented polymeric materials, Journal of Polymer Science Part B: Polymer Physics, Vol. 27 pp. 115–149. (Cited on page 101.)

Wakelin, J. H.; Virgin, H. S. and Crystal, E. (**1959**): Development and Comparison of Two X-Ray Methods for Determining the Crystallinity of Cotton Cellulose, Journal of Applied Physics, Vol. 30, No. 11 p. 1654. (Cited on pages 30 and 74.)

Wambua, P.; Ivens, J. and Verpoest, I. (**2003**): Natural fibres: can they replace glass in fibre reinforced plastics?, Composites Science and Technology, Vol. 63, No. 9 pp. 1259–1264. (Cited on pages 2 and 51.)

Wang, S.; Lee, S.-H. and Cheng, Q. (**2010**a): Mechanical properties of cellulosic materials at micro- and nanoscale levels, in **Lejeune, A. and Deprez, T.** (Ed.), Cellulose: Structure and Properties, Nova Science Publishers Inc., chapter 19, pp. 459–500. (Cited on page 216.)

Wang, S.; Lee, S.-H.; Tze, W.; Rials, T. and Pharr, G. (**2006**): Nanoindentation as a Tool for Understanding Nano-mechanical Properties of Wood Cell Wall and Biocomposites, in Proceedings of International Conference on Nanotechnology for the Forest Products Industry, Atlanta, GA, USA, pp. 1–7. (Cited on page 178.)

Wang, S. Q.; Nair, S. D.; Hurley, D. and Lee, S. H. (**2010**b): Characterizing Interphase Properties in Fiber Reinforced Polymer Composite with Advanced AFM Based Tools, Advanced Materials Research, Vol. 123 pp. 403–406. (Cited on pages 178, 189, and 216.)

Wang, X.; Ren, H.; Zhang, B.; Fei, B. and Burgert, I. (**2012**): Cell wall structure and formation of maturing fibres of moso bamboo (Phyllostachys pubescens) increase buckling resistance, Journal of The Royal Society Interface, Vol. 9 pp. 988–996. (Cited on page 178.)

Wang, Y. (**2008**): Cellulose Fiber Dissolution in Sodium Hydroxide Solution at Low Temperature: Dissolution Kinetics and Solubility Improvement, Department of Chemical and Biomolecular Engineering. (Cited on page 121.)

Wang, Y. and Chen, L. (**2011**): Impacts of nanowhisker on formation kinetics and properties of all-cellulose composite gels, Carbohydrate Polymers, Vol. 83, No. 4 pp. 1937–1946. (Cited on pages 11, 19, 40, and 109.)

Wang, Y. and Hahn, T. H. (**2007**): AFM characterization of the interfacial properties of carbon fiber reinforced polymer composites subjected to hygrothermal treatments, Composites Science and Technology, Vol. 67 pp. 92–101. (Cited on pages 178 and 189.)

Ward, K. (**1950**): Crystallinity of Cellulose and Its Significance for the Fiber Properties, Textile Research Journal, Vol. 20 pp. 363–372. (Cited on pages 58, 59, and 60.)

Wertz, J.; Bèduè, O. and Mercier, J. P. (**2010**): Cellulose Science and Technology, EPFL Press, 1 edition. (Cited on pages 2, 17, 23, 24, 25, and 153.)

Whang, S. (**1994**): Alkaline Additive for Drinking Water, United States Patent 5306511. (Cited on page 108.)

Williams, D. B. and Carter, B. C. (**2009**): Transmission Electron Microscopy, Springer, 2 edition. (Cited on page 210.)

Wisnom, M. (**1999**): Size effects in the testing of fibre-composite materials, Composites Science and Technology, Vol. 59 pp. 1937–1957. (Cited on pages xvi, 18, 77, 78, 96, 98, 99, and 100.)

Wisnom, M. and Atkinson, J. (**1997**): Reduction in tensile and flexural strength of unidirectional glass fibre-epoxy with increasing specimen size, Composite Structures, Vol. 38, No. 1 pp. 405–411. (Cited on pages 78 and 99.)

Wojdyr, M. (**2010**): Fityk: a general-purpose peak fitting program, Journal of Applied Crystallography, Vol. 43, No. 5 pp. 1126–1128. (Cited on pages 74 and 75.)

Woodings, C. (**2001**): Regenerated Cellulose Fibres, Woodhead Publishing Ltd, Cambridge. (Cited on pages xiv, 54, 55, 56, 57, 58, 73, 88, 94, 172, 210, 218, and 248.)

Wu, J.; Bai, J.; Xue, Z.; Liao, Y.; Zhou, X. and Xie, X. (**2014**): Insight into glass transition of cellulose based on direct thermal processing after plasticization by ionic liquid, Cellulose, Vol. 22, No. 1 pp. 89–99. (Cited on pages 154, 155, and 162.)

Wunderlich, D. and Zimmerer, B. (**2011**): Techincal Rayon: Present and Future, in 50th Dornbirn Man-Made Fibers Congress, pp. 1–20. (Cited on pages xxiii, 54, and 66.)

Xiong, B.; Zhao, P.; Cai, P.; Zhang, L.; Hu, K. and Cheng, G. (**2013**): NMR spectroscopic studies on the mechanism of cellulose dissolution in alkali solutions, Cellulose, Vol. 20 pp. 613–621. (Cited on page 39.)

Xiong, R.; Han, Y.; Wang, Y.; Zhang, W.; Zhang, X. and Lu, C. (**2014**): Flexible, highly transparent and iridescent all-cellulose hybrid nanopaper with enhanced mechanical strength and writable surface., Carbohydrate polymers, Vol. 113 pp. 264–71. (Cited on page 247.)

Xu, Z. W.; Fang, F. Z. and Dong, S. (**2011**): Carbon Nanotube AFM Probe Technology, in **Marulanda, J. M.** (Ed.), Electronic Properties of Carbon Nanotubes, InTech, chapter 7, pp. 105–124. (Cited on pages xix and 188.)

Yamane, C.; Aoyagi, T.; Ago, M.; Sato, K.; Okajima, K. and Takahashi, T. (**2006**): Two Different Surface Properties of Regenerated Cellulose due to Structural Anisotropy, Polymer Journal, Vol. 38, No. 8 pp. 819–826. (Cited on page 45.)

Yamane, C.; Hirase, R.; Miyamoto, H.; Kuwamoto, S. and Yuguchi, Y. (**2015**): Mechanism of structure formation and dissolution of regenerated cellulose from cellulose/aqueous sodium hydroxide solution and formation of molecular sheets deduced from the mechanism, Cellulose, Vol. 22, No. 5 pp. 2971–2982. (Cited on page 175.)

Yang, Q.; Lue, A. and Zhang, L. (**2010**): Reinforcement of ramie fibers on regenerated cellulose films, Composites Science and Technology, Vol. 70, No. 16 pp. 2319–2324. (Cited on pages 11, 19, 40, and 109.)

Yang, Q.; Qin, X. and Zhang, L. (**2011**): Properties of cellulose films prepared from NaOH/urea/zincate aqueous solution at low temperature, Cellulose, Vol. 18 pp. 681–688. (Cited on pages 135 and 141.)

Yousefi, H.; Nishino, T.; Faezipour, M.; Ebrahimi, G. and Shakeri, A. (**2011**): Direct fabrication of all-cellulose nanocomposite from cellulose microfibers using ionic liquid-based nanowelding, Biomacromolecules, Vol. 12 pp. 4080–4085. (Cited on pages 10 and 44.)

Yousefi, H.; Nishino, T.; Shakeri, A.; Faezipour, M.; Ebrahimi, G. and Kotera, M. (**2013**): Water-repellent all-cellulose nanocomposite using silane coupling treatment, Journal of Adhesion Science and Technology, Vol. 27, No. 12 pp. 1324–1334. (Cited on pages 9, 248, and 249.)

Zhang, H.; Wu, J.; Zhang, J. and He, J. (**2005**a): 1-allyl-3-methylimidazolium chloride room temperature ionic liquid: A new and powerful nonderivatizing solvent for cellulose, Macromolecules, Vol. 38, No. 20 pp. 8272–8277. (Cited on page 171.)

Zhang, L.; Liu, H.; Zheng, L.; Zhang, J.; Du, Y. and Feng, H. (**1996**): Biodegradability of regenerated cellulose films in soil, Industrial & Engineering Chemistry Research, Vol. 35, No. 12 pp. 4682–4685. (Cited on page 247.)

Zhang, L.; Mao, Y.; Zhou, J. and Cai, J. (**2005**b): Effects of Coagulation Conditions on the Properties of Regenerated Cellulose Films Prepared in NaOH/Urea Aqueous Solution, Industrial & Engineering Chemistry Research, Vol. 44, No. 3 pp. 522–529. (Cited on pages 20, 44, 92, 93, 94, and 135.)

Zhang, L.; Ruan, D. and Gao, S. (**2002**): Dissolution and regeneration of cellulose in NaOH/thiourea aqueous solution, Journal of Polymer Science Part B: Polymer Physics, Vol. 40, No. 14 pp. 1521–1529. (Cited on pages 10 and 31.)

Zhang, L.; Ruan, D. and Zhou, J. (**2001**): Structure and Properties of Regenerated Cellulose Films Prepared from Cotton Linters in NaOH/Urea Aqueous Solution, Industrial & Engineering Chemistry Research, Vol. 40, No. 25 pp. 5923–5928. (Cited on pages 48 and 141.)

Zhang, L.; Zhou, J.; Huang, J.; Gong, P.; Zhou, Q.; Zheng, L. and Du, Y. (**1999**): Biodegradability of Regenerated Cellulose Films Coated with Polyurethane / Natural Polymers Interpenetrating Polymer Networks, Industrial & Engineering Chemistry Research, Vol. 38 pp. 4284–4289. (Cited on page 247.)

Zhang, X. P.; Feng, S. F.; Hong, X. T. and Liu, J. Q. (**2013**): Orientation-related specimen thickness effects on mechanical properties of hot extruded AZ31B magnesium alloy, Materials and Design, Vol. 46 pp. 256–263. (Cited on page 101.)

Zhao, D.; Liao, Y. and Zhang, Z. (**2007**): Toxicity of Ionic Liquids, Clean, Vol. 35, No. 1 pp. 42–48. (Cited on pages 19, 107, and 150.)

Zhao, Q.; Yam, R. C. M.; Zhang, B.; Yang, Y.; Cheng, X. and Li, R. K. Y. (**2009**): Novel all-cellulose ecocomposites prepared in ionic liquids, Cellulose, Vol. 16, No. 2 pp. 217–226. (Cited on pages 10 and 44.)

Zhou, F.; Balendran, R. and Jeary, A. (**1998**): Size effect on flexural, splitting tensile, and torsional strengths of high-strength concrete, Cement and Concrete Research, Vol. 28, No. 12 pp. 1725–1736. (Cited on page 101.)

Zhou, J. and Zhang, L. (**2000**): Solubility of Cellulose in NaOH/Urea Aqueous Solution., Polymer Journal, Vol. 32 pp. 866–870. (Cited on page 10.)

Zhou, Q.; Malm, E. and Nilsson, H. (**2009**): Biomimetic design of cellulose-based nanostructured composites using bacterial cellulose, Polymer Preprints, Vol. 50, No. 2 pp. 7–8. (Cited on page 8.)

Zhu, S.; Wu, Y.; Chen, Q.; Yu, Z.; Wang, C. and Jin, S. (**2006**): Dissolution of cellulose with ionic liquids and its application: a mini-review, Green Chemistry, Vol. 8 pp. 325–327. (Cited on pages 19, 41, and 197.)

Zugenmaier, P. (**2008**): Crystalline Cellulose and Cellulose Derivatives, Springer. (Cited on page 28.)

Zweben, C. (**1994**): Is there a size effect in composites?, Composites, Vol. 25, No. 6 pp. 451–454. (Cited on pages 18, 77, 78, and 98.)

A

APPENDIX

DRYING AND MOISTURE ABSORPTION OF RAYON

The rayon textile used as precursor was conditioned at 23 °C and 50 % RH for 7 days and then dried at 95 °C in a vacuum oven for 24 h. Subsequently, the dried textile was exposed to 23 °C and 50 % RH while measuring mass changes with a laboratory balance (ED2249, accuracy 0.1 mg, Sartorius AG, Göttingen, Germany).

Table 17: Mass loss of rayon textile dried at 95 °C in a vacuum oven.

	mass of sample in mg			mass loss of sample in wt.%		
time in h	A	B	C	A	B	C
0	194	199.1	229.4			
1.5	174.5	178.8	206.1	10.1	10.2	10.2
4	174.3	178.5	206.1	10.2	10.3	10.2
18	173.4	177.8	205.6	10.6	10.7	10.4
24	173.5	177.9	205.1	10.6	10.6	10.6
final mass loss in wt.%	10.6	10.6	10.6			

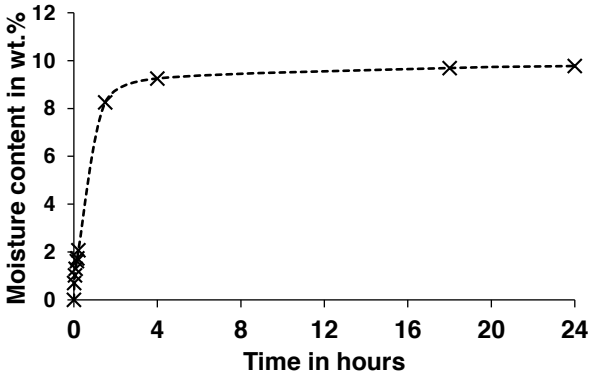

Figure 99: Moisture uptake of rayon at 23 °C and 50 % RH.

ANALYSIS OF FOURIER-TRANSFORMED INFRARED SPECTRA IN OPUS

The analysis of FTIR spectra was automated by using the integration tool available in OPUS 7.2 (Bruker, Billerica, MA, USA). The height of each peak for the TCI (I_{2900}/I_{1372}) and LOI (I_{1420}/I_{890}) were determined by setting up a method according to the baselines given by Nelson and O'Connor [1964] and O'Connor et al. [1958]. The boundaries for the left and right edge of the peak determination and the points for setting the baselines are given in Figure 100 for TCI and in Figure 101 for LOI.

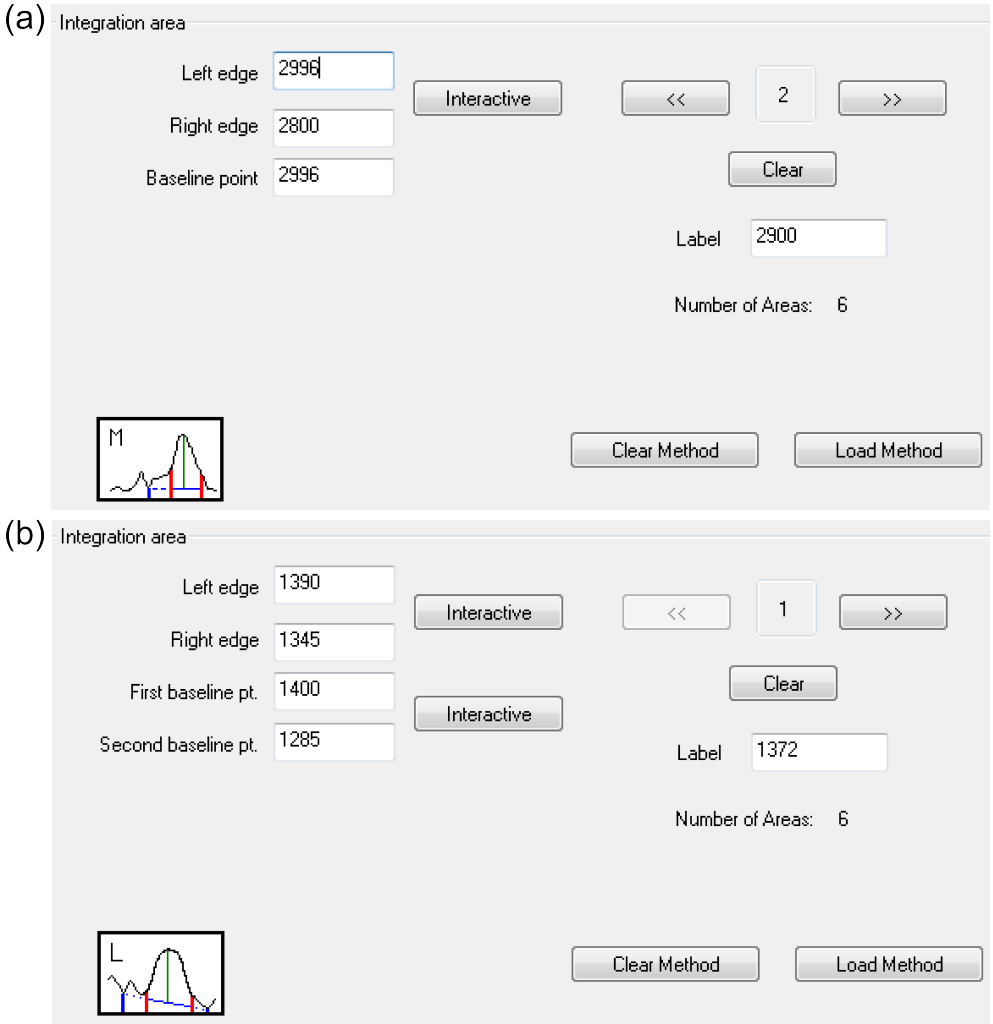

Figure 100: Settings for integration routine of I_{2900} and I_{1372} to determine TCI in OPUS 7.2.

Figure 101: Settings for integration routine of I_{1420} and I_{890} to determine LOI in OPUS 7.2.

COPYRIGHT CLEARANCE

Permission to reproduce artwork was sought from publishers, where applicable (Table 18).

Table 18: Reproduced figures with corresponding reference, publisher and licence number of requested copyright clearance.

Figure	Reference	Publisher	Licence number
1	[Bledzki et al., 2006]	John Wiley and Sons	3735780407750
8	[Fink et al., 1995]	Springer	3735761331129
14	[Cai and Zhang, 2005]	John Wiley and Sons	3735770974083
15	[Bergenstrahle et al., 2010]	Elsevier	3738130825140
18	[Miyamoto et al., 2009]	Elsevier	3735771367902
19	[Miyamoto et al., 2009]	Elsevier	3735771367902
73	[Reich et al., 2001]	Elsevier	3738240452322

STATISTICS

The results of the statistics for determining significant differences in the experimental data are given below.

Size effect in all-cellulose composite laminates

ULTIMATE TENSILE STRENGTH

```
Shapiro-Wilk normality test
data:  1 lamina
W = 0.9296, p-value = 0.5772
data:  2 laminae
W = 0.6584, p-value = 0.002184
data:  4 laminae
W = 0.8939, p-value = 0.3392
data:  8 laminae
W = 0.891, p-value = 0.3235

Fligner-Killeen test of homogeneity of variances
Fligner-Killeen:med chi-squared = 1.7067, df = 3, p-value = 0.6354

Analysis of variances
Kruskal-Wallis rank sum test
data:  r and tm
Kruskal-Wallis chi-squared = 21.376, df = 3, p-value = 8.795e-05

Pairwise comparisons using Wilcoxon rank sum test (paired=F, p.adjusted by Holm method)

data:  r and tm

X1layer X2layers X4layers
X2layers 0.015   -        -
X4layers 0.013   0.015    -
X8layers 0.013   0.015    0.013
```

```
Sample labels:
m matrix
o one lamina
t two laminae
f four laminae
e eight laminae

Shapiro-Wilk normality test
data:  m
W = 0.8702, p-value = 0.1515
data:  o
W = 0.8619, p-value = 0.2351
data:  t
W = 0.8736, p-value = 0.2411
data:  f
W = 0.9794, p-value = 0.9313
data:  e
W = 0.9341, p-value = 0.6188

Bartlett test of homogeneity of variances
data:  V by F
Bartlett's K-squared = 19.46, df = 4, p-value = 0.0006381

Kruskal-Wallis rank sum test
data:  V by F
Kruskal-Wallis chi-squared = 15.3521, df = 4, p-value = 0.004024

POST HOC
Pairwise comparisons using Wilcoxon rank sum test
data:  V and F
Eight Four  M     One
Four 0.987 -     -     -
M     0.036 0.031 -     -
One  0.127 0.195 0.889 -
Two  0.857 0.987 0.356 0.987

P value adjustment method: holm
```

YOUNG'S MODULUS

```
Shapiro-Wilk normality test

data:  m (MATRIX FILM)
W = 0.8508, p-value = 0.1251
data:  one
W = 0.8372, p-value = 0.1236
data:  two
W = 0.9435, p-value = 0.6873
data:  four
W = 0.9871, p-value = 0.7828
data:  eight
W = 0.9339, p-value = 0.6173

Bartlett test of homogeneity of variances
data:  v by f
Bartlett's K-squared = 6.1788, df = 4, p-value = 0.1862

ANALYSIS OF VARIANCES
Df Sum Sq Mean Sq F value  Pr(>F)
f            4  5.305  1.3264   5.172 0.00464 **
Residuals   21  5.386  0.2565
---
Signif. codes:  0 ?***? 0.001 ?**? 0.01 ?*? 0.05 ?.? 0.1 ? ? 1

POST HOC TEST
Tukey multiple comparisons of means
95% family-wise confidence level
factor levels have been ordered

Fit: aov(formula = v ~ f)
$f
diff         lwr      upr     p adj
Matrix-One   0.5368571 -0.30249188 1.376206 0.3450553
Eight-One    0.9600000 -0.01384522 1.933845 0.0545721
Two-One      1.0836667  0.21263302 1.954700 0.0102539
Four-One     1.2853333  0.21853934 2.352127 0.0133380
Eight-Matrix 0.4231429 -0.52246895 1.368755 0.6745259
Two-Matrix   0.5468095 -0.29253950 1.386159 0.3277926
Four-Matrix  0.7484762 -0.29260814 1.789561 0.2401652
Two-Eight    0.1236667 -0.85017855 1.097512 0.9953026
Four-Eight   0.3253333 -0.82693587 1.477603 0.9146126
Four-Two     0.2016667 -0.86512732 1.268461 0.9789942
```

NANOINDENTATION

```
*****************************
NORMAL DISTRIBUTION = TRUE FOR ALL
*****************************

Shapiro-Wilk normality test
RAYON
W = 0.9163, p-value = 0.0841
IL_15min_H2O_fibre A
W = 0.9197, p-value = 0.09771
IL_15min_H2O_matrix B
W = 0.9547, p-value = 0.4722
IL_6h_H2O_fibre C
W = 0.9573, p-value = 0.491
IL_6h_H2O_matrix D
W = 0.9476, p-value = 0.3059
IL_6h_acetone_fibre E
W = 0.9416, p-value = 0.1467
IL_6h_acetone_matrix F
W = 0.9731, p-value = 0.8697

***********************************************
HOMOGENEITY OF VARIANCES = TRUE
***********************************
Bartlett test of homogeneity of variances
data:  v by c
Bartlett's K-squared = 8.6888, df = 6, p-value = 0.1918
```

```
************************************************
ANALYSIS OF VARIANCES = NOT ALL MEANS EQUAL
************************************************
Df Sum Sq Mean Sq F value Pr(>F)
c             6 140.07  23.346    99.9 <2e-16 ***
Residuals   133  31.08   0.234
---
Signif. codes:  0 ?***? 0.001 ?**? 0.01 ?*? 0.05 ?.? 0.1 ? ? 1

Tukey multiple comparisons of means
95% family-wise confidence level
factor levels have been ordered
Fit: aov(formula = v ~ c)
$c
diff        lwr       upr     p adj
B-D 0.59707502  0.1388046 1.0553455 0.0028262
F-D 0.66595299  0.1937421 1.1381639 0.0008616
C-D 1.42834351  0.9761279 1.8805591 0.0000000
A-D 2.14515636  1.6929407 2.5973720 0.0000000
E-D 2.33027359  1.8934249 2.7671223 0.0000000
R-D 2.93726456  2.4850489 3.3894802 0.0000000
F-B 0.06887797 -0.4143235 0.5520795 0.9995226
C-B 0.83126849  0.3675880 1.2949490 0.0000071
A-B 1.54808134  1.0844009 2.0117618 0.0000000
E-B 1.73319857  1.2844922 2.1819049 0.0000000
R-B 2.34018954  1.8765091 2.8038700 0.0000000
C-F 0.76239052  0.2849275 1.2398535 0.0000919
A-F 1.47920337  1.0017404 1.9566663 0.0000000
E-F 1.66432061  1.2013857 2.1272555 0.0000000
R-F 2.27131157  1.7938486 2.7487745 0.0000000
A-C 0.71681285  0.2591156 1.1745101 0.0001346
E-C 0.90193008  0.4594094 1.3444508 0.0000002
R-C 1.50892105  1.0512238 1.9666183 0.0000000
E-A 0.18511723 -0.2574035 0.6276379 0.8719296
R-A 0.79210820  0.3344110 1.2498054 0.0000163
R-E 0.60699097  0.1644703 1.0495117 0.0013328
```

```
******************************************************
Comparison of skin and core
******************************************************
ANOVA
Df Sum Sq Mean Sq F value   Pr(>F)
c            7  24.07   3.438   15.58 2.24e-12 ***
Residuals   74  16.33   0.221
---
Signif. codes:  0 ?***? 0.001 ?**? 0.01 ?*? 0.05 ?.? 0.1 ? ? 1

Tukey multiple comparisons of means
95% family-wise confidence level
factor levels have been ordered

Fit: aov(formula = v ~ c)
$c
diff         lwr       upr     p adj
CS-CC 0.19811763 -0.47064866 0.8668839 0.9827435
AC-CC 0.79874516  0.04043547 1.5570548 0.0318069
AS-CC 0.85557326  0.19717607 1.5139704 0.0029699
ES-CC 0.87582042  0.19500333 1.5566375 0.0034023
EC-CC 1.10854769  0.42773060 1.7893648 0.0000726
RS-CC 1.51189626  0.85349907 2.1702934 0.0000000
RC-CC 1.84302587  1.08471619 2.6013356 0.0000000
AC-CS 0.60062754 -0.09621098 1.2974660 0.1425240
AS-CS 0.65745563  0.07090880 1.2440025 0.0173316
ES-CS 0.67770280  0.06609651 1.2893091 0.0195020
EC-CS 0.91043007  0.29882378 1.5220364 0.0003734
RS-CS 1.31377863  0.72723180 1.9003255 0.0000000
RC-CS 1.64490825  0.94806974 2.3417468 0.0000000
AS-AC 0.05682810 -0.63006522 0.7437214 0.9999958
ES-AC 0.07707526 -0.63133669 0.7854872 0.9999727
EC-AC 0.30980253 -0.39860942 1.0182145 0.8702797
RS-AC 0.71315110  0.02625778 1.4000444 0.0362426
RC-AC 1.04428071  0.26110184 1.8274596 0.0020765
ES-AS 0.02024716 -0.58000342 0.6204977 1.0000000
EC-AS 0.25297443 -0.34727615 0.8532250 0.8904571
RS-AS 0.65632300  0.08162682 1.2310192 0.0142285
RC-AS 0.98745262  0.30055930 1.6743459 0.0006651
EC-ES 0.23272727 -0.39203334 0.8574879 0.9400194
RS-ES 0.63607584  0.03582526 1.2363264 0.0300872
RC-ES 0.96720545  0.25879351 1.6756174 0.0014738
RS-EC 0.40334857 -0.19690202 1.0035991 0.4270723
RC-EC 0.73447818  0.02606623 1.4428901 0.0366904
RC-RS 0.33112962 -0.35576370 1.0180229 0.8030355

NO DIFFERENCE BETWEEN SKIN AND CORE OF THE RESPECTIVE FIBRES
```

```
****************************
NORMAL DISTRIBUTION = ALL NORMAL
****************************
15min_Fibre
data:  a
W = 0.9458, p-value = 0.7074
15minM
data:  b
W = 0.8453, p-value = 0.228
6h_H2O_F
data:  c
W = 0.8473, p-value = 0.1862
6hH2O_M
data:  d
W = 0.9156, p-value = 0.3216
6h_acetone_F
data:  e
W = 0.9062, p-value = 0.2903

************************************
HOMOGENEITY OF VARIANCES = EQUAL
************************************
data:  v by f
Bartlett's K-squared = 1.2079, df = 4, p-value = 0.8768

************************************************
ANALYSIS OF VARIANCES = NOT ALL MEANS EQUAL
************************************************
Df Sum Sq Mean Sq F value   Pr(>F)
f            4 1.2105 0.30262   9.875 4.68e-05 ***
Residuals   27 0.8275 0.03065
---
Signif. codes:  0 ?***? 0.001 ?**? 0.01 ?*? 0.05 ?.? 0.1 ? ? 1

*************************
POST HOC TEST
*************************
diff         lwr       upr     p adj
15F-15M 0.1617457 -0.21165353 0.5351450 0.7139940
6HM-15M 0.2797908 -0.05678675 0.6163684 0.1384625
6HF-15M 0.4506755  0.07727626 0.8240748 0.0122164
6AF-15M 0.6007645  0.25989921 0.9416299 0.0001856
6HM-15F 0.1180451 -0.16200438 0.3980945 0.7336968
6HF-15F 0.2889298 -0.03444346 0.6123030 0.0967320
6AF-15F 0.4390188  0.15383042 0.7242072 0.0010326
6HF-6HM 0.1708847 -0.10916472 0.4509342 0.4040175
6AF-6HM 0.3209737  0.08604853 0.5558990 0.0038191
6AF-6HF 0.1500890 -0.13509938 0.4352774 0.5484592
```